Electronic Theses and Dissertations

1987

Dynamic characteristics of post-tensioned prestressed concrete beams with openings.

Saadallah. Chami
University of Windsor

NOTICE

AVIS

Canadä

DYNAMIC CHARACTERISTICS OF
POST-TENSIONED PRESTRESSED
CONCRETE BEAMS WITH OPENINGS

by

SAADALLAH CHAMI

A thesis
presented to the University of Windsor
in partial fulfillment of the
requirements for the degree of
Master of Applied Science
in
Civil Engineering

Windsor, Ontario, 1987

I hereby declare that I am the sole author of this thesis. I authorize the University of Windsor to lend this thesis to other institutions or individuals for the purpose of scholarly research.

SAADALLAH CHAMI

I further authorize the University of Windsor to reproduce this thesis by photocopying or by other means, in total or in part, at the request of other institutions or individuals for the purpose of scholarly research.

SAADALLAH CHAMI

- iii -

The University of Windsor requires the signatures of all persons using or photocopying this thesis. Please sign below, and give address and date.

LEAF V OMITTED IN

PAGE NUMBERING.

PAGE V OMISE DANS

LA PAGINATION.

DEDICATION

To My Dear Father

ABSTRACT

The influence of opening size, eccentricity and location on redundant natural frequencies, mode shapes, viscous damping ratio, strains and deformations under both dynamic and fatigue loading are presented. An experimental study was conducted on six post-tensioned prestressed concrete rectangular beams provided with an opening in regions of large shear and bending stresses. A fundamental resonance frequency of about 18 Hz was observed for all the tested beams. Such a frequency did not change when varying the opening length and eccentricity for beams containing an opening in the shear span but did increase slightly for beams with an opening at midspan. A reduction between 1.0 and 1.5 Hz was observed in the value of the first natural frequency as well as a loss of 30 to 35 percent in the maximum amplitude of vibration at the first mode shape occurred due to fatigue loading before beam failure. Also, a viscous damping ratio of about 2 percent existed in all the tested beams before the application of any fatigue loading. The local behaviour of the top and bottom chords of the opening resembled that of a Vierendeel panel during fatigue loading. In addition, increasing tensile strains

were observed in the tension field region due to fatigue loading for beams provided with eccentric shear span and centric midspan openings.

A theoretical study was conducted by the Finite Element Method to determine the natural frequencies and mode shapes of vibration of rectangular, T- and I-beams. Good agreement existed between the experimental and theoretical first natural frequency values. Also, for all the cross sections considered with a midspan opening, the values of the second and fourth natural frequencies decreased rapidly and that of the first and third increased slightly with increasing opening length.

ACKNOWLEDGEMENTS

My deepest thanks and gratitude are due to HIS ALMIGHTY, ALLAH, for helping and blessing me during the course of my studies.

I would like to take this opportunity to thank the people involved in making this dissertation possible. My sincere thanks and appreciation are to my advisor Dr. J.B. Kennedy who has been a continuous source of support, encouragement and creative insight throughout the duration of the work. I am indeed indebted to him. Several other people deserve special mention. I would particularly like to thank Dr. Z.P. Reif for his interest, time and generosity towards the use of some of his equipment. Also, my appreciation is directed to Dr. N.P. Grace for his added help and to Giffels Associates for the use of their computer facilities which made the parametric study possible.

Thanks to the entire staff of the department of Civil Engineering at the University of Windsor and to the Natural Science and Engineering Research Council of Canada for their financial support throughout the research project.

Finally, I am extremely grateful to my parents Mohamed and Zahra for their continuous encouragement, support and patience.

TABLE OF CONTENTS

LIST OF FIGURES

LIST OF TABLES

NOMENCLATURE

A/D = Analog to digital conversion

A_s = The area of steel required to guard against potential horizontal splitting caused by force T

A_w, A = The area of the web and the total cross section respectively

B = The beam width

B_1 = Top flange width

B_2 = Bottom flange width

c = The distance from the center of the opening to the bottom of the beam

D/A = Digital to analog conversion

d_t, d_c = The tension and compression distances respectively

EI_{eff} = Effective section rigidity

EI_g = Gross section rigidity

EI_{rep} = Unloading - reloading section rigidity

P = Externally applied load

e = Eccentricity of the prestressing force from the centroidal axis of the section

f'_c = Compressive strength of concrete

f_s = The allowable tensile stress in the steel reinforcement

f_1 =   First natural frequency of vibration

f_2 =   Second natural frequency of vibration

f_3 =   Third natural frequency of vibration

f_4 =   Fourth natural frequency of vibration

H =   The depth of the beam

H_1 =   First flange depth

H_2 =   Second flange depth

h =   The depth of the opening

h_t , h_b =   The depths of the top and bottom chords respectively

h_2 =   Depth of the second opening

I/O =   Input-Output operation

L =   Length of the beam

ℓ =   Distance between the support and the edge of the opening

n =   Number of cycles

P_s , P =   Total prestressing force

P_1 =   Prestressing force applied to the web

P_2 =   Prestressing force applied to the flange

T =   The vertical tensile force

v =   Length of the opening

v_2 =   Length of the second opening

w/c =   Water Cement ratio

$\ddot{x}_1$ =   Acceleration, initial single peak

$\ddot{x}_n$ = Acceleration, single peak after n cycles

$\bar{y}$ = The distance of the centroidal axis from the bottom of the cross section

ρ = Percentage of tensile steel

α = $\bar{y} - e - [(h_b) / 2]$

β = $d_t + d_c$

γ = $h + [(h_t) / 3] + [(h_b) / 2]$

ξ = Viscous damping ratio

Chapter I

INTRODUCTION

1.1 General

Earthquakes, blast loadings and repetitions of high live loads on buildings and bridges are examples of dynamic loads on structures. Earlier on most structural applications were limited to regularly reinforced concrete beams. Such structural components were bulky and somewhat stiff which provided them with a high resistance against vibrational excitation. With the invention of new building techniques for both economy and structural shape, prestressed concrete structures started to come into the picture. Their high cracking resistance, rigidity and the possibility of complete utilization of high strength steel, afford prestressed concrete structures a number of advantages over plain reinforced concrete.

After the experimental work on utilization of prestressed reinforced concrete in civil construction working mostly under static conditions yielded good results, the material began to be widely used in bridge construction as well. To accurately predict the structural response of such components it becomes necessary to study among other aspects

- 1 -

the dynamic behaviour of the structures. When the natural
frequencies of the structure are determined, they are
compared to the applied transient loads frequency to
determine if the state of resonance is available in such
excitation or not.

The provision of holes in beams is sometimes necessary to
accommodate services in residential, commercial and
industrial buildings and in bridge construction as well. In
residential and commercial construction, air conditioning
ducts, electrical conduits, sanitary pipes and similar
utility components can be carried within the depth of the
beams and girders. This in turn eliminates a significant
amount of dead space between the soffit of the beams and the
suspended ceiling maintaining a minimum storey headroom. In
industrial buildings beams with openings are used for
passing through the same utility components but are mainly
concerned in providing working space for large manufacturing
machinery and internal mobile cranes, while in bridge
construction openings are provided for passing through and
supporting utility pipes to provide enough headroom for the
underpass traffic (especially large trucks which demand high
vertical clearances).

All the previously mentioned structural applications of
prestressed concrete beams with openings can be easily
subjected to vibrational excitation. With the addition of

seismic effects, residential and commercial buildings have to be concerned with human occupancy while in industrial buildings, heavy manufacturing machinery produces a lot of vibration onto supporting beams and in bridges, ongoing traffic, blast loading and wind effects are a number of important factors. Therefore practicing engineers are usually interested in the dynamic characteristics of such members in order to account for it in the design procedure to build safe and economical structures.

1.2 Objectives

After reviewing previous work by El-laithy and Kennedy (1982) who studied the effects of openings on prestressed rectangular concrete beams under static loading conditions it became evident that nowadays due to the wide range of structural applications of such members, their dynamic-fatigue characteristics are of increasing demand and importance.

Before embarking on such a research project a considerable amount of interest was shown in determining the following:

1.   The dynamic characteristics of such members which included frequency spectrums, flexural mode shapes and material damping coefficient before and after fatigue loading.

2.   The variation in strains around the opening during the fatigue process.

3.   The influence of dynamic-fatigue loading on the tension field present at either side of the opening.

4.   The deformations of the opening chords at the first flexural natural frequency.

5.   The location and pattern of cracks under the influence of dynamic-fatigue loading.

The provision of openings complicates the analysis of such members to a great extent. In view of such complexity the dynamic characteristics, stresses and deformations cannot be determined by the application of classical methods such as beam theory. To deal with the problem, both an experimental and a theoretical investigation were conducted. The experimental work investigated all the previously mentioned points of interest while the theoretical work included a parametric study which investigated the influence of different opening lengths and location, the presence of more than one opening and use of different beam cross sections such as T- and I- sections on the flexural natural frequencies and mode shapes of vibration.

1.3 Scope

The following investigation covers experimentally the effects of: the length,   eccentricity and horizontal location of an opening under the influence of a concentrated dynamic load at midspan on the dynamic characteristics, strains and deformations of rectangular prestressed concrete beams.

The experimental work comprised   of six   rectangular post-tensioned prestressed concrete beams   provided with one opening each.   The location of the opening was away from midspan in five beams and at midspan in the sixth.   Their results are analyzed and discussed from the standpoint of dynamic characteristics, strains, cracking and deformations. Theoretical flexural frequencies and   mode shapes of vibration are also presented for the above six beams and for other beams in the parametric study chapter.

A review of previous experimental and theoretical research conducted on reinforced and prestressed concrete beams with openings under static loading conditions and on reinforced   and   prestressed   concrete   beams   under dynamic-fatigue loading is presented.   A description of the finite   element   package   programs   used   (SAP-IV   and STRUDL-DYNAL) is included.   Comparisons between the results of plane stress finite element and beam theory for a solid prestressed concrete beam is also presented.

A comparison between the experimental and theoretical results with regard to natural flexural frequencies and mode shapes for six beams is presented. Also conclusions and recommendations are drawn.

Chapter II

LITERATURE SURVEY

2.1 General

Previous research in the area of structural dynamics on prestressed and regularly reinforced concrete beams has been scarce and very general with most of it being concentrated in the area of fatigue.

Most of the current codes of practice when concerned with the design of structures that are being subjected to dynamic loads specify values of the dynamic load allowance (DLA) related to the fundamental natural frequency of the structure assuming beam-type mode shapes. Such factors are used to magnify the imposed static live loads to simulate dynamic effects before analyzing and designing the structure. The application of such factors is very limited due to the number of constraints surrounding their use such as, the range of imposed exciting frequency, material damping value and the existing boundary conditions.

The survey conducted is best presented when subdivided into the following sections:

1. Concrete beams with openings subjected to static loads
2. Concrete beams subjected to dynamic loads

3.   Concrete beams subjected to fatigue loads

4.   Dynamic response of composite bridges and plates

2.2   Concrete Beams With Openings Subjected to Static Loads

Regan and Warwaruk (1967), published work related to tests conducted on prestressed concrete T-beams with large web openings. A testing program involving four model beams and two full size beams was decided upon with all beams being subjected to a two-point symmetrical loading arrangement. It was observed that the inclined cracks began at the corner of an opening located between the load and reaction point. Also, just prior to collapse the inclined cracks widened considerably and, as a result of high shearing forces present, a mechanism actually occurred with final collapse resulting from large deformations of the mechanism.

Sargious and Dilger (1977), conducted theoretical research using the finite element method on single span concrete deep beams with two openings prestressed with straight tendons. Openings of various sizes relative to the size of the beam were considered, and the maximum stresses and forces were determined at the critical locations due to the beam's own weight, external load and prestressing forces. They concluded that it is important to limit the

height of the opening and have it located closer to the bottom edge of the beam so that the top chord above the opening will have sufficient depth to resist the bending moments and shearing forces due to applied loads, since this part carries most of the bending moments and shearing forces in the beams.

In 1977 Barney, Hanson, Corley and Parmelee published literature on tests carried out on eighteen full size T-beams containing large rectangular web openings under the influence of distributed loading. The principal variables in the test program were the size and location of openings, type and amount of web shear reinforcement and amount of primary reinforcement. The results showed that of the variables considered, those having the greatest effect on specimen strength and behaviour were the location of the web openings along the span and the amount of web shear reinforcement. Also, the behaviour of beams with openings was similar to that of a Vierendeel truss concluding that large web openings can be placed in prestressed concrete beams without sacrificing strength or serviceability.

El-laithy (1978) presented a thesis containing experimental and theoretical research on the behaviour of prestressed concrete beams with rectangular openings at the transfer stage. Analytical and experimental results for strains, stresses, deformations and cracking loads were

obtained. The experimental results were based on tests conducted on ten post-tensioned prestressed concrete beams of rectangular cross section while the theoretical results were obtained by means of the finite element method. The influence of the horizontal and vertical location of an opening as well as its depth was examined. Results from the finite element method were substantiated and verified by the experimental test results. He concluded that the presence of an opening gives rise to a potentially splitting tension field, followed by a compression field, whose distances are functions of both the depth and vertical location of the opening; and, that such a tension field can be effectively contained by transverse reinforcement around the opening. Also, the maximum tensile stress occurs at or near the midheight of the opening. Furthermore the presence of the opening gives rise to significant shear stresses near the four corners and the assumption of plane stresses remaining plane does not apply in the vicinity of the opening with deflection only increasing slightly at the transfer stage. In conclusion a proposed method based on truss analogy was presented to estimate and design for the vertical tensile force around the opening for beams with one or more openings.

Abdus Salam and Harrop (1979) conducted an experimental study to provide a design method for prestressed concrete

beams with transverse circular holes. Steel liners, bonded ring reinforcement in the concrete around the holes and vertical stirrups on both sides of the opening, were reinforcing methods that were investigated. It was concluded that compensation for the presence of the holes is best provided by vertical stirrups at the sides of the opening because such reinforcement takes care of both the horizontal splitting due to prestress and the diagonal tensile stress at working load. Summarizing they mentioned that the suggested methods of design for this additional reinforcement and the corresponding test results show that perforated beams can be as strong as a similar solid beam provided the holes do not protrude in the ultimate rectangular stress block required at flexural failure.

In 1984 Dinakaran and Sastry investigated the behaviour of post-tensioned prestressed concrete T-beams with large web openings under the influence of two point loads. The variables considered were the size of the openings, location of openings, and type of reinforcement around openings. The results indicated that; of the variables considered, the location of the opening has the greatest effect on the strength and behaviour of the beams; vertical stirrups and hooks remarkably contain cracking and thereby increase the load carrying capacity of the beam while trimming of opening with reinforcement neither contains cracking nor increases

the ultimate capacity; the region around the opening behaves similar to a Vierendeel panel; the influence of openings on deflection is minor in properly reinforced beams. Concluding they stated that large web openings can be accommodated in post-tensioned prestressed concrete T-beams without sacrificing the strength.

Mansur, Tan and Lee (1985) proposed a design method for reinforced concrete beams with large rectangular openings that are subjected to both bending and shear. The model was based on the collapse load analysis in which the conditions of equilibrium, yield, and a four hinge opening failure mechanism were satisfied simultaneously. Twelve beams were designed under the proposed guidelines and tested in the laboratory. The major variables considered were the length, depth, eccentricity and location of openings, and the amount and arrangement of corner reinforcement. They concluded that: at a particular load, both the maximum crack width and maximum beam deflection increase with an increase in opening length, opening depth, or moment-shear ratio at the center of the opening. The effect of opening eccentricity is insignificant for the small eccentricities used in this test program; diagonal bars for corner reinforcement are more effective than full depth vertical stirrups in controlling crack width and reducing beam deflection and in increasing the ultimate strength of the beams; provided that the solid

sections are adequately reinforced, the beam fails by the formation of a mechanism with four hinges in the chords, with one at each corner; the position of contraflexure point in a chord member depends on the disposition of longitudinal reinforcement; if a symmetrical arrangement exists it occurs approximately at midspan of the chord members. In summary they mentioned that the proposed design method has been found to be safe and satisfactory but is only applicable to beams when the chord members are not directly loaded. Also, the slenderness ratio for the compression chord should be limited to 22 as suggested in the ACI code for unbraced compression members.

Elaborating on previous work by Mansur, Tan and Lee (1985), Mansur and Ong (1985) published a paper on epoxy repaired beams. Six reinforced concrete beams with large rectangular openings which were tested to failure previously were repaired by replacing cracked regions with epoxy mortar and by filling cracks with epoxy injection. After being cured for one day, the repaired beams were tested in the same manner as the original ones. From the results they concluded that: the repaired beams fail in the same manner as the original beams, by the formation of a mechanism with four hinges, one at each corner of the opening; the maximum crack widths in the repaired beams are, in general, smaller than those in the original beams because of the delayed

development of cracks at the four critical corners of the opening. The epoxy mortar strenythened the regions of high stress concentration; the presence of hairline cracks in the repaired beams caused a reduction in stiffness and hence higher deflection; therefore, if maximum deflection governs the design, epoxy bonded steel plates should be used at critical sections to stiffen the beam. Summarizing they mentioned that the repaired beams are stronger than the original ones.

2.3 Concrete Beams Subjected to Dynamic Loads

In 1960 Marshall and Ozell published a paper on the behaviour of prestressed concrete under dynamic loading. A very small testing program was conducted where the subject was a prestressed diving board. The means at which the board was excited (a diver springing at its end) did not provide any information about the first natural frequency with only the response at the second mode of vibration being presented. In conclusion it was mentioned that the mass of members subjected to similar loads has great effect upon their response to dynamic loads.

In 1964 Zavriev published literature related to the response of prestressed structures to dynamic loading. Most of the contents of the paper were based on personal observation and experience. In conclusion he mentioned that

due to the similarity of dynamic characteristics for both prestressed reinforced concrete and metal span construction, it would be correct for the time being to calculate dynamic coefficients for prestressed spans with the aid of empirical formulas accepted by the codes of metal bridges. Also, the idea of using prestressed construction for increased seismic resistance of structures should be considered from a positive point of view.

Jacobs, Rankin and Hill (1968) published work on the behaviour of prestressed concrete beams under reversed cyclic loading. Twelve beams were tested at alternating moments varying from a negative value, through a zero value, to a positive value having a maximum magnitude between 60 and 100 percent of the ultimate static moment. The rate of testing was varied from a relatively slow value of 1/900 cycle per second to 1/2 cycle per second. The loading was applied until either failure occurred or a predetermined number of cycles was attained. The results showed: a considerable change in beam stiffness occurred with the number of applied cycles of moment. A more rapid change occurred at higher values of moment; the energy dissipated in a beam under loading was due to material damping in the concrete behaving in an inelastic manner.

Coles and Hamilton (1969) presented research on repetitive dynamic loading applied to pretensioned

prestressed beams. Eight beams were subjected to repeated applications of dynamic blast-type loading at midspan. The number of applications of the dynamic load varied from five to seven with a magnitude ranging between 0.93 to 1.32 times the actual static failure load. Some of the conclusions drawn were: The calculated static ultimate load is a satisfactory design criterion when a beam is subjected to a low number of blast-type loadings; bond failure did not seem to be a critical factor in such beams under repetitive dynamic loads; with each successive loading, regardless of magnitude, the maximum deflection increased, thus indicating a loss of beam stiffness.

Inomata (1971) conducted experimental work on twelve prestressed and reinforced concrete beams under loading reversals. The flexural ultimate limit load was used as a design criterion. It was based on the design strength of the material and on limiting steel elongation to less than one percent. From the results he concluded that prestressed concrete beams have less energy absorption as long as the applied load remains smaller that the ultimate limit load. Also, residual deflection seems to be higher for regular reinforced concrete members than for prestressed members up to the ultimate limit load.

Sokolovsky, Livolant, Gauvain and Hoffmann (1980) conducted a study on the progressive damage to reinforced

concrete structures when subjected to dynamic reversed loads. Theoretically, a non-linear computation model was worked out for unidirectional behaviour while experimentally a column was subjected to two typical earthquake time histories on a shaking table. The time histories used were the Taft [1952] north-south component and the San Francisco [1957] north-south component. In conclusion they mentioned that: significant safety factors appear between the experimental seismic load level leading to collapse and acceptable limit levels predicted in accordance with the French code by means of the elastic theory. However, if the ultimate load prediction is usually conservative, the opposite is true for the prediction of displacement values; the non-linear analysis conducted showed good agreement with the experimental results because it took into account the progressive decrease of stiffness due to cracking at all stages of loading.

Johns and Belanger (1981) explored experimentally which value of stiffness (EI) might be appropriately used in dynamic calculations for flexurely loaded concrete beams to accurately predict resonant frequencies. The beams were tested by applying a static load increment at a distance L from both ends followed by a small intentional perturbation at midspan, causing a decaying free vibration. This response is noted on an oscillograph output permitting the

determination of the frequency. The results established that neither gross section rigidity EI_g, effective rigidity EI_{eff}, nor unloading-reloading rigidity EI_{rep} can be used with accuracy in dynamic response calculations. A formula for predicting dynamic stiffness was tentatively proposed, such a formula has the form of the EI_{eff} formula, but is linear rather than cubic in the moment term.

In 1983 Stanton and McNiven proposed an non-linear theoretical dynamic model for predicting the flexural response of reinforced concrete beams to severe cyclic loads. The model is constructed with the aid of system identification, which permits the coefficients in it to be so tuned as to replicate with the maximum possible accuracy the results of physical experiments. The uniaxial constitutive behaviour of the concrete and steel are considered separately, and they are combined through a bond-slip relationship to form a global model for the composite material. They concluded that: the layered model is able to reproduce complicated physical behaviour with remarkable accuracy. It works best in situations where its assumptions (of behaviour dominated by flexure and of reinforcement which does not buckle) are not violated; the constitutive non-linear law chosen for steel is particularly critical in modelling reinforced concrete. Summarizing, they mentioned that the analytical model contained no

mechanism for predicting shear deformations and that it is still too complicated for practical use.

2.4   Concrete Beams Subjected to Fatigue Loads

Warner (1960) presented research on the fatigue and shear characteristics of prestressed concrete. Tests were carried out on three pairs of beams, one beam in each pair was tested statically while its companion was tested under repeated loading. A repeated cycle of 55 to 60 percent of the static ultimate load caused failure in all tests. Comparisons between the results of the experiments and the theory of fatigue failure developed for constant cycles of repeated loading showed good agreement.

Warner and Hulsbos (1962) presented a report concerned with the probable fatigue life of prestressed concrete flexural members. The work consisted of a program of fatigue tests on prestressed concrete beams, an experimental study of the fatigue properties of high steel strand reinforcement, and a theoretical analysis of the stresses and deformations in such members under fatigue loading. A method was developed for predicting the fatigue life of such members failing by fatigue in the steel reinforcement under repeated constant cycle and cumulative damage loading. Also, a means of obtaining a lower bound estimate of beam fatigue life as limited by concrete fatigue failure was also

presented.   The results indicated that after an initial

sequence of repeated loading representing about ten percent

of the fatigue life, the beam normally settles down to a

fairly regular and consistent response to load.   Also, steel

fatigue failure of a prestressed beam occurs by successive

fracture of the elements of steel reinforcement in the beam.

A considerable number of load cycles may separate the first

and second steel failures,   but the interval separating

successive failures will tend to decrease as the number of,

failed elements increases. Failure of each steel element is

accompanied by a corresponding decrease in beam rigidity.

In conclusion, they mentioned that comparisons of predicted

and observed fatigue lives for the test beams showed

satisfactory correlation.

Abeles (1965) conducted studies on crack widths and

deformations of reinforced concrete beams under sustained

fatigue loading.   A two-point loading arrangement was

applied to the test beams varying from 45 to 80 percent of

the static ultimate load.   From these tests it seems

appropriate to limit the permissible maximum crack width at

static loading to 0.004 inch (0.102 mm), which might result

in a width of 0.01 inch (0.254 mm)   under sustained or

repeated loading.   Also, the tensile stress permissible for

a definite crack width depends mainly on the distribution of

the steel around the tensile zone and on the percentage p of

steel although ρ seems to be the more important factor in this case. In conclusion an empirical formula was presented for calculating limiting crack widths based on nominal permissible concrete tensile stresses.

In 1970 Hanson, Hulsbos and VanHorn published work on the behaviour of concrete I-beams under fatigue loading. Tests were conducted on six simply supported beams with each beam being subjected to a symmetrical two-point loading arrangement having a repeated cycle magnitude of 19 to 45 percent of the ultimate flexural capacity applied at a rate of 250 cycles per minute. Based on the results, the following conclusions were drawn: the flexural fatigue life of the test beams was less than expected from the available information on the fatigue strength of the strand; cracks have an effect on the fatigue strength of a strand in a beam (most strand fatigue failures occured where there was a crack present); limit the nominal tensile stress in the bottom fibres to $6\sqrt{f_c'}$; shear fatigue failures do not occur suddenly, but rather give considerable warning as indicated by increasing deflection and increasing inclined crack width before failure occurs.

In 1971 Price and Edwards investigated experimentally the fatigue strength of bonded post-tensioned concrete I-beams. Ten beams were loaded at a rate of 300 cycles per minute under a constant load having a maximum amplitude varying

from 68 to 74 percent of the ultimate flexural load. The results showed that the response of cracked sections is significantly affected by repeated loading of a magnitude sufficient to cause flexural cracks to open. This change is brought about by both progressive breakdown of bond and by changes in the stress-strain relationship of concrete. The change in response occurs rapidly in the early load cycles but reaches very nearly stable values later on. Also, fatigue failure of normal under-reinforced sections generally occurs by fracture of the prestressed reinforcement. However, if the section contains a high number of steel elements, a large number of load cycles will be resisted before structural collapse. Concrete compression fatigue failures are possible at high load levels in under-reinforced sections and at lower load levels in over-reinforced beams. Finally, a theory based of the fatigue fracture of the reinforcement is presented for the prediction of the fatigue strength of prestressed concrete members in flexure. This theory applies to repeated loading between extremes that are of constant magnitude.

Kulkarni and Ng (1979) investigated the behaviour of limited prestressed beams under repeated loading. Eight T-beams were tested under severe combinations of repeated loads on a universal testing machine. Each beam was subjected to a frequency of testing of 7 cycles per second

with the criteria that the application of 2 million cycles of repeated loads being critical for design considerations. The results showed that: the effect of repeated loading on beam deformation is predominant only in the early stages; theoretical computations of deflections neglecting concrete in the tension zone always gives overestimated values of deflection; in extreme stage cracking the contribution of concrete in the tension is significant and needs attention during the design process.

In 1981 Balaguru presented a theoretical model to predict the fatigue life, increase in deflection and crack width of prestressed concrete beams using the fatigue properties of the constituent materials, namely concrete, prestressed and non-prestressed steel. The model takes into consideration the following: 1) cyclic creep of the concrete in the compression zone, 2) cyclic creep or strain-softening of reinforcing and prestressing steel under cyclic loading, 3) progressive decrease of stiffness contribution of tension zone concrete. The author proved the adequacy of his model by comparing its results to previous experimental research. In conclusion the author mentioned that the proposed method compares favorably with experimental data but hoping that with the availability of more experimental data and better understanding of some of the complex behaviour, the model can be further simplified to expedite design calculations.

2.5   Dynamic Response of Composite Bridges and Plates

Although the above research topic is not directly concerned with the one presented in this publication, the author felt that the experimental tests and procedures discussed in two papers presented a meaningful aid to this investigation.

In 1984 Grace and Kennedy presented research concerned with the dynamic-fatigue response of continuous composite bridges. Experimentally, four tests were conducted to determine the dynamic-fatigue characteristics: 1) the sweep or sine-wave test, 2) the log-decay test, 3) the normal-mode test, 4) the resonance fatigue test. From the results it was observed that deck cracking produces a substantial reduction in the natural frequencies of the structure. Furthermore, a study of the damping response of the cracked model revealed a damping ratio of about 3 percent. Also, fatigue loading close to the resonance frequencies can cause very rapid increase in the stress range, thus leading to sudden failure of the structure.

Grace and Kennedy (1985) investigated the dynamic response of orthotropic plate structures with fixed-simply supported and free-free boundary conditions. A very similar experimental testing procedure to the one above was followed. The analytical results, verified by experimental test results, confirm that for this class of structures the

natural frequencies beyond the first cannot be reliably estimated by beam theory. In conclusion they mentioned that a reliable estimate of the lower natural frequencies of such structures will make it possible to design against resonance.

Chapter III

THEORETICAL ANALYSIS

3.1 General

The finite element method is generally-acceptable for deducing the natural frequencies and associated mode shapes of vibration of structural members.   The basic idea behind the finite element method is to divide the structure, body, or region being analyzed into a large number of finite elements. These elements are connected together at discrete nodal points where continuity is expressed.

Two finite element computer programs, SAP-IV and STRUDL-DYNAL, were adopted for the theoretical analysis of prestressed concrete beams with or without openings.   A brief description of each program is presented in this chapter followed by the area of application that each one was used in.

3.2 Structural Analysis Computer Program SAP-IV

SAP-IV, the Structural Analysis Program developed for the Static and Dynamic Response of Linear Systems at the University of California, Berkely (1974) was used to determine the natural frequencies and mode shapes of

vibration of solid prestressed rectangular concrete beams. The first version of SAP was published in September 1970. Work was then continued to produce an improved static and dynamic analysis program resulting in the release of SAP-III at the end of 1972. In relation to SAP-III, the current version SAP-IV has improvements throughout, such as a variable number of nodes for thick shells and three dimensional elements, as well as out of core direct integration for time history analysis.

A three dimensional beam element which complies completely with beam theory was used. Figure 3.1 shows the associated number of degrees of freedom and the local axes orientation for such an element with respect to the global axes. Since only flexural modes were of interest the beam elements were restrained from moving in direction 3 and from rotating about axis 2 and 3. The beam model consisted of 19 beam elements and 21 nodes as shown in Figure 3.2.

3.3 Structural Design Language Computer Program STRUDL-DYNAL

The original version of STRUDL was developed and initially released by the Massachusetts Institute of Technology (MIT). McDonnell Douglas Automation Company (MCAUTO) provides a much enhanced version of STRUDL compared to the one developed by MIT. In particular, a major

enhancement has been the implementation of a reliable dynamics analysis capability. The dynamics portion of STRUDL is called STRUDL-DYNAL (1985). This program is a series of subprograms for solving different dynamic problems in structural engineering. The commands are interpreted by the Integrated Civil Engineering System (ICES). These commands are made of engineering words which are available in the commands manual.

This program was used to conduct a theoretical parametric study on prestressed concrete beams. The investigation considered a number of factors which could influence the natural frequencies and mode shapes of vibration. Such factors consisted of:

1. The influence of different opening length and location.

2. The presence of more than one opening.

3. The use of different beam cross sections (T- and I-sections).

3.3.1 The Influence of Length and Location of Openings

Two opening locations were chosen for the investigation dealing with beams of rectangular cross sections; one was within the shear span twenty four inches away from the support while the other was centred about the midspan.

3.3.1.1   Beams With Openings in the Shear Span (Side Opening)

Eight different cases were investigated. One case represented a solid beam while the others were for beams with openings varying in length from 4 to 32 inches and having a constant depth of 3 inches. Figures 3.3 and 3.4 show the associated number of degrees of freedom and the local axes orientation with respect to the global axis of Plane Stress Rectangular (PSB) and Constant Strain Triangular (CSTG) elements. Figure 3.5 shows a typical finite element mesh which was used in this series of investigations. This mesh consisted of 58 elements and 92 nodes which was used for the analysis of a 24 inch by 3 inch opening. Also Table 3.1 shows the different cases studied showing opening sizes, location and beam dimensions.

3.3.1.2   Beams With Openings at Midspan

Here four different opening lengths were investigated. The length varied from 8 to 32 inches at an increment of 8 inches while the depth was kept constant at 3 inches. Figure 3.6 shows a typical finite element mesh which was used in this series of investigations. This mesh consisted of 70 elements and 100 nodes. The elements employed in the mesh are identical to the ones used previously. Table 3.2 lists the different cases considered.

3.3.2   Beams With More Than One Opening

All the beams considered in this part of the investigation contained two openings with varying lengths and located in the shear span, with a constant depth of 3 inches. The first opening was located at 24 inches away from the support and was followed by a vertical chord which separated the two openings. The chord's length varied from 4 to 16 inches in all the cases considered. Table 3.3 shows the three cases investigated and Figure 3.7 shows a typical mesh for the analysis of a beam containing an 9 inch by 3 inch and a 12 inch by 3 inch openings. This mesh consisted of 61 elements and 92 nodes with all the elements being identical to the ones used previously.

3.3.3   Beams Having Different Cross Sections

The influence of different beam cross sections (other than rectangular) on the natural frequencies and mode shapes of vibration was investigated. T- and I-beams provided with openings at midspan were considered.

3.3.3.1   T-Beams With Openings at Midspan

Two different T-beam cross sections were considered in this part of the investigation. In one cross section the dimensions of the top flange were relatively large resulting in the neutral axis lying well within the flange while the other cross section contained a smaller flange with the

neutral axis falling within the web. Four different cases were considered for the first cross section and two others were studied for the second cross section (refer to Table 3.4). The web of the cross section was made up of PSR and CSTG elements while the flange consisted of a new Linear Strain Rectangular (LSR) element. Figure 3.8 shows the associated number of degrees of freedom and the local axis orientation of the LSR element with respect to the global axis. Also, Figure 3.9 shows a typical finite element mesh which was used for a large flange section having a 32 inch by 3 inch opening at midspan.

3.3.3.2 I-Beams With Openings at Midspan

Three different cases were investigated herein. One case represented a solid beam while the others were for beams with openings varying in length from 16 to 32 inches and a depth of 3 inches (refer to Table 3.5). Figure 3.10 shows a typical finite element mesh which was used for the case of a 32 inch by 3 inch opening. The same elements used previously for a T-beam were again used here with the only difference being the addition of a bottom flange consisting of a number of LSR elements.

Chapter IV

EXPERIMENTAL INVESTIGATION

4.1 General

Experimental tests were carried out on six simply supported post-tensioned prestressed concrete beams with openings. Figure 4.1 shows the overall beam layout and Table 4.1 indicates the dimensions, opening sizes and location, eccentricity and amount of prestressing force and the experimental ultimate compressive strength of concrete for such beams. The main objective was to study the behaviour of such structures under pulsating loads. The main issues of the investigation were the overall dynamic characteristics of the beams and the local behaviour of the opening region when subjected to vibrational excitation. The experimental work consisted of five tests:

1.   The free vibration hammer test;

2.   The sine wave sweep test;

3.   The natural frequency test;

4.   The log-decrement test; and,

5.   The fatigue test.

Such tests provide information on the dynamic response such as natural frequencies, material damping ratio, mode shapes and associated fatigue strain ranges.

4.2   Materials

4.2.1   Concrete

All concrete mixes used were composed of high early strength cement, coarse aggregates, fine aggregates, sand and water. The high early strength portland cement accelerates the hydration process which is accompanied by rapid hardening and rapid development of strength. This made it possible to test the beams shortly after casting. The coarse aggregates consisted of crushed durable stone having a maximum diameter of 0.4 inch (10 mm) and a minimum diameter of 0.2 inch (5 mm). The fine aggregates consisted of small stones with a maximum diameter 0.2 inch (5 mm). Fine sand was used and care was taken to make sure it was free of chemicals, coatings of clay and fine material that may effect hydration and in turn bond of the cement paste. Natural tap water having no impurities was used. Water cement ratics of 0.43 to 0.45 were required to achieve the desired concrete compressive strength of 6000 to 8000 psi. Three 6 inch by 12 inch cylinders were cast for each beam; such cylinders were tested at the first day of beam testing to determine the concrete compressive strength. (Appendix A contains the concrete mix design)

4.2.2   Steel

The following types of steel were used:

1.   High tensile strength prestressing wires having a diameter of 0.276 inch (7 mm).   The ultimate strength as documented by the manufacturer was given as 255,000 psi (1760 MPa).   The above value was checked in the laboratory, and the results were in good agreement. Each wire had one end deformed as shown in Figure 4.2.

2.   Mild steel stirrup bars having a 3/16 inch (4.9 mm) diameter.

3.   Two end steel bearing plates, 3/4 inch (19.1 mm) thick were used to distribute the prestressing force over an area of 3 inch by 8 inch (76 mm by 203 mm) at each end of the beams.   Figure 4.3 shows such a plate.

4.2.3   Formwork

The forms consisted of 3/4 inch (19.1 mm) thick plywood. After the wood was cut to the appropriate dimensions, 1.5 inch wood screws were used to keep it together.

4.2.4   Other Materials

The following items were used during beam preparation:

1.   Plastic tubes having a 7/16 inch (11.1 mm) diameter, were properly greased with oil and used to house the prestressing tendons during the casting operation.

2. Small steel chairs were used to rest the bottom of the
   stirrups on to provide the appropriate clearance from
   the bottom of the forms.

3. Thin steel wire was used to tie the stirrups to two
   1/8 inch (3.2 mm) diameter mild steel reinforcing bars
   at the top of the beam to keep them in place.

4.3   Experimental Equipment

4.3.1   Post-tensioning Equipment

the following items were used during the post-tensioning
operation:

1. A hydraulic jack having a capacity of 20 kips (89 kN)
   was used to tension each cable separately to the
   desired force. Figure 4.4 shows the jack.

2. Anchorage wedges and cylinders of the open grip type
   were used to anchor the tendons after tensioning them.
   Refer to Figure 4.5.

3. Two steel end bearing plates 3 inch by 8 inch (75 mm
   by 200 mm) having a thickness of 3/4 inch (19 mm) were
   used at both ends of the beams to distribute the
   prestressing force over the entire bearing area and in
   turn put the concrete in a precompression loading
   state.

4. Three cylindrical wire load cells were used to monitor
   the prestressing force in the wires during and after
   post-tensioning (refer to Figure 4.6).

4.3.2   Vibration Loading System

The Gilmore closed-loop electrohydraulic system was used to control the jack operation during all phases of loading.

Looking at the Gilmore structural loading system in more detail showed that it can be classified into:

1.   An electronic console unit which includes servo-amplifiers, signal conditioners, rate programmers and a numbers of other features such as a pump on-off switch and a cycle counter module (refer to Figure 4.7).

2.   An actuator, model 433-20 having a built in position and velocity feedback transducers plus an external static-dynamic loadcell (refer to Figure 4.8).

3.   A 20 GPM hydraulic pump.

The electronic console unit provided complete control of the jack displacement and frequency of loading which in turn maintained the applied load constant during testing. The following is a brief description of the console controlling features:

1.   Servo amplifiers controlled the servo valve on the actuator which in turn controlled the rate of oil flow into the actuator. They also contain the jack gain and damping controls.

2.   Two signal conditioner models 429 and 416. The model 429 was primarily responsible for generating the

required wave function accommodating the testing frequency range of 1 to 22 Hz. The model 416 position signal conditioner controlled the mode of the actuator through the gain and phase adjustments. When the conditioner was placed in displacement control mode, the actuator LVDT output signal was fed directly into the servo-amplifier and from there out into a volt meter for displacement monitoring.

4.3.3   Actuators

The Gilmcre model 433-20 kip (89.9 kN) hydraulic actuator was used in all the experiments. The actuator was supported at the top to the structural flanges of the frame as shown in Figure 4.9. Due to the fact that the travelling stroke of the actuator's piston was so small in the higher frequency range when compared to the beam's displacement amplitude at the natural frequency, a new loading arrangement had to be worked out at the bottom end of the jack. The arrangement used consisted of two steel pieces, one installed on the jack and the other installed on a steel plate resting on the beam's point of loading. Both pieces were lined up by a groove that fits into the top piece on the jack. Four springs having a stiffness of 790 lb/inch (0.1383 kN/mm) were housed in between the two steel components. With the aid of the LVDT mounted on the jack, a desired displacement was applied by the jack onto the

springs which in turn transmitted a constant load to the beam's surface. The steel piece resting on the top of the beam was supported to the bottom concrete surface by using grooved mild steel bars, steel plates and nuts as shown in Figure 4.10.

4.3.4 Supports

The beams were simply supported resting on steel rollers having a 3 inch (75 mm) diameter whose housing was welded onto I flange sections which were clamped to base supports. The ends of the concrete beams were tied down by means of a small piece of steel pipe resting on the top concrete surface. It was supported by two U shaped grooved mild steel bars one at each end of the pipe running right through the supporting flanges and fixed by nuts as shown in Figure 4.11.

4.4 Experimental Instrumentation

4.4.1 General
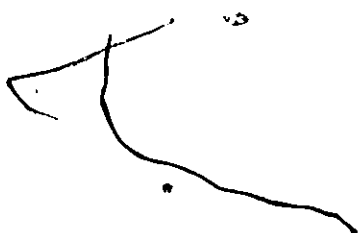
Due to the scope of the research project a large number of sensors and instruments was used to acccmodate the desired measurements and analysis. The sensors employed in the investigation included dynamic-fatigue concrete strain gages , piezoelectric accelerometers, linear variable differential transformers and tendon loadcells. The

instrumentation used included the Megadac 2000 data acquisition system, FFT dynamic analyzer, accelerometers power supply and IBM microcomputers and mainframes.

4.4.2   Dynamic-Fatigue Concrete Strain Gages

The strain gages used to monitor the entire experimental work were of the type EAE-06-750FF-350, manufactured by Micro Engineering II (ME2). The reasons for selecting such a gage were due to its capability of measuring strains up to 3% elongation with an accuracy of 5%, fatigue life of 10 million cycles at 1500 microstrain and gage length of 0.75 inch (19 mm). Relatively speaking, the gage length was small under the classification that concrete strain gages fall under but was necessary due to the high number and mounting of the strain gages around the opening. Refer to Figure 4.12.

Before any strain gages were mounted, the concrete surface was prepared by applying an epoxy of high durability and strength (RTC); it is prepared by mixing equal quantities by volume of activators A and B. The epoxy's main function is to fill up the surface voids to create a smooth surface before the strain gages are mounted. After smoothening the surface the gages were mounted using CA-200SL adhesive and catalyst. A three-wire system was used to monitor the gages with each wire containing seven conductors. One end of the wires was soldered onto the gage

terminals (black and white wires on one terminal, red on the other) while the other end was connected to the SCI excitation boxes on the Megadac. After the completion of the soldering operation the gages were protected by applying polyurethane coating which was left to dry for one day followed by a second coat of Gagekote #5.

4.4.3 Piezoelectric Accelerometers

Dytran model 3100A 25(g) accelerometers were used in all stages of the experimental investigation. Figure 4.13 shows a typical accelerometer. Inside the silver housing, the accelerometer's two main parts are self generating quartz crystals and a seismic mass (similar to a single degree of freedom spring and mass system). The quartz crystals are preloaded to a specific force, such a force would vary depending on the type of the accelerometer used. When the base of the accelerometer is subjected to any acceleration, it is automatically transferred to the mass through the crystals creating a force equal to the mass times the acceleration based on Newton's second law of action. This transfer of acceleration releases some of the preloaded force in the quartz crystals; such a change in force is converted to a low impedance electronic signal having a voltage magnitude proportional to the measured acceleration. Such a signal is fed into an amplifier and from there into an A/D converter. The voltage output range monitored in all

the experiments was between ±2 volts, while the accelerometer sensitivity was about 100 mv/g over a frequency range of 1 to 3500 Hz at 0.5 dB.

One inch (25.4 mm) by 0.5 inch (12.7 mm) stiff plexi-glass cylinders were used for mounting the accelerometers. Each cylinder had a 0.159 inch (4.0 mm) diameter by 0.25 inch (6.35 mm) deep threaded hole drilled in the middle of its upper surface. After securely fixing the bottom of the cylinders to the smooth concrete surface by a 5 minute epoxy compound, the accelerometer was mounted in place by screwing the stud at its base into the threaded hole and tightened so that no differential movement existed between the accelerometer and the plexi-glass cylinders. Voltage readings were transmitted to the power supply by co-axial cables model 6010 having a BNC connector at the power supply end and a microdot connector at the accelerometer end.

4.4.4   Linear Variable Differential Transformers.

All the LVDTs used were of the D-500 series made by Schaevitz em limited. Six of the LVDTs had a displacement capacity of ±1.0 inch while one had a ±0.5 inch capacity. Such sensors were excited by voltage supply modules (SCV) on the Megadac. Approximately a ±7.0 voltage output range was monitored and digitized for all the displacements encountered in the experimental work. Each LVDT was mounted

very similarly to the accelerometers with the only difference being the fixation of the outside cylindrical LVDT surface to steel flanges by using magnetic mechanical arms identical to the ones used to support static dial gages as shown in Figure 4.14. The threaded rod that is inserted into the bored core of the LVDT was mounted into a 0.5 inch (12.7 mm) by 0.25 inch (6.4 mm) stiff plexi-glass cylinder which was glued onto the concrete surface. Any differential movement that is detected by the rod after the LVDT is zeroed is sent to the data acquisition unit as a voltage signal where it was digitized and stored on mass storage 3M tapes.

4.4.5 Prestressing Loadcells

Three cylindrical loadcells were used to measure the prestressing force in the steel bars during both jacking and beam loading. The loadcells were excited by (SCI-884-350) current energization modules on the Megadac. The maximum available 400:1 gain setting was used for such sensors. Figure 4.15 shows a typical calibration curve for load cell #27.

4.4.6 Megadac 2000 Data Acquisition Unit

The Megadac is a flexible modular data acquisition and control system, it embodies numerous options necessary for accurate dynamic capture of analog data from a wide range of

active and passive transducers (refer to Figure 4.16). A
number of the options were particularly useful in setting up
the experiment during and after the prestressing operation
and in capturing specific experimental data during the
dynamic and fatigue testing. The unit has a maximum
sampling rate of 20,000 samples per second and a capacity of
128 channels of input. Only 64 input channels were
available in our system with 43 of them used in all the
experiments. The sampling rate used was equal to 120 cycles
per second in the burst mode (an option available on the
Megadac which allows it to sample all the channels the
same time increment), such sampled data was stored on a 300
foot (91.5 m) long 3M magnetic tape cartridge having a
capacity of about 30 mega bits.

The Megadac's front panel keyboard and display allows it
to operate as a "stand-alone" device while conducting
experiments which is an important added feature. A number
of signal conditioning and bridge completion modules are
available on the Megadac. The following is a brief
description of the available ones.

1.   Four 16 channel analog to digital input modules
      (AD-1614D) with differential inputs and 15 input
      scaling ranges with a maximum system gain of 400:1
      (1:1 gain being ±10 volts).

2.   Four   constant   current   energization   modules
     (SCI-884-350) for strain gage and loadcell excitation,
     with each module providing eight constant current
     pairs.   Each current pair (A , B) is made up of two
     precision current sinks carrying 8.9285 mA each and a
     350 chm bridge completion connection for quarter
     bridge operation.   Figure 4.17 shows a quarter bridge
     3-wire current energization schematic circuit diagram
     for strain gage excitation while Figure 4.18 shows a
     full bridge current energization schematic circuit
     diagram for loadcell excitation.

3.   Two constant voltage energization modules (SCV-884).
     Each module is capable of supplying 12,10,8,6,4 or 2
     volts depending on the type of sensor used.   Such
     modules are designed only for full bridge application.
     Figure 4.19 shows a typical voltage energization
     schematic circuit diagram for LVDT excitation.

Before the Megadac was used for data sampling, two
experimental tables were set up through the front panel
keyboard (the mode and scan tables) and saved in battery
protected CMOS memory.

The mode table's main function is to   the Megadac
to establish a profile for communicat   a host
computer.   This is particularly important in data reduction
and analysis operations, and for the control of the Megadac

by a computer through an RS-232 interface. The scan table
contains input-output channel processing information for the
Megadac. It is composed of two sections, base and scan
entries. The base entries section contains information
which applies to all scan entries; ex. , number of channels,
sampling rate and mode of sampling. The scan entries
section contains processing information pertaining to the
mapping from hardware A/D ports to positions in the recorded
data block. Each scan entry contains a channel port address
(number) which is used for extraction of data samples, a
high low limit which is used for starting and stopping the
recording process (depending on user preset triggering
limits), a post gain option and an autobalance value
display. All data was recorded using a high 12 bit
resolution mode; also for reduction purposes a 19.2K baud
rate was used for data transmission to the host computer.
If any more detailed information is needed with regard to
recording and transmitting of the experimental data please
refer to Appendix B.

In order to establish circuit connections between the
Megadac and the experimental sensors, four terminal boxes
designed and built by the electronic design centre at the
University of Windsor were used (refer to Figure 4.20).
These boxes consisted of:

1. An A/D terminal box having 144 gold plated terminals representing four (AD-1614D) modules each having 16 channels (32 terminals) and 16 ground terminals.

2. Two SCI terminal boxes labeled SCI-1 and SCI-2 having 64 gold plated terminals each representing four (SCI-E84-350) modules each having 8 channels (32 terminals).

3. An SCV terminal box having 72 gold plated terminals representing two (SCV-884) modules having 8 channels each (32 terminals) and 8 ground terminals.

All of the modules at the back of the Megadac consisted of a 37 pin connector. Cables with an opposite 37 pin connector to the Megadac's at one end having appropriate wires soldered onto the terminals in the boxes at the other end were used.

To generalize the circuit connections to any application a 49 pin ribbon connector was used to externally connect the A/D box to the SCI-1, SCI-2 and SCV terminal boxes.

4.4.7 FFT Dynamic Analyzer II (SD375)

The model SD375 dynamic analyzer is a stand-alone, hard wired, dual channel instrument that combines a 400 line per channel analyzer, and a dual trace roster scan crt in a single portable unit (manufactured by Scientific Atlanta Spectral Dynamics Division in San Diego). Refer to Figure 4.21.

The instrument is a microprocessor base FFT analyzer and signal processor that accommodates front panel selection of twenty one frequency ranges covering 1 to 100 ·kHz for data analysis.   It contains a 12 bit analog to digital·converter and a resolution of 1024 data points in time domain and 400 data lines in frequency domain.   The SD375 contains a built in averager for signal to noise enhancement in the frequency or time domain.   The number of averages can be specified by the number of ensembles (N) or total averaging time (T) to the nearest second which is entered through the keyboard and can be any integer number.   When in linear averaging mode, the   FFT   analyzer   performs a   linear average   (ideal integrater)   until   the preselected number of averages has been reached.   Also the spectrum information is normalized at each step of the number of averages performed and stored onto processor memories M1 or M2.   When in peak averaging mode,   the FFT retains the highest   level in each of the 400 filter locations.   Information for all filter locations is updated every 100 or 200 milliseconds depending if single or dual channel processing has been selected and stored onto processor memories M1 or M2.

The SD375 was used in two stages of the work, the first being during experiments while conducting the hammer test, and the   other during   data analysis.   To establish communication between the FFT analyzer and the Megadac, the

D/A card on the back console of the Megadac was connected to the input BNC connector on the front panel of the analyzer.

After capturing the beam transient response while conducting the hammer test, the plot available on the scan crt was dumped onto a video hardcopy printer (SD422) which was connected to a composite video BNC connector on the back of the FFT analyzer. After data transmission and analysis, plots showing beam frequency spectrums, decay envelope and mode shape acceleration values were available. FFT analyzer front panel options allowed the plots to be dumped onto an HP plotter which was connected to an IEEE 488 multipin connector on the back of the analyzer. Figure 4.22 shows a typical dual channel plot and a brief description of the displayed variables.

4.4.8   Accelerometer Power Supply

Dytran model 4121 power unit for voltage mode 2-wire accelerometers was used (refer to Figure 4.23). The unit contained a regulated DC power supply and 12 channels having an adjustable constant current circuit of 2 tc 20 mA. A maximum voltage excitation of up to 24 volts DC can be supplied by such a unit but only 12 volts DC was needed for the specific accelerometers used. The front cf the power supply contained 12 output BNC connectors which were directly connected to the A/D modules on the data acquisition unit, while the rear contained 12 input BNC

connectors for energizing the accelerometers. A channel monitor switch was available on the front cf the power supply unit to indicate the value of the energizing voltage being supplied to the accelerometers.

4.4.9   IBM Microcomputers and Mainframes

An IBM personal computer was used for both data reduction and transmission. The microcomputer was interfaced with the data acquisition unit via an RS-232 port with the data reduction operation being controlled by company written software for the Megadac. After the data was reduced and stored on disk, it was again transmitted to the University of Windsor's IBM mainframe for reorganization and plotting for its final representation. Such an operation was done by using an external modem interfaced to an RS-232 port on the microcomputer and using an intertalk software called X-talk.

4.5   Preparation of the Tested Beams

The following is a list of the beam preparation period:

1.   First, the top, bottom, side and ends of the forms were cut to the desired lengths from an 8 feet by 4 feet by 0.75 inch (2.44m by 1.22m by 19.1mm) plywood sheet. Three 0.5 (12.7 mm) inch holes were drilled into each end to pass through the plastic tubes housing the prestressing tendons. After applying two coats of oil to the inside of the plywood to avoid

undesirable bond with the concrete and leaving it to dry for one day, one inch screws were used to put the side and bottom forms together.

2. After preparing the number of required stirrups from 3/16 inch (4.76 mm) mild steel bars, they were distributed throughout the length of the beam according to the shear reinforcement design (Appendix C contains the truss analogy design method used for stirrup spacing at either side of the opening). The stirrups were tied onto 1.5 inch (38.1 mm) steel cable staples which were nailed into the bottom form providing the needed concrete clearance of 0.75 inch (19.1 mm). In order to keep the stirrups in a vertical position, two 1/8 inch (3.18 mm) mild steel bars were tied onto the top of the stirrups. Refer to Figure 4.24.

3. Three prestressing tendons were cut about 4 feet (1.22 m) longer than the beam length to provide enough jacking distance during the prestressing operation. The bars were then inserted into 0.375 inch (9.5 mm) external diameter plastic tubes.

The outside surface of the tubes was well greased and tied down to the stirrups at the proper locations (two at the bottom and one at the top). After making sure that the tendons are tied down securely so that

no movement occurs during the casting operation, the top and end forms were screwed into the side and bottom forms respectively. After cleaning the surface of the prestressing bed, two sheets of plywood were placed between the side form and the bed to form a more even pouring surface. The beam was then traced to the bed sides by 2 inch by 4 inch (50.8 mm by 101.6 mm) wood pieces to keep the sides straight during the casting operation and a styrofoam piece having the desired opening dimensions was glued onto the inside of the side form by 5 minute epoxy. refer to Figure 4.25.

4. The required weights of all the concrete ingredients were prepared. Initially, all the ingredients were mixed together in the concrete mixer except for the the water which was added in stages until a uniform mix resulted. During the casting operation, care was taken to make sure that appropriate compaction resulted by vibrating the concrete with special attention being given to the ends and around the opening. After casting the beam and three 6 inch by 12 inch (152.4 mm by 304.8mm) cylinders, all surfaces were given a smooth final finish by hand troweling.

5. Approximately three hours after casting, wet burlap and nylon sheets were placed on the concrete surface

to moist-cure it. Such a curing operation continued for two days until the concrete surface seemed sufficiently wet. The three concrete cylinders were stripped and put in a water bath in the curing room after one day of casting.

6. After letting the beam air-cure for one day, the styrofoam was removed and the surfaces around the opening and at midspan were prepared by applying RTC epoxy to them and letting it dry for one day. The concrete surfaces were prepared to a final smooth finish by using an air powered sanding gun. The strain gages are then mounted in the desired arrangement and protected against any damage by applying two coats of Polyurethane and Gagekote #5.

7. The prestressing tendons and tubes were pulled out of the beam then it was rotated 90° to stand on its bottom surface and the top, side and end forms were removed. The two end bearing plates were placed in position and the prestressing bars were passed through them. At one end three cylindrical wire load cells were placed on the tendons followed by anchorage wedges, cylinders of the open grip type and the prestressing jack. At the other end anchorage was provided by the deformed ends on the prestressing bars. All the strain gages and loadcells were

autobalanced by the Megadac through the SCI terminal
boxes before any prestressing force was applied. The
tendons were pulled one at a time starting with one of
the bottom bars which was originally prestressed to
half its final force, second in line was the other
bottom bar which was also prestressed in an identical
fashion to the first one and from there to the top
tendon which was prestressed to its full force. After
that the jacking returned to the bottom two bars to
complete their prestressing. Note all the bars were
tensioned to an equal force of approximately 8 kips
(35.58 kN) resulting in a downward eccentricity about
the primary bending axis.

8. The beam was moved onto the supports by a crane
lifting it at two points located approximately at 1/3
the span from either end. After placing the beam on
the rollers and removing the bottom form, it was
centred with respect to the point of loading. The
ends were tied down as described in an earlier section
and the bottom part of the loading assembly which
contains the springs was put in place and tightened at
centre span. All the plexi-glass cylinders needed for
accelerometer and LVDT mounting were glued onto the
desired points on the beam using 5 minute epoxy.

9.   All the remaining sensors which consisted of LVDTs and
      accelerometers were mounted at the desired locations
      along the beam length and connected to the Megadac
      through the SCV terminal box and power supply unit.
      Only the new channels monitoring such sensors were
      autobalanced on the Megadac (a feature which balances
      only the desired channels indicated in the scan entry
      table).   With the experiment ready to be conducted,
      all the initial sensor readings were sampled and
      recorded on mass storage.

4.6   Experimental Test Procedure

The testing procedure carried out was designed to
experimentally determine the dynamic and fatigue
characteristics of the concrete beams under cyclic loading.
With interest being confined to in-plane vibrational
behaviour, only the first flexural mode of vibration was
important.   Also because all the beams were simply
supported, the second and third flexural modes of vibration
were fairly high and quite apart and were not considered an
important part of the investigation.   In order to determine
the dynamic and fatigue characteristics of the beams, the
following tests were conducted:

1.   Free vibration hammer test;

2.   Sine wave sweep test;

3.   Natural frequency test;

4.   Log-decrement test (transient test); and,

5.   Fatigue test.

The first test was only conducted at the beginning of every experiment to determine the location of the first three flexural modes of vibration while the next three tests were conducted once before the fatigue test and once after the completion of the fatigue test (refer to Grace (1986)).

4.6.1   Free Vibration Hammer Test

The free vibration hammer test was conducted by mounting an accelerometer at one of the centre span locations and striking the beam once with a heavy hammer in the direction of the flexural plane of bending. The acceleration output was directly fed into an FFT dynamic analyzer placed in the frequency domain mode. The dynamic analyzer stores such a response in memory and when recalled, a plot of voltage response versus frequency is presented. By observing such a plot, the flexural modes of vibration can be determined by simply locating the frequency values at which the highest voltage response peaks appear. The magnitude of such peaks was not of interest but only their location. Such a plot was immediately dumped onto a video output printer for a hard copy which was interfaced with the dynamic analyzer.

4.6.2   Sine Wave Sweep Test

The sine wave sweep test was performed by continuously subjecting the beams to a varying excitation frequency which ranged between one and twenty two cycles per second (Hz). Such a frequency range was well within the value of the first flexural vibration mode. The application time of each frequency was equal in all the tests (approximately 5 seconds). The data acquisition unit was continuously sampling the data at a rate of 120 samples per second in the burst mode and recording it on tape.

With the data available on tape, the Megadac was interfaced with FFT dynamic analyzer via a D/A output card on the back of the Megadac. By specifying jumper locations on the card, only the one desired channel data is transmitted for analysis. Before any accelerometer data was transmitted, a calibration signal was sent to the dynamic analyzer to determine the equivalent voltage value corresponding to one (g) of acceleration. Such a calibration signal was generated using an accelerometer calibrater which imposes a one (g) excitation on the accelerometer. After inputing the calibration value into the dynamic analyzer through its front panel numeric keyboard and placing it in frequency domain mode, the accelerometer data was transmitted to form a frequency spectrum. Such a chart defined the beam acceleration

response at every imposed excitation frequency at that one specific location that the accelerometer was mounted on. Also, the natural frequency was very evident in such a chart. Only the response chart of one of the accelerometers mounted near midspan was produced because that is the location of maximum acceleration and displacement under the influence of the first mode of flexural vibration.

4.6.3 Natural Frequency Test

After experimentally determining the value of the first flexural natural frequency as a result of conducting the sine wave test, the beams were excited at their natural frequency for approximately 10 seconds. Such a steady state response was monitored by six accelerometers mounted at different locations along the length of the beam with their data being sampled and recorded by the Megadac. Such data was transmitted from the data acquisition unit to the FFT analyzer placed in frequency domain to determine the magnitude of acceleration at the different beam locations. The final acceleration amplitudes were then plotted resulting in the experimental mode shapes.

4.6.4 Log-decrement Test (Transient Test)

This test simultaneously follows the natural frequency test. With the beam resonating at its natural frequency, the load was removed and the beam was left to undergo a

decaying free vibration. The entire period of transient response was monitored and recorded. Such response was transmitted to the FFT analyzer in time domain and dumped onto an HP plotter. As a result the associated material damping was determined by using the logarithmic decrement method.

4.6.5 Fatigue Test

The fatigue test was carried out right after the sine wave sweep test and continued on until the beams developed a significant number of cracks and in-turn lost a lot of their flexural stiffness (very close to failure). The dynamic strains imposed on the area surrounding the opening and at centre span were monitored and recorded throughout the loading period at selected fatigue cycles.

The data acquisition unit was interfaced to an IBM personal computer via an RS-232 port and the data was transmitted to be reduced and converted to engineering units. With the final data stored on disks, the personal computer was linked up to the university's mainframe for data transmission. From there SAS/GRAPH was used to represent such data in graphical form showing concrete strain versus the number of fatigue cycles at different locations around the opening and at midspan.

Chapter V

DISCUSSION ON RESULTS

5.1   Analysis of the Dynamic Test Results

5.1.1   Free Vibration Hammer Test

The objective of the free vibration hammer test was to
determine the response (natural frequencies) of the
prestressed concrete beams before the application of any
loading. Two different cases were examined, one having the
beams resting on the supports without the loading jack
resting at midspan (loading point) and the other having the
ends tied and the jack resting at midspan. The latter
situation simulates the supporting and loading arrangement
of the beams during the sweep and natural frequency tests.
Table 5.1 shows the observed results for all the beams. It
is evident that very little change occurred in the natural
frequencies as the opening size increased from 8 to 16
inches at an increment of 4 inches (beams 1 to 3). Also,
when the opening centre was moved vertically providing an
eccentricity from the beam's neutral axis (beams 4 and 5),
the first and second natural frequency values increased
slightly but for all practical situations they could be

assumed to be the same as the previous three beams. As for beam #6 which contained an opening centred about midspan, an increase in the fundamental natural frequency was observed. Such a response indicates that the loss of mass at midspan influenced the first natural frequency to a greater extent than did the loss of stiffness (the centre of the opening coincided with the neutral axis of the beam resulting in a loss of stiffness of about 5%).

With the loading jack resting at midspan the free vibration natural frequencies increased between 1 and 5 Hz for all the beams (refer to Table 5.1). What is most important is the increase of 1 to 2 Hz that was observed in the first natural frequency value. Such an increase was further verified when the sine wave sweep test was conducted. Figures 5.1 and 5.2 show typical free vibration response curves for beam #4 with and without the jack resting at midspan.

5.1.2 Sine Wave Sweep test

In order to determine the frequency spectrums of the tested beams, the vibration signature of the acceleration time history at different locations on each beam model was needed. Such information was obtained by sweeping the beam models through a range of frequencies under the influence of a constant forcing function. Figure 5.3 shows a segment of the sinusoidal forcing function at 18 Hz. Also, Table 5.2

indicates the maximum amplitudes of such a function that each beam was subjected to.

With the acceleration time history responses available, the Fast Fourier Transform algorithm was used to present the data in frequency domain. The FFT Spectral Dynamics Analyzer (SD375) was used to conduct such an operation. In order to reduce the affects of Gibbs oscillations and side lobes while conducting the FFT operation, the Hamming window function was used. Such a function was available on the FFT analyzer and is automatically applied to the changing input memory before its transfer to CPU memory. With the final frequency response available in CPU memory, it was recalled onto the screen to mark the frequency with the maximum vibration amplitude and from there onto an HP plotter for a hard copy.

Both the (before) and (after) fatigue frequency spectrums were of interest. Figure 5.4 shows the (before) fatigue frequency spectrum of beam #1. It clearly indicates that the beam resonated at 20 Hz. Such a frequency is higher than the 18 Hz observed by the free vibration hammer test with the loading jack resting at midspan. This can be attributed to the fact that too much static precompression was applied to the load springs before the application of any dynamic loading (refer to Table 5.2). This in-turn provided a bit of an elastic support at midspan resulting in

a higher resonance frequency. With beam #1 heavily cracked the sine wave sweep test was repeated resulting in the frequency spectrum shown in Figure 5.5. Comparing the (before) and (after) fatigue spectrums indicated a decrease of 1.1 Hz in the resonance frequency (refer to Table 5.3) and a definite loss in vibration amplitude at all frequency values. This is very evident at the resonance frequency where the vibration amplitude decreased from 5.08 g to 2.70 g (1 g = 10 m/s^2). Such a reduction is attributed to the loss of beam stiffness as fatiguing continued which in-turn increased the material viscous damping and reduced the vibration amplitudes.

Before conducting the sine wave sweep test on beam #2, the initial spring static precompression was reduced by 0.06 kips (refer to Table 5.2). The results of such a test are shown in Figure 5.6. The frequency spectrum indicates a resonance frequency of 18.9 Hz which is almost identical to the 18.5 Hz that was observed in the free vibration hammer test. This in-turn indicated that the beam is no longer being elastically supported at midspan. After 1.8 million cycles of fatigue loading with the beam heavily cracked the test was repeated. Figure 5.7 shows the corresponding frequency spectrum. Comparing the (before) and (after) fatigue spectrums indicated a decrease of 1 Hz in the resonance frequency (refer to Table 5.3) and as before a

definite loss in vibration amplitude at such a frequency (from 4.07 g to 2.90 g).

Beam #3 was tested under the same loading conditions and frequency range as beam #2. The (before) fatigue frequency spectrum for such a beam is shown in Figure 5.8. A resonance frequency of 17.8 Hz was observed which is almost identical to the 18 Hz indicated by the free vibration hammer test. After 1.48 million cycles of fatigue loading the sweep test was repeated resulting in the frequency spectrum shown in Figure 5.9. Comparing the (before) and (after) fatigue frequency spectrums indicated a decrease of 1 Hz in the resonance frequency (refer to Table 5.3) and as observed earlier a loss in vibration amplitude from 4.88 g to 3.05 g at such a frequency.

Beam #4 was tested under the same loading conditions and frequency range as beams 2 and 3. The (before) fatigue frequency spectrum is shown in Figure 5.10. A resonance frequency of 18 Hz was observed which is identical to the one indicated by the free vibration hammer test. After 1.6 million of fatigue cycles the sweep test was repeated resulting in the frequency spectrum shown in Figure 5.11. Comparing both spectrums indicated a decrease of 1.1 Hz in the resonance frequency (refer to Table 5.3) and a reduction in vibration amplitudes at all frequency values.

The (before) fatigue frequency spectrum for beam #5 is shown in Figure 5.12. It is evident that the beam resonated at 17.8 Hz which is almost identical to the 18 Hz observed by the free vibration hammer test. After 1.5 million cycles of fatigue, the sweep test was repeated resulting in the frequency spectrum shown in Figure 5.13. Comparing both spectrums indicated a reduction of 1 Hz in the resonance frequency (refer to Table 5.3) and a loss in vibration amplitude of 2.5g at such a frequency.

Beam #6 was tested in an identical manner to beams 2 through 5. The (before) fatigue frequency spectrum is shown in Figure 5.14. The beam resonated at a frequency of 19.4 Hz which is almost equal to the frequency of 19.0 Hz which was observed during the free vibration hammer test. After 0.35 million cycles of fatigue loading the sweep test was repeated resulting in the frequency spectrum shown in Figure 5.15. Comparing both spectrums indicated a reduction of 1.4 Hz in the resonance frequency (refer to Table 5.3) and as before a reduction in the vibration amplitudes at all frequency values.

Examining the results for all the tested beams indicated that there was hardly any change in the fundamental resonance frequency with increasing opening length and with varying opening eccentricities for beams provided with openings in the shear span (side openings). As for beam #6

the fundamental resonance frequency increased when compared to beams 2 through 5 which indicated that when openings are provided at midspan, the loss of mass has a greater influence on the first natural frequency than the loss of stiffness. This same observation was confirmed by the finite element results, discussed later on in this chapter. Also, after the completion of the fatigue process, a decrease of 1 to 1.5 Hz was observed in the fundamental natural frequency; and a further decrease in vibration amplitude at all frequency values of the spectrum curve were observed. Both of the two previously mentioned points can be attributed to the fact that as the beams lost some stiffness due to cracking with increasing fatigue cycles, the material damping increased causing reductions in both the resonance frequency and vibration amplitudes.

5.1.3 Natural Frequency Test

The objective of conducting the natural frequency test on the beams was to obtain the experimental mode shapes for such structures when subjected to vibrational excitation at the first natural frequency. The forcing function and maximum loading amplitudes employed in this test were the same as those used earlier in the sine wave sweep test. The steady state vibration was measured at six different locations along the length of the beam and eventually plotted on SAS/GRAPH. To extract such vibration amplitudes,

the acceleration time histories at the first natural frequency were fed into the FFT Dynamic Analyzer which was placed in frequency domain mode. Figure 5.16 shows the accelerometer locations along the length of the beam and Figure 5.17 shows a typical frequency spectrum of accelerometer #3 of beam #2 at the fundamental natural frequency (before) fatigue loading. It was observed that the vibration levels for beams 2 through 6 ranged between 4.06 and 5.36 g. As for beam #1 a vibration level up to 7.2 g was observed. This is attributed to the fact that beam #1 was subjected to 0.83 kips of dynamic loading as compared to 0.45 kips that the other beams were subjected to.

The natural frequency test was conducted twice on every beam, once before the application of fatigue loading and then after the beams were heavily cracked. Figure 5.18 shows the corresponding mode shapes for beam #1. As expected the beam's deflected shape at the fundamental frequency resembled a half sine wave. With the beam heavily cracked the mode shape did not change, only the amplitude of vibration decreased. The mode shapes of beam #2 are shown in Figure 5.19. As before the deflected shape is identical to that of beam #1 with the only difference being the maximum amplitude of vibration at midspan which was considerably less due to the smaller applied load. With the beam heavily cracked the test was repeated. A loss of 45%

in vibration amplitude was observed at any location along the length of the beam. This is attributed to the fact that beam #2 withstood about 0.6 million cycles of added fatigue loading than any other beam due to the lower amplitude of loading. Such a high number of fatigue cycles (about 2.2 million) reduced the stiffness of such a beam considerably resulting in the loss of vibration amplitude indicated earlier.

The beam #3 mode shapes were identical to those of beams 1 and 2 but only showed a loss in the order of 13% in vibration amplitudes due to the fatiguing process. Figure 5.20 shows such mode shapes. The 13% loss in vibration amplitude is considerably less than the one observed for beam #2. This is due to the fact that the (after) fatigue natural frequency test was conducted before the beam was heavily cracked (200,000 cycles before failure occurred). Therefore ideally the test should have been conducted at about fifty or sixty thousand cycles before failure as was the case for beams 4 and 5.

The mode shapes of beams 4 and 5 at the first natural frequency are shown in Figures 5.21 and 5.22. Again as before both beams exhibited mode shapes that resembled a half sine wave with the maximum amplitude of vibration occurring at midspan. When the test was repeated with both beams heavily cracked after 1.6 and 1.5 million cycles of

fatigue loading, losses of 36 and 30 percent, respectively, were observed in vibration amplitude at any location along the length of the beams.

Figure 5.23 shows the corresponding mode shapes for beam #6. Again, such mode shapes are identical to the ones observed for beams 1 to 5. It is evident that a loss in vibration amplitude of about 13% occurred due to fatigue loading. This again can be attributed to the fact that the (after) fatigue natural frequency test was conducted before the beam was heavily cracked (75,000 cycles before failure occurred).

Therefore from the observed results it can be concluded that the presence of side and midspan openings in the beams tested herein did not have any local affects on the first mode shape. Also, the beams deflected as expected in a half sine wave manner with the maximum amplitude of vibration occurring at midspan. Such a mode shape did not change with fatigue loading; only the maximum vibrational amplitude was reduced by 30 to 35 percent. In addition, the amplitude of vibration seemed to be consistent at the same locations for beams that were tested under identical loading conditions for both (before) and (after) fatigue mode shapes.

5.1.3.1   Chords Displacement at the First Natural Frequency

The objective of conducting such measurements was to determine the local behaviour of the opening region at the first natural frequency.   This consisted of displacement amplitudes and overall deflected shapes.

Seven LVDTs were used with four being placed in the corners of the top and bottom chords and two others in the middle of such chords. Also, a reference LVDT was placed at midspan directly under the load.   The maximum upward and downward displacement amplitudes registered by the LVDT were considered as the reference quantities with the rest of the LVDT readings being plotted for such amplitudes only. Plots of the response of the opening region (before) and (after) fatigue are presented for all the beams except teams 1 and 3 where only the (before) fatigue responses are presented.

Figure 5.24 shows the (before) fatigue chords displacement for beam #1.   The ends of the top and bottom chords closer to the load displaced a total amplitude of 0.31 and 0.3 inches respectively.   The maximum observed midspan displacement amplitude was equal to 0.653 inches. The (before) and (after) fatigue chords displacement for team #2 are shown in Figures 5.25 and 5.26.   Before fatigue, the ends of the top and bottom chords closer to the load displaced 0.20 and 0.195 inches respectively with a maximum observed beam midspan amplitude of 0.34 inches.

Such amplitudes are lower than the one observed for beam#1. This can be attributed to the lower load of 0.45 kips that beam #2 was subjected to instead of the 0.83 kips applied to beam #1. After fatigue the beam's loss of stiffness was evident when lower total amplitudes of displacement were observed for the chords and at midspan.

Figure 5.27 shows the (before) fatigue chords displacement for beam #3. The ends of the top and bottom chords closer to the load indicated a total displacement amplitude of 0.331 and 0.324 inches respectively. The maximum observed total displacement amplitude at midspan was equal to 0.53 inches. It is evident from the previous results for beams 1 to 3 that as the size of the opening increased, the amplitude of the maximum displacement at any point along the chords increased as long as they were subjected to identical loading conditions. The above conclusion was reached when the results of beam #1 were reduced by the factor of 0.45/0.8 to be compatible in loading to beams 2 and 3.

Beam #4 chords displacement (before) and (after) fatigue at the first natural frequency are shown in Figures 5.28 and 5.29. Before fatigue, the ends of the top and bottom chords closer to the load indicated a total displacement amplitude of 0.349 and 0.345 inches with a maximum observed total midspan amplitude of 0.54 inches. Comparing such

values to the ones observed for beam #3 shows · hardly any

change. Therefore moving the opening vertically upward did

not influence the displacement amplitudes and deflected

shape at the first natural frequency when compared to

providing an opening centred about the neutral axis of the

beam (beam #3). After fatigue, the loss of beam stiffness

was again evident where a loss in displacement amplitude was

observed for the chords and at midspan.

Figures 5.30 and 5.31 show the (before) and (after)

fatigue chord response at the fundamental frequency for beam

#5. Before fatigue, the ends of the top and bottom chords

closer to the load displaced a total amplitude of 0.333 and

0.321 inches. Also, the maximum total amplitude of

displacement observed at midspan was 0.51 inches. Comparing

the results to the ones observed for beams 3 and 4 indicates

hardly any variation in displacement amplitudes. Therefore

as was observed for beam #4 earlier the movement of the

opening vertically downward did not influence the

displacement amplitudes and deflected· shapes at the first

natural frequency. After fatigue, the loss of beam

stiffness was very evident where much lower amplitudes of

total displacement were observed at every location that

contained an LVDT (the chords or midspan).·

Figures 5.32 and 5.33 show the chords displacement.

(before) and (after) fatigue for beam #6. It is observed

that the ends of the top and bottom chords displaced a total
amplitude of approximately 0.41 and 0.42 inches. Due to
fatigue loading, the bottom chord displacement increased by
0.05 inches at the two ends and by 0.1 inches at midspan
when the beam was moving down at the first natural
frequency. Also, the displacement of the two corners of the
top chord increased by 0.1 inches when the beam moved
downward. Looking at the total amplitude of chord
displacement (after) fatigue indicated a reduction in value
when compared to the (before) fatigue amplitude of
displacement. This reduction is due to the expected loss of
stiffness resulting from fatigue loading.

Looking over the values of midspan deflection at the
first natural frequency and comparing them to the
theoretical static deflection values at the same location
under the same loading conditions indicated a dynamic
magnification factor in displacement of approximately 3.0.
In conclusion, it can be stated that the size of the side
opening affects the amplitude of displacement at the first
natural frequency. The larger the opening size the higher
the amplitude under the same loading conditions. Also,
moving the opening vertically up or down did not influence
the chords displacement values when compared to same size
openings centred about the neutral axis of the beam. No
local affects were evident when the beams were excited at

the first natural frequency. This is due to the fact that hardly any differential displacement occurred at the same locations in the top and bottom chords when the beam was either moving up or down. After fatigue the loss of beam stiffness was evident. When the chords displaced downward at the natural frequency, a larger displacement was observed than the one before fatigue but, when the chords displaced upward, a such smaller displacement was observed resulting in a smaller total displacement amplitude than before. Finally it seems that providing the same size opening in the side of the beam is better than having it at midspan due to the following two reasons: (i) the smaller total amplitudes of chord displacement at the first natural frequency, and (ii) the much longer fatigue life observed by side openings.

5.1.4 Free Vibration Transient Decay Test

The objective of conducting the free vibration transient decay test was to obtain the amount of viscous damping available in the prestressed concrete beams. There are a number of dynamic methods that are employed to approximate the damping ratio. The logarithmic decrement method was used herein, Such a method is valid for a multi degree of freedom system provided that the beams are vibrated in a single mode. It is fairly easy to apply by utilizing the solution of the equation of motion for a single degree of

freedom system; the natural logarithm of the ratio of an initially selected single peak to the nth successive single peak is given by:

$$\xi \approx \frac{1}{2 \pi n} \ln [(\ddot{X}_1) / (\ddot{X}_n)]$$

where: ξ = Viscous damping ratio

$\ddot{X}_1$ = acceleration, initial single peak

$\ddot{X}_n$ = acceleration, single peak after n cycles

n = number of cycles

The free vibration transient decay test was conducted twice on every beam before the application of, any fatigue loading. The final calculated damping ratio was based on the average of such tests. Each corresponding decay curve was obtained from the acceleration response of accelerometer #3 which was mounted 9 inches away from midspan. The decay curve at the fundamental frequency for beam #1 is shown in Figure 5.34. Applying the logarithmic decrement method resulted in a damping ratio of 2.0%. Such a damping ratio also included Coulomb damping due to the friction that existed between the beams and the supports.

Figure 5.35 shows the decay curve for beam #2. The corresponding damping ratio was calculated as 1.9%. Such a

value was very close to the 2% calculated earlier for beam #1. The calculated damping ratios for beams 3 and 4 were 1.9% and 2.1% respectively. Figures 5.36 and 5.37 show the corresponding decay curves for these beams.

Figures 5.38 and 5.39 show the decay curves for beams 5 and 6. Applying the logarithmic decrement method resulted in the same damping ratio of 2.1% . Therefore there seems to be a steady trend of consistency in the values of the viscous damping ratio for all the tested beams.

In conclusion it is evident that hardly any change existed in the values of the viscous damping ratio between the tested beams. Therefore, the variation of opening size and location did not influence the amount of damping present. Also, it can be assumed that a viscous damping ratio of about 2% exists in such structural members. Theoretically speaking, such a percentage is fairly low, but for structural application it seems to be fairly reasonable.

5.2   Analysis of the Fatigue Test Results

5.2.1   General

In order to simplify the discussion of the results observed by the strain gages due to fatigue loading, it was decided to place the 26 strain gages into four groups. Group one which included gages 1 through 8 was primarily

responsible for monitoring the strain variations in the top chord (refer to Figure 4.12). Group two which included gages 11 to 16 was responsible for monitoring the strain variations in the vertical directions within the tension field that existed at either side of the opening. Group three consisted of gages 19 through 24 which monitored the strain variations in the bottom chord and group four, which was made up of strain gages 25 and 26, monitored the extreme compression and tension fibres at midspan under the concentrated load. Only the results of beams 2 to 6 will be discussed herein since the original compressive strain values due to prestressing of beam #1 were not taken into account before loading was commenced.

The strain gage results of beam #3 show the actual strain fluctuation at specific cycles of loading throughout the fatigue life of the structure. To reduce computer time, the results of beams 2,4,5 and 6 only display the maximum, average and minimum strain values observed at specific cycles of loading throughout the fatigue life of the beams in addition to regression best-fit curves for each data set.

5.2.2   The Top Chord

Beam #2 top chord indicated increases in the compression strain values at the location of strain gages 1, 2, 4, 5, 7 and 8 (refer to Figure 4.12) with increasing number of fatigue cycles. The increase in compression strain value of

gage #1 was expected and evident when it was compared to strain gage #3 since it was closer to the load. But when the strain values of gage #6 were compared to those of gage #8 a lower compression strain value was found. Also, the change in strain values observed for gage #8 with increasing fatigue cycles after ignoring the original, compressive strain value due to prestressing was almost identical to that of gage #1 (refer to Figure 5.40). This in itself showed that at some stage during the fatigue process, the chord's local bending action resembled that of a Vierendeel panel, where the corner closer to the load and the one diagonally across from it exhibited compressive local bending and the remaining two corners tensile local bending. This will be further verified when the results of the bottom chord are examined.

Beam #3 top chord results showed the same trend as that of beam #2 for all gages but indicated larger strain magnitudes at a specific cycle cf loading and larger strain variations with increasing fatigue cycle. This can be attributed to the larger opening size and magnitude of loading that beam #3 was subjected to. Figure 5.41 shows the strain variations with increasing fatigue cycles of gages 1 and 8. Both gages demonstrated an increase in compressive strain up to failure with Vierendeel local bending evident in the latter stages of loading. Such local

bending action was more evident when the results of gages 3 and 6 were compared (refer to Figure 5.42). Both gages showed an increase in compressive strain values up to 1.0 million cycles of loading but as the loading continued, tensile strains due to Vierendeel local bending action came into play and eventually reduced such compressive strains.

The top chord of beam #4 behaved in a manner somewhat similar to that of beam #3. At early cycles of fatigue loading, the change in the strain magnitude was the same as that of beam #3 but as the fatiguing process continued, the increase in the strain value with increasing fatigue cycle was less than what was observed for beam #3. Gages 3 and 6 showed increasing compressive strains up to 0.5 million cycles of loading but as fatiguing continued, Vierendeel local tension strains of a much smaller magnitude than the ones observed for beam #3 came into play reducing such strains (refer to Figure 5.43). This was further verified when the change in strain values over the fatigue life of gages 1 and 9 was examined (refer to Figure 5.44). Both gages indicated changes of -325 and -180 microstrain as compared to -475 and -260 microstrain for beam #3. This proved that when the opening was moved vertically upward, Vierendeel local bending affects are not as dominant as when the opening is centred about the neutral axis.

Beam #5 top chord displaced in a very similar manner to that of beam #3. Gages 2, 4, 5 and 7 (refer to Figure 4.12) magnitudes of fluctuating strain at some fatigue cycle and the change in strain values with increasing fatigue cycles were similar to that of beam #3. The strain fluctuation at the early cycles of loading in gages 1 and 8 was again similar to that of beam #3 but the change in strain value as fatiguing continued before failure occurred was equal to -475 and -380 microstrain as compared to -475 and -260 microstrain for beam #3 (refer to Figure 5.45). This indicated that the local Vierendeel bending action is more evident in beam #5 than in beam #3. Such a conclusion was further verified when the results of strain gages 3 and 6 were examined (refer to Figure 5.46). They clearly indicate increasing tensile strains as fatiguing continued showing that the Vierendeel local bending action was evident from the beginning of the fatiguing process. The final magnitudes of such tensile strains were equal to +45 and +140 microstrain for gages 3 and 6 respectively which were much larger than the +35 and +50 microstrain observed for beam #3. Therefore moving the opening vertically downward demonstrated that the top chord becomes more vulnerable to Vierendeel local bending action than for beams provided with concentric or vertically upward eccentric openings.

The top chord results of beam #6 were totally different
from the ones observed for beams 2 through 5. Much higher
strain fluctuations occurred during the early stages of
fatigue loading with even larger changes in strain values
being observed with increasing fatigue cycles. Figure 5.47
shows the variation of strain with fatigue cycles of gages 1
and 3 (refer to Figure 4.12). Very similar response
patterns were observed for both gages with strain
fluctuations of -500 and -350 microstrain occurring before
beam failure occurred. Gages 4 and 5 also displayed very
similar response patterns showing a maximum strain
fluctuation of up to -300 microstrain early on during
fatiguing and smaller total changes in strain value with
increasing fatigue cycles than what was observed for gages 1
and 3. As for gages 6, 7 and 8 hardly any fluctuation was
observed in the original compressive strain values due to
prestressing under the influence of loading since the gages
were close to the neutral axis of the beam. Also it was
evident that as failure approached, the bending of the
bottom fibre of the chord especially at the chord's midspan,
resulted in the formation of tensile strains which ended up
reducing the original compressive strains (refer to Figure
5.48). Therefore when the opening was moved horizontally to
midspan, the response of the top chord was just as expected.
As fatiguing continued, an increase in the strain values and

variations was observed. Also, since the load was centred about midspan, no local Vierendeel bending action was evident in the top chord; only local tension bending was evident at the bottom fibre of the chord just before failure occurred.

5.2.3   The Tension Field

In this part of the discussion, the results of group two which primarily monitored the tension field that existed at either side of the opening i.e gages 11 to 16 (refer to Figure 4.12) will be examined.

Beam #2 tension field showed hardly any change in strain value with increasing fatigue cycles. Also, very little strain variations were observed at any cycle of fatigue loading during the loading process. Figure 5.49 shows the strain variation response to fatigue loading of gages 11 and 15; gage 11 showed a variation of 35 microstrain at any fatigue cycle exhibiting an undulating response to loading throughout the entire fatiguing process resulting in a final strain value that was 30 microstrain less than the original prestressing value. Gage 15 showed a variation of only 40 microstrain at any fatigue cycle with a net change in strain value of only 50 microstrain before failure occurred.

Beam #3 tension field demonstrated almost identical results to that of beam #2 indicating hardly any variation between the before failure strain values and that due to

original prestressing. Figure 5.50 shows the strain variation response to fatigue loading of gages 12 and 15 (refer to Figure 4.12). Both gages were one inch away from the ends of the opening at either side. From the plots it is evident that only about a 20 microstrain strain variation was observed at any fatigue cycle. Also, as the fatigue loading continued, unsteady variations of strain were observed throughout. But such variations were only of very small magnitude and did not influence the original prestressing values.

Beam #4 results were totally different from the ones observed for beams 2 and 3. Figure 5.51 shows the strain variation with increasing fatigue cycle of gages 12 and 13 (refer to Figure 4.12). Strain gage #12 indicated a high original tension value of +960 microstrain. During fatigue loading, a strain variation of +100 microstrain was observed at every cycle of loading and as fatiguing continued a final change of +700 microstrain was evident when compared to the original prestressing value. Gage #13 indicated an even higher original tension value of +2300 microstrain since it was closer to the opening. Again during fatigue loading, a strain variation of +100 microstrain was observed at any cycle of loading and as fatiguing continued, a final change of +900 microstrain was evident before beam failure. The results of the other gages followed the same trend as the

ones above indicating that by moving the opening vertically upward, rapid changes in strain in the tension field region are induced during loading and therefore requiring proper reinforcement to delay failure within the opening region.

Beam #5 strain variations were very similar to those observed for beam #4. Figure 5.52 shows such variations for gages 11 and 13. Both gages indicated high original prestressing values of +1750 and +800 microstrain respectively. During fatigue loading gage #11 showed a strain variation at any cycle of +50 microstrain as compared to the +300 microstrain observed for gage #13. But both indicated increases in strain values of +300 and +2200 microstrain before failure occurred. The results of gages 14, 15 and 16 indicated high original prestressing values and seemed to follow the same trend of increasing tensile strains with increasing fatigue cycles until they failed about halfway through the fatiguing process. Therefore it seems that moving the opening vertically downward influenced the tension field region and hence should be reinforced properly to avoid local fatigue failure.

The tension field in beam #6 behaved in a manner that is somewhat a combination of the observed results for the previous beams. Gages 11 and 16 (refer to Figure 4.12) which were located two inches away from the edges of the opening displayed a behaviour that is similar to that of

beams 2 and 3. Figure 5.53 shows the strain variation in these gages with increasing fatigue cycles. It is evident from the results of both gages that fairly low tensile strains existed from prestressing. Also, a fluctuation of only +30 microstrain existed in both gages at any fatigue cycle of loading with the original prestressing value changing by +30 and +40 microstrain due to fatigue loading before failure occurred. Strain gages 12 and 15 (refer to Figure 4.12) which were located one inch away from the edges of the opening displayed a behaviour that is similar to that of beams 4 and 5. Figure 5.54 shows the strain variation with increasing fatigue cycles of these gages. It is evident that much higher prestressing values were observed for the two gages when compared to those of gages 11 and 16. This is due to the fact that these gages were closer to the edges of the opening. Fluctuations in the order of +80 and +60 microstrain were observed for gages 12 and 15 respectively. Also, changes of +200 and +175 microstrain were observed from the original prestressing values due to fatigue loading. Although such changes are not equal in magnitude to the ones observed for beams 4 and 5, they are still significant in value.

5.2.4 . The Bottom Chord

The bottom chord results of beam #2 indicated higher original compressive strains due to prestressing than the top chord. This is because the net affect on the prestressing force was located at an eccentricity of 1.17 inches below the neutral axis of the beam, thus inducing large compressive strains on the bottom half of the beam. During loading, strain gages 19 and 24 (refer to Figure 4.12) indicated increasing compressive strains with increasing fatigue cycles until failure occurred. A fluctuation of about 40 microstrain was observed for both gages at any early cycle of loading with about a net change of 300 microstrain from the original prestressing value being observed before failure occurred. Vierendeel local bending action was again evident in the latter stages of loading for such gages inducing increased compressive strains. Such a phenomenon was further verified when the results of gages 21 ans 22 were examined (refer to Figure 5.55). The response of both gages to loading was almost identical where compressive strains increased up to about 1.0 million cycles but as fatiguing continued, both local Vierendeel bending and overall beam tensile bending affects reduced the compressive strains by about 200 microstrain. Gage #20 (refer to Figure 4.12) indicated an increase in compressive strain values up to about 1.0 million cycles due

to local compressive action at the top fibre of the bottom chord but as loading continued beyond that stage, tensile strains due to the overall bending of the cracked beam reduced such effects. As for gage #23 hardly any fluctuation occurred in the original prestressing compressive strains up to 1.6 million cycles. As fatiguing continued the overall bending affects of the cracked beam reduced such compressive strains by about 120 microstrain.

The bottom chord of beam #3 indicated a slight increase in the original compressive strain values due to prestressing when compared to that of beam #2. Such values were again higher than the ones observed at the top chord of beam #3 due to the eccentricity of the prestressing force. Strain gages 19 and 24 (refer to Figure 4.12) indicated high original prestressing values of -950 and -900 microstrain. As the beam was loaded, increasing compressive strains were observed throughout. Gage #19 strain fluctuation at any early cycle of loading was slightly higher than the -100 microstrain registered by gage #24. This is due to the higher moment that gage 19 was subjected to. Also, a net change of about 200 microstrain was observed before failure occurred. Such a change can again be attributed to local Vierendeel bending action at the bottom chord. This behaviour was further evident when the response to load of strain gages 21 and 22 was looked at. Both gages indicated

increases in compressive strain values up to about 1.0 million cycles of loading with a fluctuation at any early cycle of -250 and -300 microstrain, respectively. As fatiguing continued beyond 1.0 million cycles, tensile strains started to come into play primarily due to Vierendeel local bending. The magnitude of such tensile strains increased by +150 and +250 microstrain just before failure. Gage #22 registered a higher tensile strain value than gage #21 due to both Vierendeel local bending and overall bottom fibre tensile strains. Figure 5.56 shows the strain variation with increasing fatigue cycles of strain gages 22 and 24. Strain gage #22 indicates the tensile aspect of Vierendeel bending while gage #24 indicates the compressive aspect of such bending. Gages 20 and 23 (refer to Figure 4.12) which monitored the top and bottom fibres at the middle of the bottom chord indicated totally different responses. Gage #20 showed a steady increase in compressive strain as fatiguing continued indicating that the local bending of the chord influenced the top fibres more than the overall beam tensile bending. Gage #23 indicated increasing strains up to 1.2 million cycles. As fatiguing continued, tensile strains started to develop resulting in a total change of +100 microstrain before failure occurred. It is evident that slightly larger variations in strain values were observed due to Vierendeel local bending for the bottom chord of beam #3 when compared to that of beam #2.

The original prestressing compressive strain values in the bottom chord of beam #4 were smaller in magnitude than those observed for beam #3. This is due to the opening being moved vertically upward 0.5 inches which in turn shifted the overall neutral axis of the beam below that of Beam #3. Such a shift reduced the compressive strain values being applied by the prestressing moment that exists because of the eccentricity of the applied force. Strain gages 19 and 24 (refer to Figure 4.12) indicated increasing compressive strain values as the beam was subjected to fatigue loading. Such strains increased throughout the fatigue life of the beam registering changes up to -200 and -150 microstrain just before failure (refer to Figure 5.57). The actual strain fluctuation of such gages at any early fatigue cycle was -170 and -120 microstrain respectively. Such a fluctuation and the change in strain values due to fatiguing were very similar to the ones observed for beam #3. The Vierendeel local bending action was again evident in gages 19 and 24 but was further verified when the results of gages 21 and 22 were examined. Such gages showed very similar response patterns to loading. The original compressive strains in both gages were reduced due to tensile affects that influenced the bottom chord throughout the fatigue loading stage (refer to Figure 5.58). At the early stages of loading the strain variation with any cycle

was -175 and -300 microstrain, respectively.. Such values continued to decrease as loading continued due to the tensile strains resulting from the local Vierendeel bending action. Strain gages 20 and 23 (refer to Figure 4.12), which monitored the extreme fibre strains in the middle of the chord, registered hardly any variation of strain with increasing fatigue cycles. Gage #20 compressive strain value increased by only -40 microstrain when compared to the original prestressing value before failure occurred and gage #23 compressive strain value was reduced by 70 microstrain due to overall beam tensile bending.

The bottom chord of beam #5 registered higher original compressive strains than beams 3 and 4. This is due to the opening being moved vertically downward 0.5 inches which in turn shifted the overall beam neutral axis upward causing a larger distance to the extreme compressive fibre. Due to the eccentricity of the prestressing force, a moment was induced which imposed higher compressive strains at any location along the bottom chord. Strain gages 19 and 24 (refer to Figure 4.12) indicated high original compressive strain values of -1100 and -1200 microstrain. Such strains increased steadily with increasing fatigue cycles resulting in total changes of -300 and -240 microstrain before failure occurred. Such changes are larger in amplitude than the ones observed for beams 3 and 4. Vierendeel local bending

was again evident in the response of the above two gages and was further verified when the results of strain gages 21 and 22 were examined (refer to Figure 5.59). From the plots it is evident that both gages indicated the presence of tensile strains throughout the fatigue loading period which reduced the original compressive strains by +220 and +400 microstrain, respectively. The reason that gage #22 indicated a larger tensile strain amplitude was due to the presence of both maximum bending tension caused by overall beam bending and the addition of further tensile strains due to local Vierendeel bending action. The change in strain values for gages 21 and 22 was the largest amongst beams 2 to 5. Therefore it seems that moving the opening downward caused the highest variation in stresses when compared to other beams.

The bottom chord of beam #6 behaved in a totally different manner than what was observed for the previous four beams. This is because no local Vierendeel bending action was present and much higher strain variations were observed during fatigue loading. Strain gages 19, 20 and 21 (refer to Figure 4.12) showed similar behaviours and with hardly any change in the original prestressing values, up to 0.2 million cycles of fatigue loading. This is because such gages were closer to the neutral axis of the beam. As loading continued, tensile strains due to chord cracking

started to develop reducing the original compressive strains by +150 and +200 microstrain for gages 19 and 21 and by +230 microstrain for gage #20. The bottom fibre of the chord was monitored by strain gages 22, 23 and 24. Such gages indicated higher early strain variations at any cycle of fatigue than what was observed for gages 19, 20 and 21. Such variations were almost identical and equal to +300 microstrain. Gage #22 indicated a slightly lower reduction in the original compressive strain value due to tensile affects at the bottom fibre than what was observed for gage #24. The original prestressing strain values in gages 22 and 23 were reduced by +150 and +200 microstrain due to fatigue loading before failure occurred. Gage #23 which monitored the middle of the bottom tensile fibre of the bottom chord indicated the largest loss in the original compressive value due to fatigue loading. Such a loss was equal to +280 microstrain but still kept the bottom fibres in a compressive state of stress before failure occurred. Figure 5.60 shows the strain variation in strain gages 23 and 24 with increasing fatigue cycles.

5.2.5 Extreme Fibres at Midspan

As for the final group of strain gages which included gages 25 and 26 only the results of beams 2 to 5 will be discussed since the opening was provided at midspan for beam #6.

Strain gage #25 monitored the strain at the extreme compressive fibre at midspan due to bending action (refer to Figure 4.12) and as expected indicated very rapid increases in compressive strain values due to fatigue loading. Figure 5.61 shows typical responses of such a gage to loading for beams 3 and 4. It is evident that in both cases that a fluctuation of about -600 microstrain existed during any cycle of loading resulting in final increases in strain value before failure occurred of -1500 and -1100 microstrain for beams 3 and 4, respectively. The response of gage #25 to loading in beams 2 and 5 was very similar to that of beams 3 and 4 indicating similar strain variations with loading and almost equal final strain value before failure.

Strain gage #26 monitored the extreme bending tensile fibre at midspan. Figure 5.62 shows the response of such a gage to fatigue loading in beam #4. The plot indicates a continuous decrease in the original prestressing compressive strain value as fatiguing continued due to tensile bending strains at the bottom fibre. The original compressive value was reduced by +85 microstrain before failure occurred. Beams 2 and 3 also indicated similar strain reductions of +110 and +120 microstrain before failure occurred.

From all the previously observed results it is evident that providing beams with openings in the shear span is fairly safe under the influence of fatigue loading as long

as the beams are reinforced properly around the opening to intercept the tension field due to prestressing and to pick up any further increases in such tensile strains due to fatigue loading. Such increases in strain were evident in beams provided with eccentric openings (upward or downward) in the shear span or at midspan. Also Vierendeel local bending action was evident in all the beams provided with openings in the shear span. The influence of such an action seemed to be more evident in beam #3 than in beam #2 since larger strain variations were observed due to fatigue loading at identical locations. Therefore, as the length of the opening increased, the Vierendeel local bending action became more evident. Also, Beam #5 seemed to be most influenced by such bending action when compared to beams 3 and 4. This observation indicated that moving the opening vertically downward increased the influence of such an action on both the top and bottom chords. In conclusion, from a fatigue aspect point of view, providing an opening centric about the neutral axis of the beam in the shear span is much safer than providing an eccentric opening in the shear span or at midspan. This is due to the much smaller tensile strain variations within the tension field region and the longer fatigue life sustained by such beams when subjected to continuous repetitive loading.

5.3   Crack Patterns and Failure Modes

The following observations were made during the fatigue loading process for all the tested beams. Such observations indicate such characteristics as cracking patterns and final failure modes.

The first hairline cracks in beam #1 appeared about four inches away from midspan at about 25,000 cycles of fatigue loading. As fatiguing continued, such flexural cracks began to incline due to shear affects. The beam settled down in deflection response during this stage but continued to show more crack formation by having eight visible cracks, four on either side of midspan. With the beam heavily cracked, failure occurred at 1.27 million cycles of fatigue loading by simultaneous yielding of the prestressing wires and crushing of the compression zone concrete. Figure 5.63 shows the final failure mode and the still intact opening region of beam #1.

Beam #2 cracked after 85,000 cycles of fatigue loading. Two cracks one about three inches away and the other one inch away from midspan were observed. Between 0.1 and 1.6 million cycles of loading the beam settled down to a steady deflection response but showed a lot further flexural cracking symmetrically about midspan at six, twelve,fifteen and seventeen inches away. At 1.75 million cycles the original two cracks propagated vertically upward and

inclined at about 45° after reaching the centre line of the beam. Such cracks propagated as far as 2 inches above the beam neutral axis. The beam failed at about 2.15 million cycles due to the fatigue of the bottom left prestressing wire. Figure 5.64 shows the cracking pattern at midspan and the fatigued prestressing wire. After failure, the remaining prestressing force left in the two other wires was equal to 6.C and 5.6 kips which indicated a loss of 31% and 35% in the prestressing forces due to fatiguing.

After 17,000 cycles of loading, one crack was observed for beam #3 directly under the load. After 0.5 million cycles a total of five cracks were visible, the original one under the load and four others symmetrically spaced at two and five inches from midspan. Between 0.5 and 1.5 million cycles the beam settled down in deflection response to load but showed further cracking at about seven, eleven and fifteen inches away from midspan. The beam failed after 1.67 million cycles of loading at the original crack location by yielding of the prestressing wires which was simultaneously followed by the crushing of the concrete in the compression zone. Figure 5.65 shows the failure mode. This failure occurred at the end closer to the opening which was identical to the failure mode of beam #1.

Beam #4 first signs of cracking occurred symmetrically at one inch away from midspan after 18,000 cycles of loading.

Between 0.1 and 1.0 million cycles further symmetrical cracking was observed at three,seven and nine inches away from midspan. At 1.1 million cycles, the beam was heavily cracked flexurally around the midspan region but no cracks formed any where near the opening region. The final failure occurred after 1.7 million cycles of loading by yielding of the prestressing steel and crushing of the compression zone concrete (identical to beams 1 and 3). Figure 5.66 shows the final failure mode and the still intact opening region.

Cracks were observed after 30,000 cycles of fatigue loading for beam #5. Three flexural cracks were formed, one right under the load and two others symmetrically two inches away from midspan. Between the period of 0.1 million and 1.0 million cycles of fatigue loading, the beam settled down to a steady deflection response to load. During this period, further symmetrical flexural cracks were observed at six and ten inches away from midspan. After 1.57 million cycles, one of the original cracks had propagated flexurally upward to the centre line of the beam and continued in a 45° inclined fashion due to shear affects until reaching the top concrete fibre where the bottom and top prestressing wires yielded and the compression zone concrete collapsed. Figure 5.67 shows the final mode of failure and the uncracked opening region. This failure mode is again identical to the ones observed for beams 1, 3 and 4.

Beam #6 cracked after only 10,000 cycles of fatigue loading. Two flexural cracks formed right under the two corners of the chord at the extreme tension fibre. Between 0.1 and 0.25 million cycles of loading these cracks propagated vertically upward right to the two corners of the bottom chord and continued upwards beyond the corners in an inclined fashion. Also, more symmetrical flexural cracks were observed at eleven and fifteen inches away from midspan. After 0.38 million cycles of fatigue loading, the one side of the bottom chord was cracked right through forming hinges which separated it completely from the rest of the beam. Due to such a failure, it was felt that continuing the fatigue test was not of interest with only the ultimate static flexural strength being important. The beam failed statically at 3.8 kips by the simultaneous yielding of the prestressing wires and the collapse of the bottom chord at the corners and the top chord right under the load. Figure 5.68 shows the failure mechanism due to fatigue loading and the final failure after the beam was tested statically.

In conclusion it is evident that all the beams that were provided with openings in the shear span and subjected to fatigue loads equal to 80% of the cracking load (beams 1,3,4,5) failed in an identical fashion. Such a failure started by crack formation right under or near the point of

loading and ended up by crack propagation resulting in simultaneous yielding of all the prestressing wires and crushing of the compression zone concrete. For such beams, the opening region was still intact with no visible damage due to fatigue loading. As for beam #2 whose maximum amplitude of loading was only 50% of the cracking load, a different failure pattern was observed. The beam actually failed by the fatiguing of one of its prestressing wires showing that if such beams were subjected to smaller amplitudes of loading and longer cycles of fatigue loading, the steel wires will fatigue. Beam #6 failed by the formation of flexural hinges in the bottom chord corners. This type of failure indicated the vulnerability of beams that are provided with openings at midspan under the influence of fatigue loading.

5.4   Analysis of the Theoretical Work

5.4.1   Solid Beam Response by Beam Theory

The first four natural frequencies of a solid beam having a cross section of 3 by 8 inches and a length of 180 inches are presented in Table 5.4. This was a point of interest for comparison reasons with the results of the finite element analysis and with the experimental free vibration hammer test. The results of the finite element analysis overestimated the first four associated flexural natural

frequencies by 4%, 3%, 2% and 0%, respectively. The Experimental free vibration hammer test results overestimated the first three associated flexural natural frequencies by 0%, 5%, and 1%, respectively. Therefore it can be concluded that good agreement existed between theory and experiment.

5.4.2   Openings in the Shear Span (Side Openings)

The objective of this investigation was to determine the influence of side opening length on the natural frequencies and mode shapes of vibration. Table 5.5 shows the observed results which indicated that the presence of side openings with varying length did not influence the first or second natural frequencies when compared to solid beams. Also, opening lengths up to 24 inches had little effect on the third natural frequency with the exception of very long openings where, local modes of vibration were observed resulting in a sudden drop in frequency value. In addition, the values of the fourth natural frequency indicated that up to a 12 inch opening very little frequency variation existed, but when larger opening sizes were considered, a rather linear drop in frequency value was observed. The sudden drop in the third and fourth natural frequency values for large openings can be attributed to opening intervention in the area of a point of inflection at the associated mode shape (region where a node of zero deflection exists). The

opening region around such a node is subjected to excessive changes in stresses which reduce the stiffness and eventually lower the frequency. Figures 5.69 and 5.70 show the associated mode shapes for a rectangular beam containing a 32 inch by 3 inch side opening. Looking at the third and fourth mode shape indicates the point of opening intervention in the deflected shapes.

5.4.3   Openings at Midspan

The objective of this part of the investigation was to determine the influence of midspan opening length on the natural frequencies and mode shapes of vibration. The results (refer to Table 5.6) indicated an increase in the first and third natural frequencies as the length of the opening increased. This can be attributed to the fact that since all the openings centres coincided with the neutral axis of the beams, very little change occurred in the flexural moment of inertia and therefore presenting no significant reduction in stiffness. As the opening increased in length, a significant loss of mass occurred which imposed a larger influence on the fundamental and third natural frequencies (fundamental frequency $w^2=k/m$) resulting in a net increase in frequency. Also, as the size of the opening increased, the second and fourth natural frequencies decreased. This can be attributed to the same reason that was indicated earlier concerning opening

intervention in the area of nodes of zero deflection in associated mode shapes. The node occurred in the middle of the opening for the second and fourth mode shapes. Figures 5.71 and 5.72 show the associated mode shapes for a rectangular beam containing a 32 inch by 3 inch midspan opening. Looking at the second and fourth mode shapes, they clearly indicate opening intervention at midspan.

5.4.4 Beams With More Than One Opening in the Shear Span

The objective of this part of the investigation was to determine the influence of both the number and length of side openings on the natural frequencies of vibration. From the results (refer to Table 5.7) it was observed that a very similar behaviour occurred to that of beams with one opening in the shear span. There was no or very little change in the first three natural frequencies with increasing opening length. Also, an almost linear decrease in the value of the fourth natural frequency was observed with an increase in opening length which again can be attributed to opening intervention at mode shape nodes of zero deflection.

5.4.5 T-Beams With Openings at Midspan

The variation of opening length in the shear span did not exhibit any significant change in the values of the first three natural frequencies for rectangular beams; furthermore, the assumption that both T- and I-beams

provided with shear span openings would behave in a very similar manner to that of rectangular beams; therefore it was decided to analyze only the influence of midspan openings on T- and I-beam natural frequencies and mode shapes.

Two different T-beam cross sections were considered in this investigation; the effect of opening length on both cross sections is discussed. Table 5.8 shows the results for all the cases studied herein. The results of the first cross section (beams 1 to 4) show that no change in the value of the first natural frequency was evident with increasing the opening length showing that the loss of stiffness at midspan being just as critical as the loss in mass. Also, very little change in the values of the third natural frequency was observed with increasing opening length. In addition the values of the second and fourth natural frequencies seemed to decrease rapidly with increasing opening length which again can be attributed to opening intervention at mode shape nodes of zero deflection. Comparing such frequency values to the ones observed for rectangular beams with an opening at midspan indicated that for the same size openings, higher fundamental natural frequencies, as well as much lower second, third and fourth natural frequency values were evident. Therefore T-beams having a cross sectional neutral axis well within the flange

are more susceptible than rectangular beams to vibration frequencies that exceed the fundamental natural frequency. Figures 5.73 and 5.74 show the associated mode shapes for a large flange T- section containing a 32 inch by 3 inch opening at midspan.

The results of the second cross section (beams 5 and 6) followed a very similar pattern to that of the first one indicating a rapid decrease in the second and fourth natural frequency values and hardly any change in the third natural frequency value. With regard to the first natural frequency value, an increase occurred with increasing opening length indicating that the loss of mass at midspan being more critical than that of stiffness (identical to rectangular beams with openings at midspan). Comparing the results observed for both cross sections for solid beams and for other beams containing openings of the same length seemed to indicate that the second cross section was much safer against vibrational excitation (higher natural frequency values). This can be attributed to the fact of having a lower cross section neutral axis which reduced the flexural tension area and in turn increased the overall section stiffness. Therefore when using T-beams it is recommended to select a section which has a balanced tension and compression flexural moments of inertia.

5.4.6   I-Beams With Openings at Midspan

All the cases considered in this part of the investigation contained a symmetric cross section with the opening centre coinciding with the beam neutral axis. The objective of the study was to determine the influence of opening length on the response of such beams. The results indicated (refer to Table 5.9) that an increase in the first natural frequency value occurred as the opening length increased similar to that of a rectangular beam with an opening at midspan. This again is due to the higher influence of loss of mass to that of stiffness. Also, a very rapid decrease in the second and fourth natural frequency value occurred as the opening length increased. This again is attributed to opening intervention around mode shape nodes of zero deflection. As for the third natural frequency, very little change was observed with opening length. Figure 5.75 shows the first two associated mode shapes for an I-beam provided with a 32 inch by 3 inch opening at midspan.

In conclusion it can be stated that the free vibration response of symmetric I-beams provided with openings at midspan is identical to that of rectangular beams with openings at midspan. The only difference being the higher frequency values of I-beams due to the added cross sectional stiffness provided by the flanges.

5.5 Fundamental Frequency Variation Between Theory and Experiments

In this section of the results a simple comparison is made between the observed experimental and calculated theoretical fundamental natural frequency values. Theoretically beams 1 to 3 indicated a first natural frequency value of 17.2 Hz (refer to Table 5.3) with beam #6 indicating a frequency of 18.0 Hz (refer to Table 5.6). When identical beams were tested experimentally, frequencies of 20 Hz, 18.9 Hz, 17.8 Hz and 19.4 Hz were observed for beams 1, 2, 3 and 6, respectively. Beam #1 indicated the largest difference of 2.8 Hz. Such a variation can be attributed to the high amount of precompression that was applied to the springs before running the tests. This in turn provided a bit of an elastic support and increased the fundamental natural frequency. Experimentally, beams 2, 3 and 6 overestimated the theoretical fundamental natural frequency by 1.7 Hz, 0.6 Hz and 1.4 Hz, respectively. Such a difference is relatively small and for all practical engineering purposes is acceptable.

It is evident that very good agreement existed between the theoretical and experimental results for all the beams considered. Also, beams provided with openings at midspan, indicated the highest fundamental natural frequency values.

Chapter VI

CONCLUSIONS AND RECOMMENDATIONS

6.1   Conclusions

From the results of this study it is evident that prestressed rectangular concrete beams with openings are very durable structures against vibrational excitation and fatigue loading. Such structures register high natural frequency values and sustain a large number of fatigue cycles before failure occurs. But it is essential that the region around the opening be adequately reinforced with vertical stirrups and that openings be centred about the neutral axis of the beam in the shear span.

Based on the theoretical and experimental investigations the following specific conclusions are drawn.

6.1.1   Natural Frequencies and Mode Shapes

1.   No significant variation exists in the value of the first natural frequency of vibration with increasing opening length or with varying the opening eccentricity for prestressed concrete beams provided with openings in the shear span. A slight increase in the natural frequency value can be expected when the opening is at midspan.

2. The value of the first natural frequency does not significantly decrease when prestressed rectangular concrete beams are subjected to a high number of fatigue cycles. A more evident reduction in vibration amplitudes can be expected at the associated mode shape.

3. The presence of shear span and midspan openings does not induce any local affects on the first mode shape.

4. Increasing the length of shear span openings, increases the amplitude of displacement at the first natural frequency.

5. Variations in opening size, location and eccentricity do not influence the amount of damping present within such beams.

6. Increasing the opening length decreases the values of the third and fourth natural frequencies but not that of the first and second natural frequencies in prestressed rectangular concrete beams provided with an opening in the shear span.

7. No significant variation exists between the natural frequencies of prestressed rectangular concrete beams provided with one or two openings in the shear span.

8. Increasing the opening length increases the values of the first and third natural frequencies and rapidly decreases the values of the second and fourth natural

frequencies in prestressed rectangular concrete beams provided with an opening at midspan.

9. The location of the cross sectional neutral axis in T-beams significantly influences the natural frequency values.

10. I-beams provided with an opening at midspan demonstrate an identical pattern of response to that of rectangular beams with an opening at midspan.

6.1.2 Fatigue Loading

11. Vierendeel local bending action is evident under the influence of fatigue loading for rectangular beams provided with an opening in the shear span but not for beams provided with an opening at midspan.

12. The prestressing tension field is influenced by fatigue loading in rectangular beams provided with eccentric shear span and centric midspan openings.

13. Beam failure due to fatigue loading occurs away from the opening region in prestressed rectangular concrete beams provided with an opening in the shear span.

6.2 Recommendations for Future Research

For future research the following points of interest could be studied:

1. Investigate experimentally the dynamic characteristics of rectangular, T- or I-beams provided with a number

of openings. The response of such structures to resonance fatigue could also be looked at.

2. Excite such structures at a frequency range that takes into account the response at the second and even third natural frequencies. __This could be meaningful information if prestressed concrete beams are erected in industrial plants where the operation speeds of machinery are higher than the first natural frequency of vibration.

Appendix A

CONCRETE MIX DESIGN

A.1 General

The following design is based on the guidelines presented in the CPCA metric manual (1991).

A.2 Properties of the Materials

Water : tap water

Cement : high early strength (type III)

Coarse Aggregate : maximum size = 10 mm (0.4 inch)

absorption   = 0.5 %

total moisture content = 2 %

dry rodded mass = 1600 kg/m^3 (99.9 lb/ft^3)

Fine Aggregate : maximum size = 5 mm (0.2 inch)

small aggregate = 40 %

sand = 60 %

absorption = 0.7 %

total moisture content = 4 %

finess modulus (FM) = 2.56

A.3 Desired Characteristics

Compressive strength f$_c'$ = 45 MPa (6520 psi)

Slump = 80 mm (3 inch)

Air content = 0 %

A.4   Design Procedure

The design procedure is presented in the following number of steps:

1. Select the appropriate slump value from Table 7-4:
    slump = 80 mm (3 inch).

2. Maximum aggregate size = 10 mm (0.4 inch).

3. Select mixing water requirements from Table 7-6 for
    non-airentrained concrete:
    w = 225 kg/m³ (14.1 lb/ft³).

4. Select water/cement ratio:
    the average strength = f'_c + 1.4 X FM
    average strength = 45 + 1.4 X (2.56) = 49 MPa (7100 psi)
    select w/c = 0.4 from Figure 7-1.

5. Estimate the required cement:
    cement = 225/0.4 = 563 kg/m³ (35.1 lb/ft³).

6. From Table 7-1 estimate the quantity of coarse aggregate
    for a FM of 2.56 and a maximum size of 10 mm (0.4 inch):
    dry mass = 0.484 X 1600 = 775 kg/m³ (48.4 lb/ft³).

7. Estimate the needed quantity of fine aggregate using the
    estimated mass of a cubic meter of concrete:
    from Table 7-9 the total mass = 2285 kg/m³ (142.7 lb/ft³)
    F.A. = 2285 - (225 + 563 + 775) = 722 kg/m³ (45.1 lb/ft³).

8.   Estimate the needed corrections to compensate for the
      moisture in the aggregates:
      coarse aggregate = 775 X 1.02 = 791 kg/m³ (49.4 lb/ft³)
      Fine aggregate = 722 X 1.04 = 751 kg/m³ (46.9 lb/ft³).

9.   Adjust the amount of water:
      coarse aggregate = (2 - 0.5) = 1.5 %
      fine aggregate   = (4 - 0.7) = 3.3 %
      final amount of water = 225 - 0.015 X 775 - 0.033 X 722
                            = 190 kg/m³ (11.9 lb/ft³).

10.   The final estimated batch:
      a) water = 190 kg/m³ (11.9 lb/ft³)
      b) cement = 563 kg/m³ (35.1 lb/ft³)
      c) coarse aggregate = 791 kg/m³ (49.4 lb/ft³)
      d) fine aggregate = 751 kg/m³ (46.9 lb/ft³)

11.   Calculate the total volume of concrete needed for the
      beam and three 6 inch by 12 inch test cylinders:
      volume of the beam = 0.0732 m³ (2.59 ft³)
      volume of cylinders = 0.0167 m³ (0.59 ft³)
      total volume = 0.09 m³ (3.17 ft³).

12. Estimated final batch for needed volume:

a) water = 0.09 X 190 = 19 kg (40 lb)

b) cement = 0.09 X 563 = 51 kg (112 lb)

c) coarse aggregate = 0.09 X 791 = 71 kg (156 lb)

d) sand = 0.09 X (0.6 X 751) = 41 kg (90 lb)

e) small aggregate = 0.09 X (0.4 X 751) = 27 kg (60 lb).

Appendix B

MEGADAC 2000 DATA ACQUISITION UNIT

B.1   General

This appendix contains information on recording, transmitting and analog output playback of data for all the different sensors used in the experimental work.

B.2   Data Recording and Storage

The technical manual describes in detail all the different options available on the Megadac for data recording. Only the options used in this research work are described herein.

Data recording is controlled by the information present in the Scan table. Such information specifies directions to the Megadac for processing input channels. The Scan table is composed of two sections, Base Entries and Scan Entries.

B.2.1   Base Entries

There are 19 Base Entries in the Scan table. Such entries must be initialized by the user before performing any A/D activity. The following is a brief description of the chosen options.

Base Entry	Value	Description
0	43	Number of Scan Entries present
1	120	Sampling rate
2	0	Samples per second
3	0	Internal clock
4	1	Tape mark inserted after recording
5	1	Auto-balance enabled
6	0	No table expansion
7	1	Burst scan mode
8	0	Start storing immediately
9	0	Stop storing immediately
10	0	Do not repeat the recording cycle
11	42	Monitor Scan Entry #42
12	--	None specified
13	--	None specified
14	0	Start at record cycle 0
15	0	Stop at record cycle 0
16	0	Limit-Exceeded counter
17	0	No triggering of data
18	0	DO not save any pre-triggered data

B.2.2 Scan Entries

The Scan Entries contain information pertaining to the
mapping from hardware A/D or D/A ports or digital ports to
positions in the recorded data blocks.   Each Scan Entry
contains a channel port address which is used for extraction
of data samples and a high and low limit which are used for
starting   and   stopping   the   recording   process   if
pre-triggering is used.   Also,   a Gain value and an
Autobalance value are available to each channel.   The Gain
value is applied to this entry's input prior to the A/D
conversion.   Such a setting depends on the type of sensor
used since different sensors have different voltage outputs.
The Autobalance value is applied to the entry's channel
address by being   converted to an analog   signal and
subtracted from the incoming signal prior to the gain
application and the A/D conversion.

The following is an example of a Scan Entry monitoring an
LVDT:

Scan Entry	Channel Address	Low	High	Gain	Auto
029	032	-2048	+2047	+1	+10

B.3   Data Transmission

After the data was stored on 3M cassette cartridges, it was transmitted from the Megadac to an IBM-PC for data reduction and conversion and from there to the University of Windsor's mainframe.

B.3.1   Data Transmission from the Megadac to IBM-PC

Before any data transmission was possible, a profile for communication with the Megadac was established with the aid of the Mode table. The following is a brief description of the options used to establish communications:

Mode Entry	Value	Description
0	1	Only Carriage return transmitted
1	1	No line feed echoed
2	0	No Echo of commands
3	0	Status reporting enabled
4	0	No flow control
5	0	One-Up numbers sent
6	0	No delay after carriage return
7	128	Number of entries transmitted before carriage return
8	0	Wait for tape I/O operation
9	1	12-bit resolution

Mode Entry	Value	Description
10	1	Signed data (+/-)
11	0	19.2K baud rate
12	2	No parity
13	55	Channel address to be monitored
14	--	None specified
15	--	None specified
16	255	Transmit all channels
17	0	Retry reading tape errors
18	0	No auto rewind
19	0	One tape drive
20	0	No auto restart
21	0	IEEE-488 address
22	0	IEEE-488 parallel poll
23	0	ASCII data transmit format
24	0	Cassette wrap

The IBM-PC and the Megadac were interfaced via RS-232 ports and an interconnecting cable. Data transmission and reduction was controlled by company written software (Optim) for the Megadac.

B.3.2 Data Transmission from IBM-PC to IBM-4381 Mainframe.

With the reduced data on computer disks, the IEM-PC was connected to a modem via an RS-232 port. Communication was established using a computer software package called X-talk. After the data was available on the mainframe further data organization was conducted before using SAS/GRAPH for plotting.

B.3.3 Analog Output Playback from Megadac to FFT Analyzer

The playback mode causes the Megadac to use the Scan table and the data on the cassette drive and transmit the data out the D/A channels. The information in the Scan Table is used to determine channel addresses, gain and if specified, auto balance values. The table Base Entry 0, 1, 2 and 7 should be the same as when the data was recorded. However the Scan Entry "channel address" should be changed for each Scan table entry to reflect the desired output channels (use a non-existant channel for entries not to be played and the same Scan Entry number and channel address used during data recording for the channel to be played). The D/A card jumper configuration must coincide with the desired output channel before placing the Megadac in playback mode.

Appendix C

TRUSS ANALOGY DESIGN METHOD

C.1   General

Vertical Stirrups were used to intercept the tension field at either side of the opening.   The employed design method is based on Truss Analogy which was presented in a publication by Kennedy and El-laithy (1992).

C.2   Truss Analogy Formulation

The formulation of such a method is presented below, followed by a worked example.

$$A_s = \frac{T}{f_s} \qquad\qquad [\text{ C.1 }]$$

$$T = \frac{\alpha(\gamma - \alpha)}{\beta\gamma} \, P_s \qquad\qquad [\text{ C.2 }]$$

$$\alpha = \bar{y} - e - [(h_b)/2] \qquad\qquad [\text{ C.3 }]$$

$$\gamma = h + [(h_t)/3] + [(h_b)/2] \qquad\qquad [\text{ C.4 }]$$

$$\beta = d_t + d_c \qquad\qquad [\text{ C.5 }]$$

$$d_t = \frac{1}{2}(H^2/hc) \qquad\qquad [\text{ C.6 }]$$

$$d_c = \frac{2}{3} \left(H_c / h \right) \qquad\qquad [\ C.7\ ]$$

$$P_s = P_1 + P_2 \left[\left(A_w \right) / A \right] \qquad\qquad [\ C.8\ ]$$

where :
A_s	=	the area of steel required to guard against potential horizontal splitting caused by force T
f_s	=	the allowable tensile stress in the steel reinforcement
T	=	the vertical tensile force
$\bar{y}$	=	the distance of the centroidal axis from the bottom of the cross section
e	=	eccentricity of the prestressing force from the centroidal axis of the section
h_t, h_b	=	the depths of the top and bottom chords respectively
h'	=	the depth of the opening.
d_t, d_c	=	the tension and compression distances respectively
H	=	the depth of the beam
c	=	the distance from the center of the opening to the bottom of the beam
P_s	=	total prestressing force
A_w, A	=	the area of the web and the total cross section respectively
P_1	=	prestressing force applied to the web
P_2	=	prestressing force applied to the flange

C.3   Solved Example

The following example presents the design of stirrup reinforcement at either side of the opening for beam #3.

h_t = 2.5 inch (63.5 mm) h_b = 2.5 inch (63.5 mm)

h = 3 inch (76.2 mm) c = 4 inch (101.6 mm)

H = 8 inch (203.2 mm) e = 1.167 inch (29.6 mm)

$\bar{y}$ = 4 inch (101.6 mm)

γ = 3 + (2.5 / 3) + (2.5 / 2) = 5.083 inch (129.1 mm)

α = 4 - 1.167 - (2.5 / 2) = 1.583 inch (40.2 mm)

d_t = 0.5 X (64 / 12) = 2.67 inch (67.74 mm)

d_c = 0.667 X (32 / 3) = 7.111 inch (180.62 mm)

β = 2.67 + 7.111 = 9.779 inch (248.4 mm)

T = [(1.583 X (5.083 - 1.583)) / (9.779 X 5.083)] X 25.5

= 2.84 kips (12.63 kN)

A_s = (2.84 / 20) = 0.142 inch^2 (92 mm^2)

Using 3/16 inch (4.8 mm) diameter mild steel bars, the area of steel per leg equals 0.0276 inch^2 (17.81 mm^2).

Therefore place :   1 stirrup at hole edge   =   2 X (0.0276)

                         1 stirrup one inch away   =   2 X (0.0276)

                         1 stirrup two inches away   =   2 X (0.0276)

                         1 stirrup three inches away =   2 X (0.0276)

Resulting in a total steel area of 0.221 inch^2 (143 mm^2) over 3 inches (76.2 mm) which exceeds the required area of 0.1412 inch^2 (92 mm^2).

Appendix D

<u>FIGURES</u>
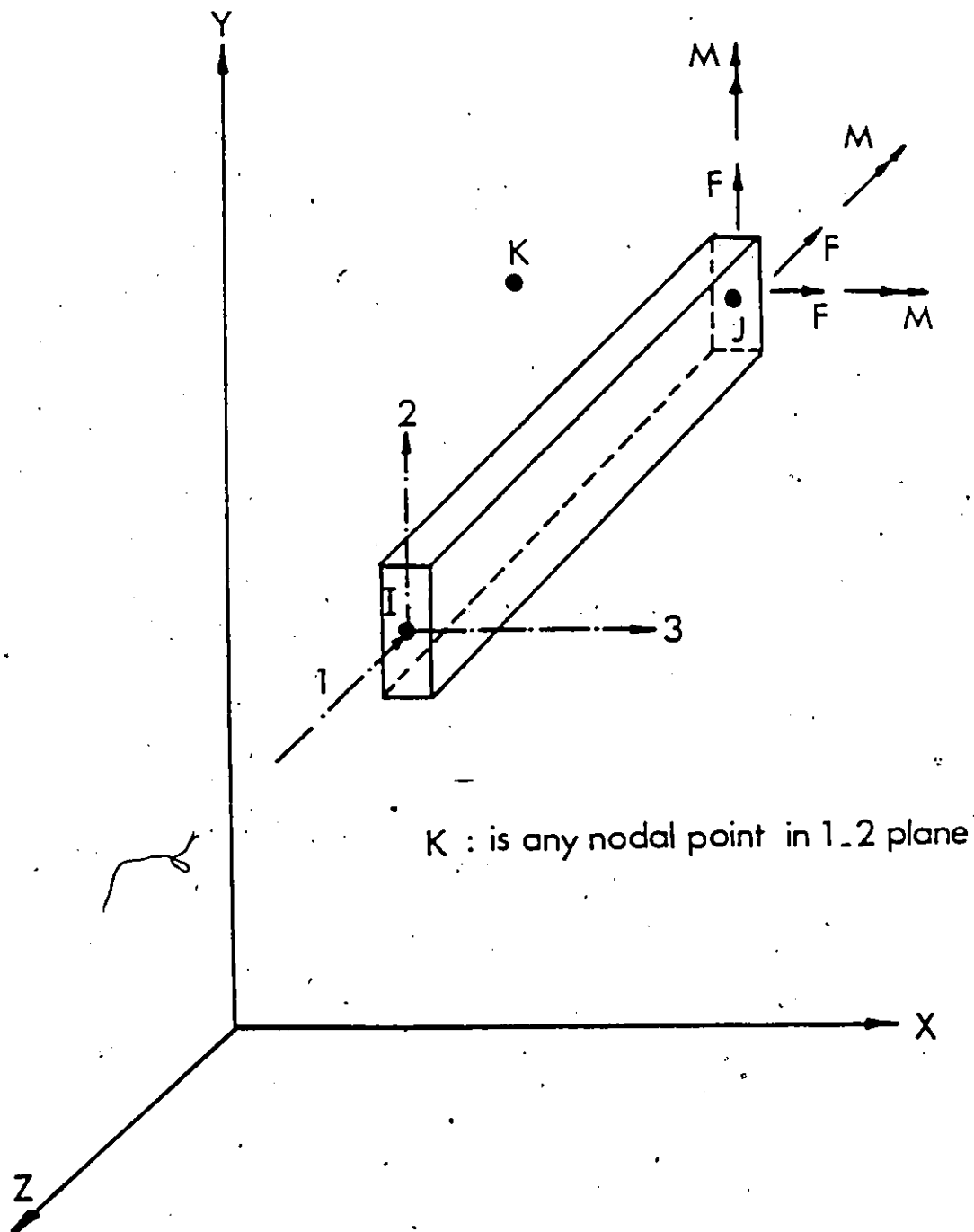
Figure 3.1: Local and Global Axes for a Three Dimensional Beam Element
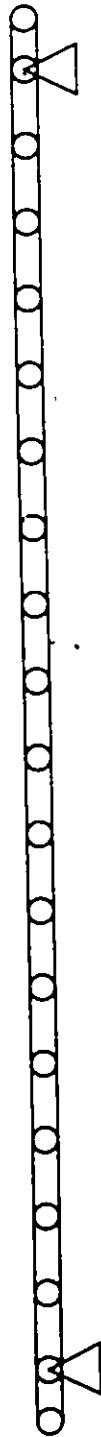
No. of Nodes = 21
No. of 3-D Beam Elements = 19

Figure 3.4: Solid Beam Model Used in SAPIV
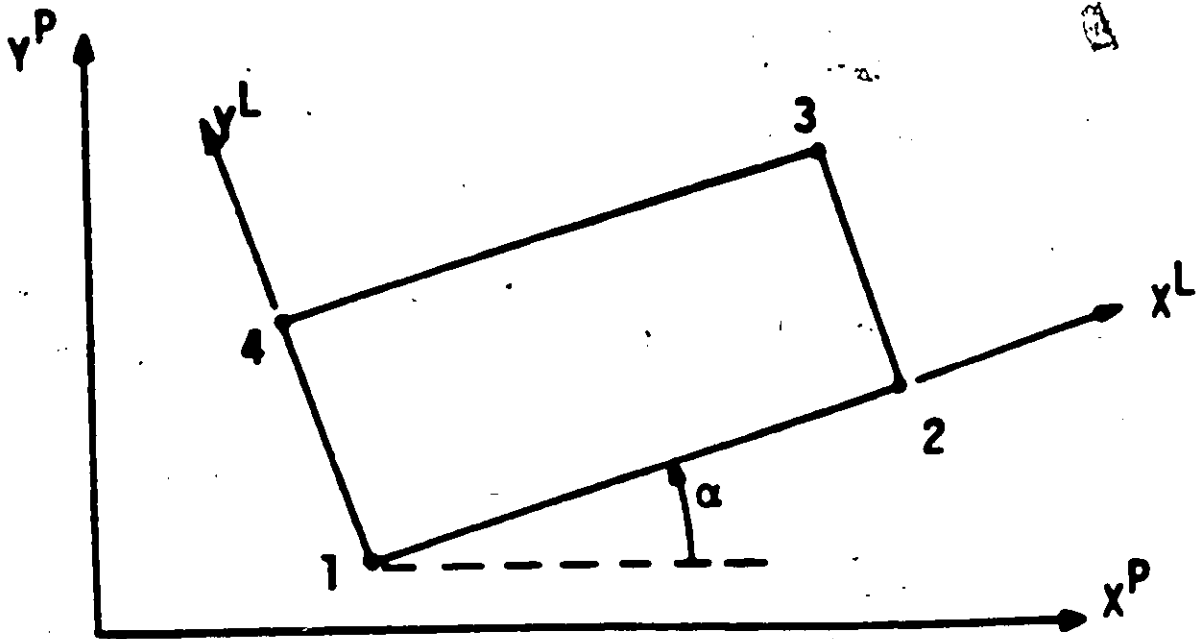
Figure 3.3: Local and Global Axes for a PSR Element
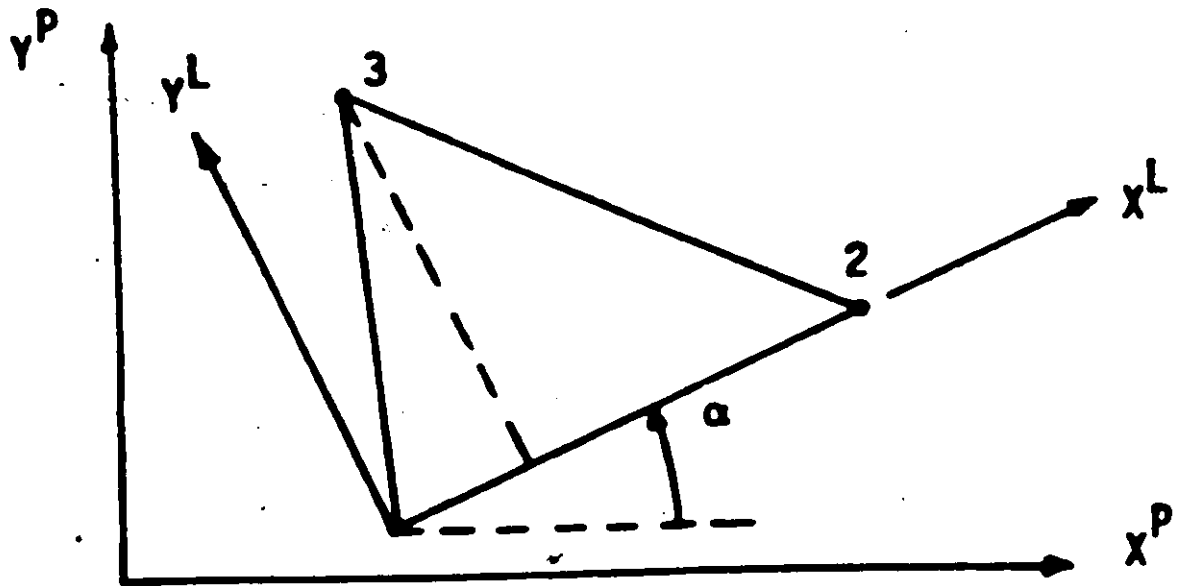
<u>**Figure 3.4**</u>:   Local and Global Axes for a CSTG Element
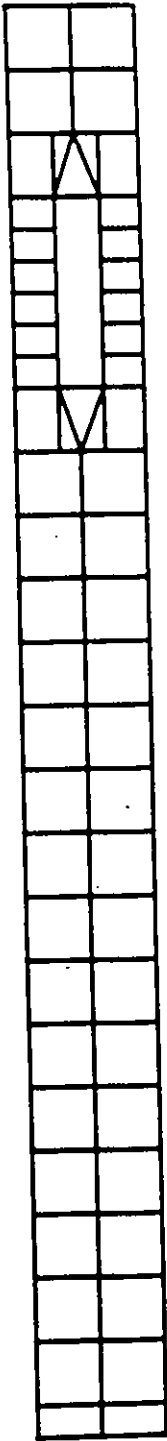
Figure 3.5: Typical Finite Element Mesh for a Rectangular Beam With an Opening in the Shear Span
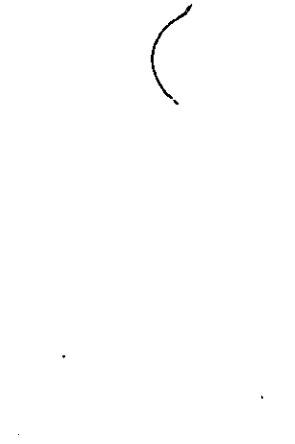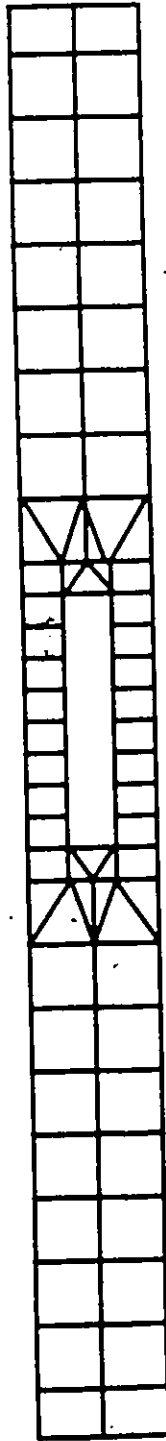
Figure 3.6: Typical Finite Element Mesh for a Rectangular Beam With an Opening at Midspan
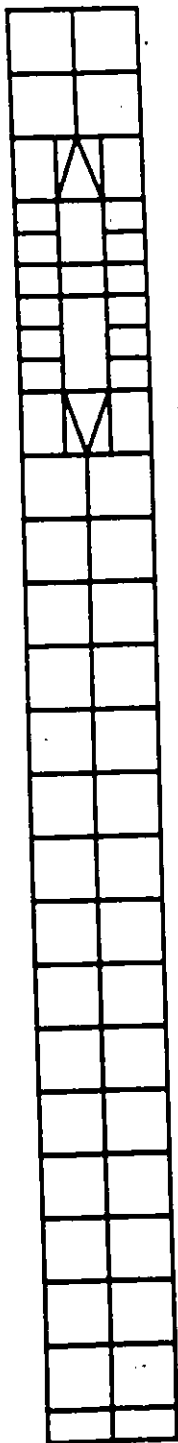
Figure 3.1: Typical Finite Element Mesh for a Rectangular Beam With Two Openings in the Shear Span
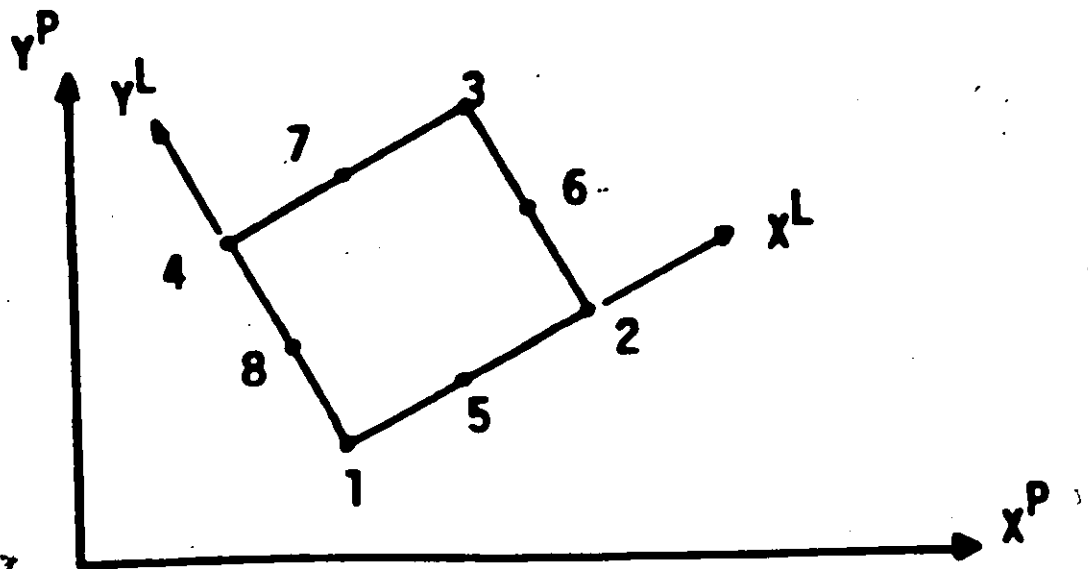
Figure 3.8: Local and Global Axes for an LSB Element
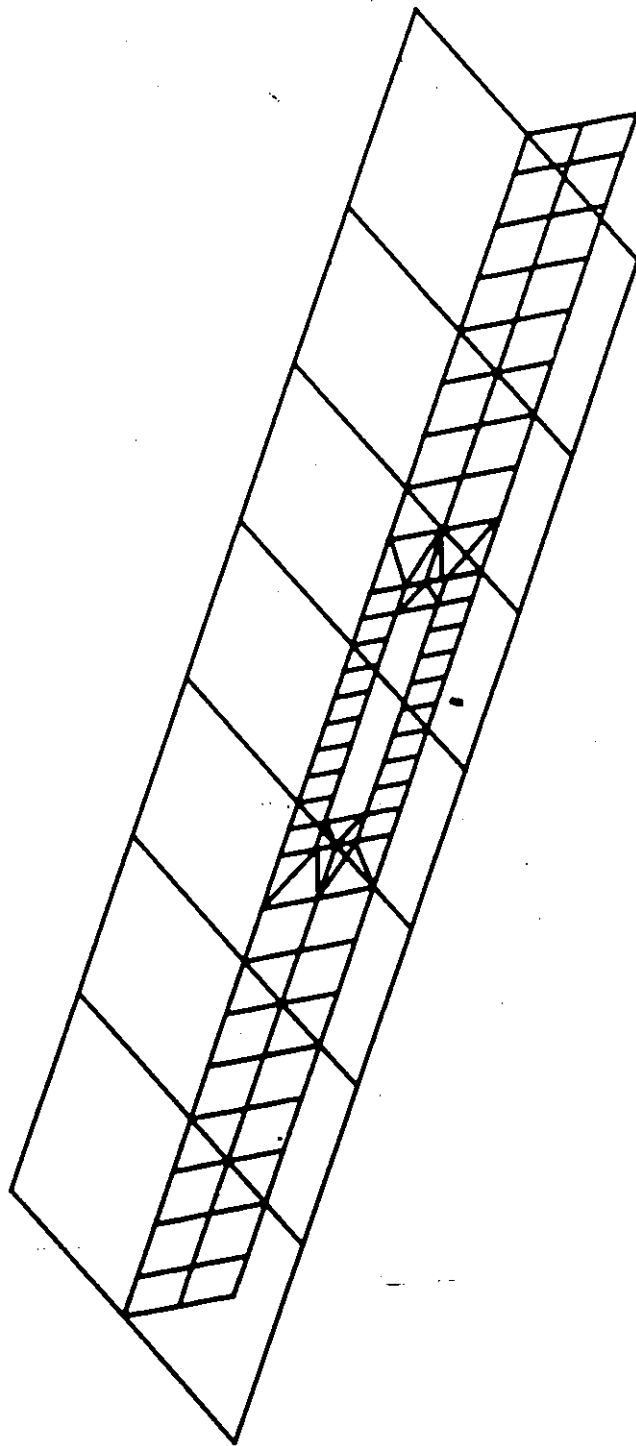
Figure 3.9: Typical Finite Element Mesh for a Tee Beam With
an Opening at Midspan
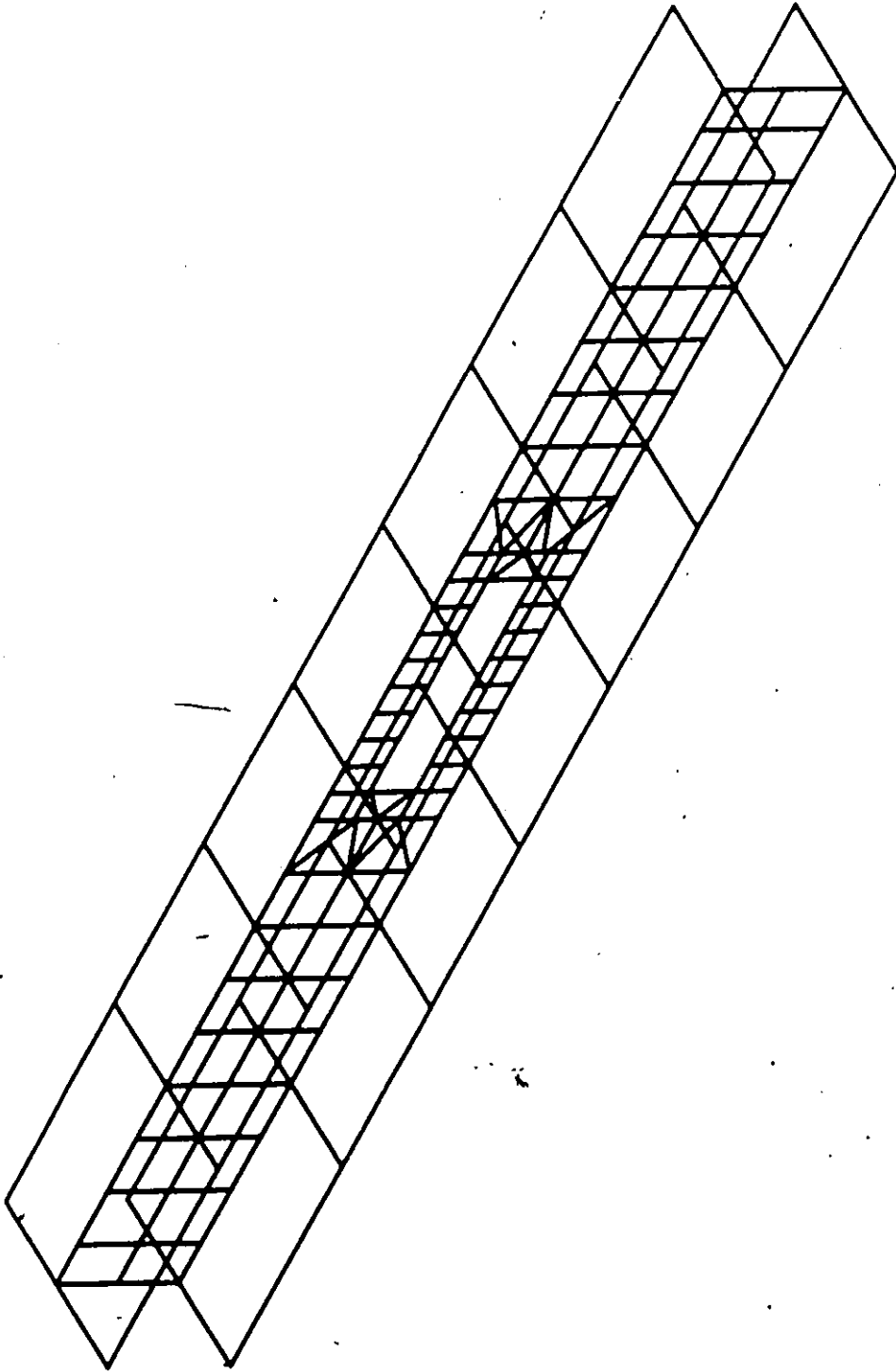
Figure 3.10: Typical Finite Element Mesh for an I Beam With an Opening at Midspan
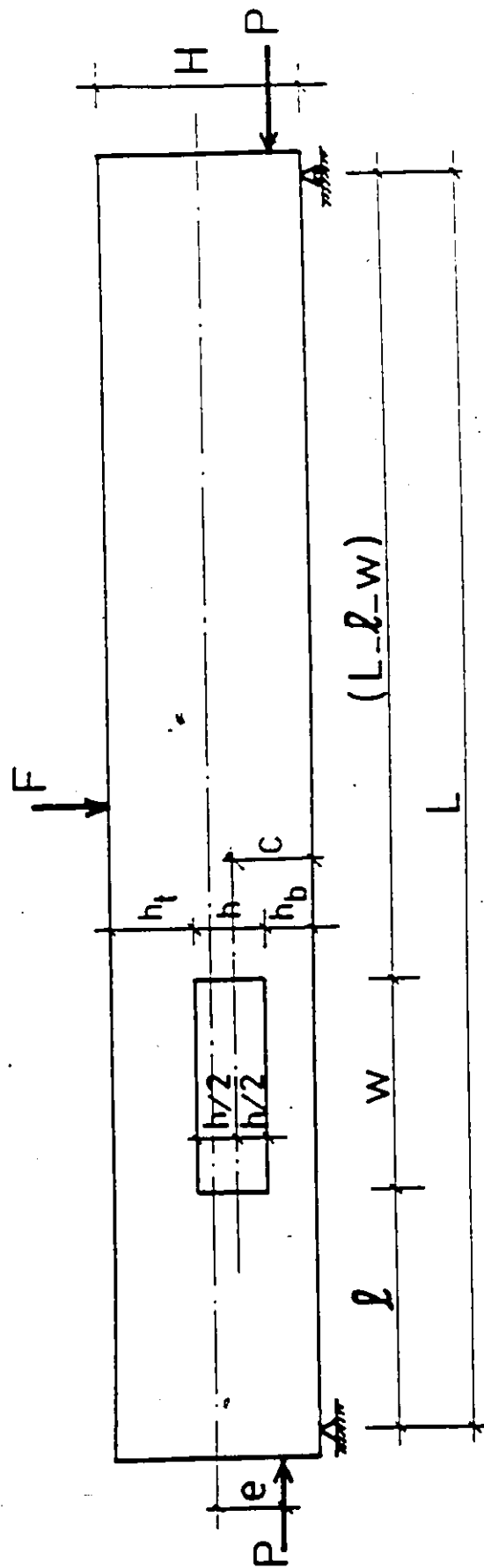
Figure 4.1: Typical Beam Layout
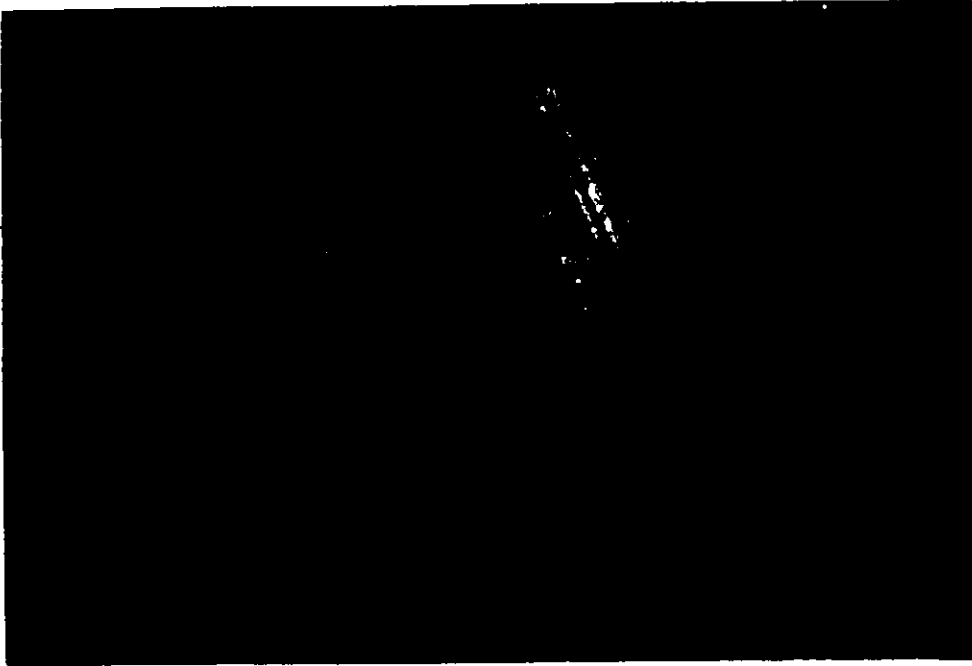
Figure 4.2: Deformed End of the Prestressing Wires
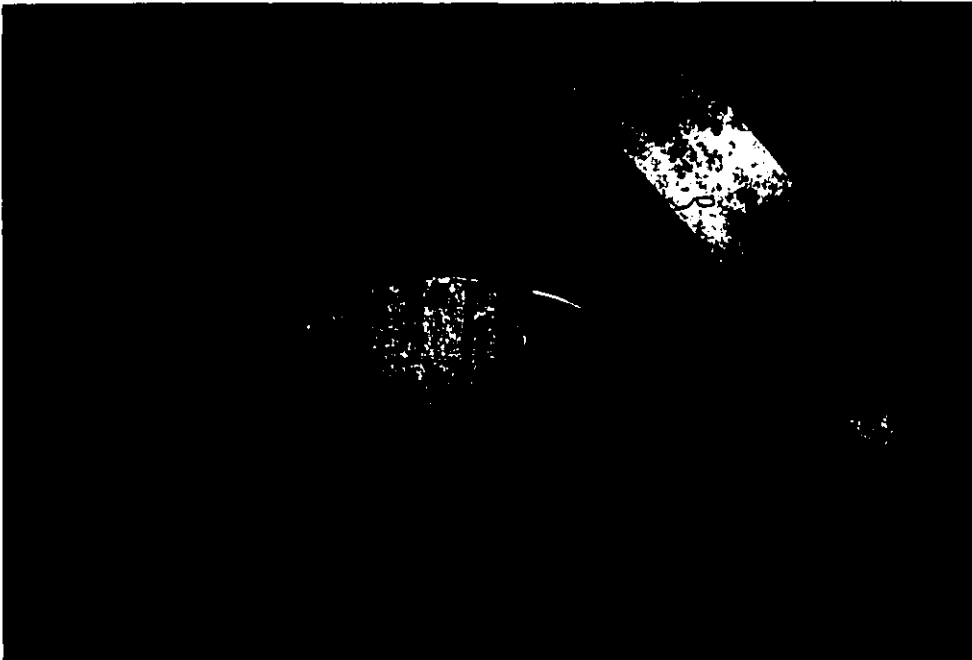
Figure 4.3: Prestressing End Bearing Plates
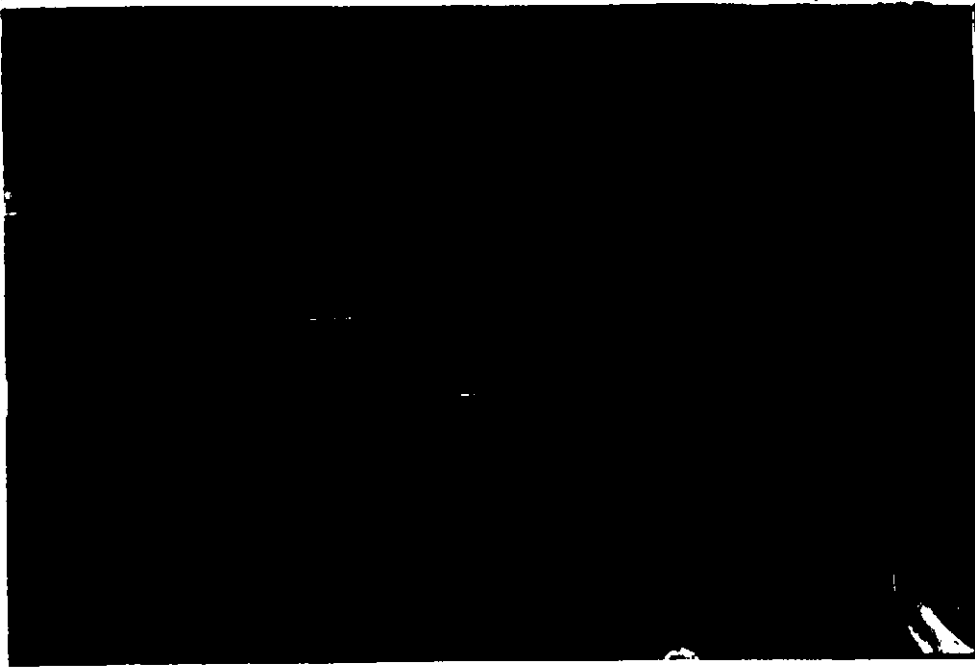
Figure 4.4:   The Hydraulic Prestressing Jack
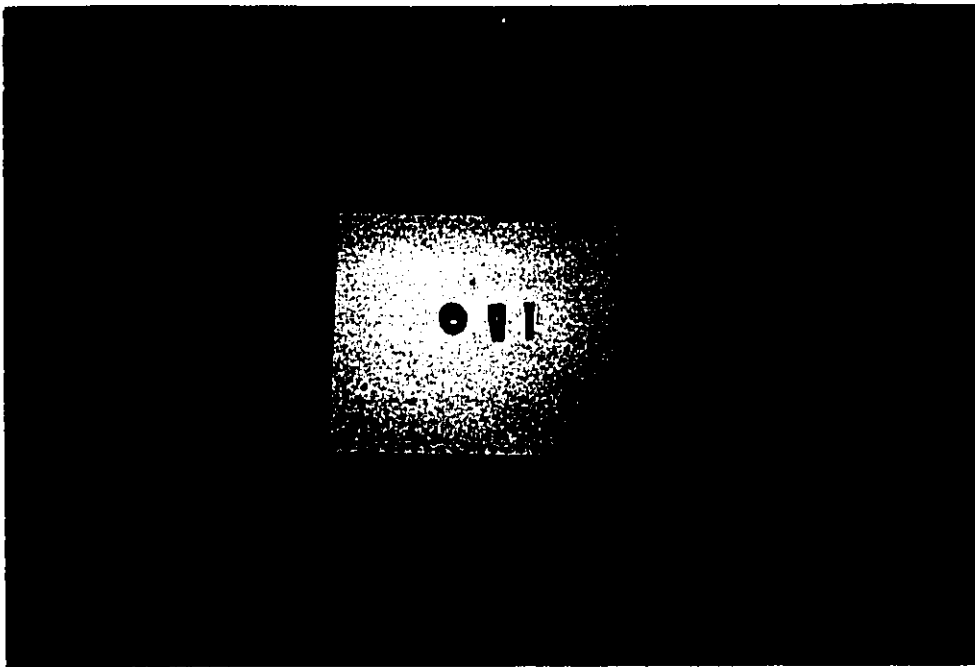
Figure 4.5:   Anchorage Wedges and Cylinders

Figure 4.6: Cylindrical Wire Load Cell
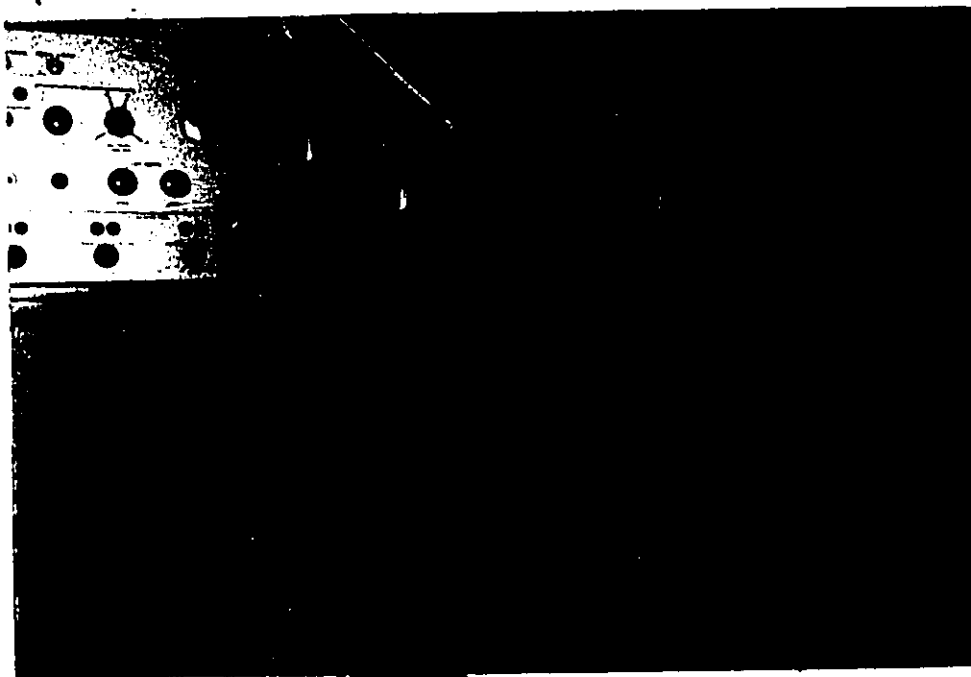
Figure 4.7: Gil... ...ctronic Console Unit

Figure 4.3: Gilmore Model 433-20 Actuator
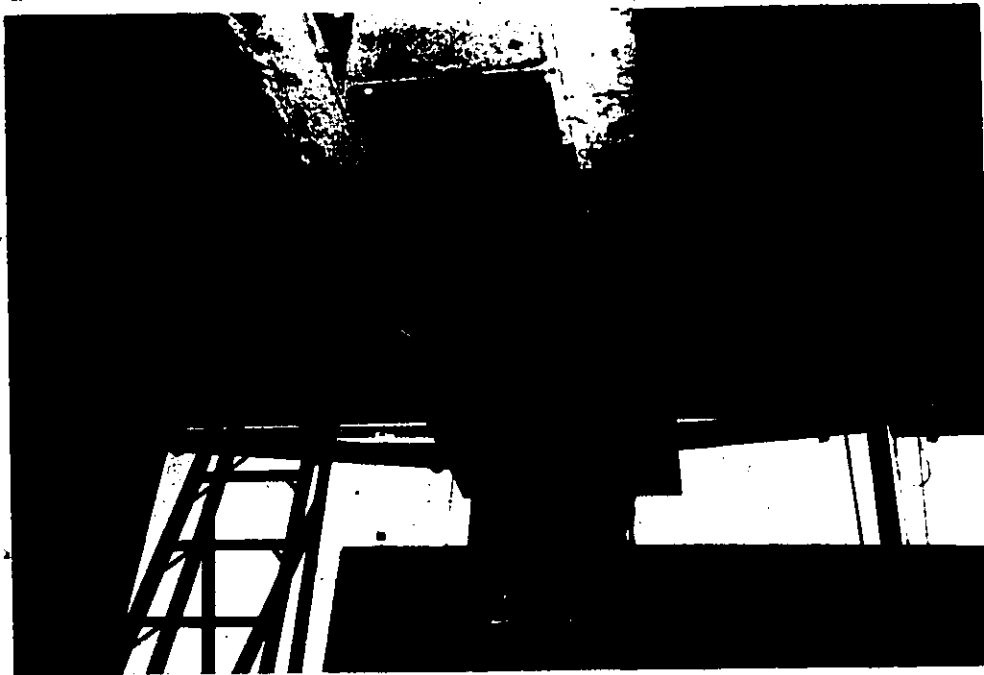
Figure 4.9: Supporting Flanges at the Top End of the Actuator
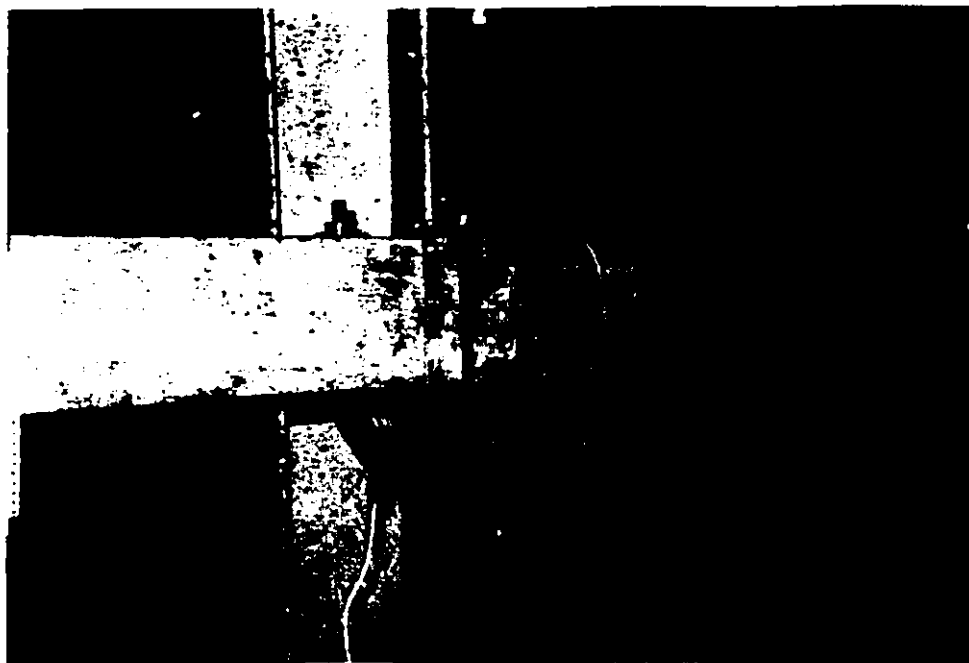
Figure 4.10: Loading Assembly at the Bottom End of the
Actuator

Figure 4.11: End.Support of Beams
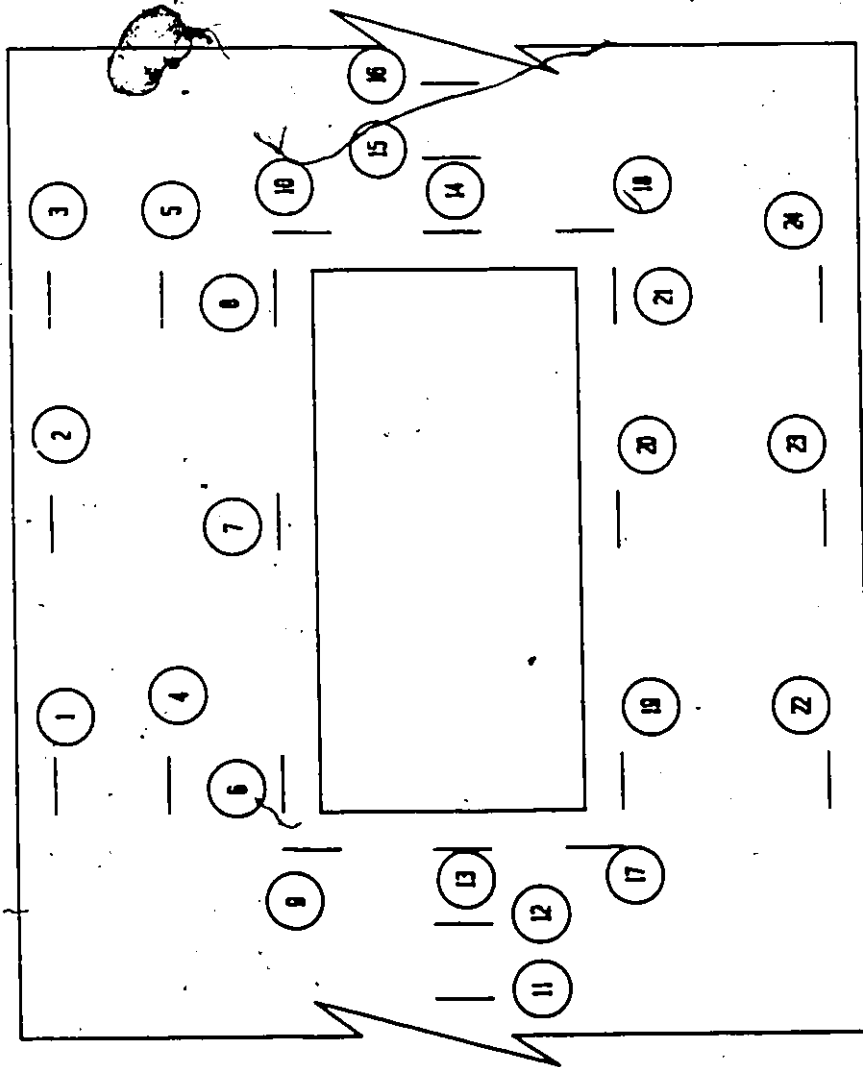
Figure 4.12: Strain gage Arrangement Around the Opening
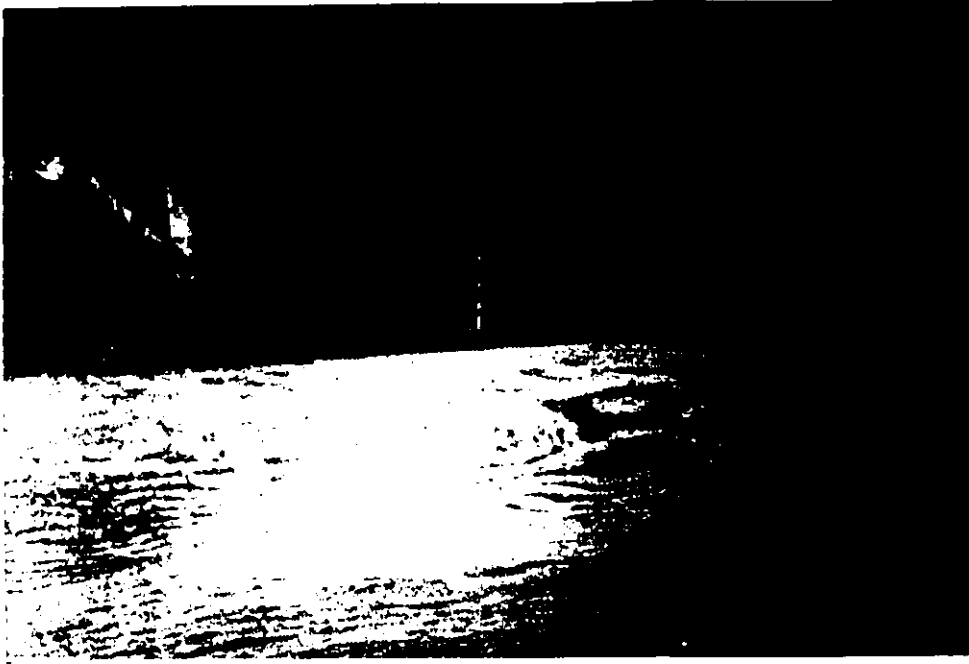
Figure 4.13:   Dytran 3100A 25(g) Accelerometer

Figure 4.14:   LVDT Supporting Arrangement
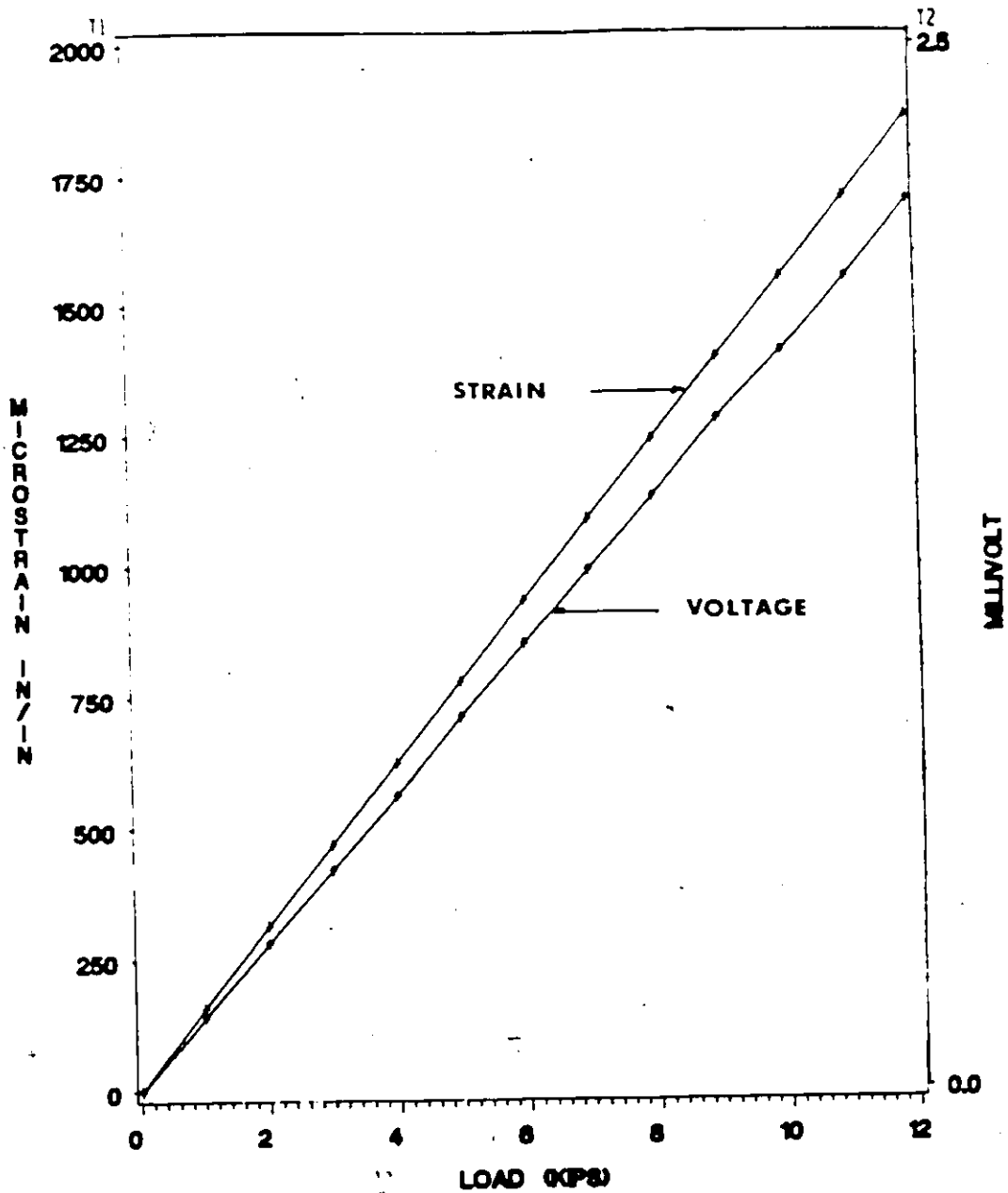
Figure 4.15: Calibration Curve for Load Cell #27

Figure 4.16: Megadac Data Acquisition Unit

Strain Gage

Red

Black

White

I./ P. (−) {A/D}
ENG. {SCI}
A

I./ P. (+) {A/D}
ENG. {SCI}
B

B. C. {SCI}
ENG. {SCI}
G.
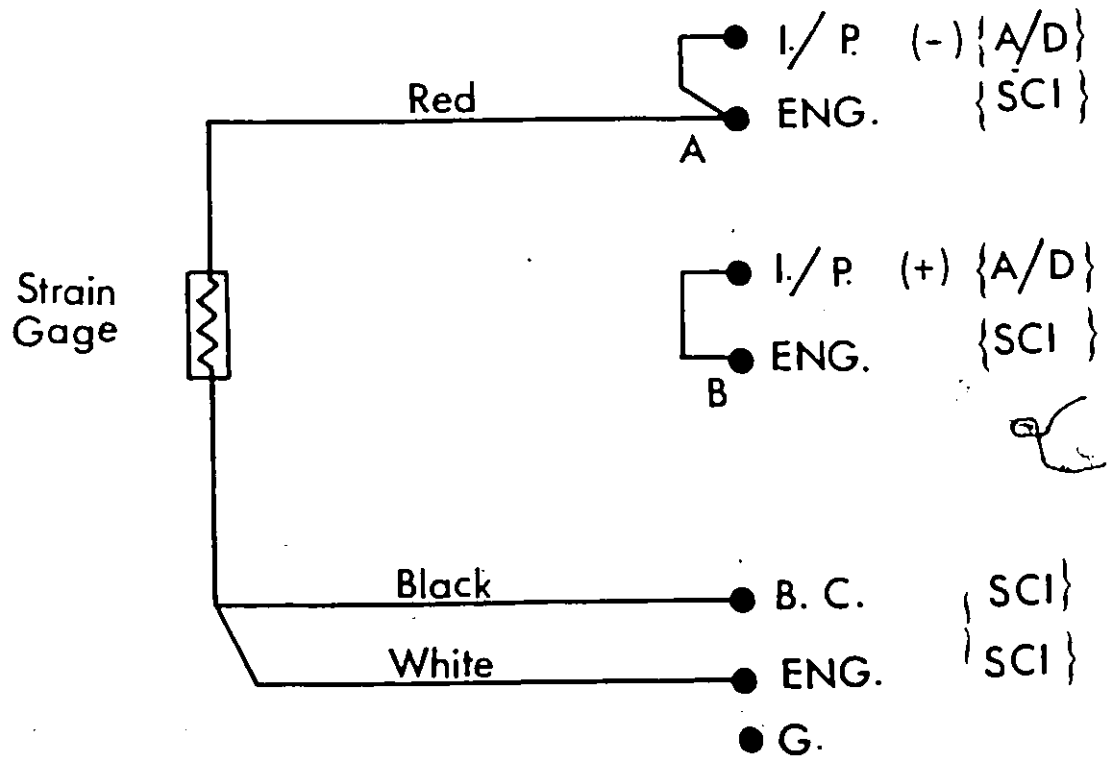
Figure 4.17: Schematic Circuit Diagram for Quarter Bridge 3-Wire Current Energization

Figure 4.18: Schematic Circuit Diagram for Full Bridge Current Energization
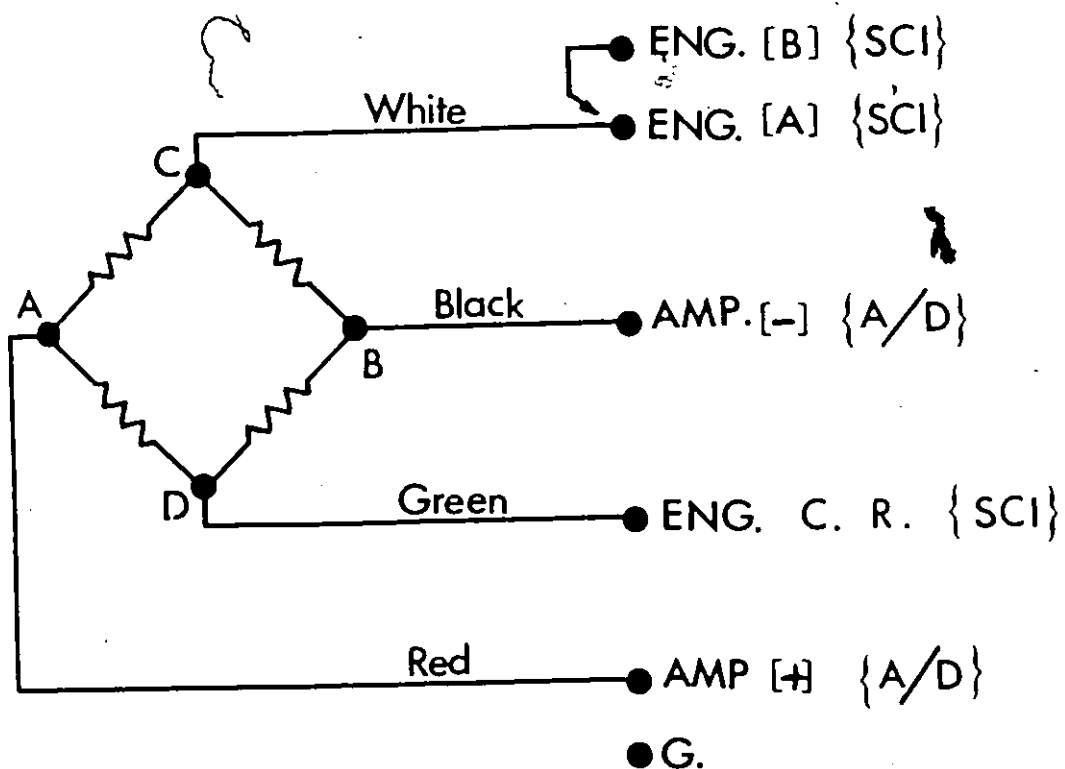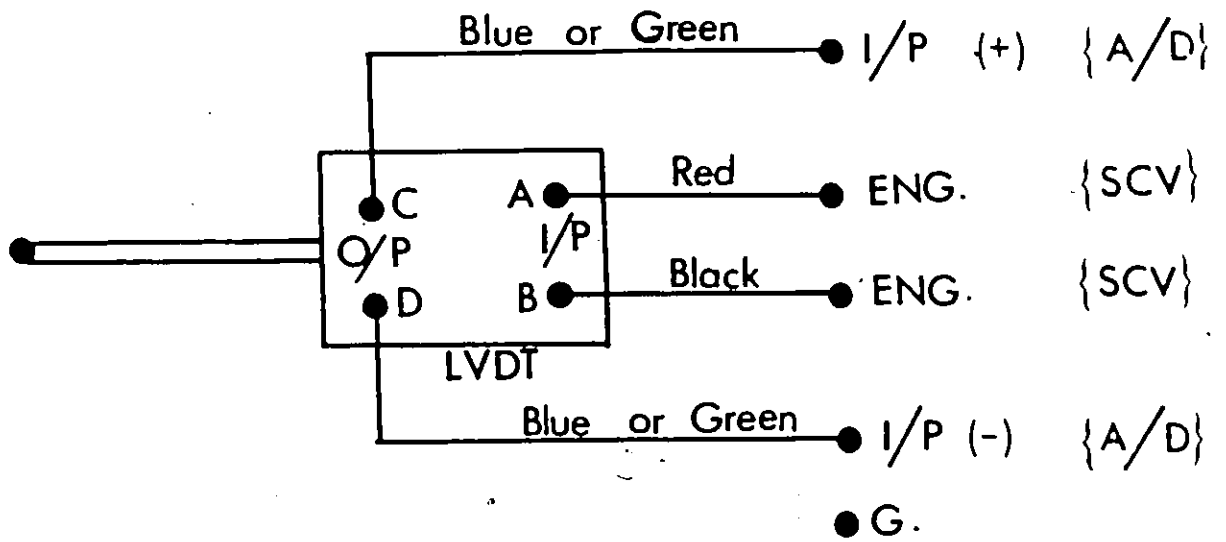
Figure 4.19: Schematic Circuit Diagram for Full Bridge Voltage Energization
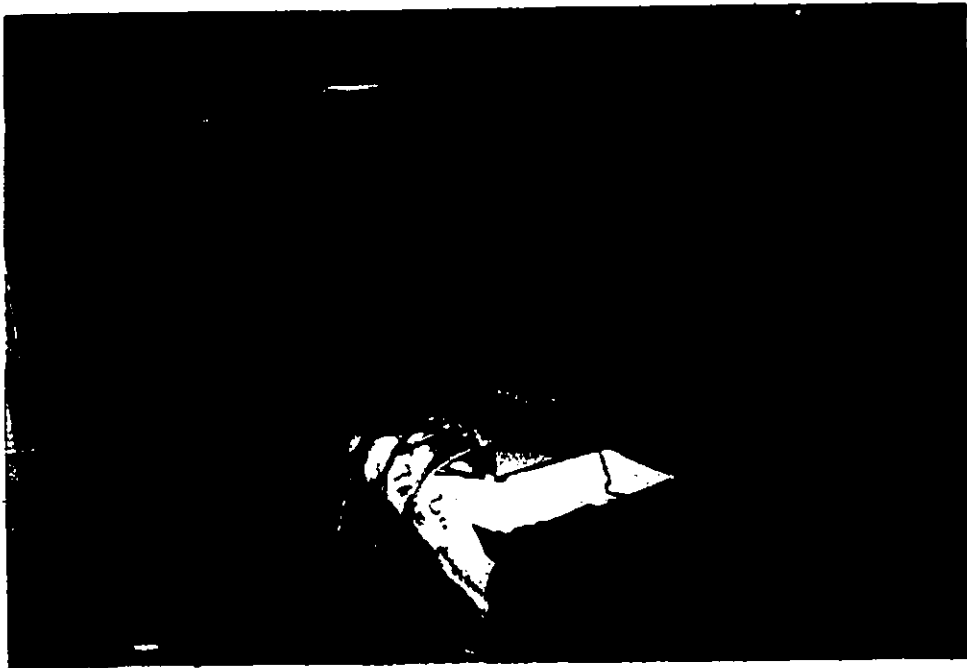
Figure 4.20: A/D, SCI-1, SCI-2 and SCV Terminal Boxes
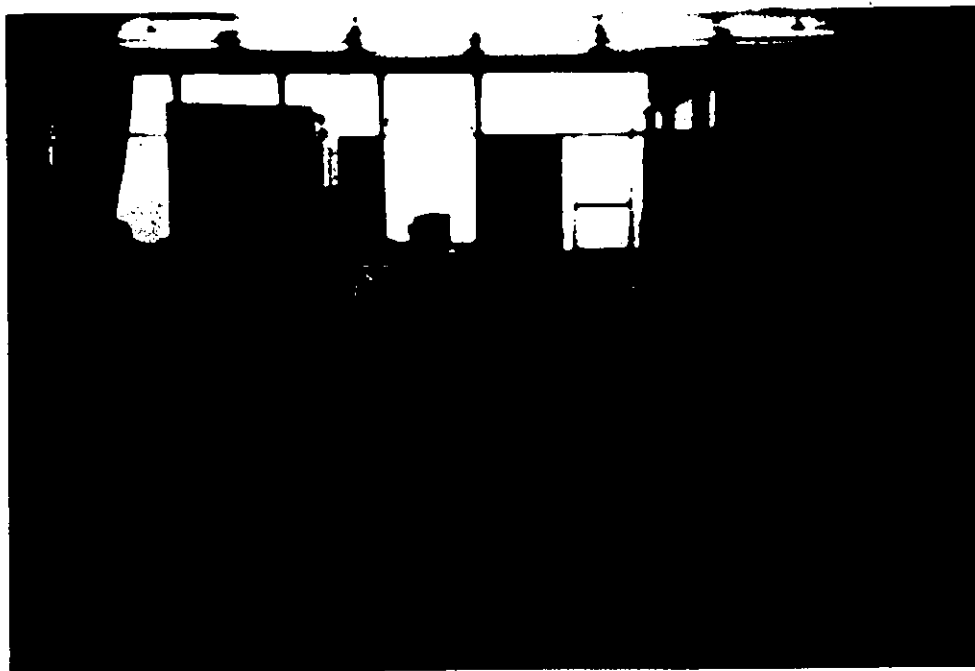
Figure 4.21: FFT Dynamic Analyzer

Figure 4.22: Typical SD375 Plot With Possible Display Variables
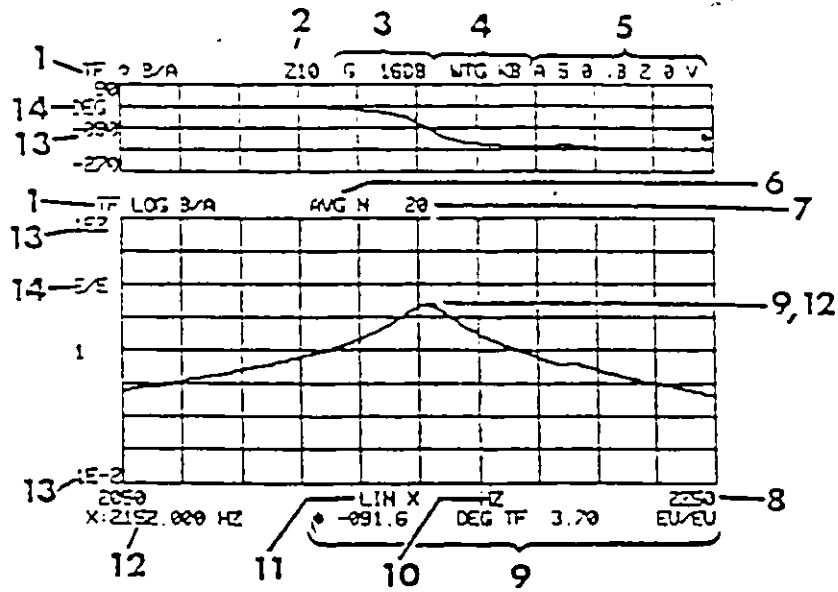
1. Upper & lower trace identification

2. Spectrum mode
   NB—narrowband
   Z—zoom

3. Output display gain

4. Weighting selected:
   H—Hanning
   KB—Kaiser Bessel
   TR—transient
   R—rectangular

5. Ch A & Ch B selected full scale input level

6. Averager mode:
   AVG—linear sum
   EXPO—exponential
   PK—peak

7. Ensemble number N or average time T in seconds

8. Full scale analysis range or memory period

9. Y-axis cursor value for upper & lower trace in deg, γ^1, dB, V, V^1, EU, EU^1, EU^1/Hz

10. X-axis parameter in Hz, kcpm, order, sec

11. X-axis format in Lin or Log

12. X-axis cursor value in Hz, kcpm, order, msec

13. Scaled grid values of Y-axis display parameter

14. Y-axis parameter for upper & lower trace in deg, γ^1, dB, V, EU, PSD

$1 g \cong EU \cong 10 \ m/s^2$

Figure 4.23:   Dytran Model 4121 Power Supply Unit
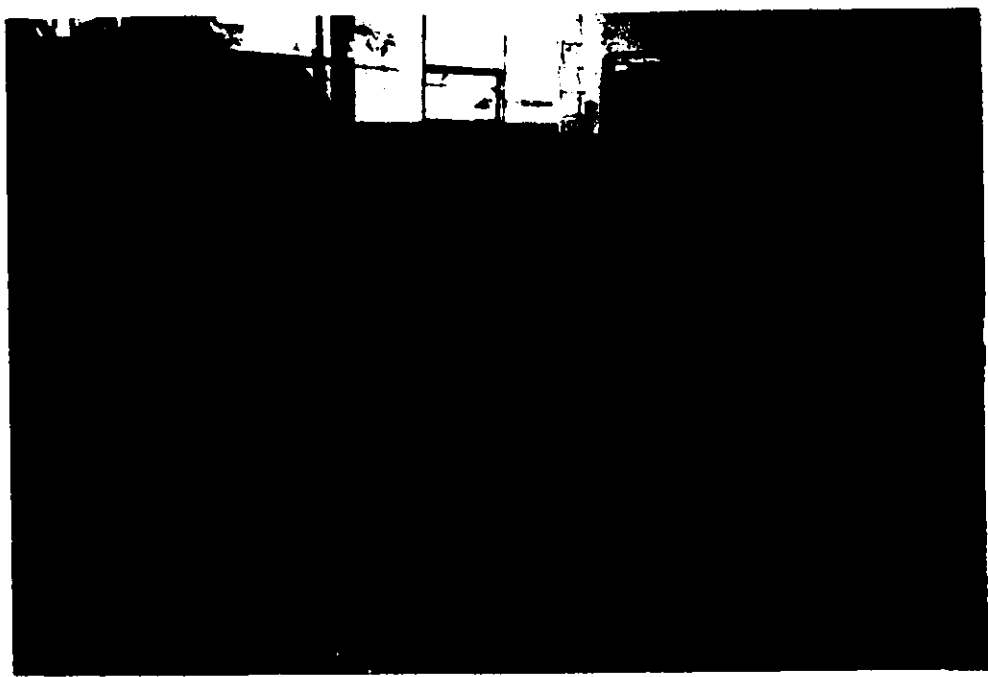
Figure 4.24:   Stirrups Supporting Arrangement
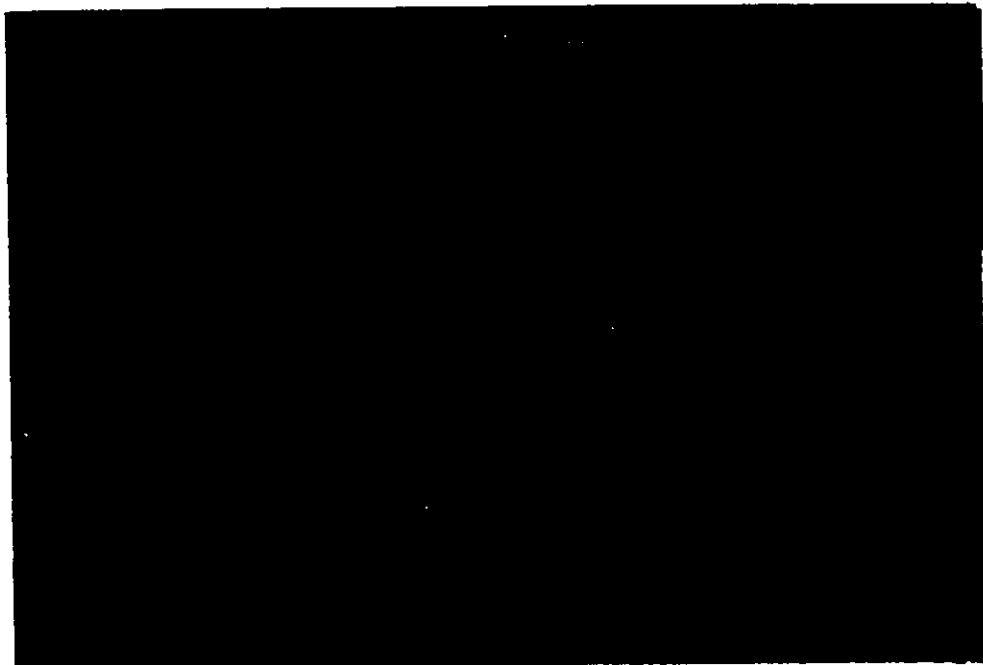
Figure 4.25: Opening Region Before Casting

LIN A   NB   G 30DB WTG H A 0.05 V RMS

2E-3

V

0

0.0   LIN X   HZ   200.0

X: 17.0   HZ   Y(A) 1.57E-3 V   PEAK T   5
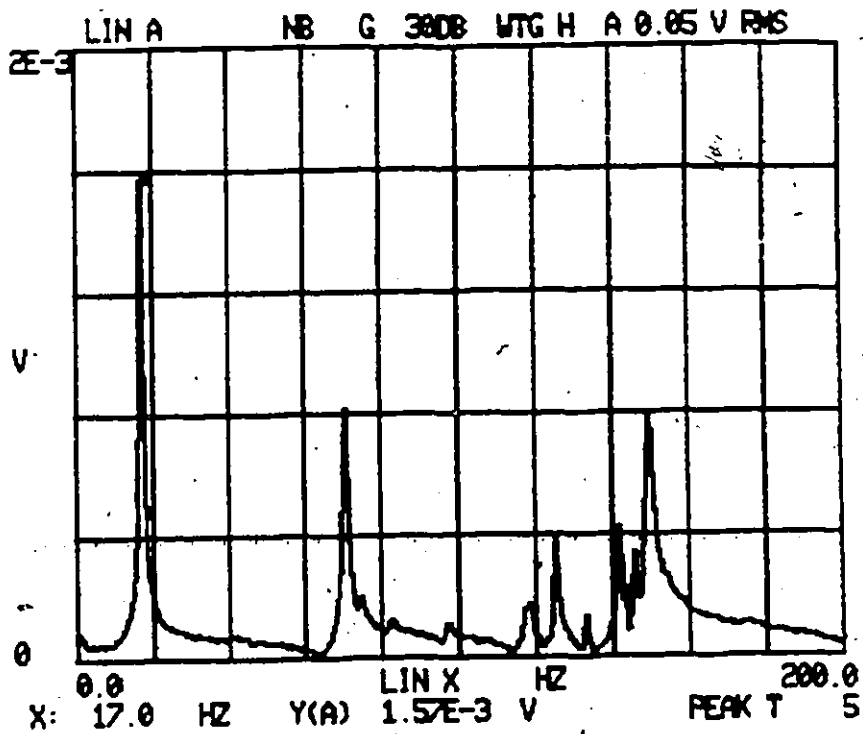
Figure 5.1: Free Vibration Response Curve For Beam   #4
Without the Loading Jack Resting at Midspan

LIN A   NB   G 30DB WTG H A 0.05 V RMS

2E-3

V

0

0.0   LIN X   HZ   200.0

X: 18.0   HZ   Y(A) 1.77E-3 V   PEAK T   5
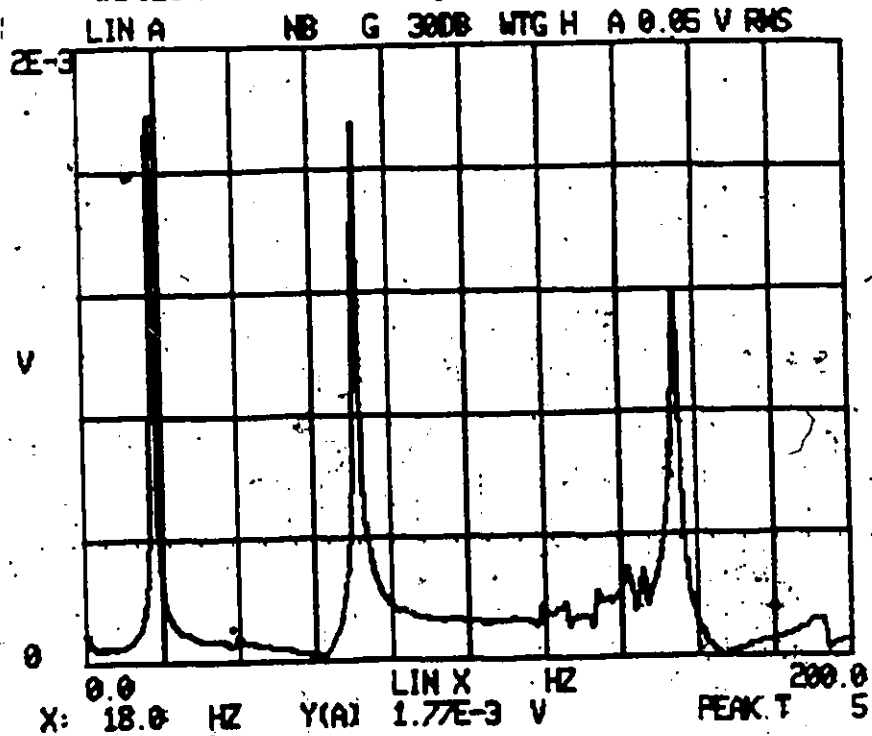
Figure 5.2: Free Vibration Response Curve For Beam #4 with
the Loading Jack Resting at Midspan.

**TYPICAL SWEEP TEST SINUSOIDAL
FORCING FUNCTION AT 10 HZ**
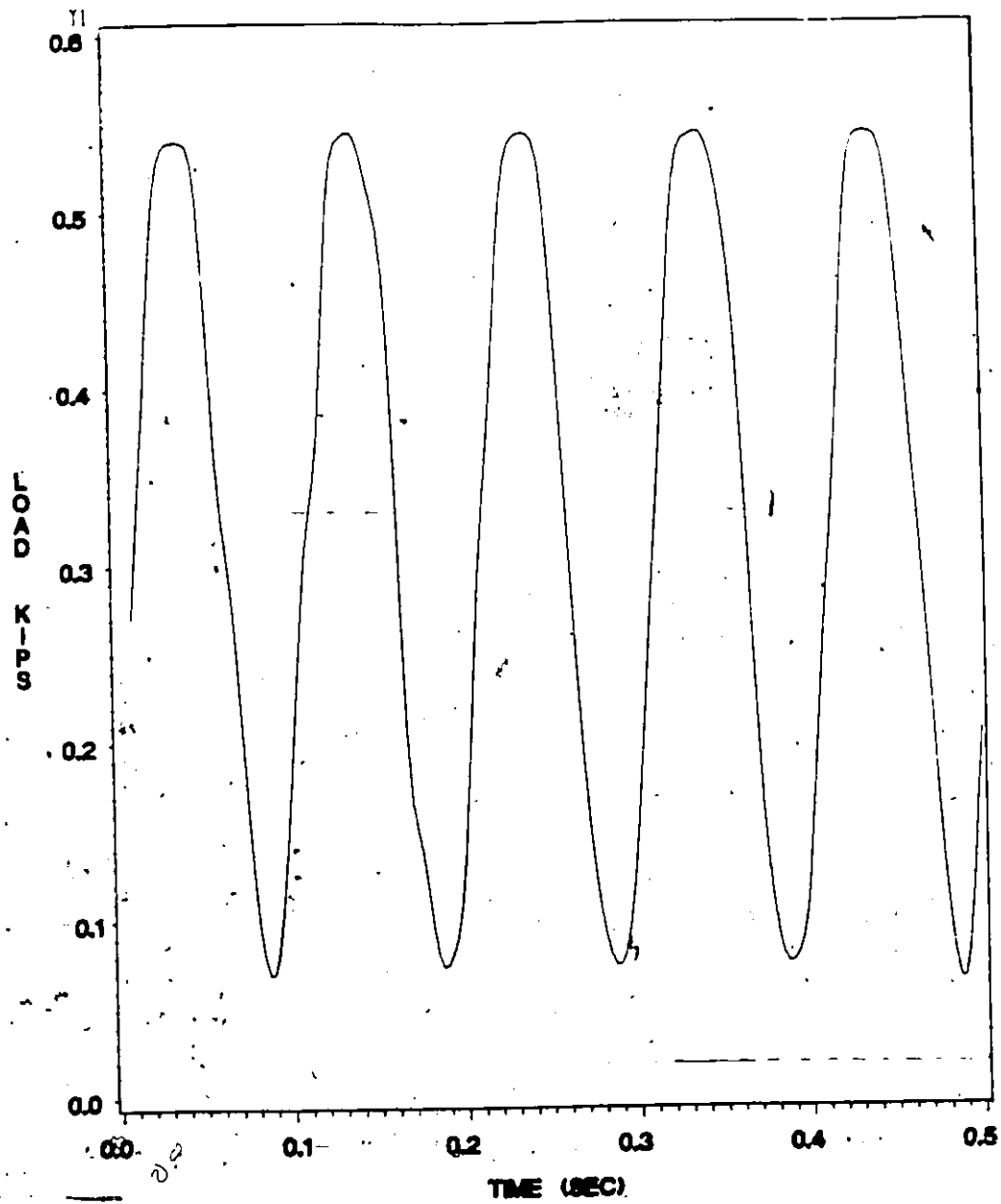
Figure 5.3: Sinusoidal Forcing Function for the Sweep Test
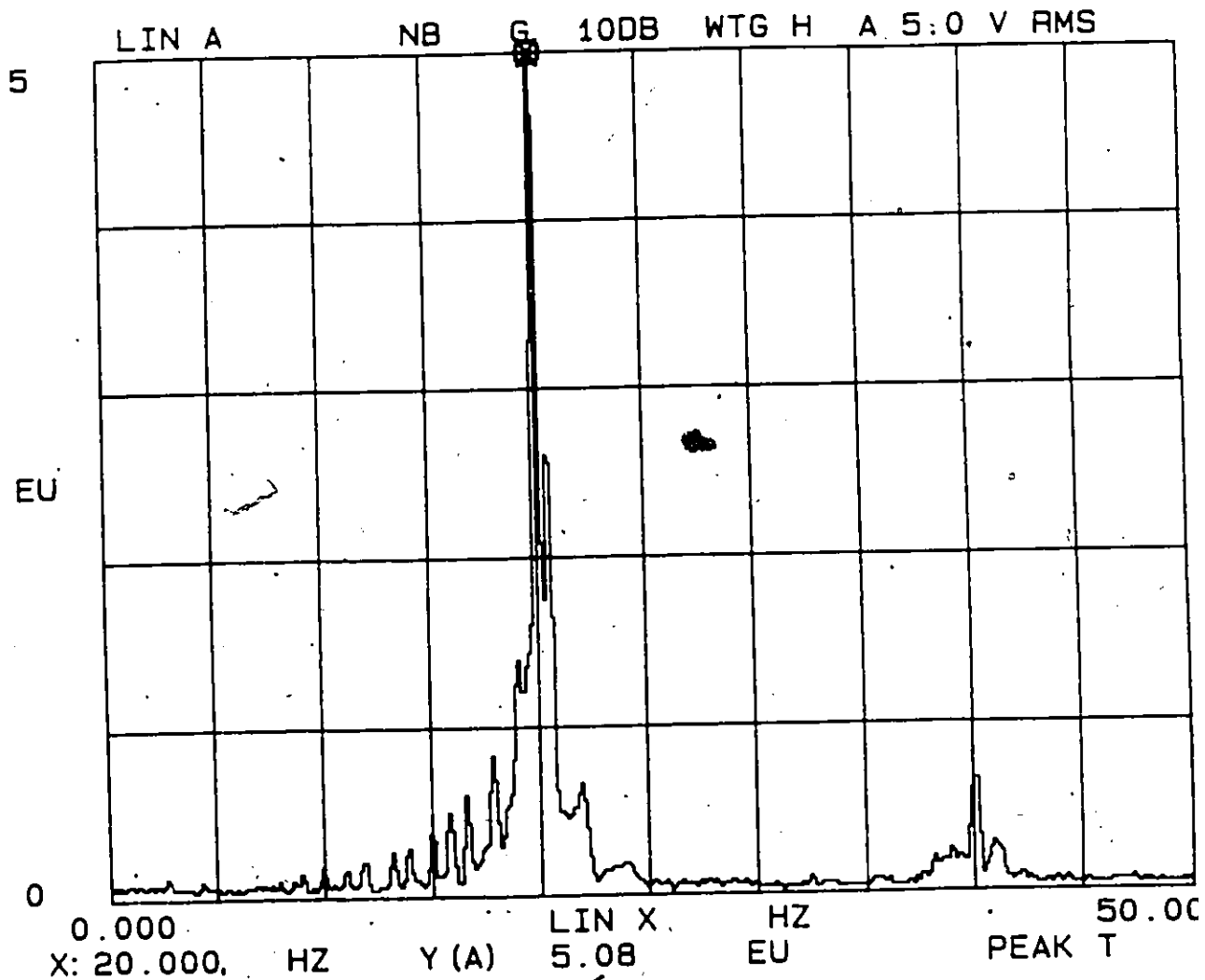
Figure 5.4:   Frequency Spectrum   of Beam   #1 Before   Fatigue
               Loading
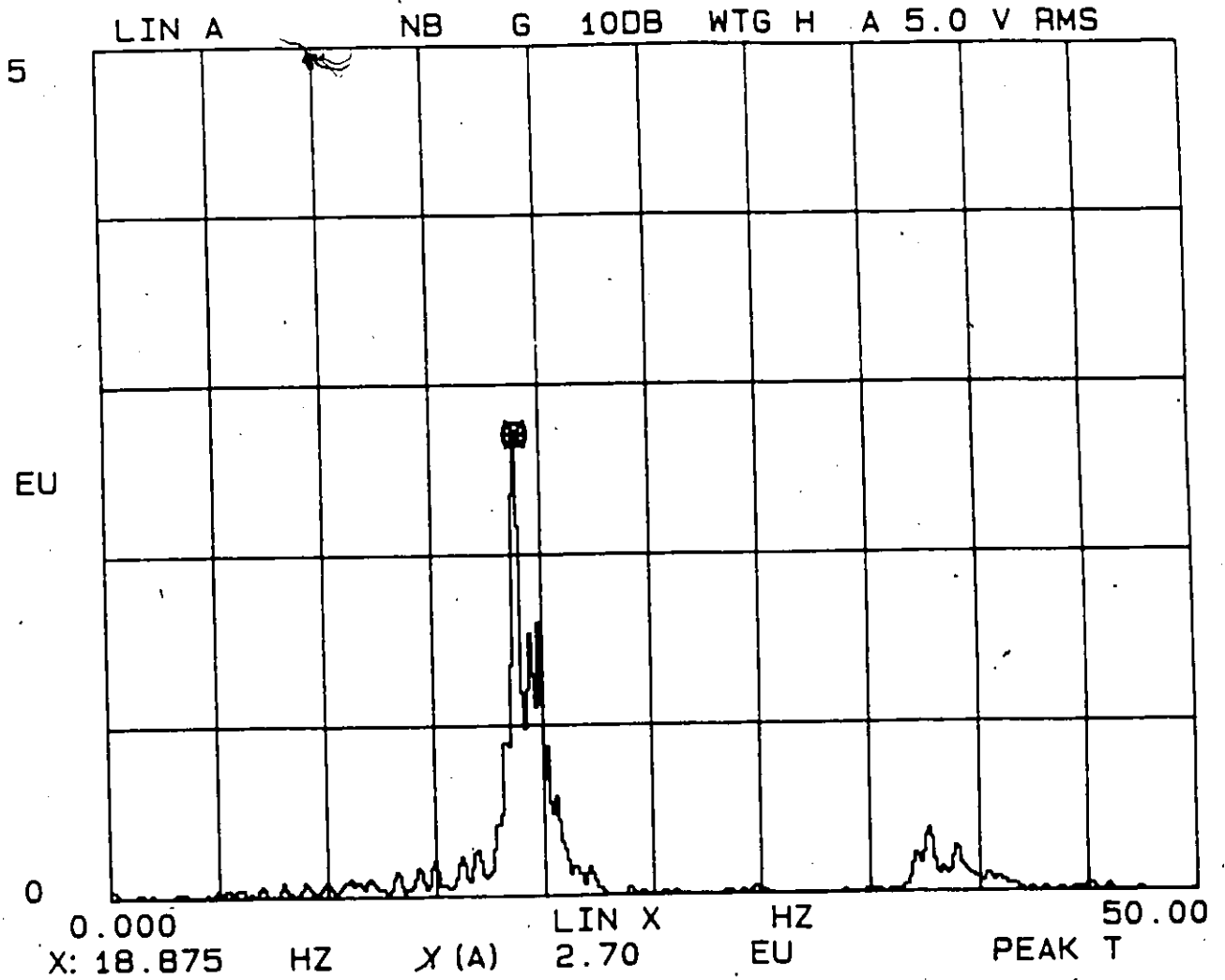
Figure 5.5: Frequency Spectrum of Beam #1 After Fatigue Loading
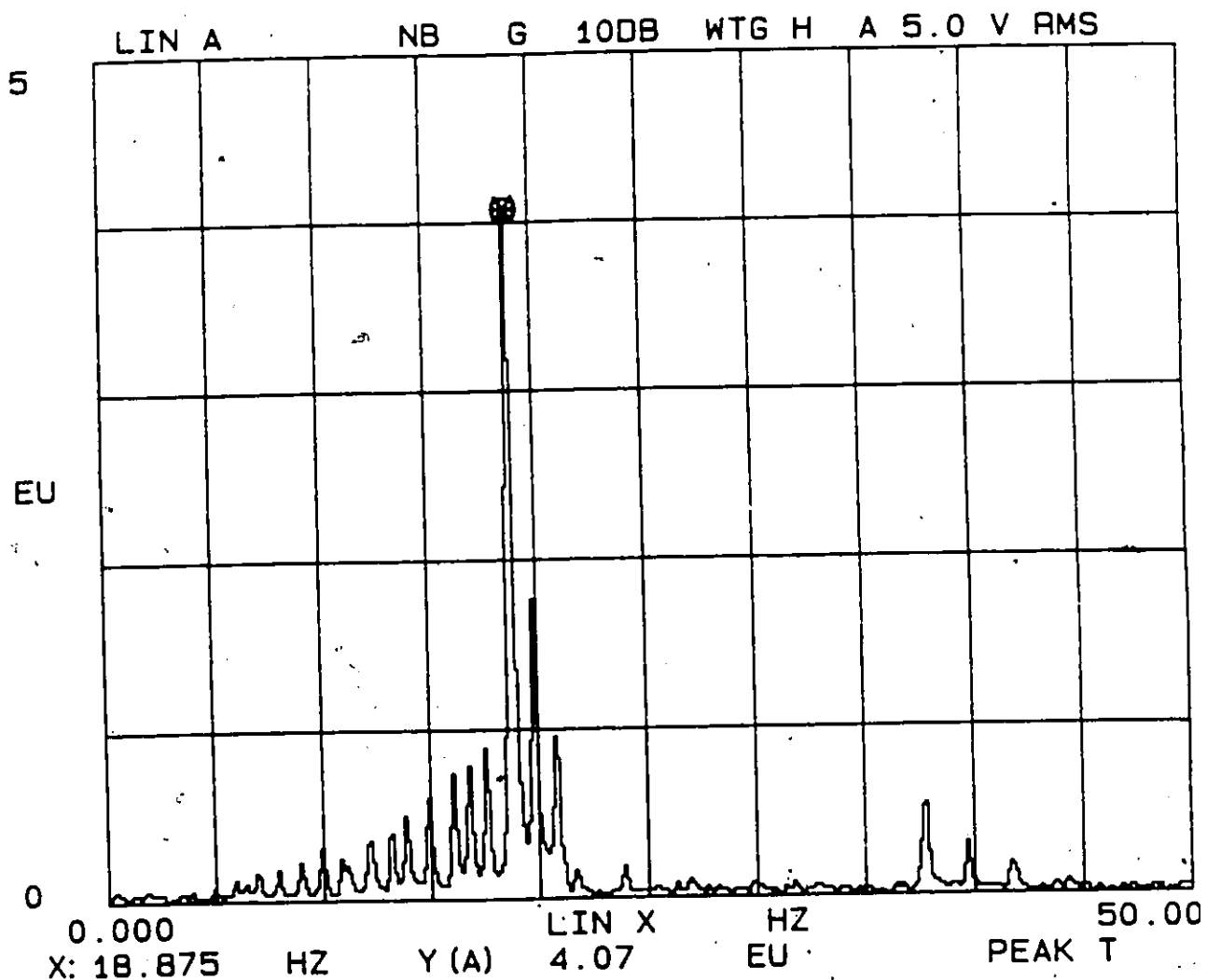
Figure 5.6: Frequency Spectrum of Beam #2 Before Fatigue Loading

LIN A   NB   G   10DB   WTG H   A 5.0 V RMS

X: 17.875 · HZ   Y (A)   2.90   EU   PEAK T
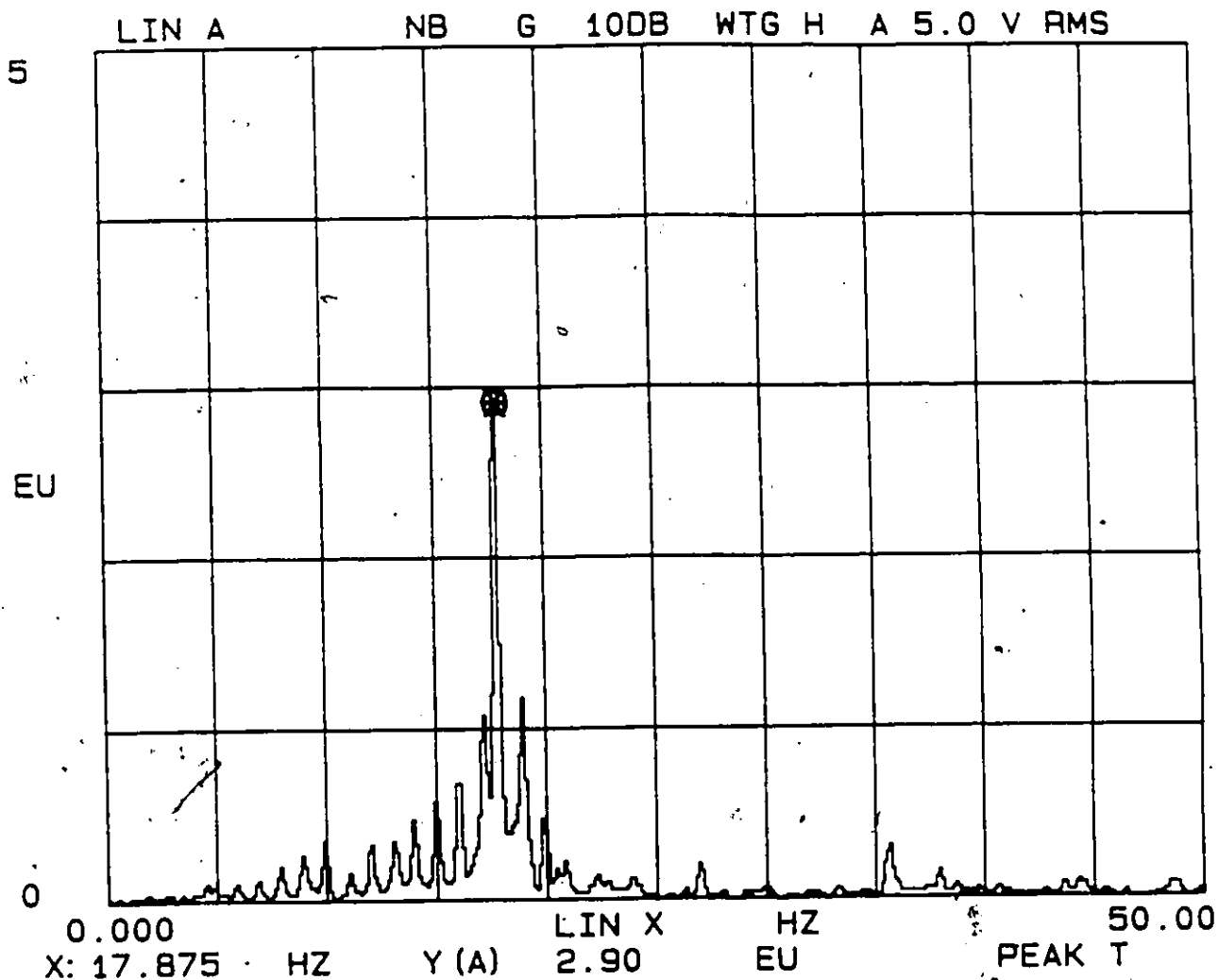
Figure 5.7: Frequency Spectrum of Beam #2 After Fatigue Loading
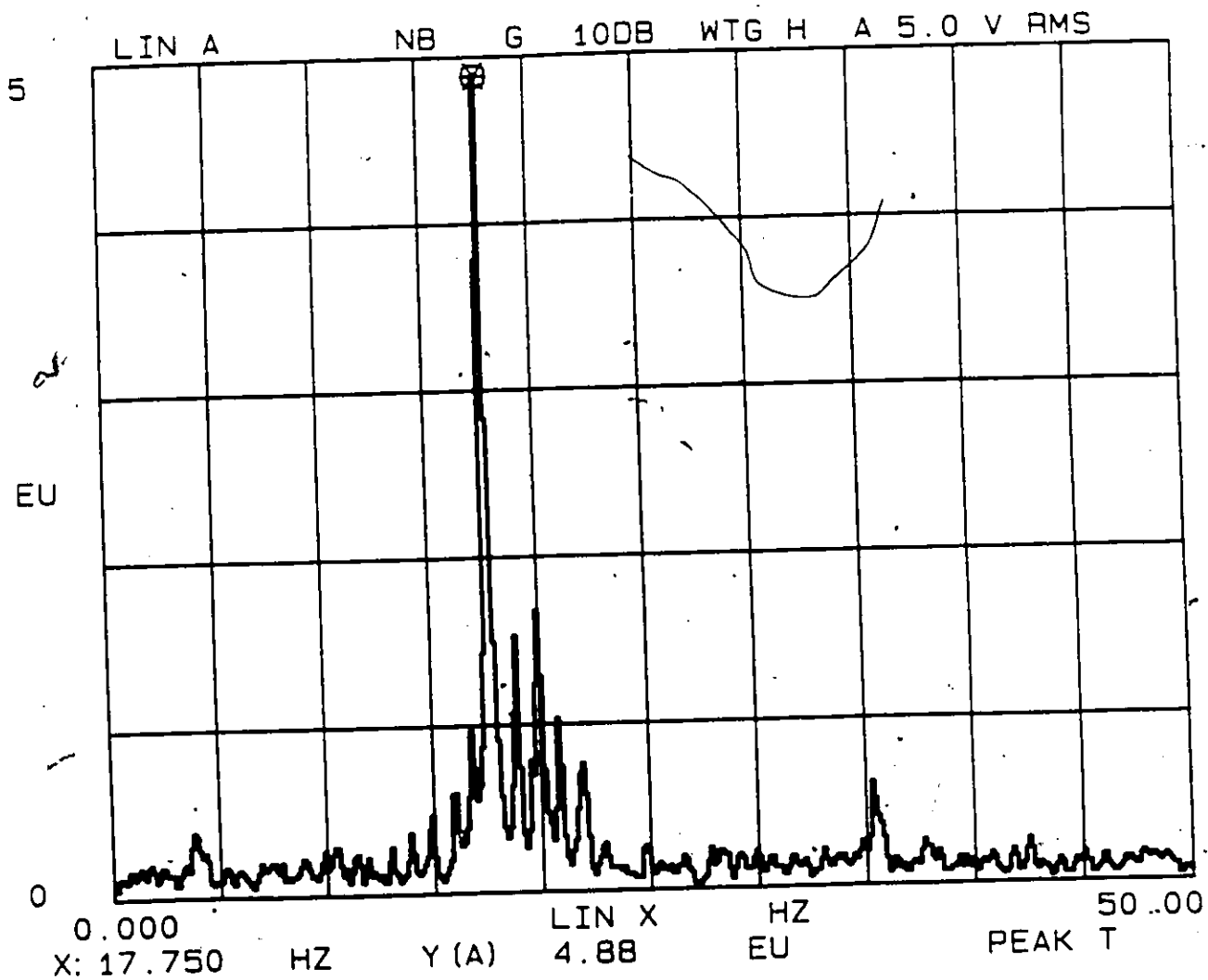
Figure 5.8: Frequency Spectrum of Beam #3 Before Fatigue Loading
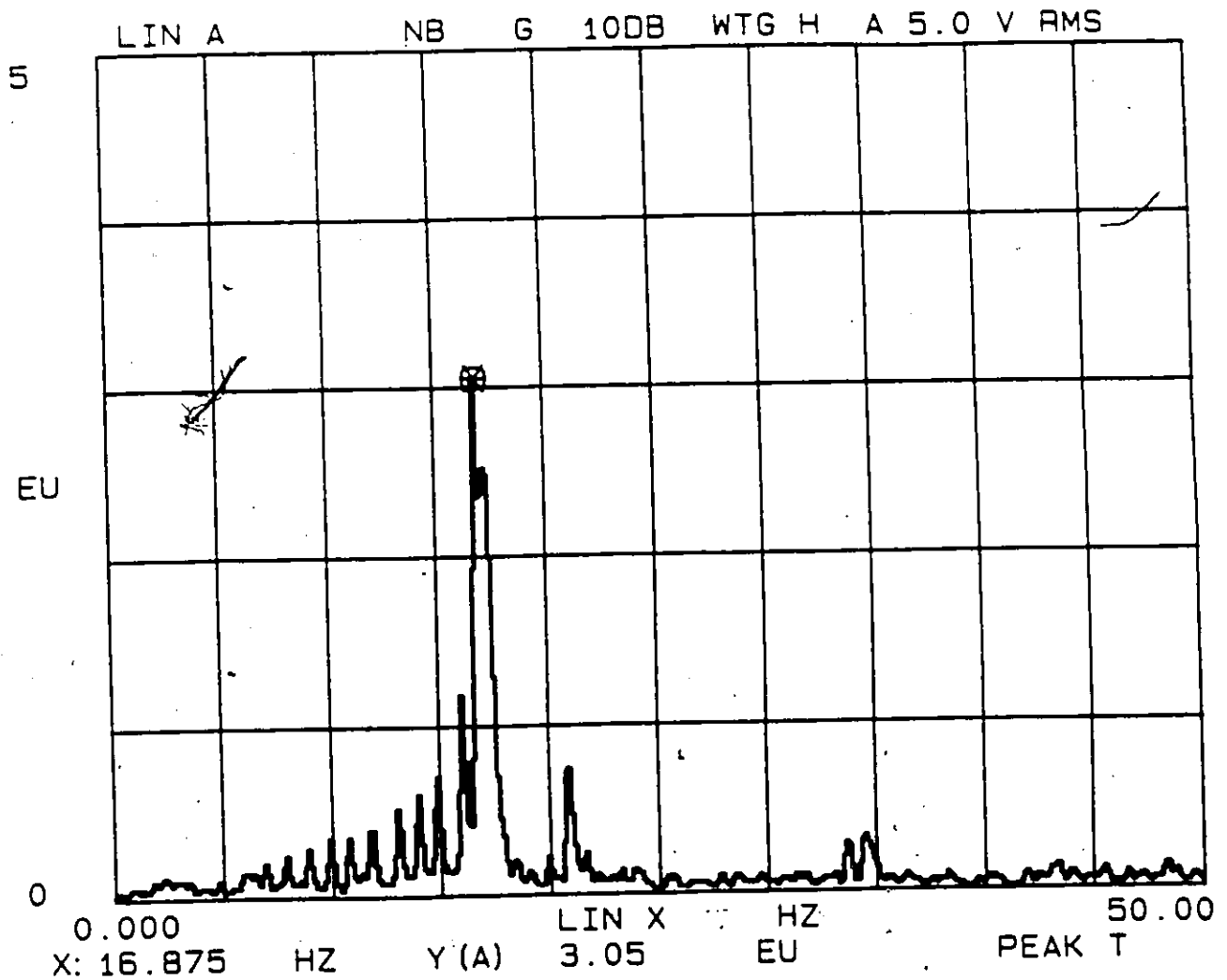
Figure 5.9: Frequency Spectrum of Beam #3 After Fatigue Loading

LIN A   NB G 10DB WTG H A 5.0 V RMS
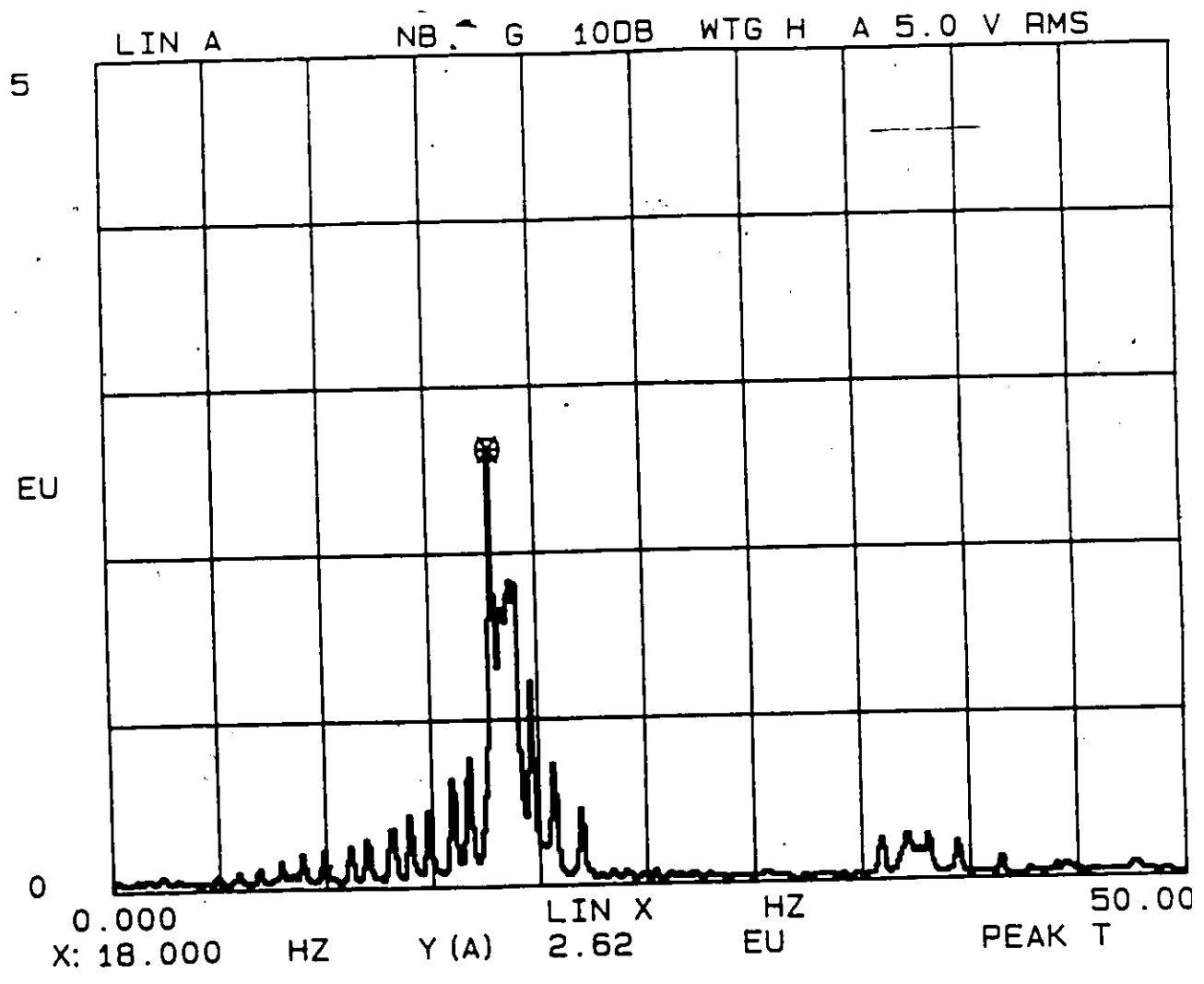
Figure 5.10: Frequency Spectrum of Beam #4 Before Fatigue Loading

LIN A   NB   G   10DB   WTG H   A 5.0 V RMS

X: 16.875   HZ   Y(A)   2.60   EU   PEAK T
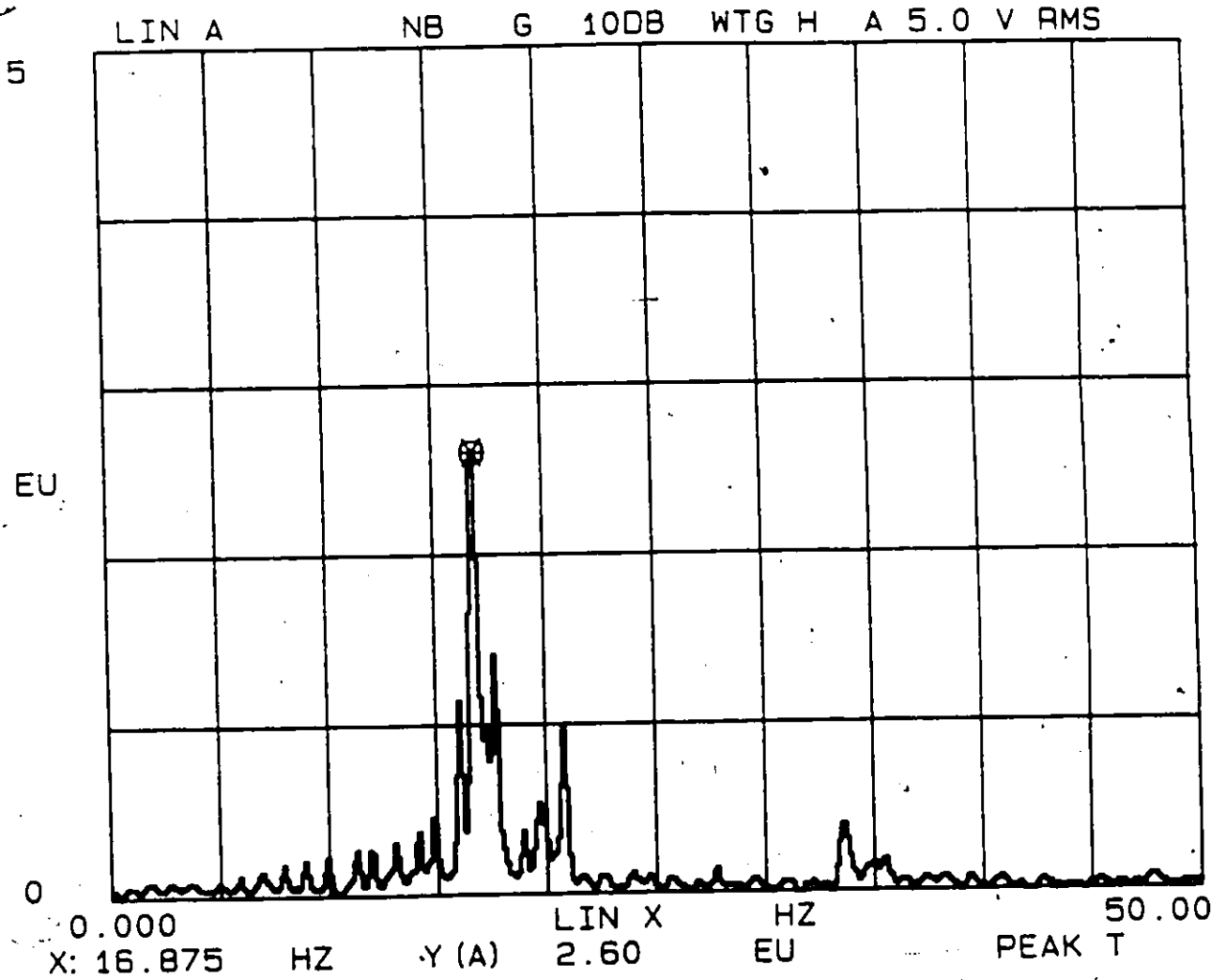
Figure 5.11:   Frequency Spectrum of Beam #4 After Fatigue
                   Loading
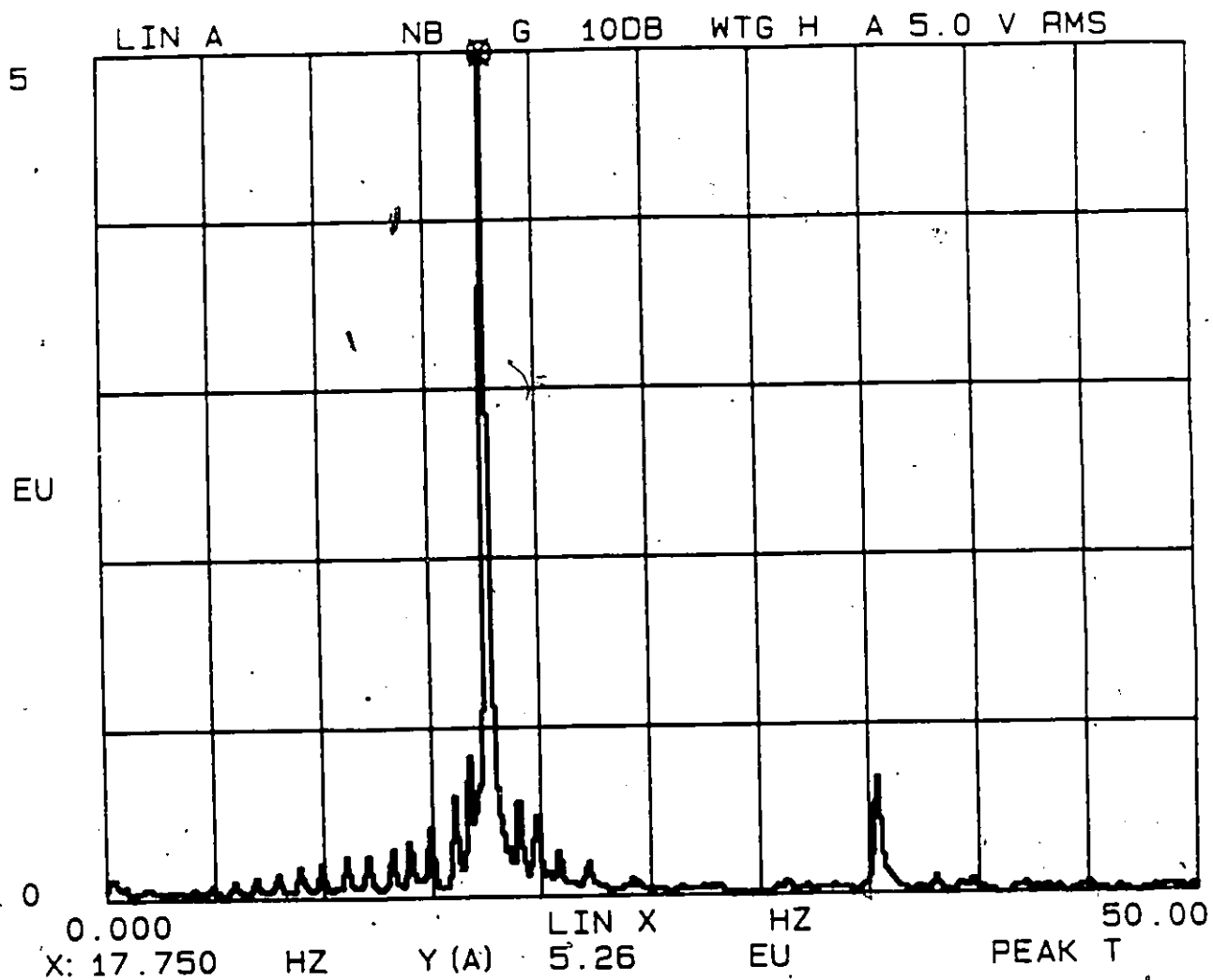
Figure 5.12: Frequency Spectrum of Beam #5 Before Fatigue Loading
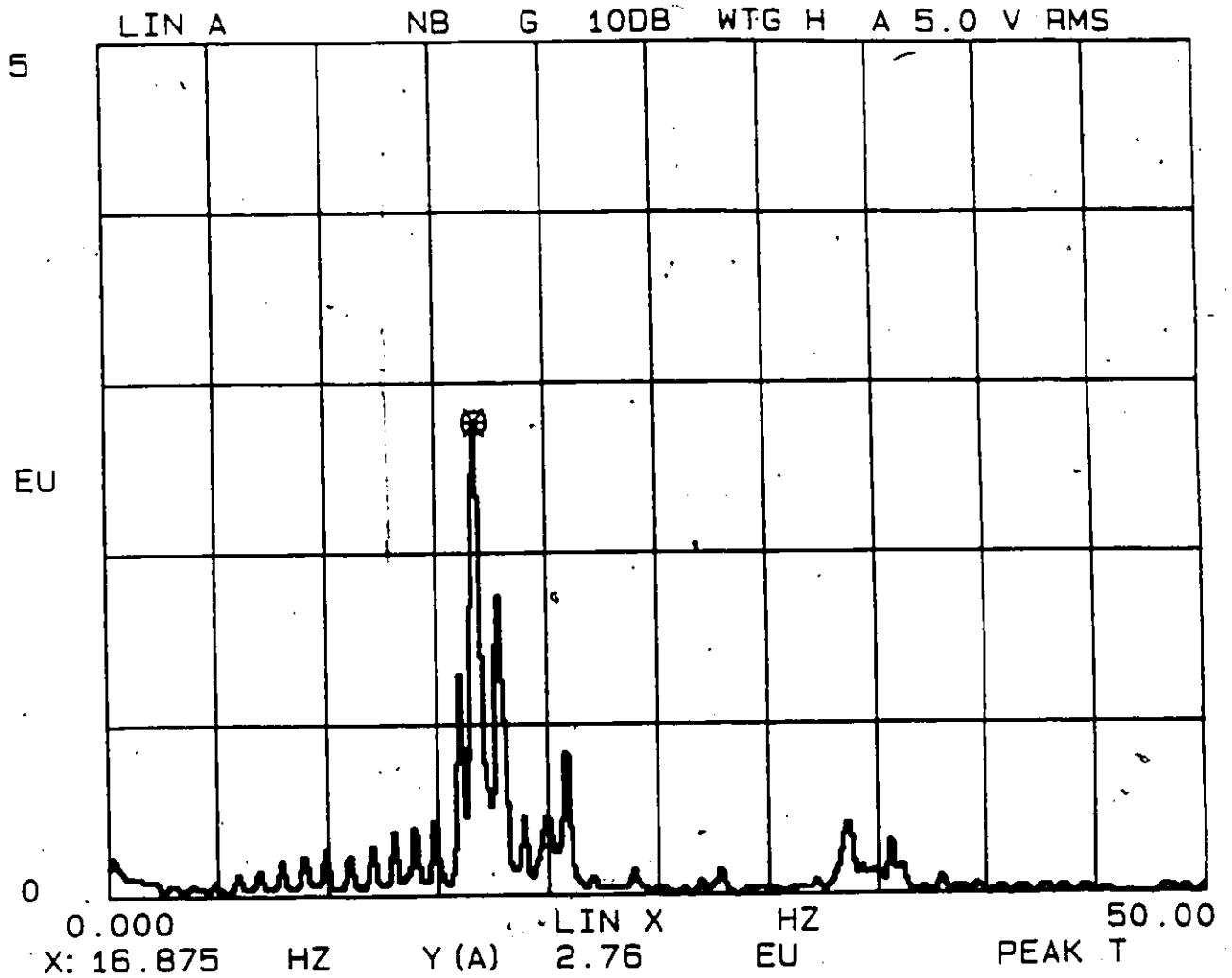
Figure 5.13: Frequency Spectrum of Beam #5 After Fatigue Loading

LIN A   NB   G   10DB   WTG H   A 5.0 V RMS

```
5

EU

0
  0.000                        LIN X      HZ              50.00
  X: 19.375    HZ    Y(A)    3.06        EU            PEAK T
```
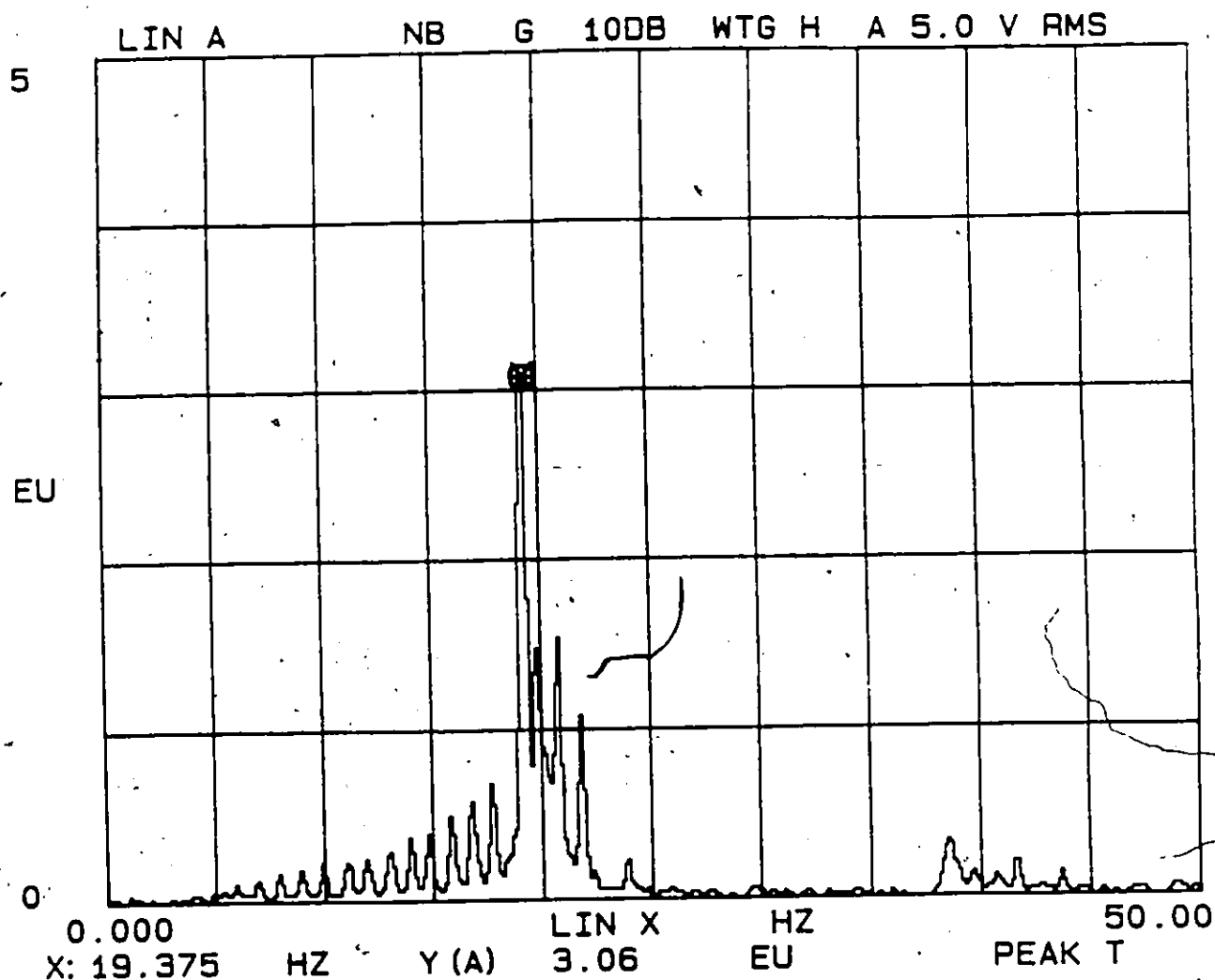
Figure 5.14: Frequency Spectrum, of Beam #6 Before Fatigue
              Loading .
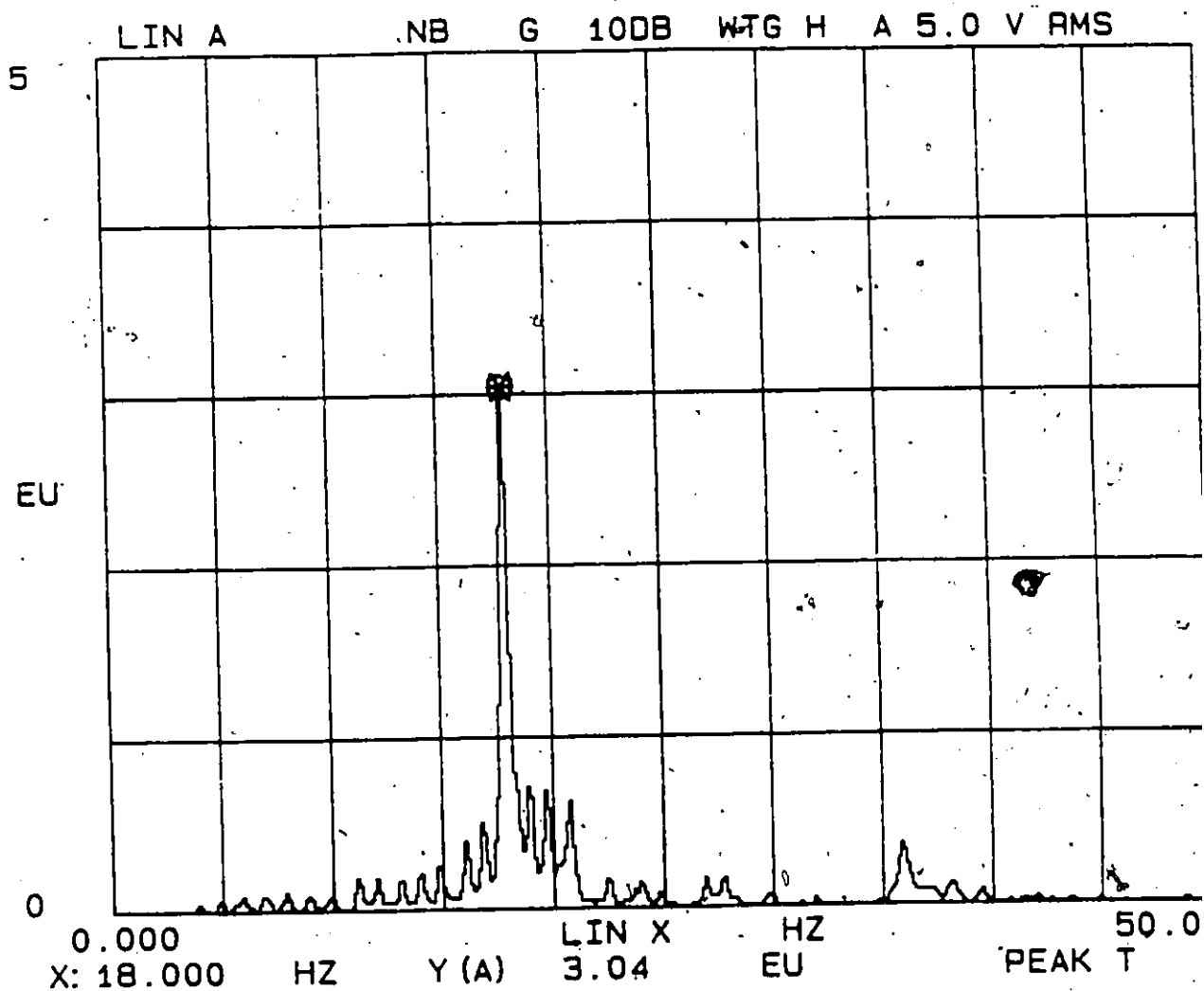
Figure 5.15: Frequency Spectrum of Beam #6 After Fatigue Loading
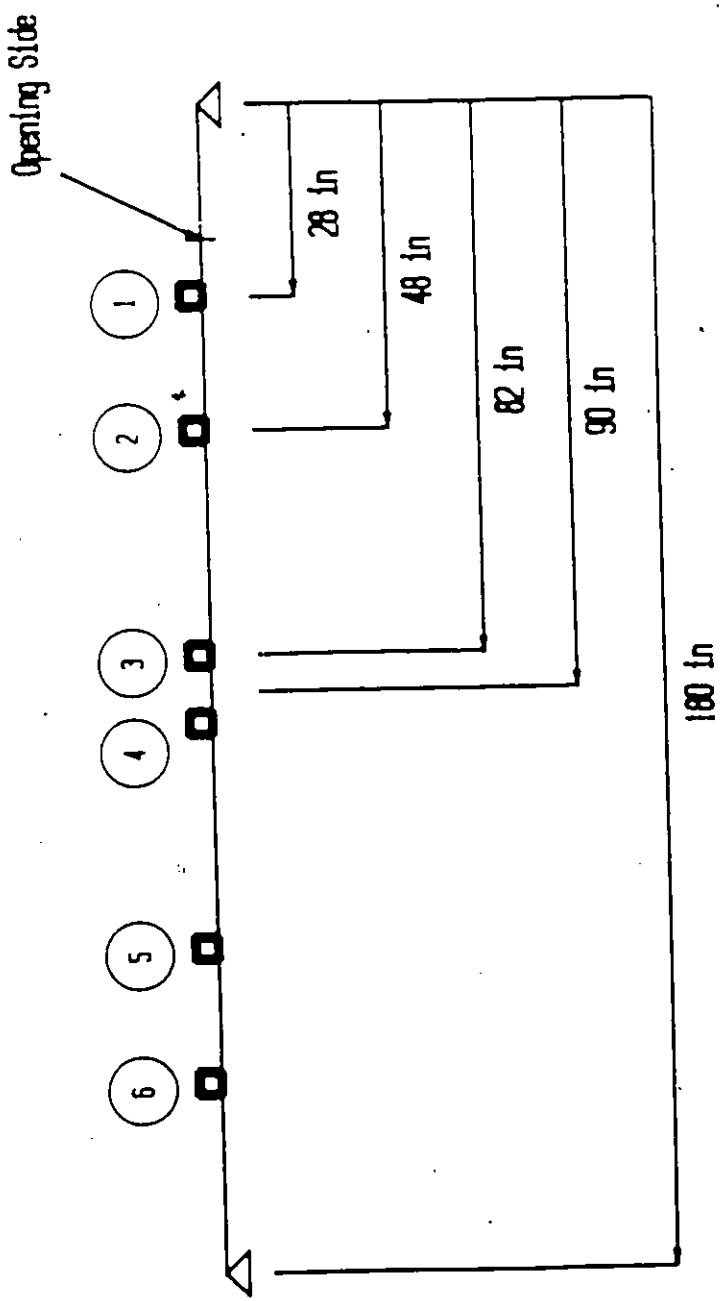
Figure 5.16: Accelerometer Locations Along the Beam Length

LIN A   NB   G   10DB   WTG H   A 5.0 V RMS


```
 5

EU

 0
   0.000                        LIN X        HZ          50.00
 X: 19.125     HZ      Y (A)    4.44         EU         PEAK T
```
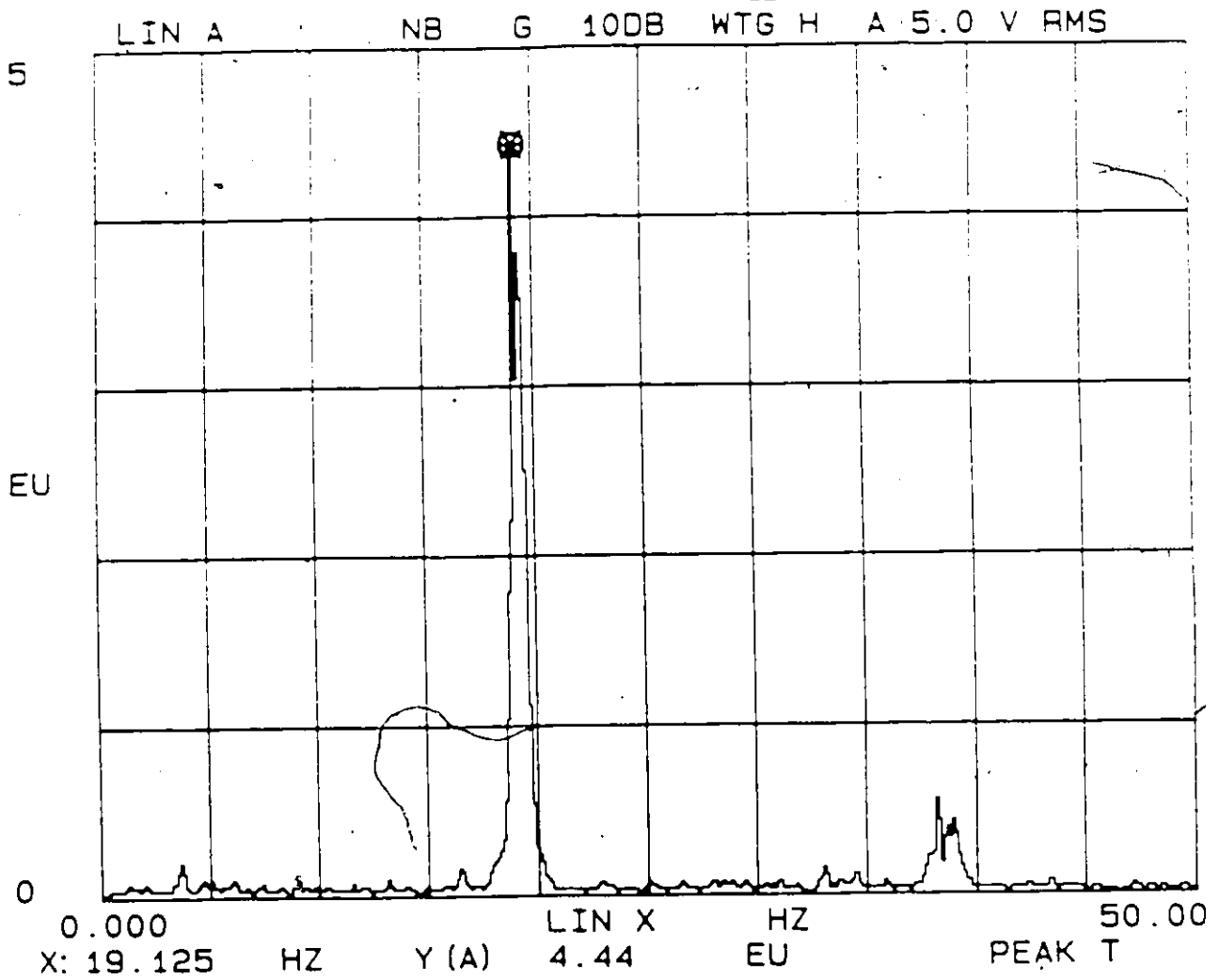
<u>Figure 5.17</u>:   Frequency Spectrum of Accelerometer #3 of Beam
#2 at the Fundamental Frequency Before Fatigue
loading

EXPERIMENTAL MODESHAPES BEAM 1
FLEXURAL MODE 1
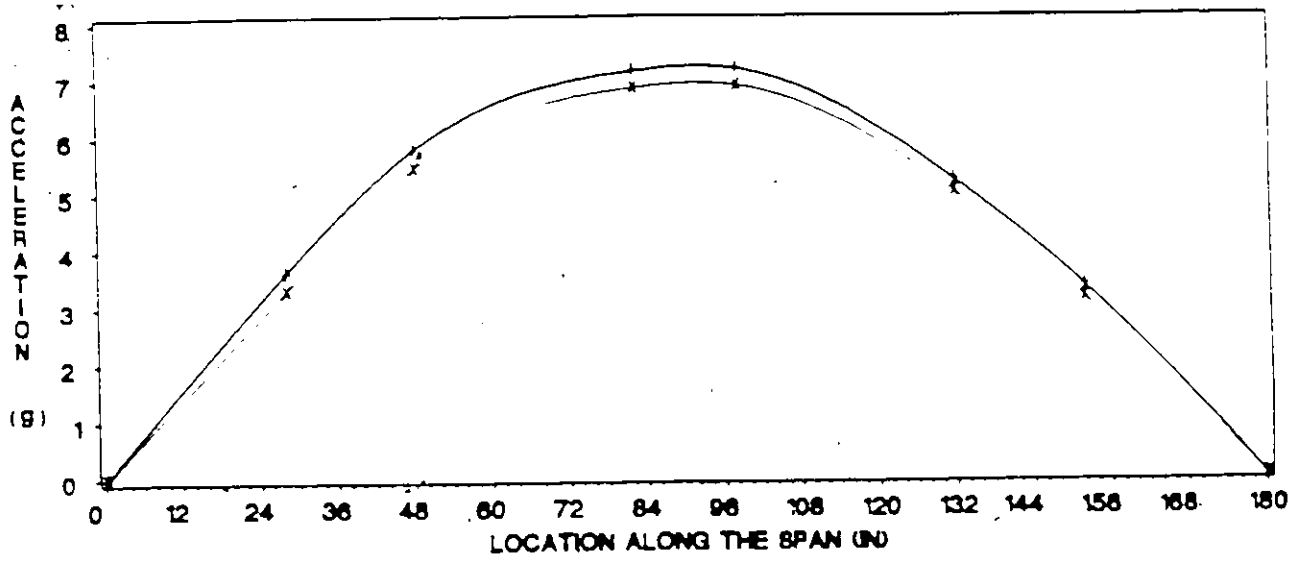
Figure 5.18: Beam #1 Mode Shapes at the First Natural Frequency

EXPERIMENTAL MODESHAPES BEAM 2
FLEXURAL MODE 1
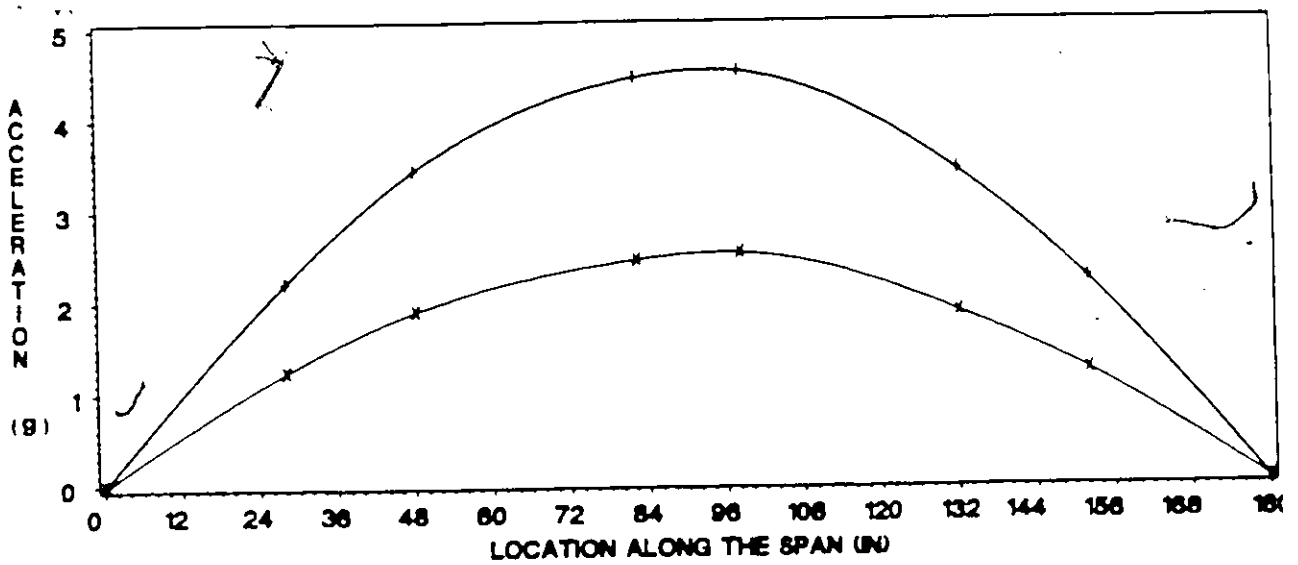
Figure 5.19: Beam #2 Mode Shapes at the First Natural Frequency

EXPERIMENTAL MODESHAPES BEAM 3
FLEXURAL MODE 1
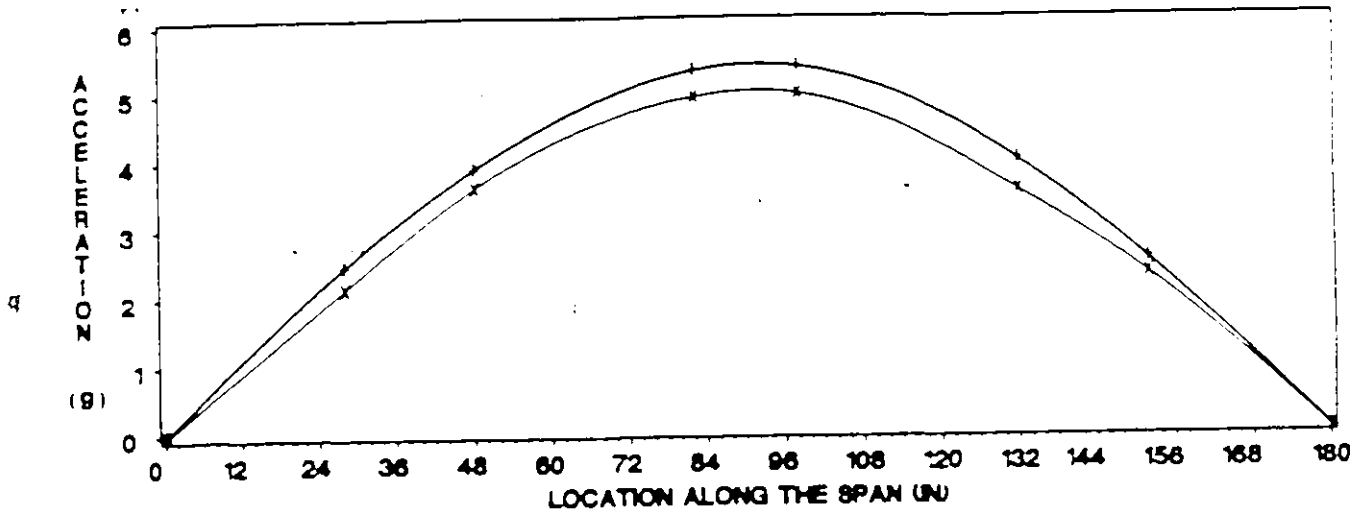
Figure 5.20: Beam #3 Mode Shapes at the First Natural
Frequency

EXPERIMENTAL MODESHAPES BEAM 4
FLEXURAL MODE 1
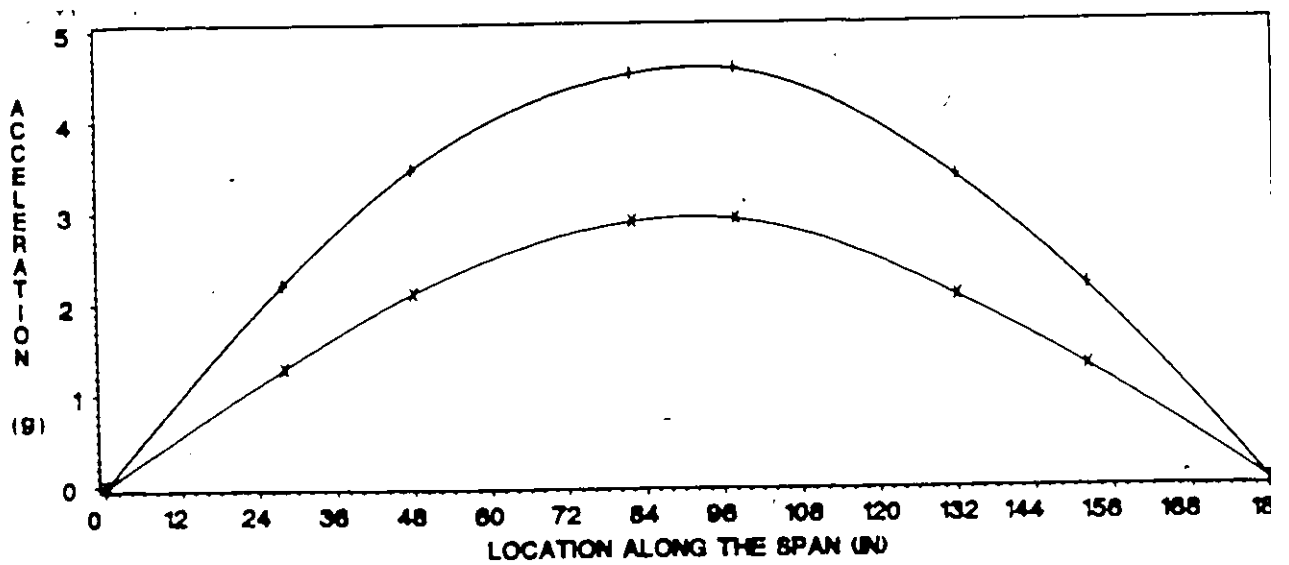
Figure 5.21: Beam #4 Mode Shapes at the First Natural
Frequency

EXPERIMENTAL MODESHAPES BEAM 5
FLEXURAL MODE 1
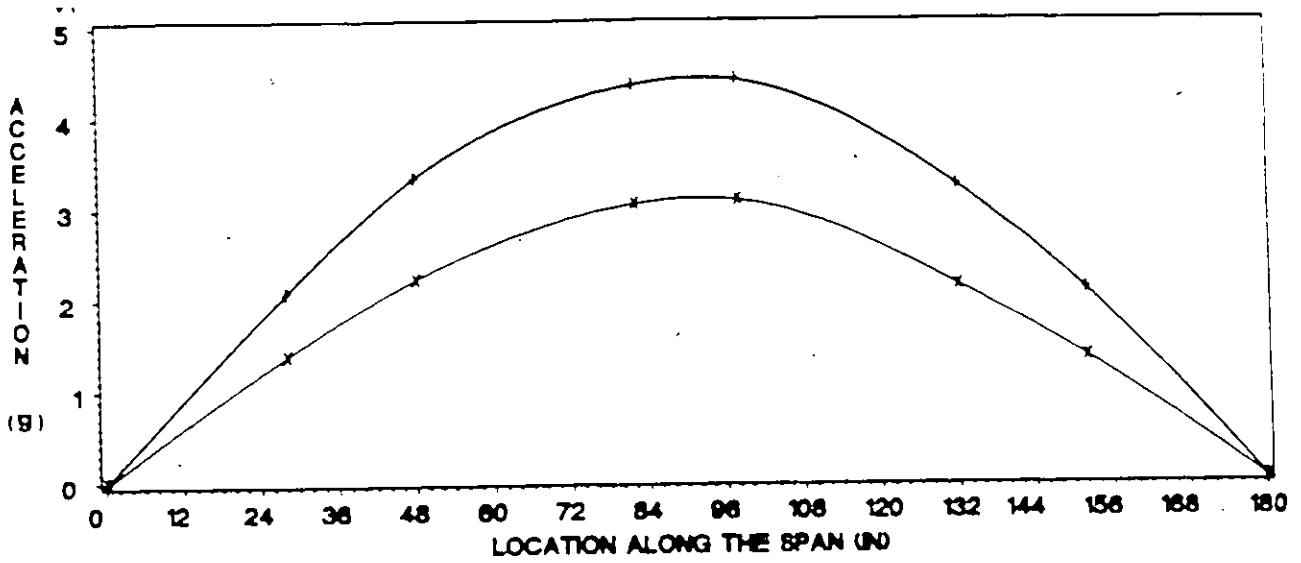
Figure 5.22: Beam #5 Mode Shapes at the First Natural Frequency

EXPERIMENTAL MODESHAPES BEAM 6
FLEXURAL MODE 1
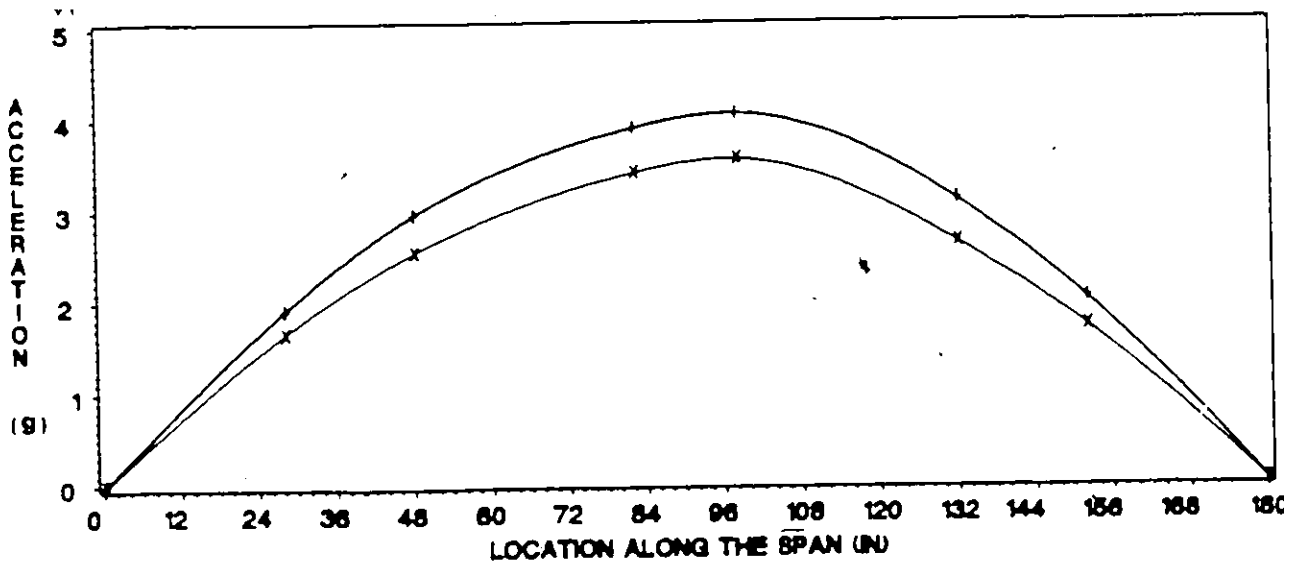
Figure 5.23: Beam #6 Mode Shapes at the First Natural Frequency

BEAM 1 CHORDS DISPLACEMENT
BEFORE FATIGUE AT FIRST
NATURAL FREQUENCY
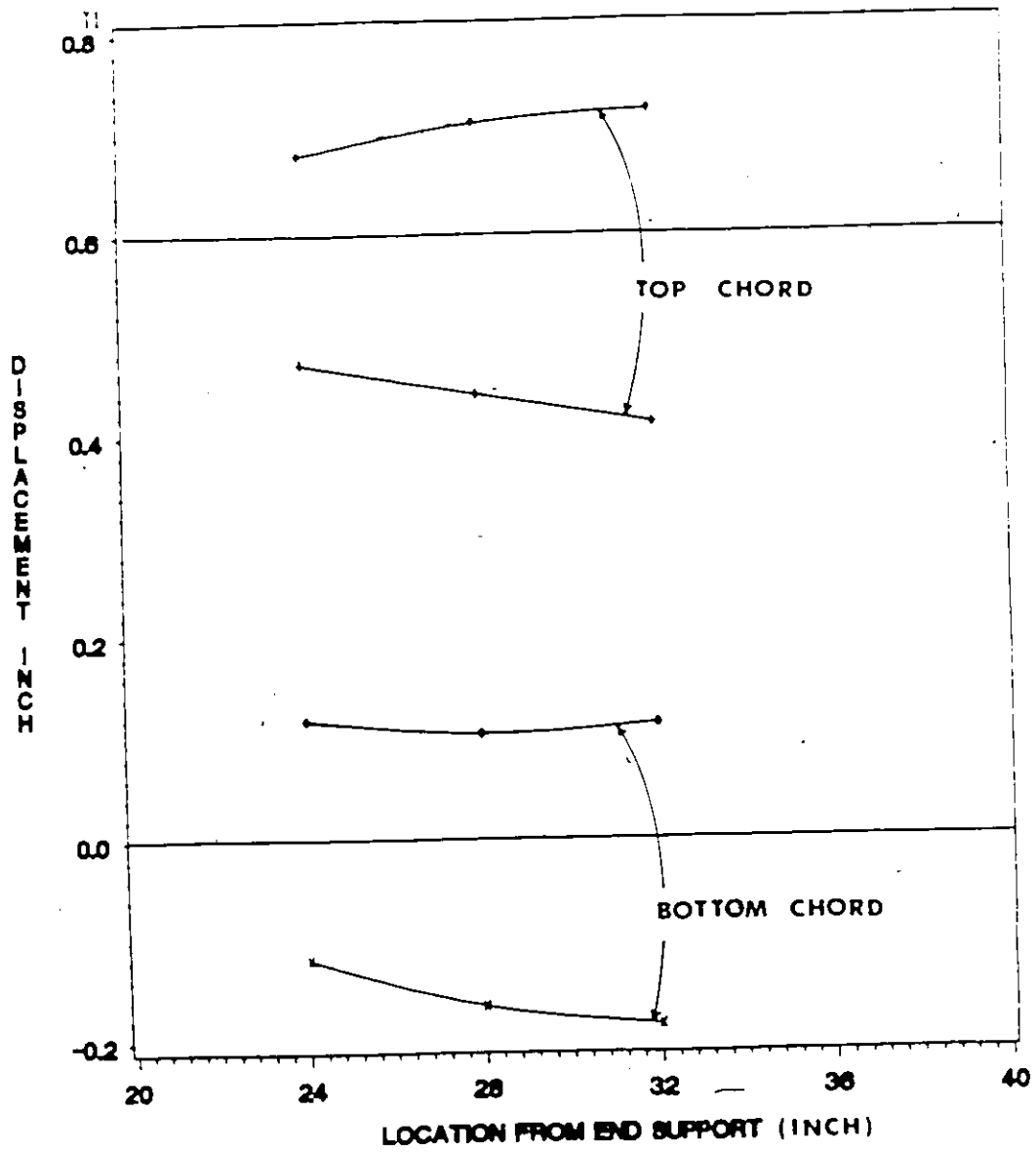
Figure 5.24: Before Fatigue Chords Displacement for Beam #1

BEAM 2 CHORDS DISPLACEMENT
BEFORE FATIGUE AT FIRST
NATURAL FREQUENCY
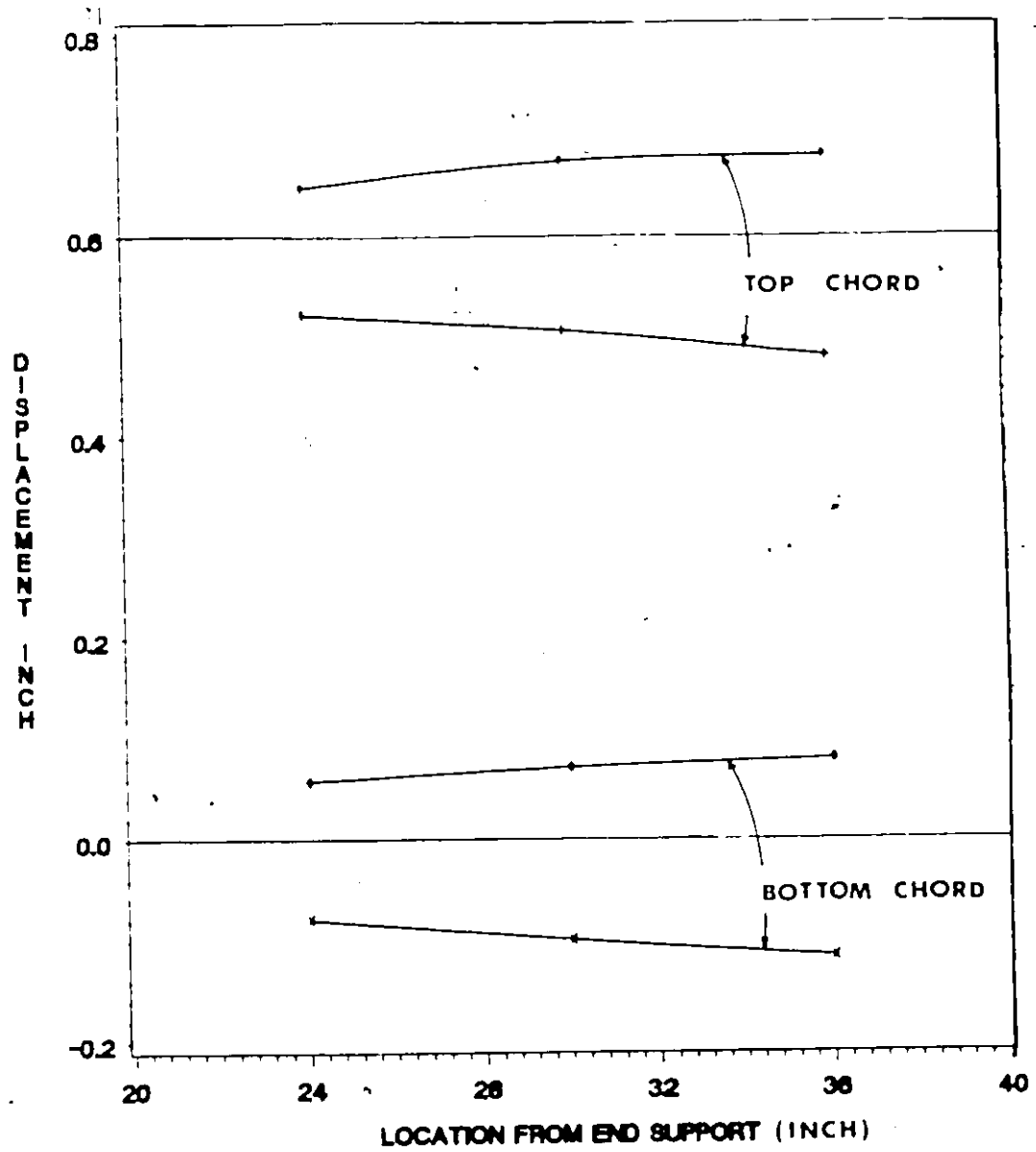
Figure 5.25:   Before Fatigue Chords Displacement for Beam #2

BEAM 2 CHORDS DISPLACEMENT
AFTER FATIGUE AT FIRST
NATURAL FREQUENCY
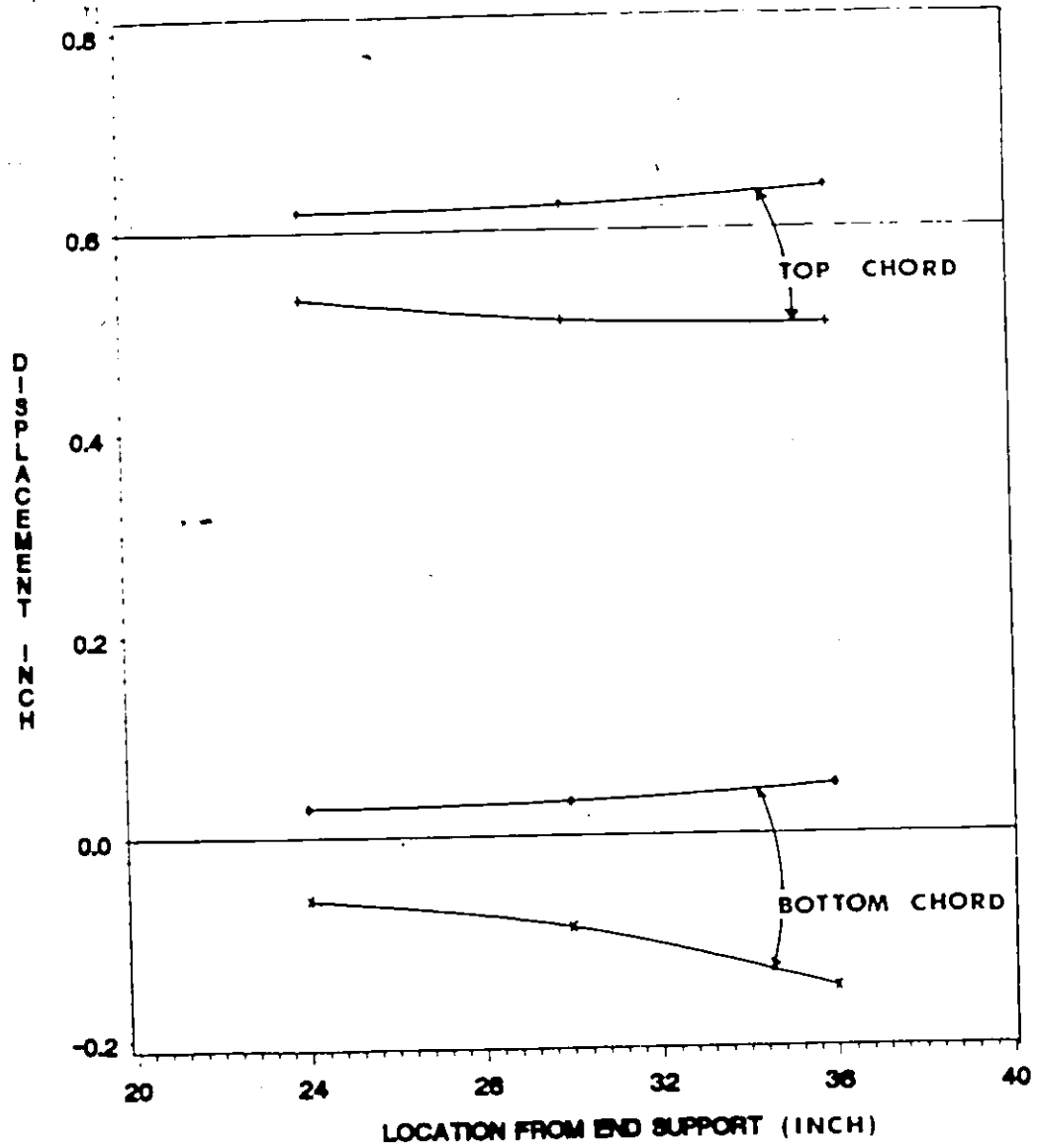
Figure 5.26: After Fatigue Chords Displacement for Beam #2

BEAM 3 CHORDS DISPLACEMENT
BEFORE FATIGUE AT FIRST
NATURAL FREQUENCY
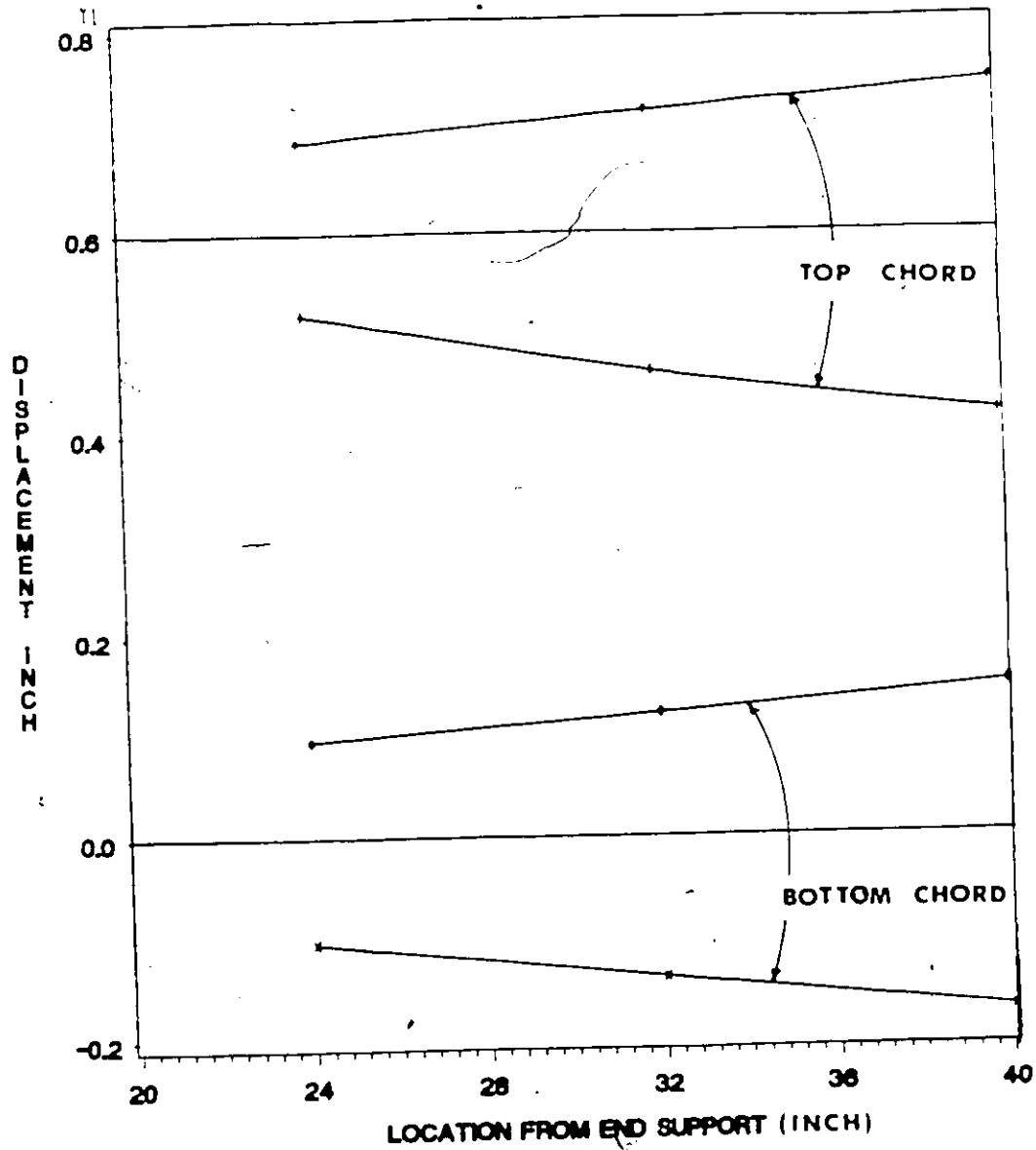
Figure 5.27:   Before Fatigue Chords Displacement for Beam #3
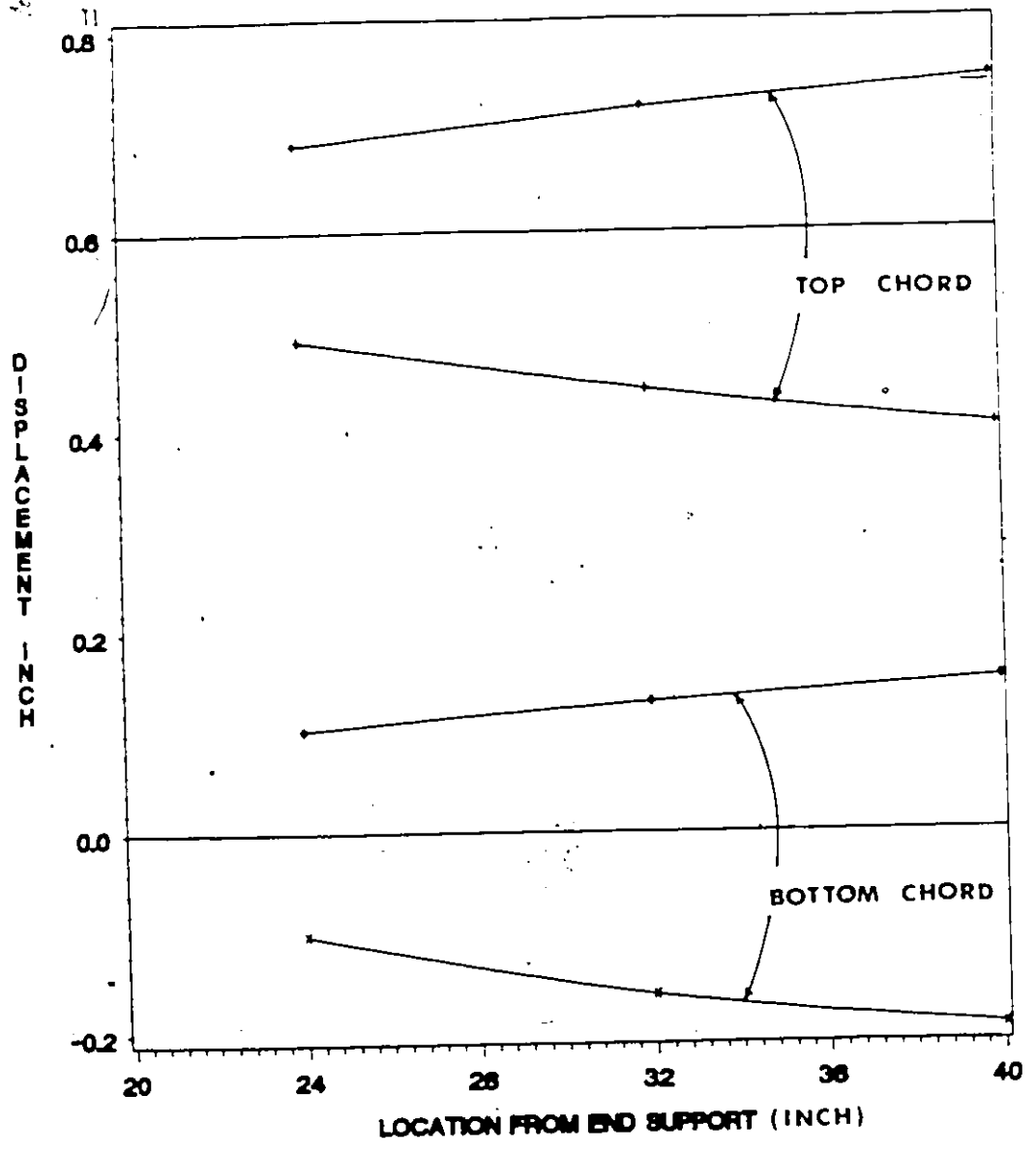
Figure 5.28: Before Fatigue Chords Displacement for Beam #4

BEAM 4 CHORDS DISPLACEMENT
AFTER FATIGUE AT FIRST
NATURAL FREQUENCY
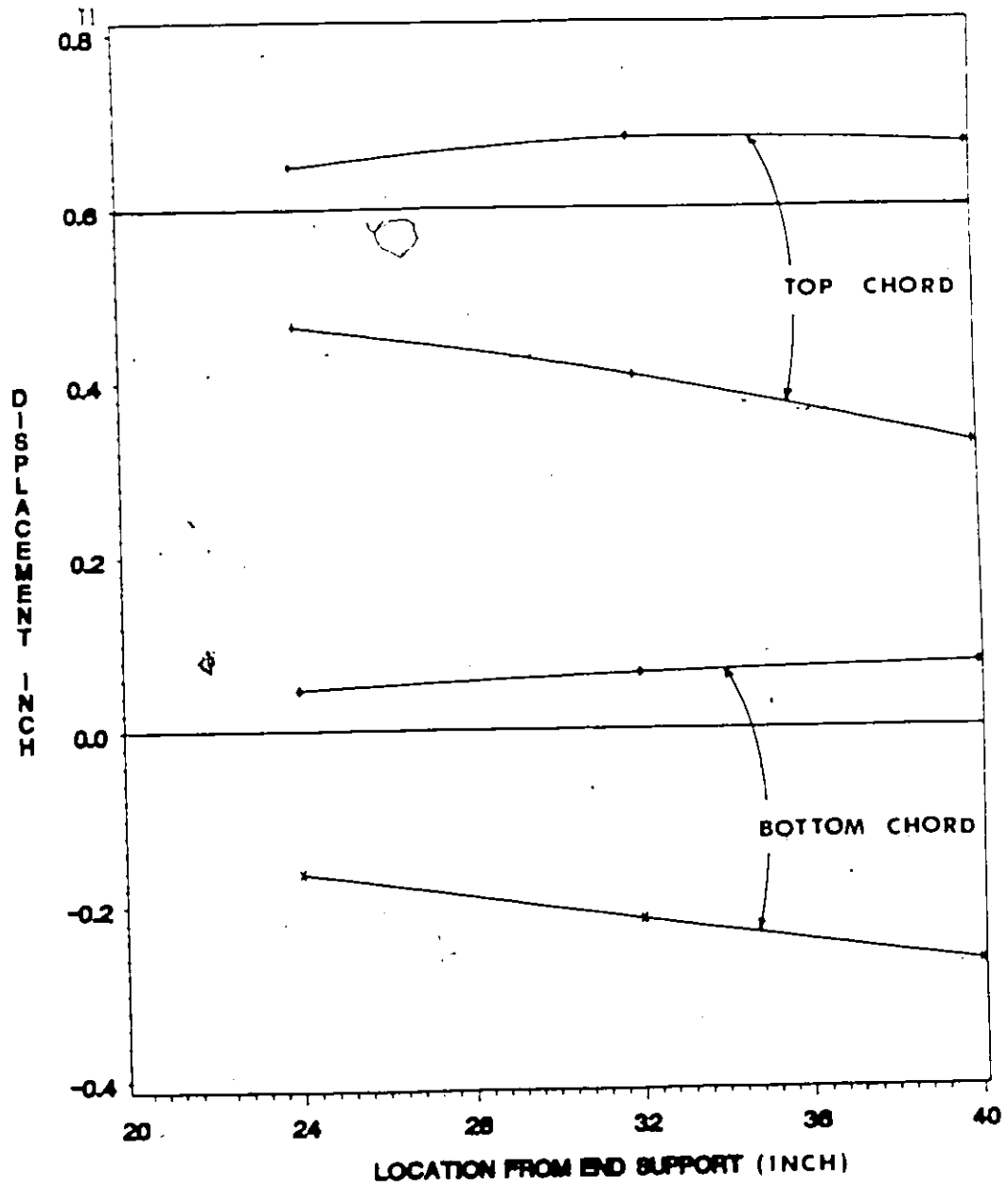
Figure 5.29: After Fatigue Chords Displacement for Beam #4

**BEAM 5 CHORDS DISPLACEMENT
BEFORE FATIGUE AT FIRST
NATURAL FREQUENCY**
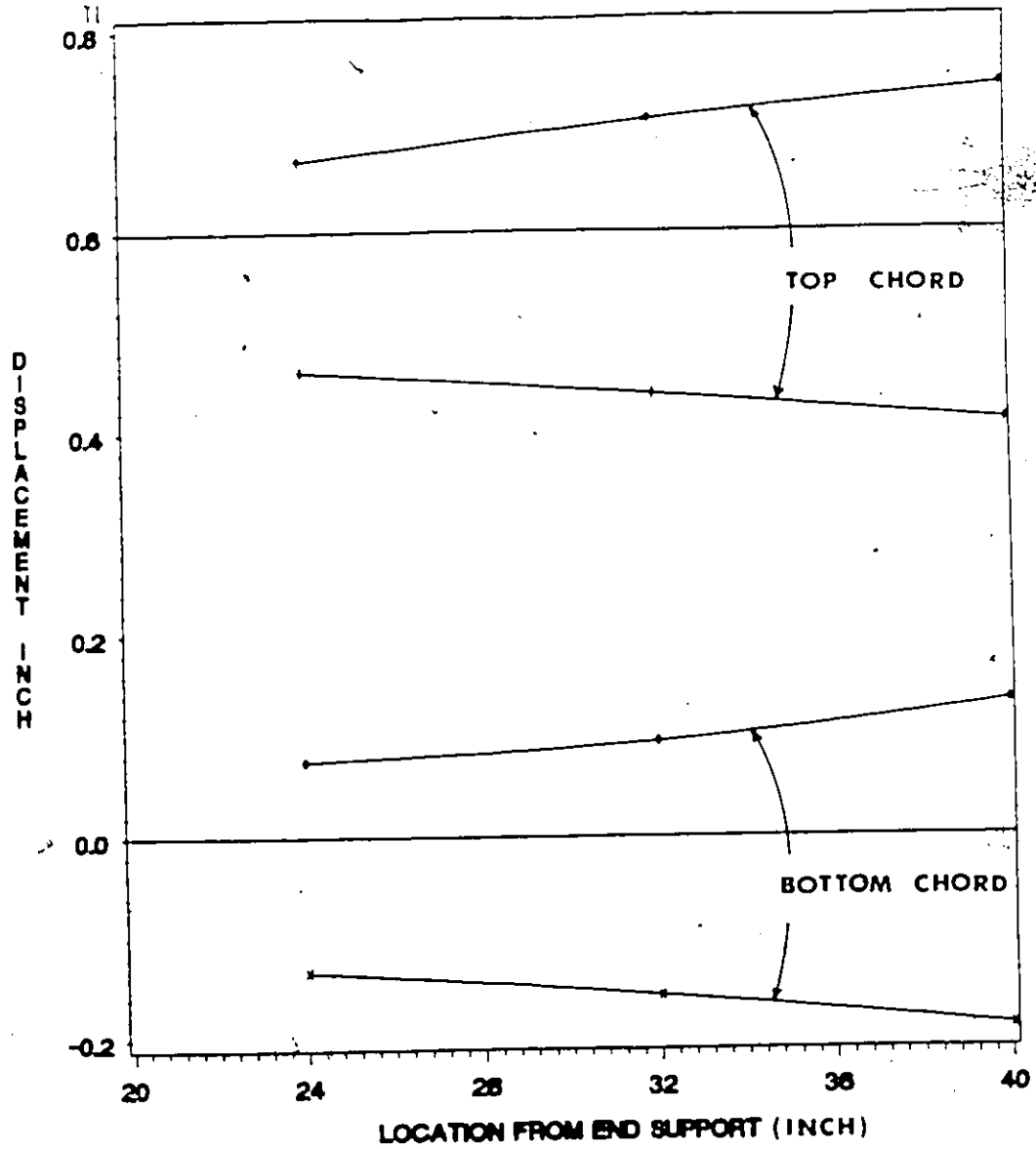
Figure 5.10: Before Fatigue Chords Displacement for Beam #5

BEAM 5 CHORDS DISPLACEMENT
AFTER FATIGUE AT FIRST
NATURAL FREQUENCY
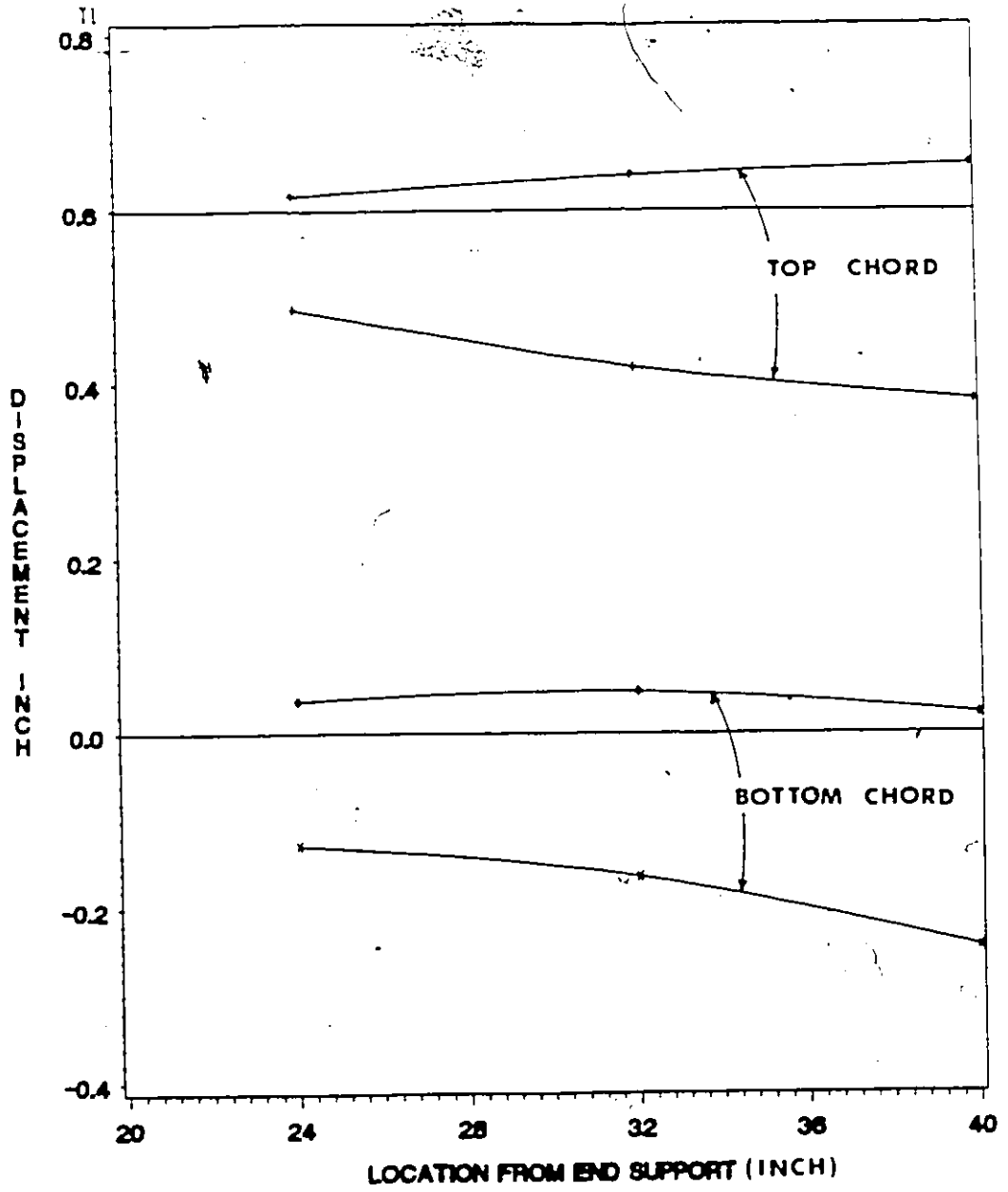
Figure 5.31:   After Fatigue Chords Displacement for Beam #5

Figure 5.32: Before Fatigue Chords Displacement for Beam #6

**BEAM 6 CHORDS DISPLACEMENT
AFTER FATIGUE AT FIRST
NATURAL FREQUENCY**
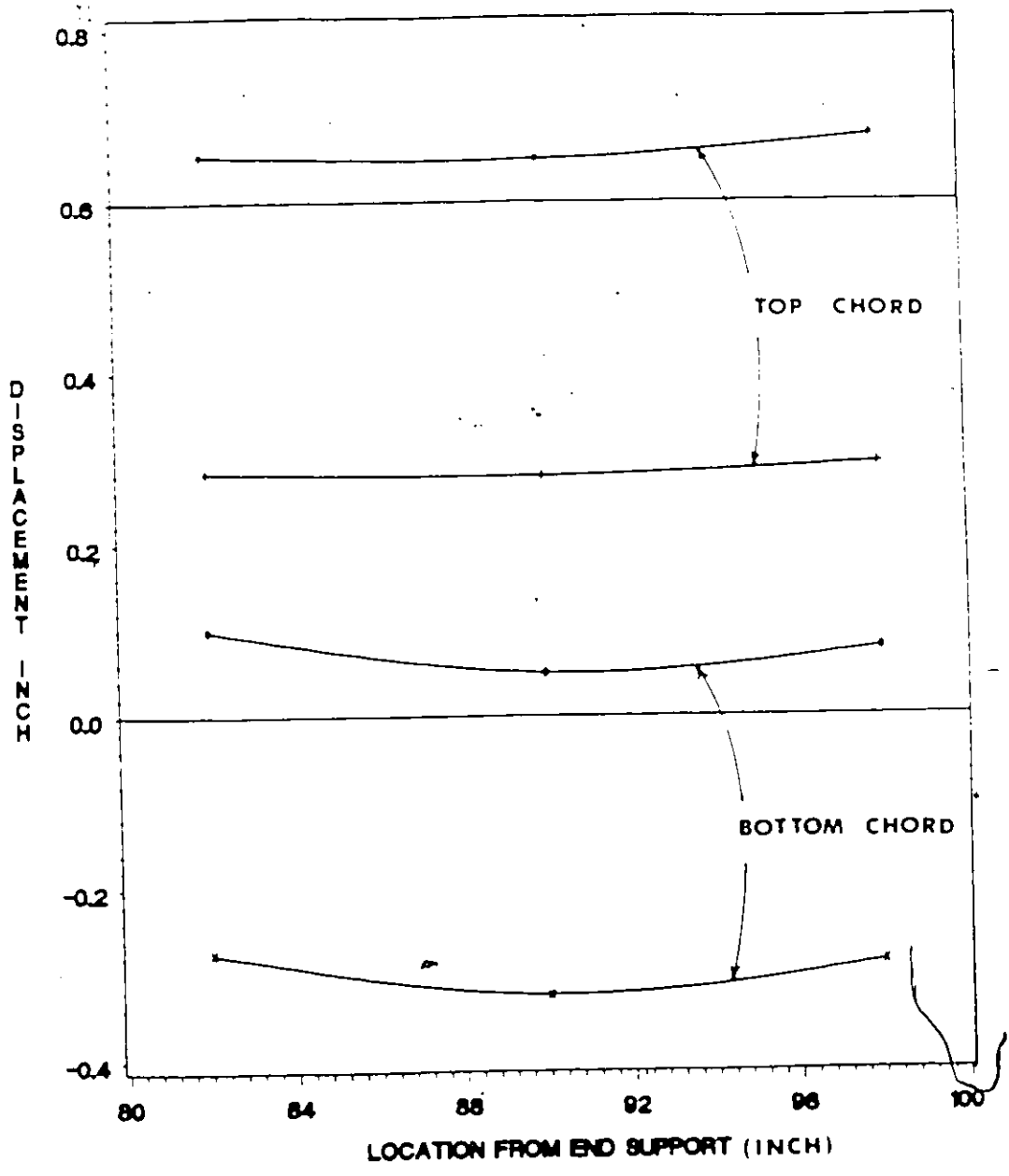
Figure 5.33: After Fatigue Chords Displacement for Beam #6
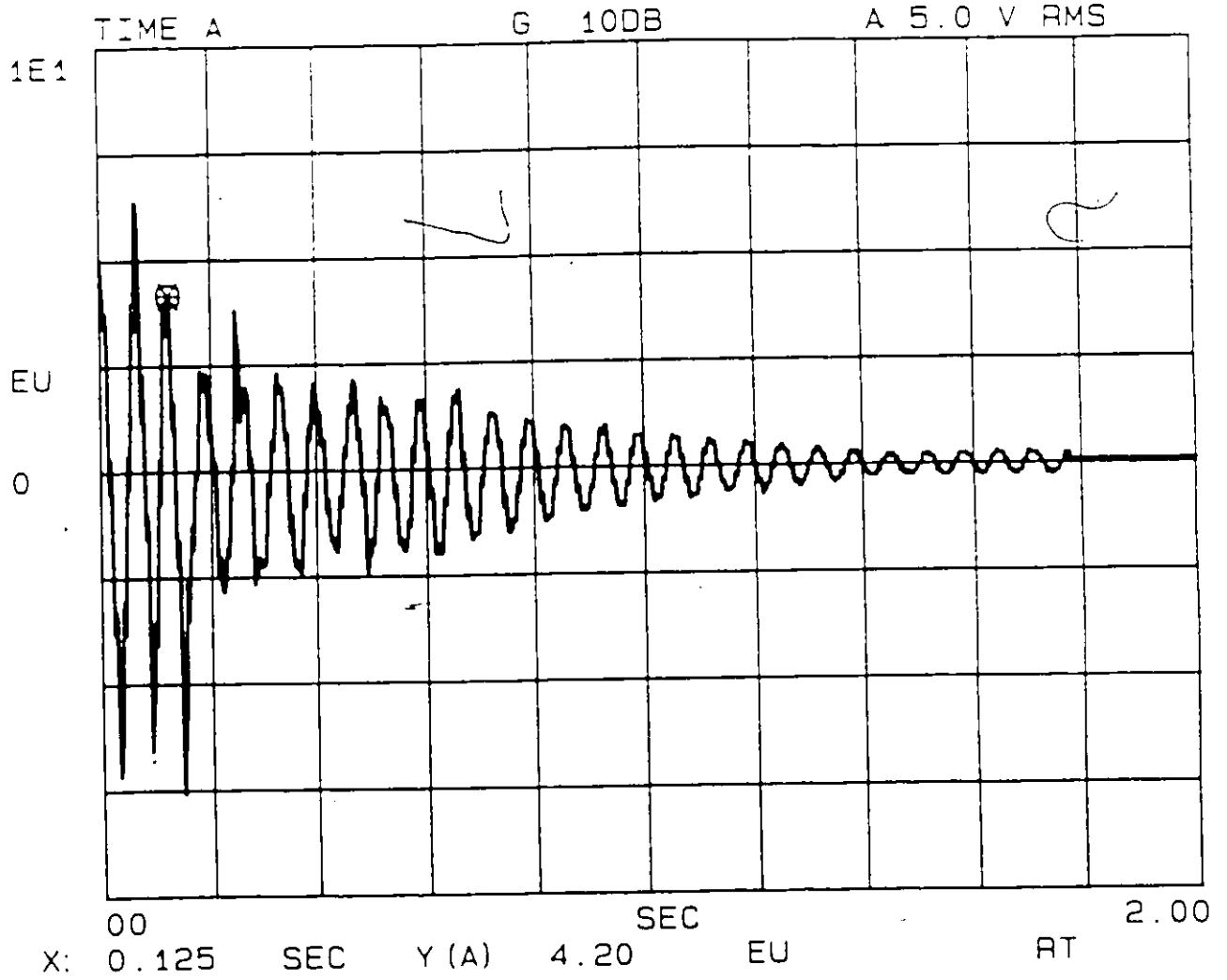
Figure 5.34: Beam #1 Decay Curve at the First Natural Frequency
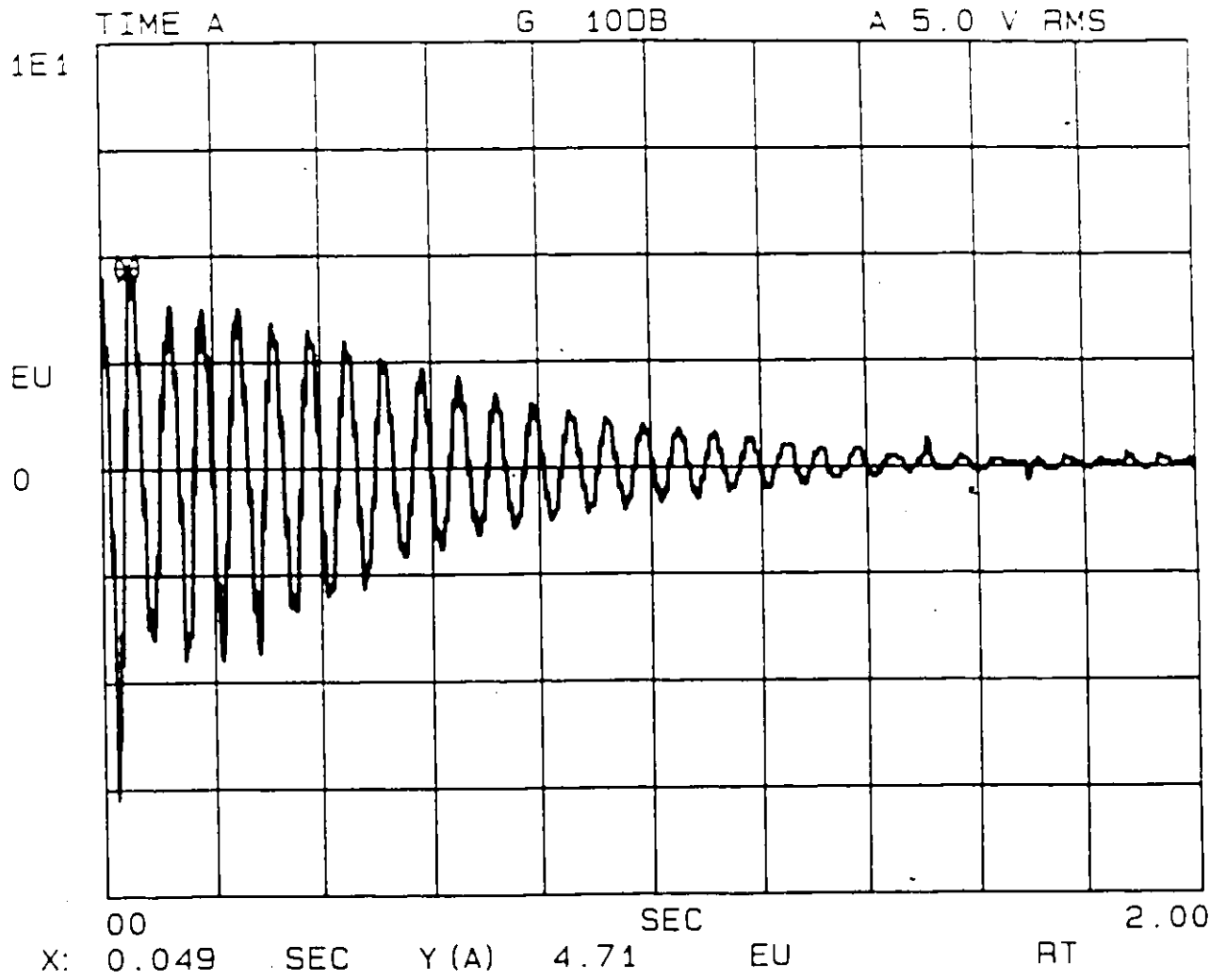
Figure 5.35: Beam #2 Decay Curve at the First Natural Frequency
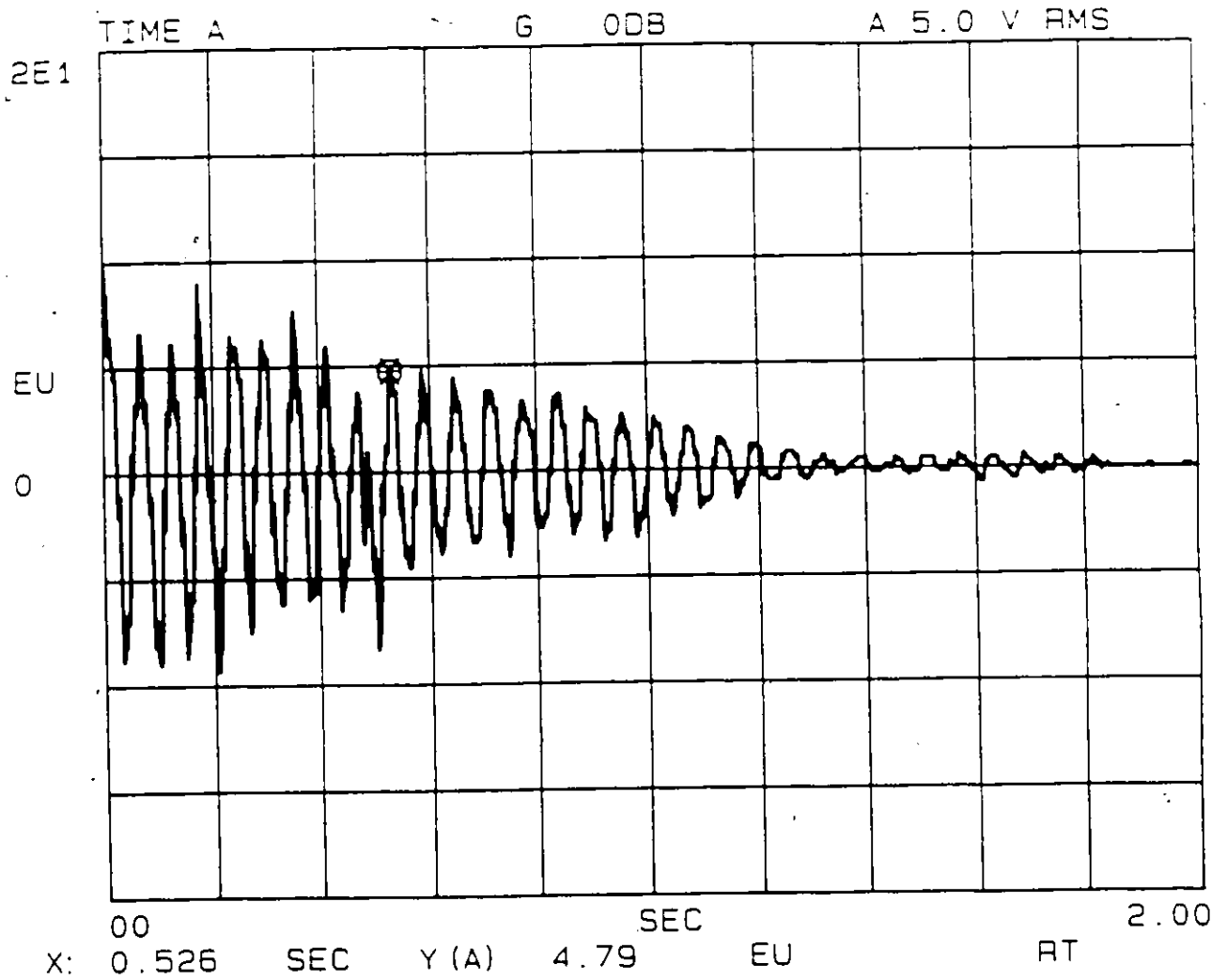
Figure 5.36: Beam #3 Decay Curve at the First Natural Frequency

Figure 5.37: Beam #4 Decay Curve at the First Natural Frequency

TIME A   G   10DB   A 5.0 V RMS

1E1

EU

O

00   SEC   2.00
X: 0.061   SEC   Y(A)   7.63   EU   RT
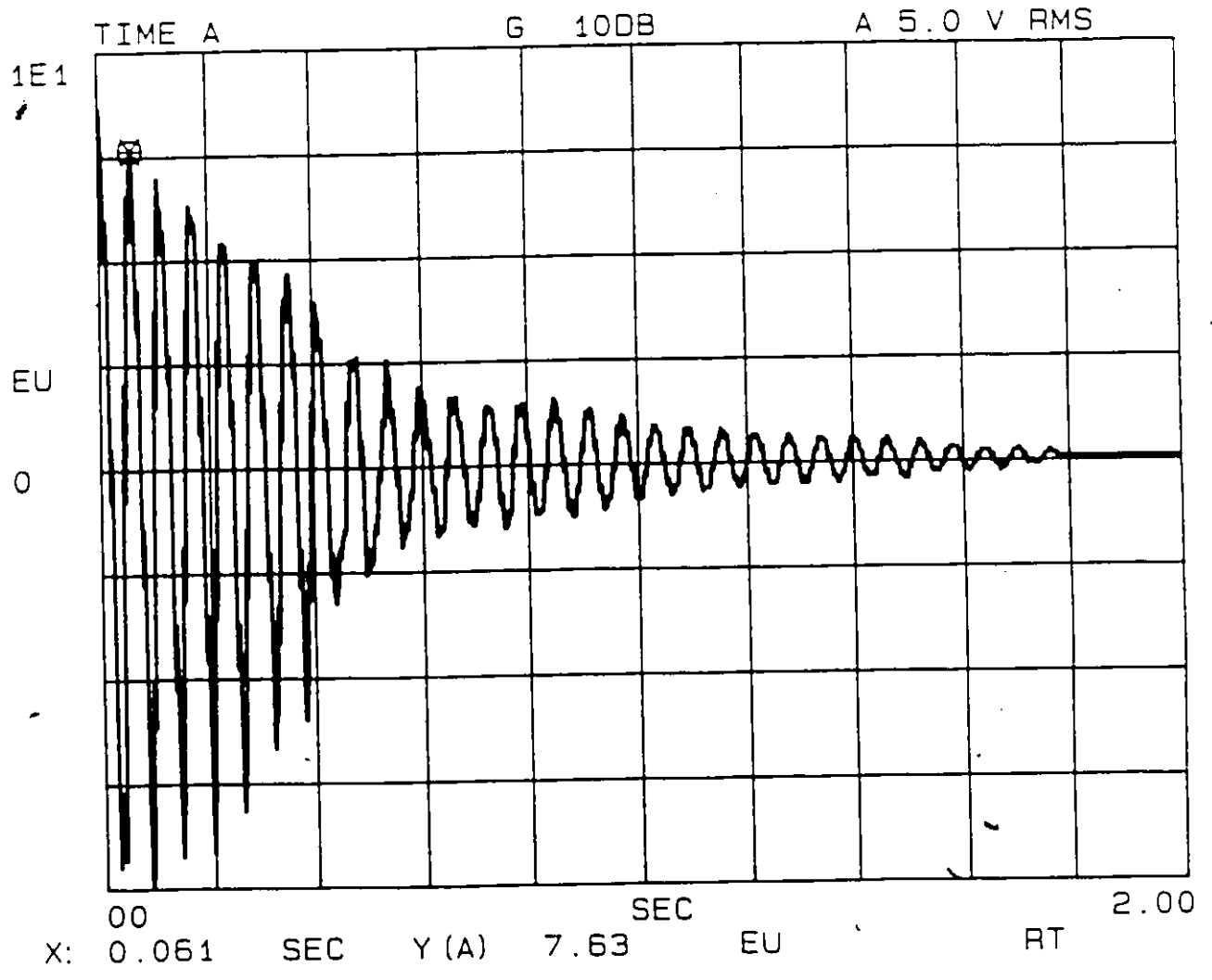
<u>Figure 5.38</u>:   Beam #5 Decay Curve at the First Natural
                      Frequency

Figure 5.39: Beam #6 Decay Curve at the First Natural Frequency
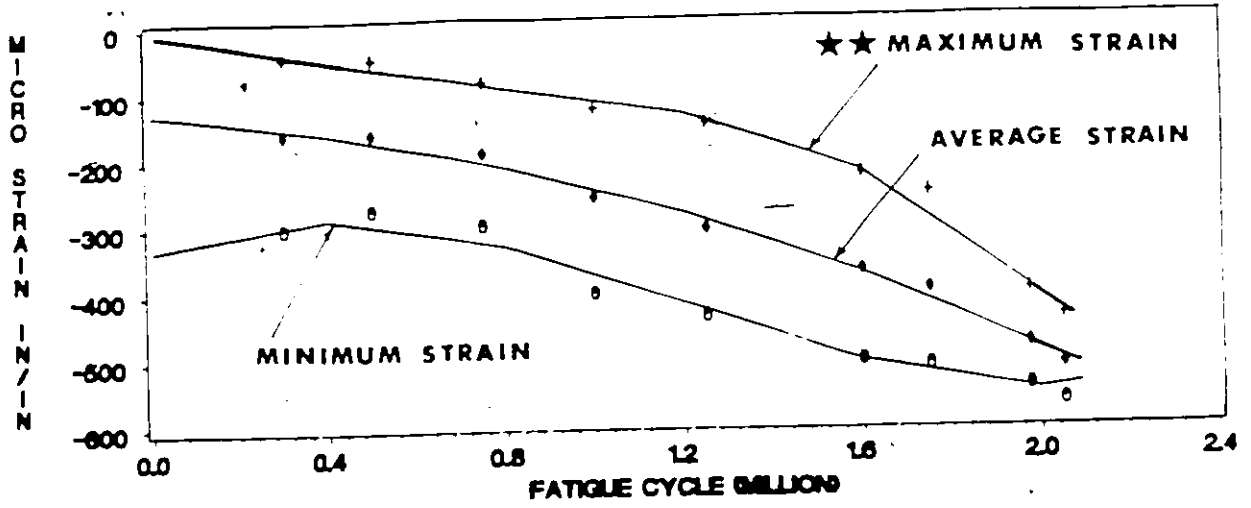
★★ This identification applies to the remaining figures of beams 2,4,5 and 6
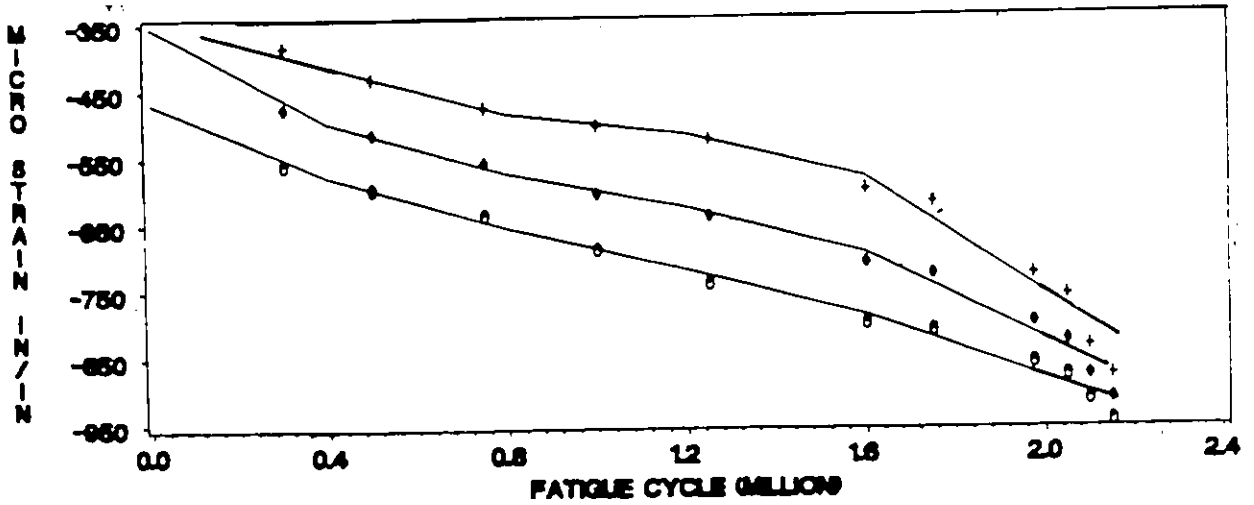
Figure 5.40: Strain Variation of gages 1 and 8 of Beam #2
With Increasing Fatigue Cycles

FATIGUE READINGS OF STRAINGAGE 1
BEAM 3
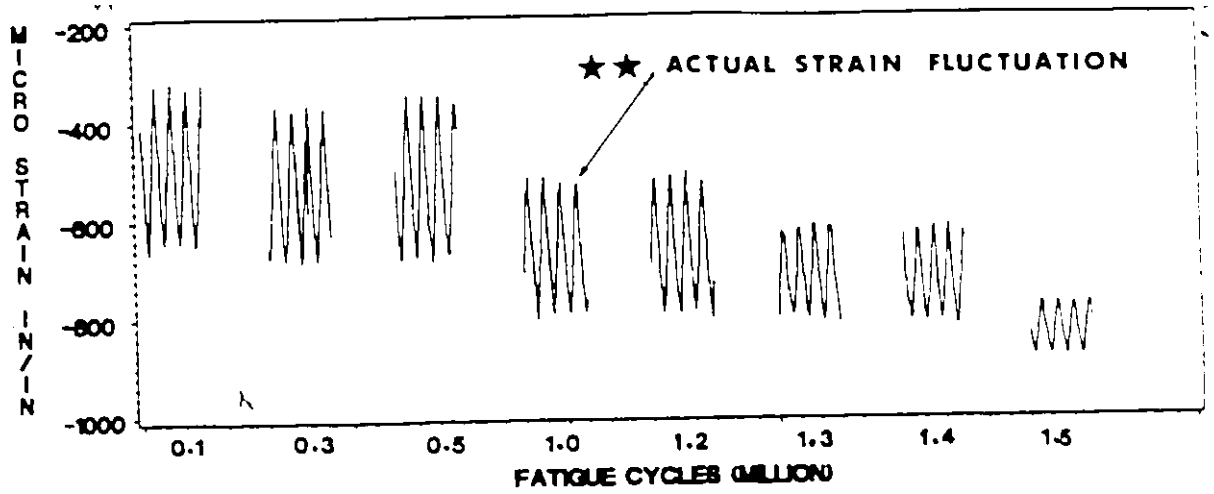
★★ This identification applies to the remaining figures of beam #3

FATIGUE READINGS OF STRAINGAGE 8
BEAM 3
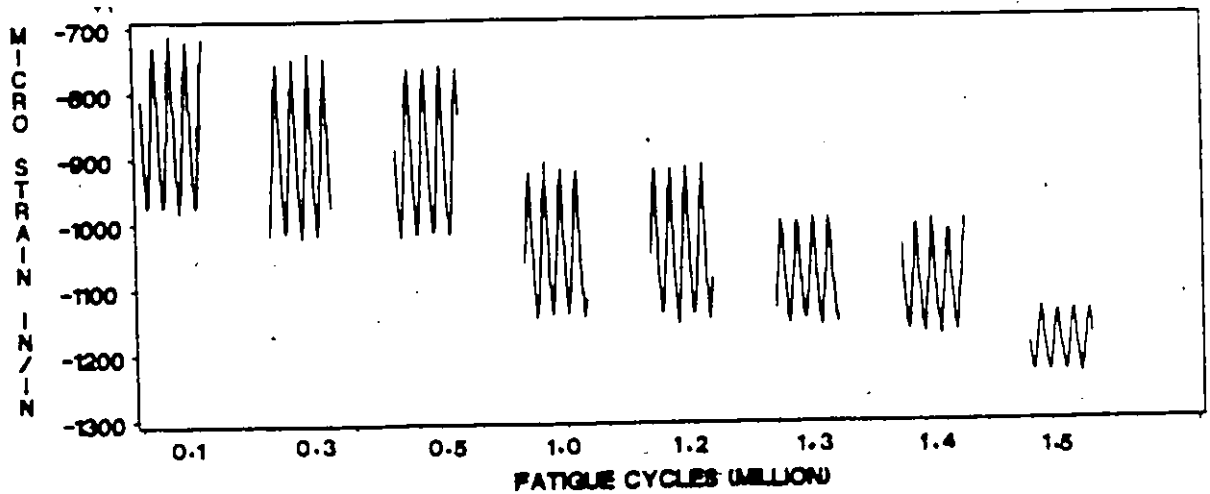
Figure 5.41: Strain Variation of gages 1 and 8 of Beam #3 With Increasing Fatigue Cycles

FATIGUE READINGS OF STRAINGAGE 3
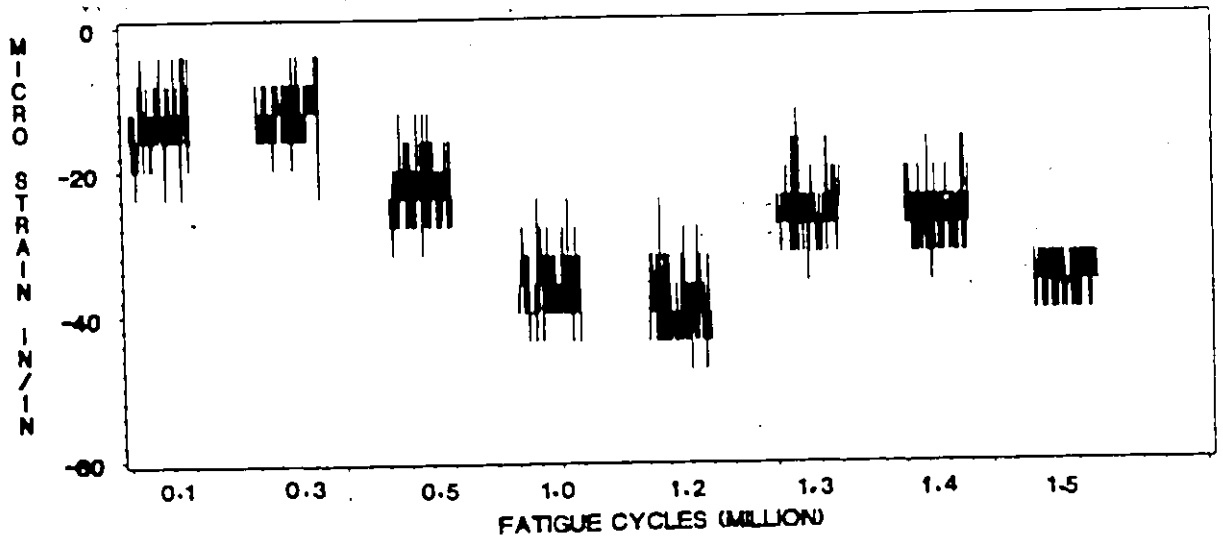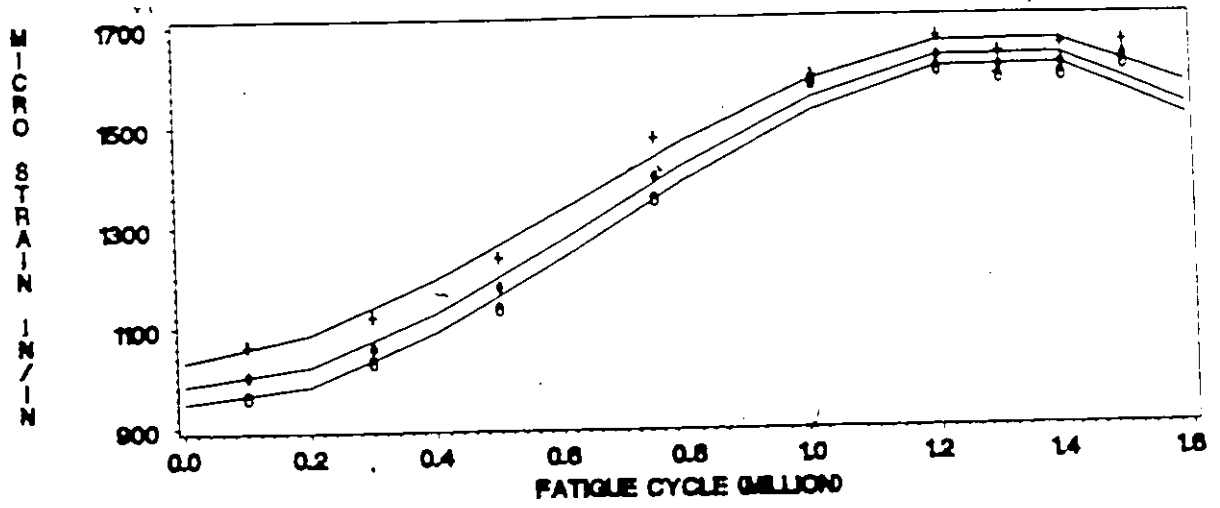BEAM 3

FATIGUE READINGS OF STRAINGAGE 6
BEAM 3
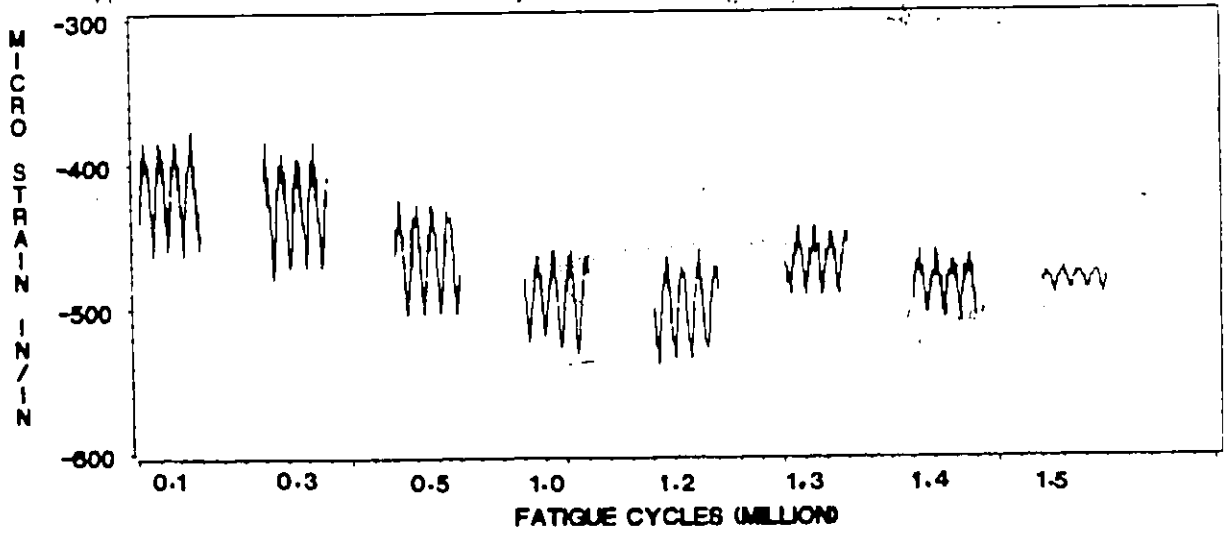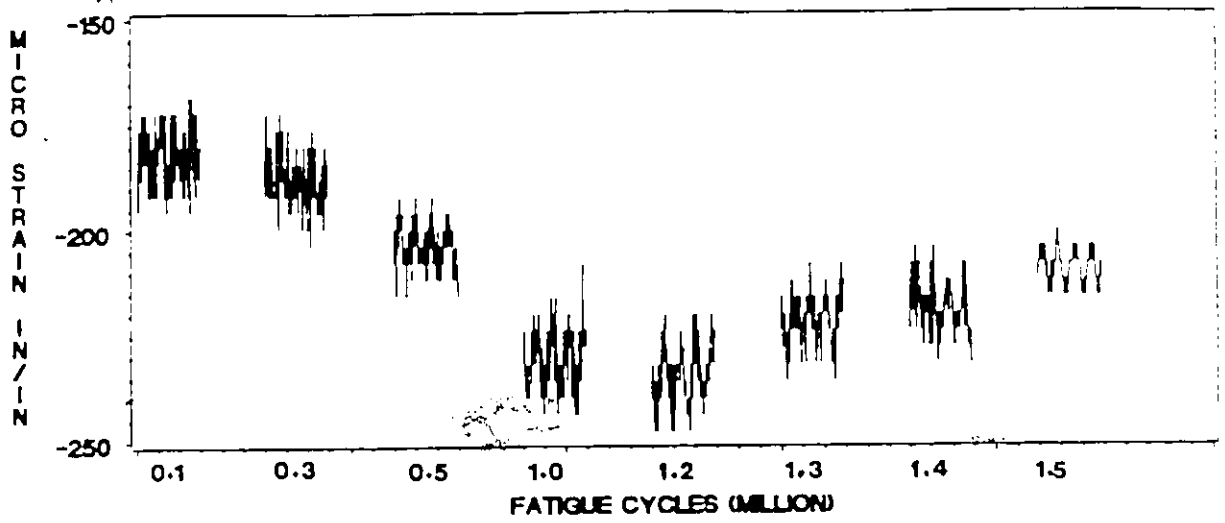
Figure 5-42:   Strain Variation of gages 3 and 6 of Beam #3
With Increasing Fatigue Cycles

FATIGUE READINGS OF STRAINGAGE 3
BEAM 4
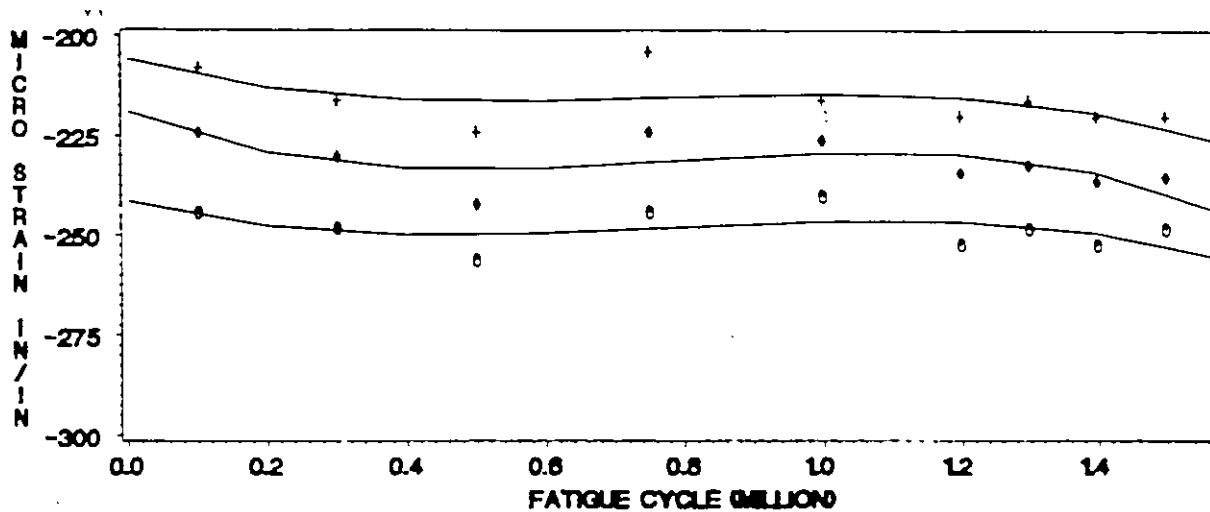
FATIGUE READINGS OF STRAINGAGE 6
BEAM 4
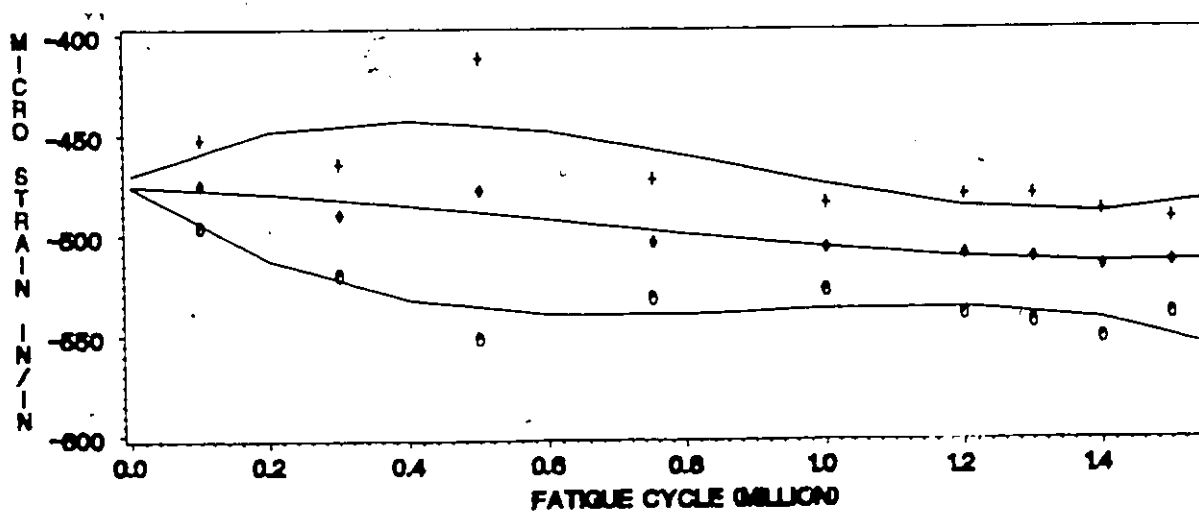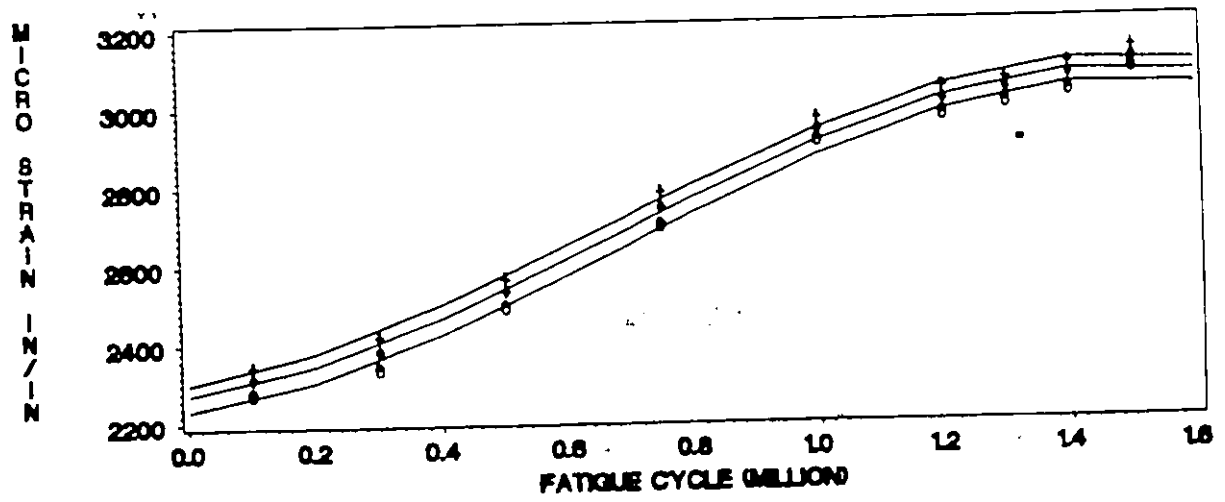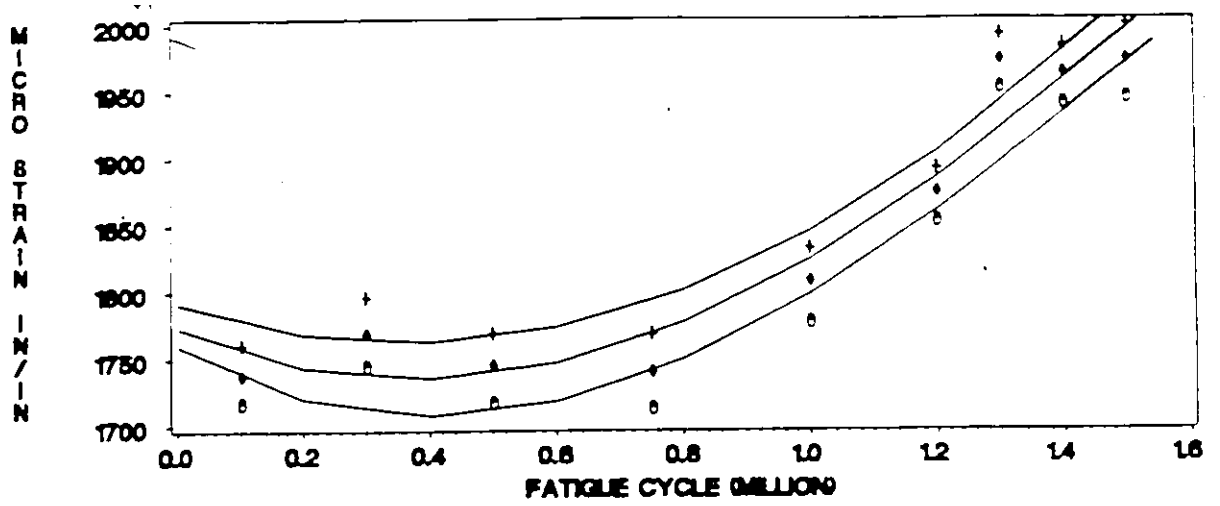

Figure 5.43: Strain Variation of gages 3 and 6 of Beam #4
With Increasing Fatigue Cycles

FATIGUE READINGS OF STRAINGAGE 1
BEAM 4
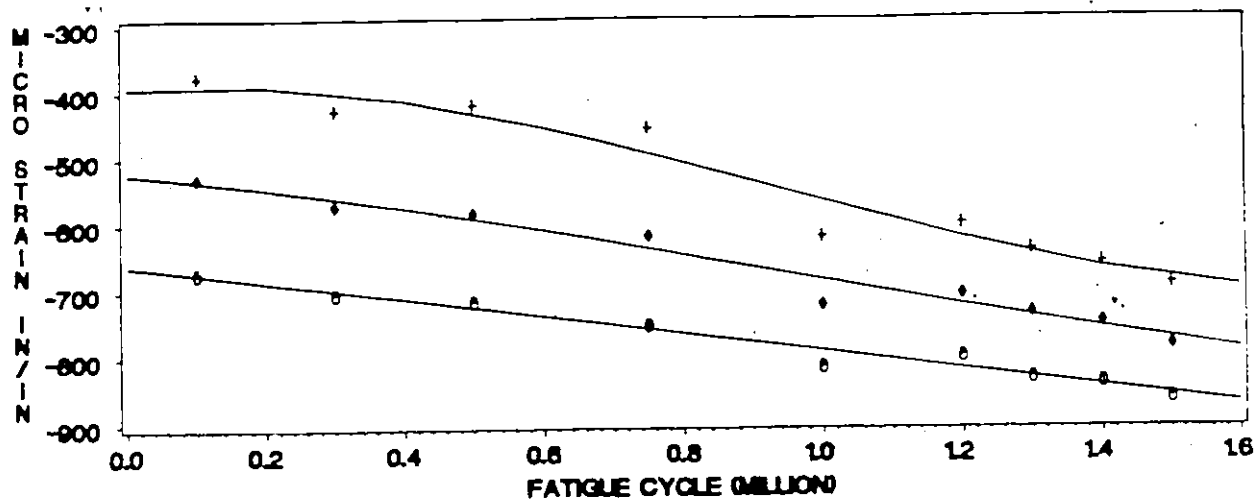
FATIGUE READINGS OF STRAINGAGE 8
BEAM 4
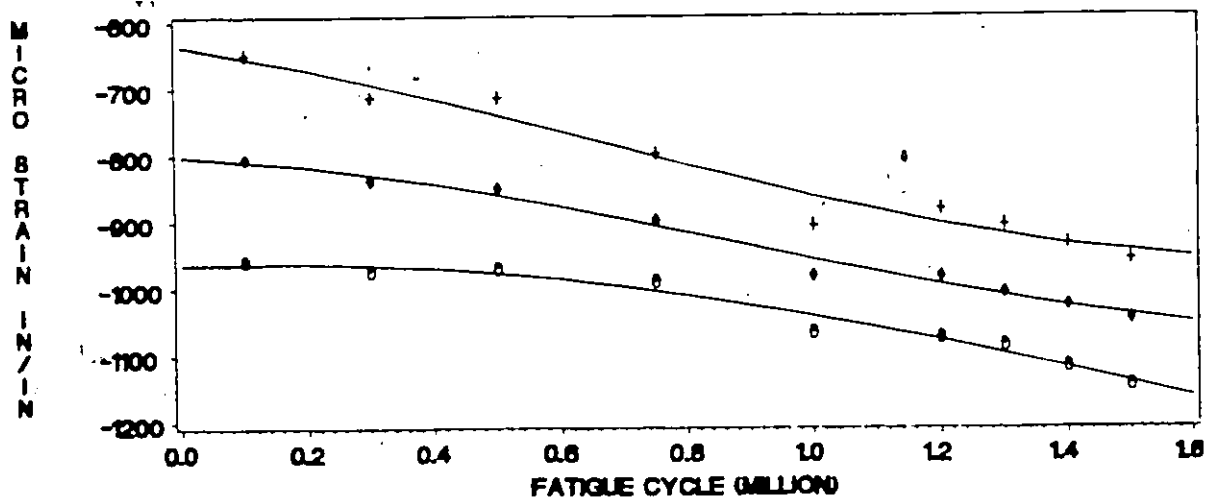
Figure 5.44:   Strain Variation of gages 1 and 8 of Beam #4
With Increasing Fatigue Cycles
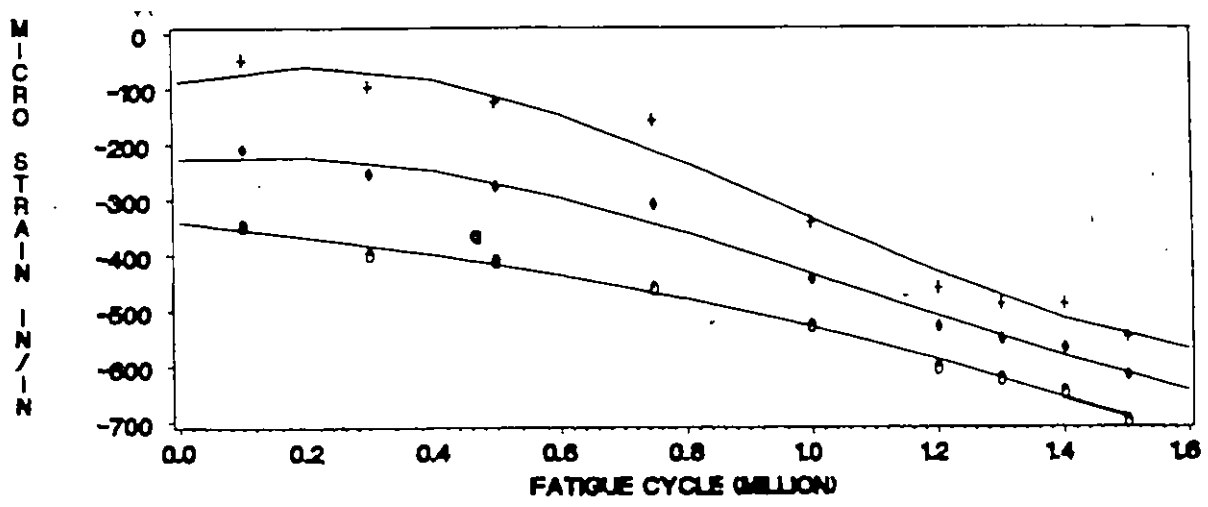
FATIGUE READINGS OF STRAINGAGE 8
BEAM 5
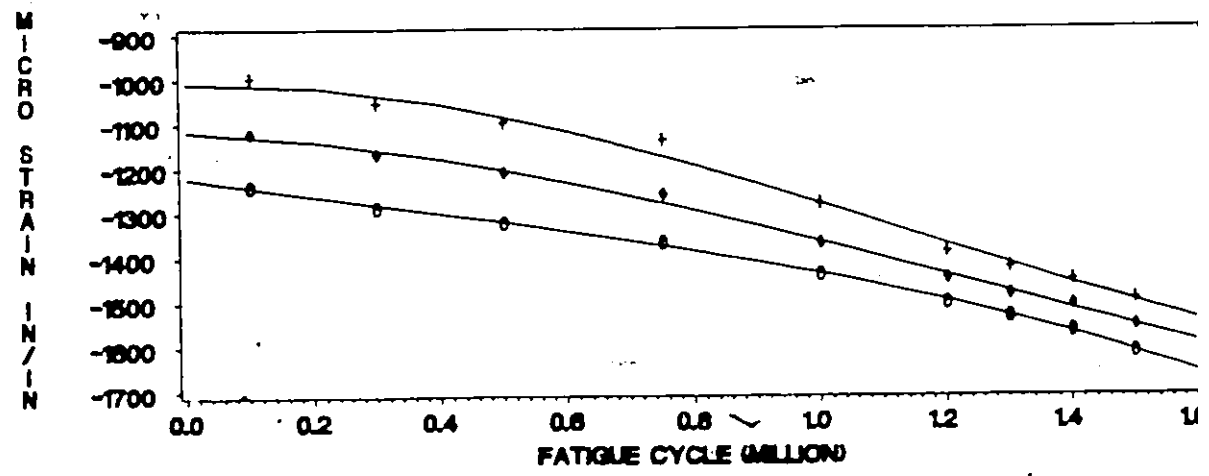
Figure 5.45: Strain Variation of gages 1 and 8 of Beam #5
With Increasing Fatigue Cycles

FATIGUE READINGS OF STRAINGAGE 3
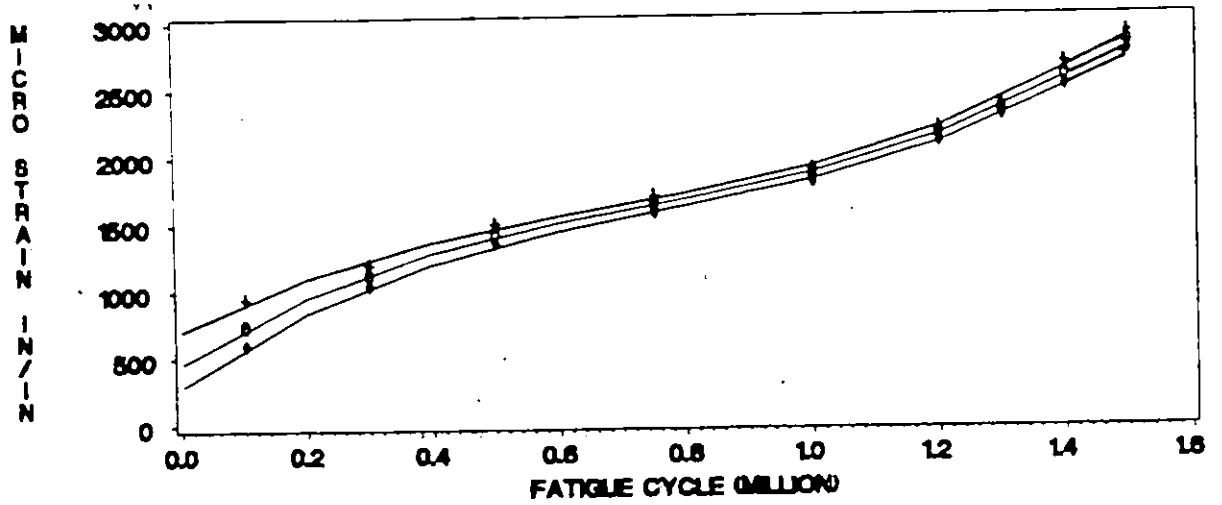BEAM 5
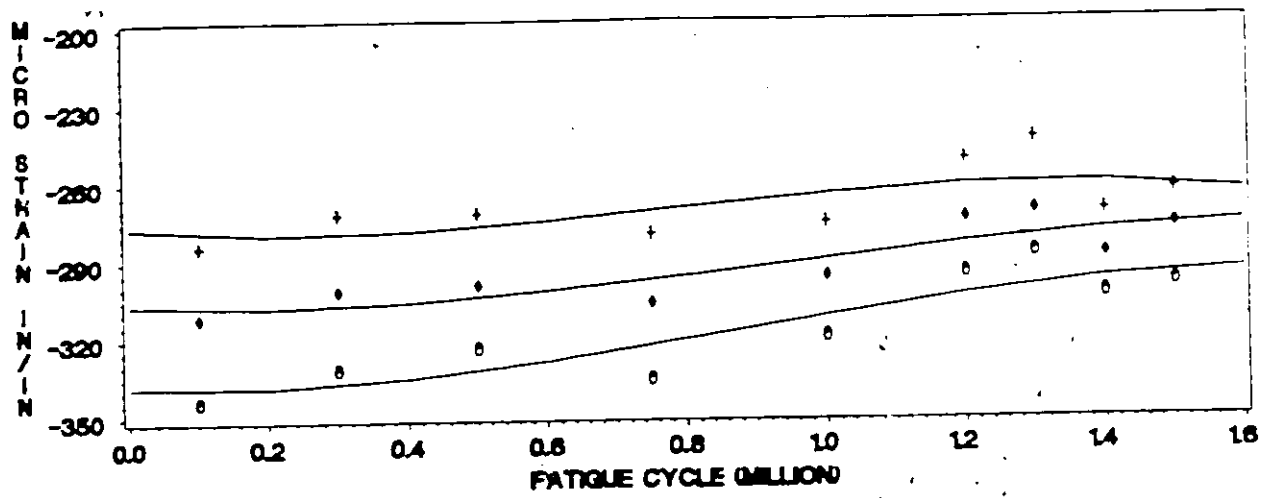
FATIGUE READINGS OF STRAINGAGE 6
BEAM 5
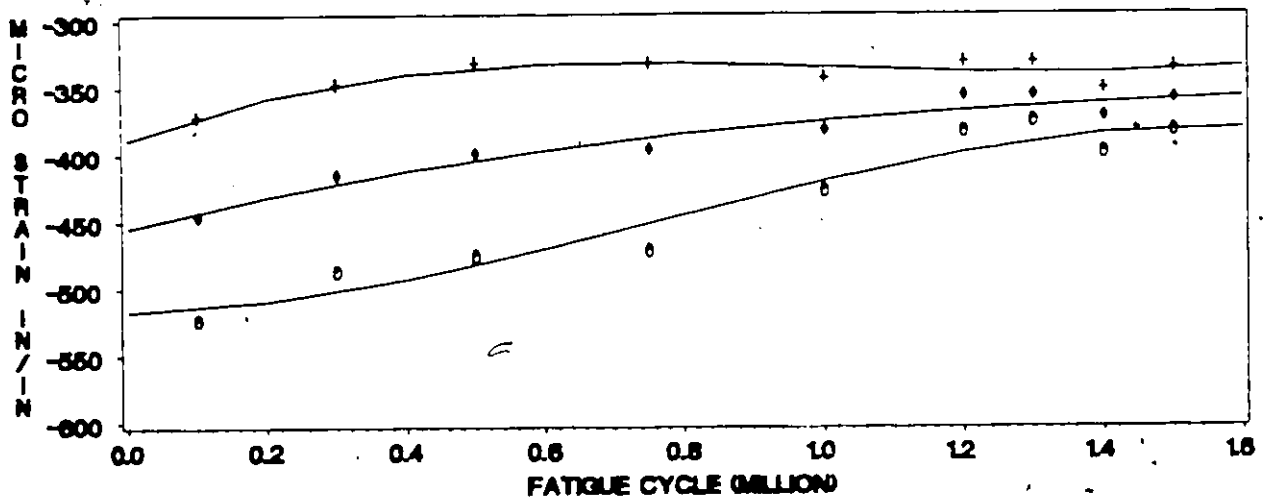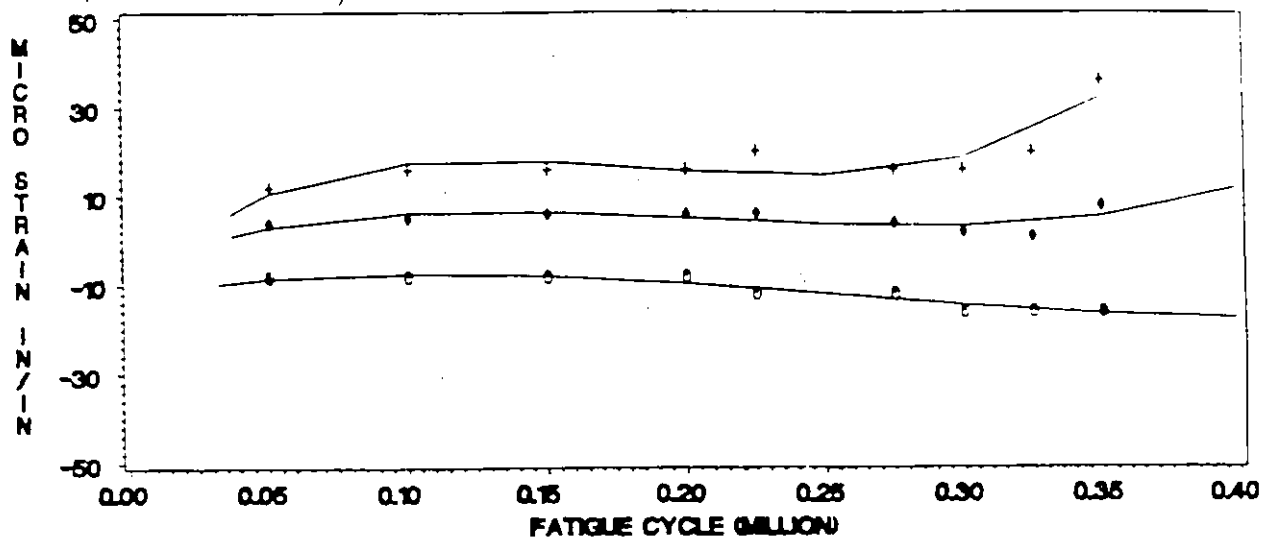

Figure 5.46: Strain Variation of gages 3 and 6 of Beam #5
With Increasing Fatigue Cycles
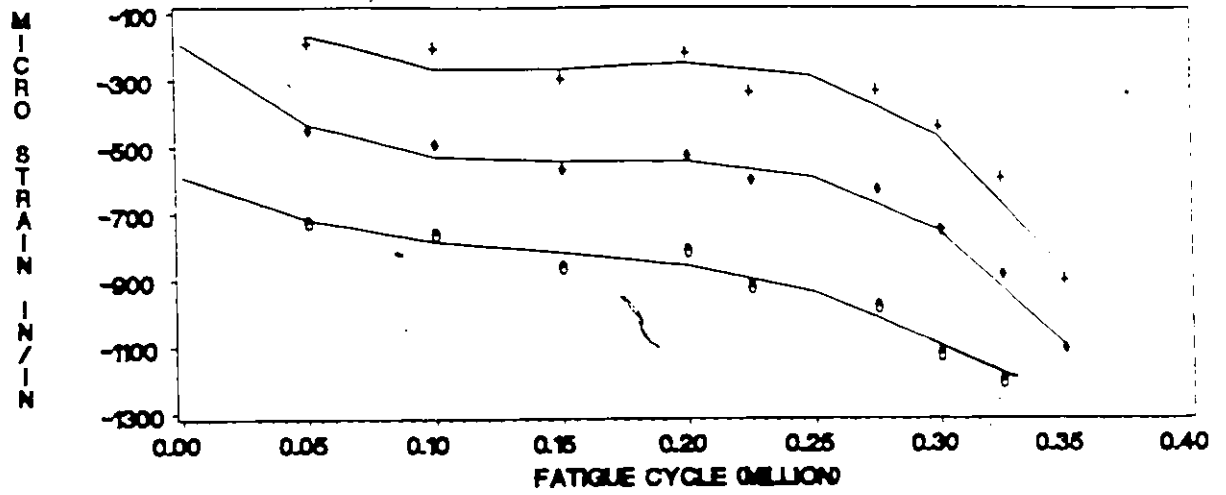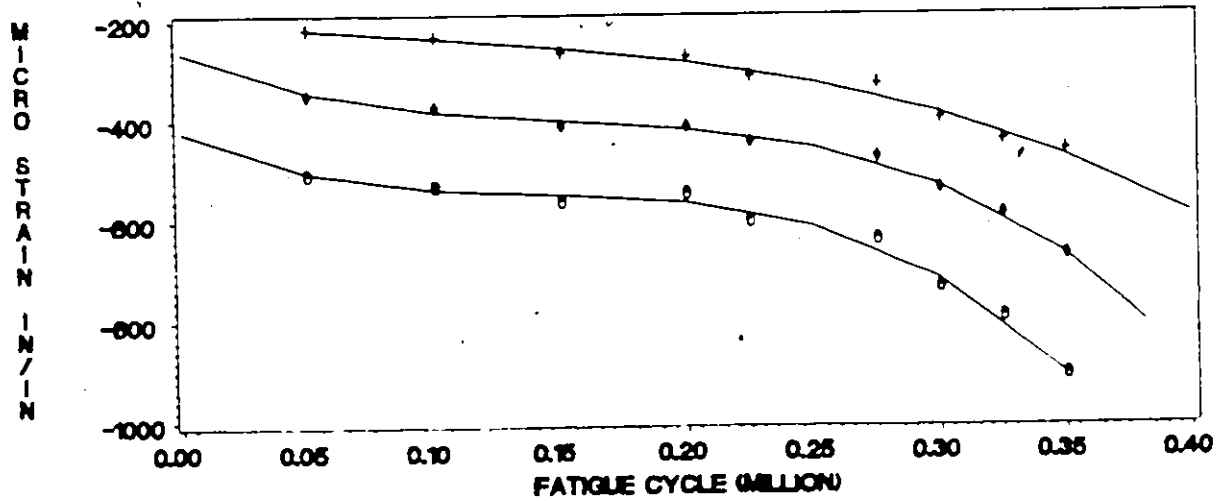
Figure 5.47:   Strain Variation of gages 1 and 3 of Beam #6
With Increasing Fatigue Cycles

FATIGUE READINGS OF STRAINGAGE 7
BEAM 6
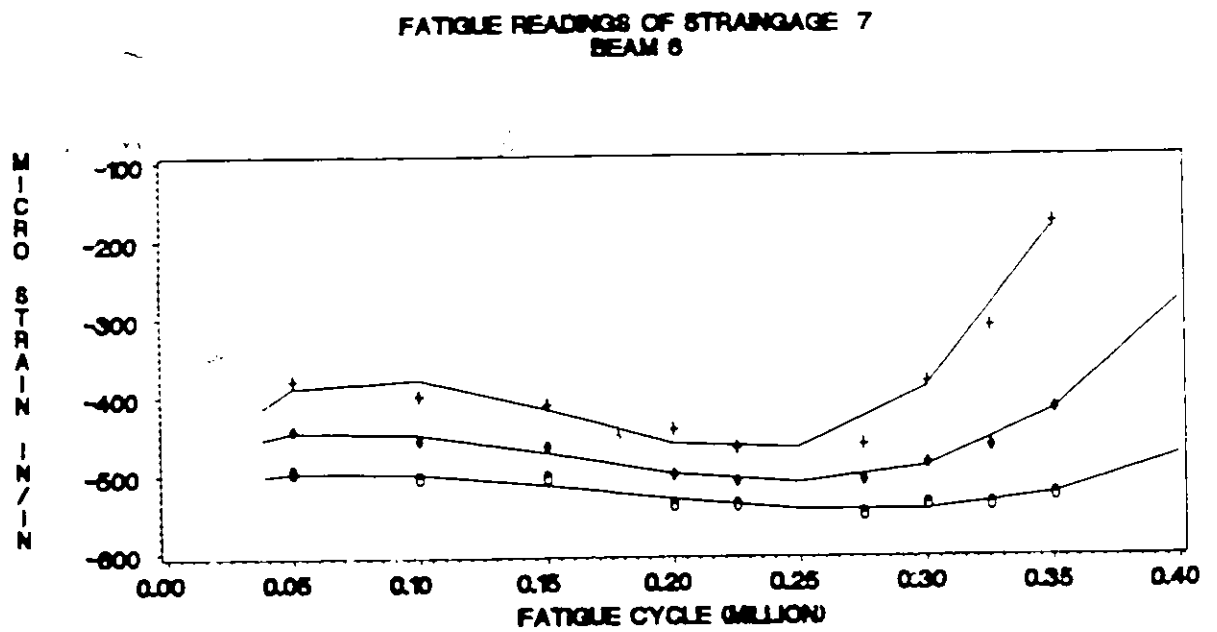
Figure 5.48: Strain Variation of gage #7 of Beam #6 With Increasing Fatigue Cycles
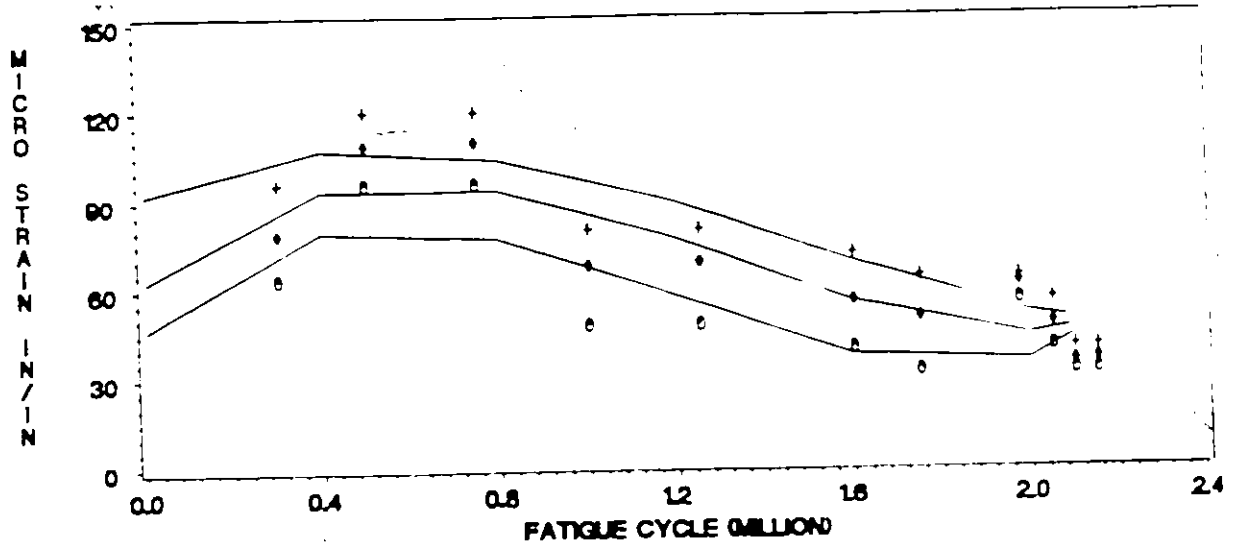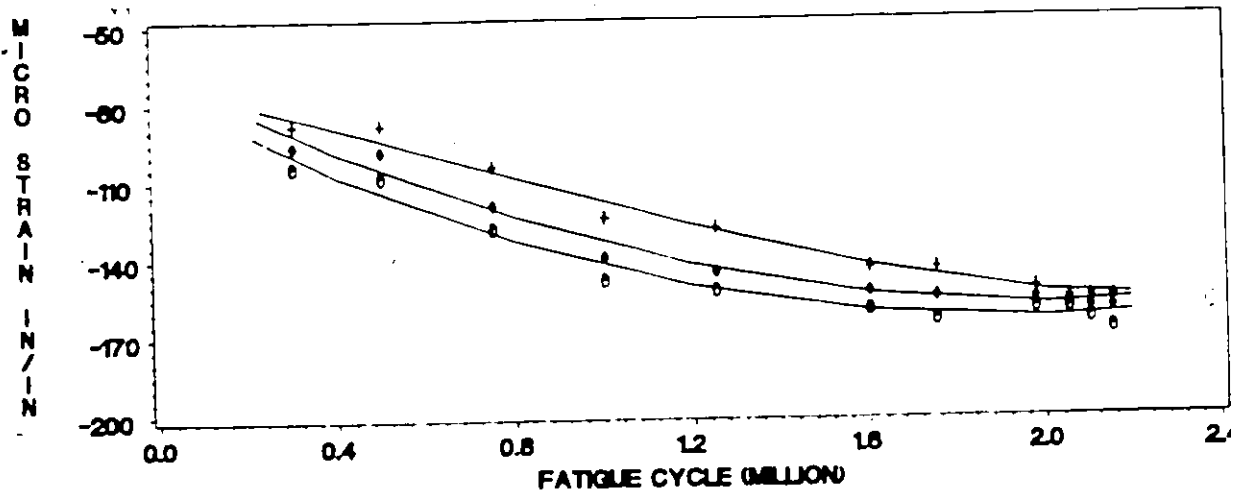
Figure 5.49:   Strain Variation of gages 11 and 15 of Beam #2
With Increasing Fatigue Cycles

FATIGUE READINGS OF STRAINGAGE 12
BEAM 3
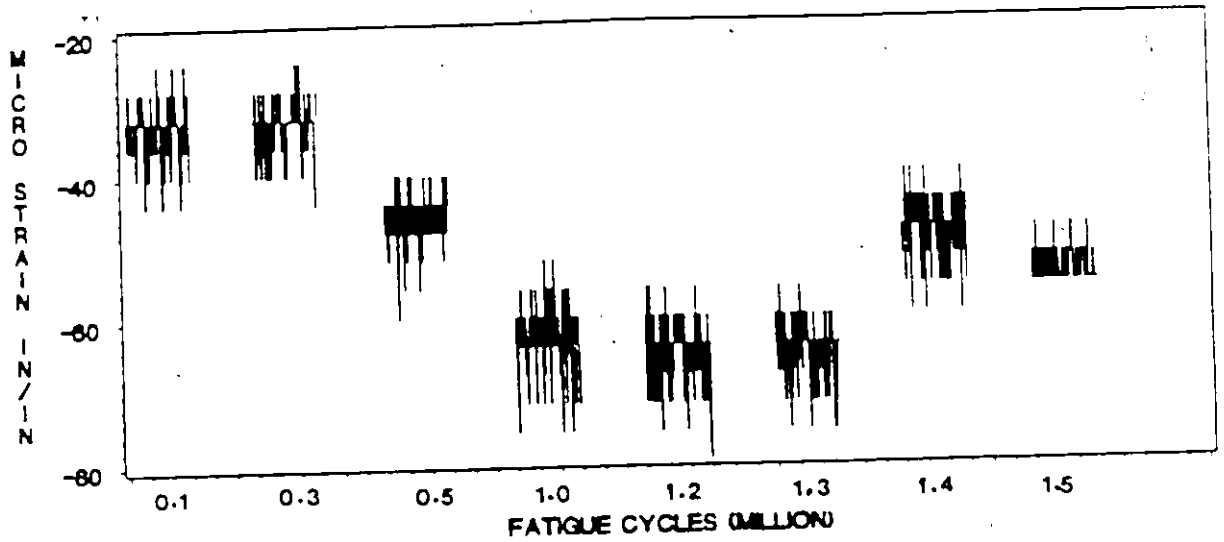
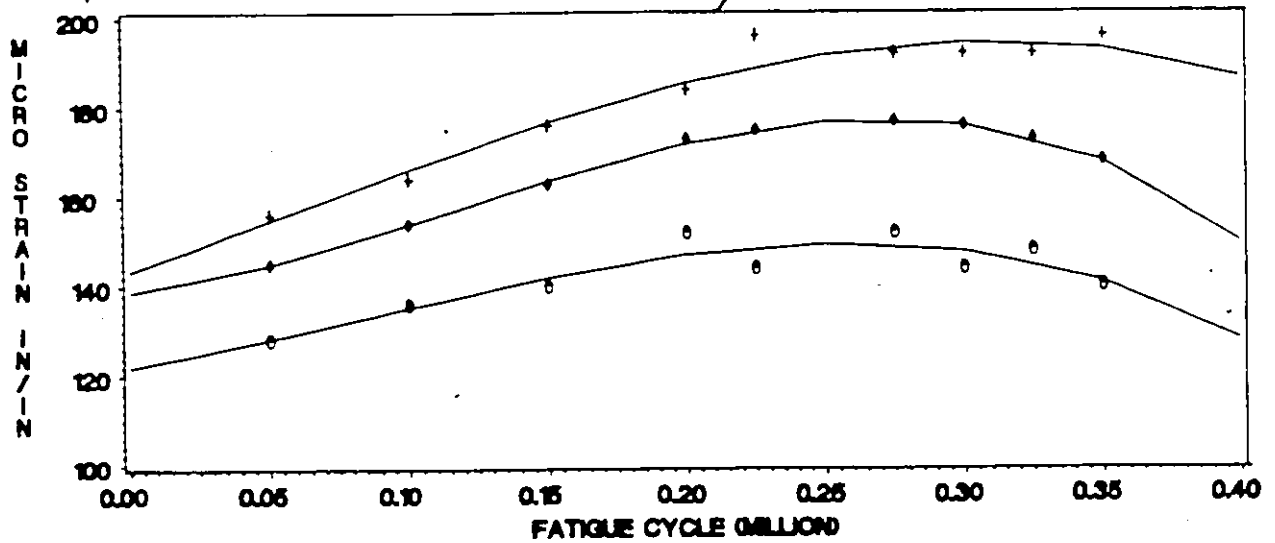

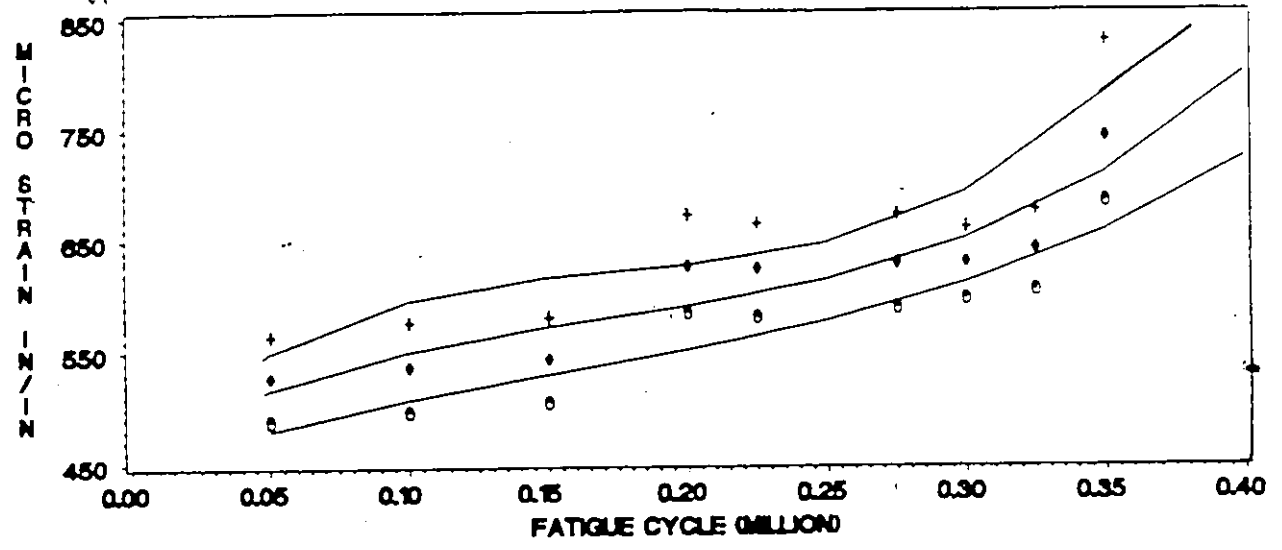FATIGUE READINGS OF STRAINGAGE 15
BEAM 3

Figure 5.50:   Strain Variation of gages 12 and 15 of Beam #3
With Increasing Fatigue Cycles

FATIGUE READINGS OF STRAINGAGE 12
BEAM 4

FATIGUE READINGS OF STRAINGAGE 13
BEAM 4

Figure 5.51: Strain Variation of gages 12 and 13 of Beam #4
With Increasing Fatigue Cycles

FATIGUE READINGS OF STRAINGAGE 11
BEAM 5

FATIGUE READINGS OF STRAINGAGE 13
BEAM 5

Figure 5.52:   Strain Variation of gages 11 and 13 of Beam #5
With Increasing Fatigue Cycles

FATIGUE READINGS OF STRAINGAGE 11
BEAM 6

FATIGUE READINGS OF STRAINGAGE 16
BEAM 6

Figure 5.53: Strain Variation of gages 11 and 16 of Beam #6 With Increasing Fatigue Cycles

FATIGUE READINGS OF STRAINGAGE 12
BEAM 6

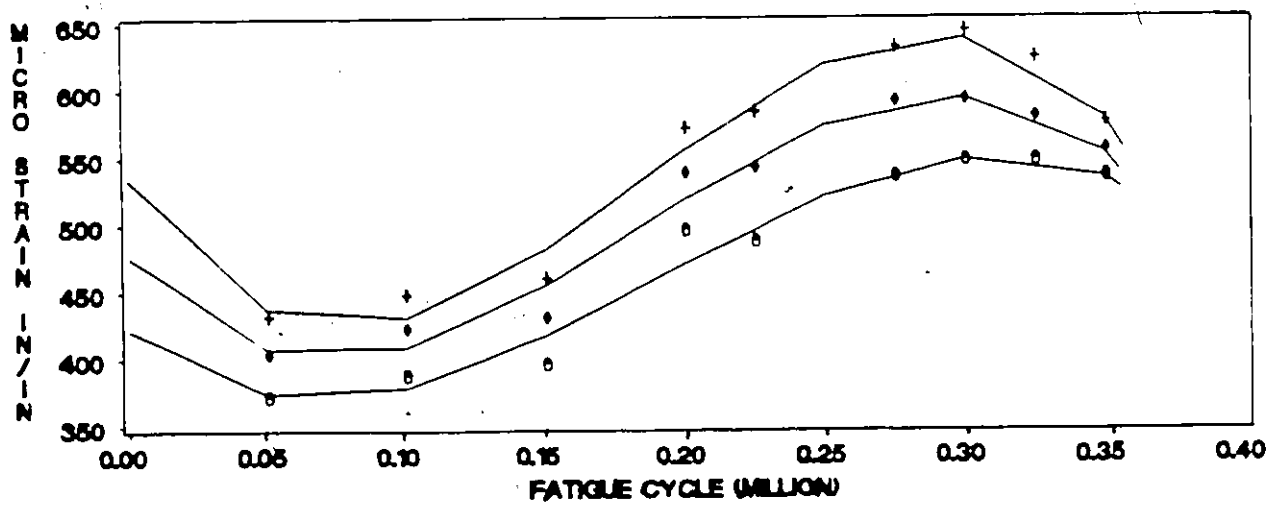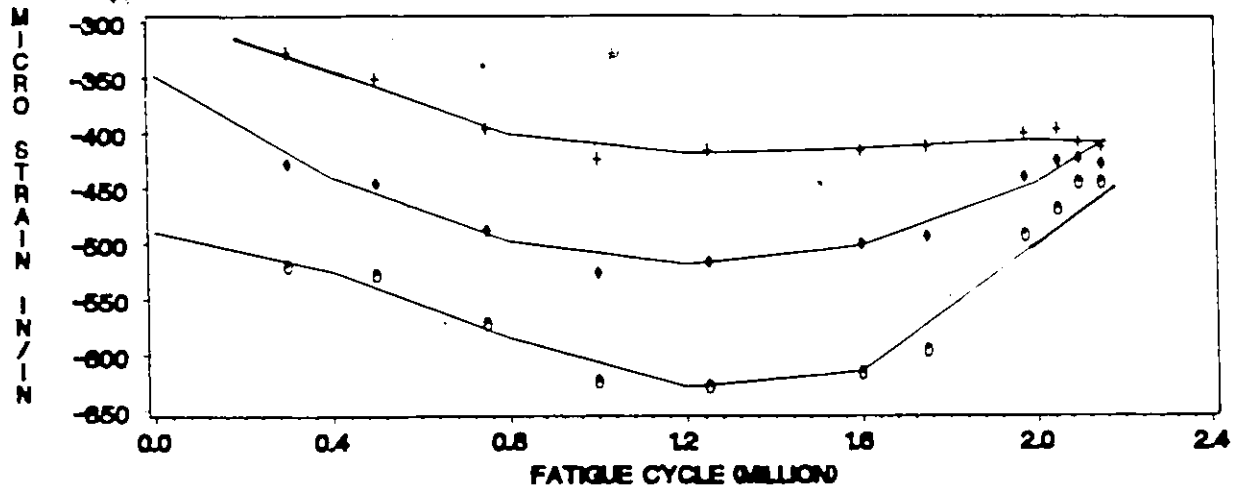FATIGUE READINGS OF STRAINGAGE 15
BEAM 6

Figure 5.54: Strain Variation of gages 12 and 15 of Beam #6
With Increasing Fatigue Cycles
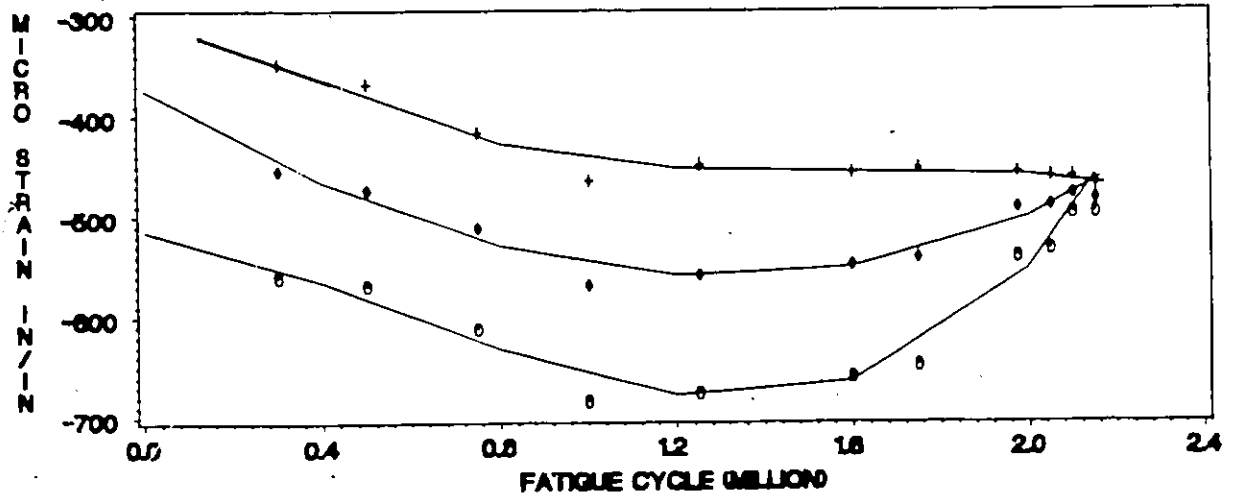
FATIGUE READINGS OF STRAINGAGE 21
BEAM 2

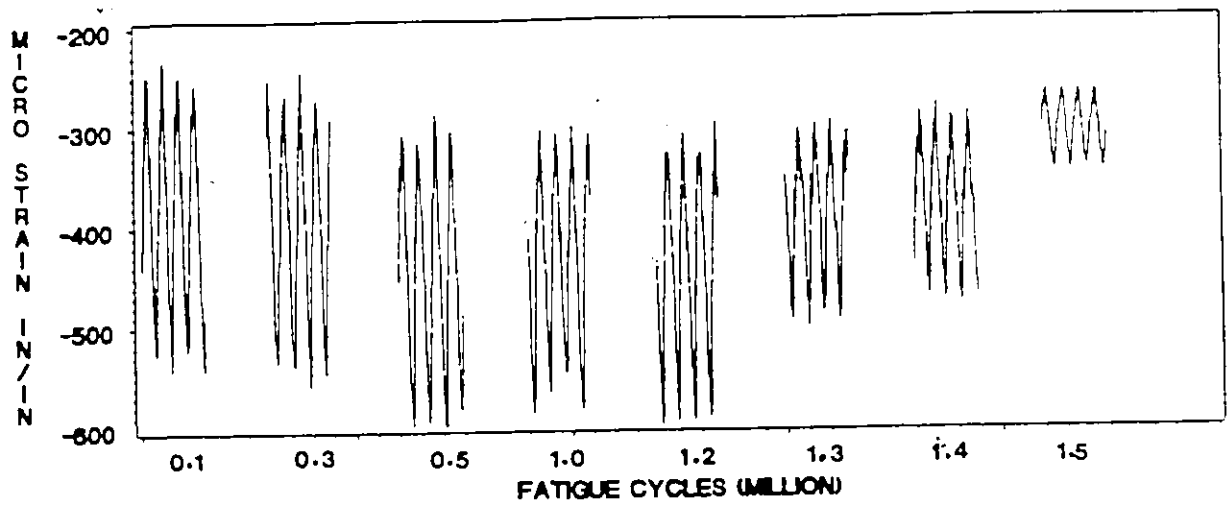FATIGUE READINGS OF STRAINGAGE 22
BEAM 2

Figure 5.55: Strain Variation of gages 21 and 22 of Beam #2
With Increasing Fatigue Cycles

FATIGUE READINGS OF STRAINGAGE 22
BEAM 3

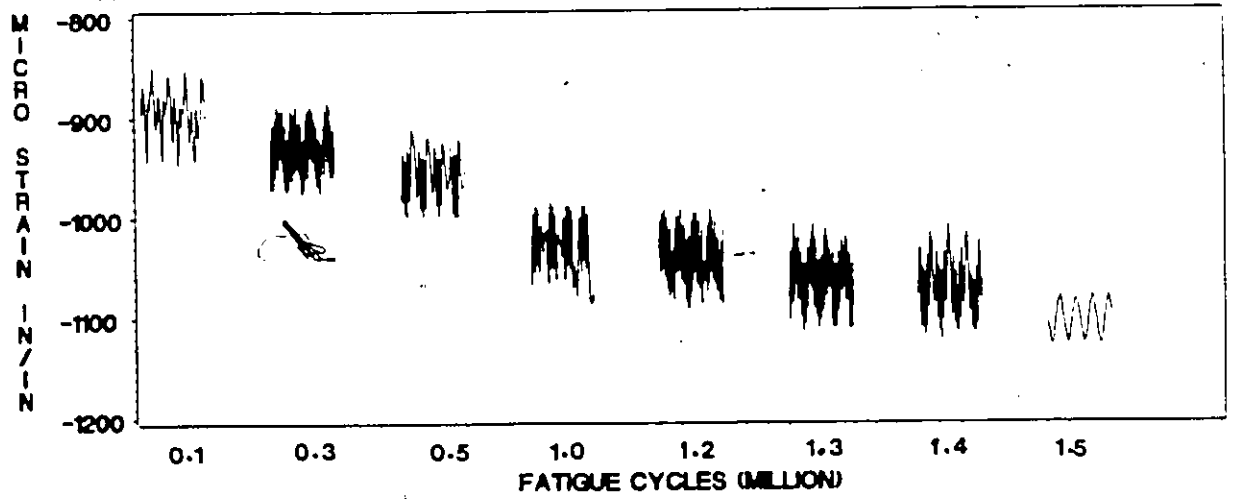FATIGUE READINGS OF STRAINGAGE 24
BEAM 3

Figure 5.56:   Strain Variation of gages 22 and 24 of Beam #3
With Increasing Fatigue Cycles

FATIGUE READINGS OF STRAINGAGE 24
BEAM 4

Figure 5.57: Strain Variation of gages 19 and 24 of Beam #4
With Increasing Fatigue Cycles

FATIGUE READINGS OF STRAINGAGE 21
BEAM 4

FATIGUE READINGS OF STRAINGAGE 22
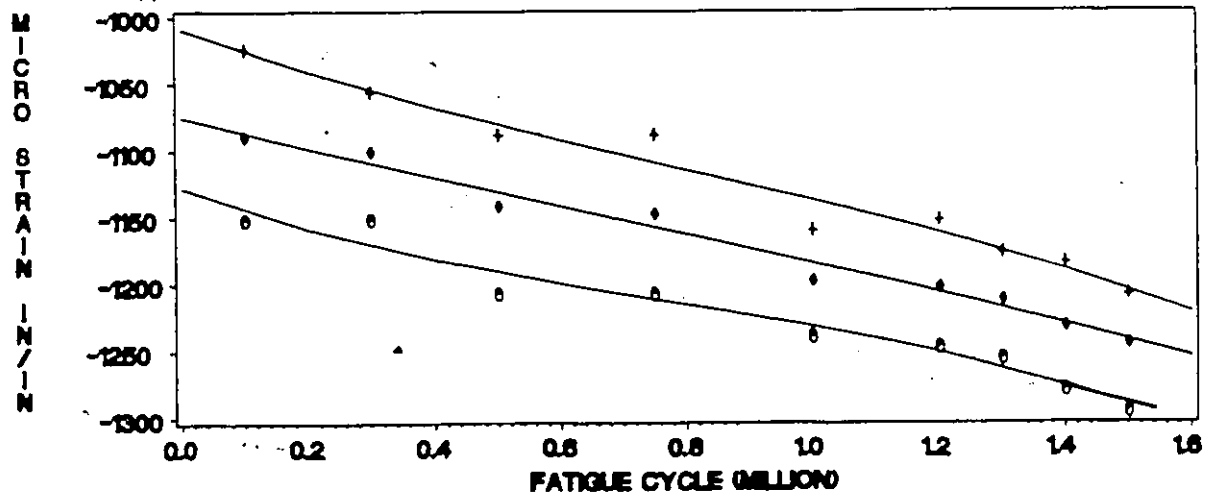BEAM 4
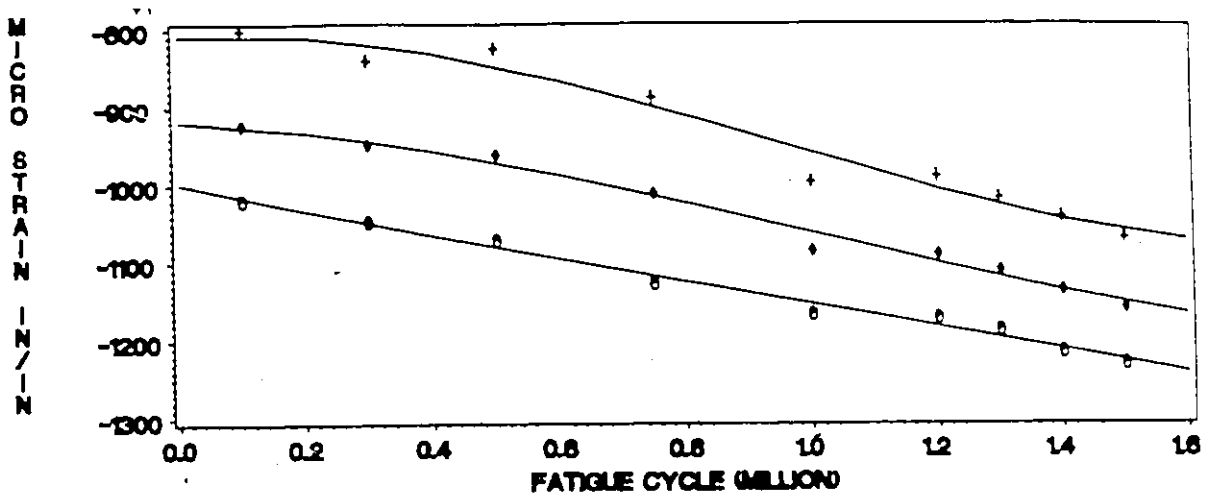

Figure 5.58: Strain Variation of gages 21 and 22 of Beam #4
With Increasing Fatigue Cycles

FATIGUE READINGS OF STRAINGAGE 21
BEAM 5

FATIGUE READINGS OF STRAINGAGE 22
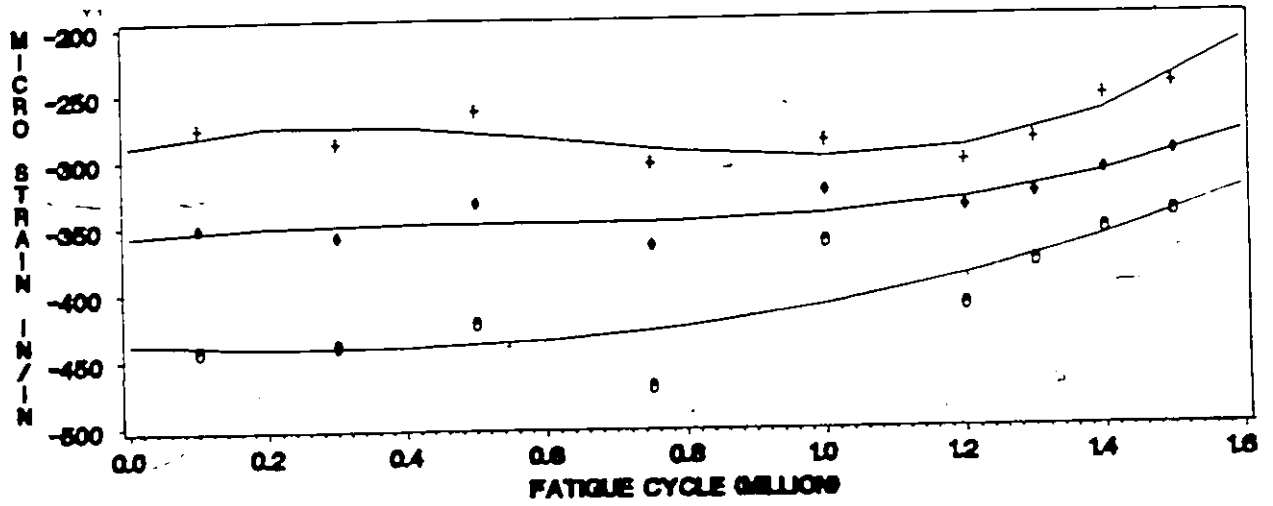BEAM 5
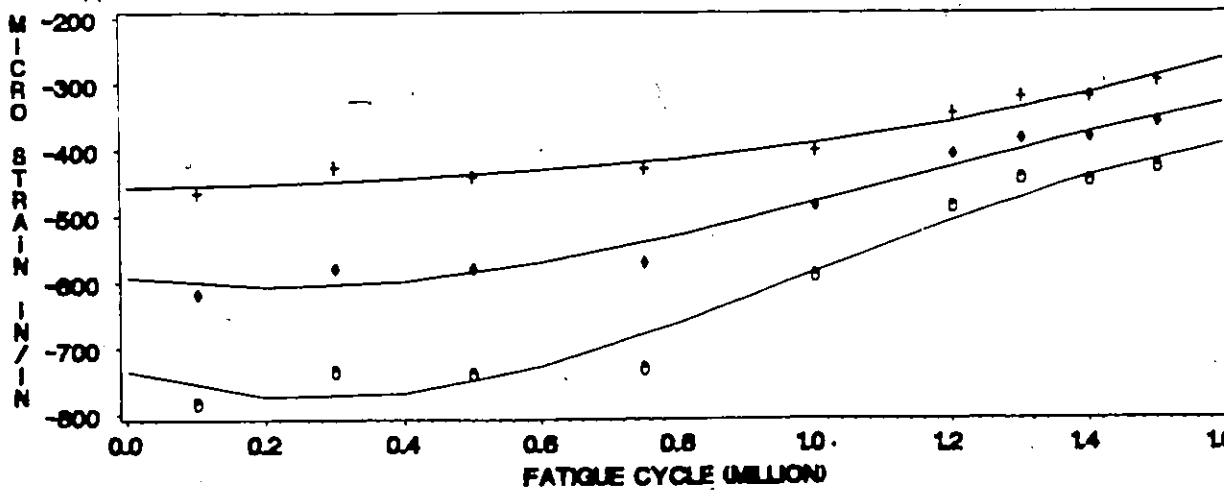
Figure 5.59: Strain Variation of gages 21 and 22 of Beam #5
With Increasing Fatigue Cycles

FATIGUE READINGS OF STRAINGAGE 23
BEAM 6
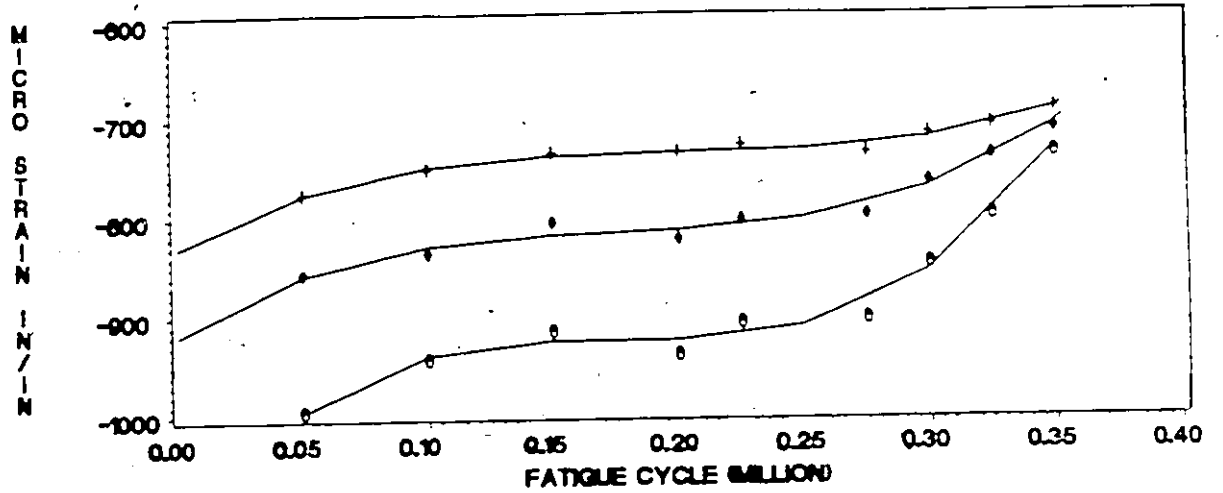
FATIGUE READINGS OF STRAINGAGE 24
BEAM 6
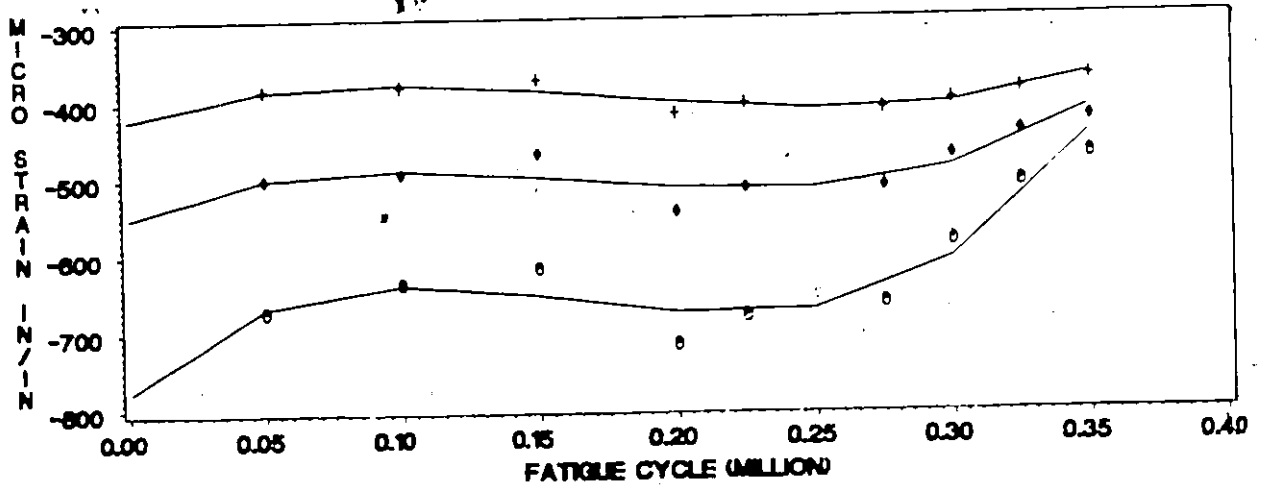
Figure 5.60: Strain Variation of gages 23 and 24 of Beam #6
With Increasing Fatigue Cycles

FATIGUE READINGS OF STRAINGAGE 25
BEAM 3

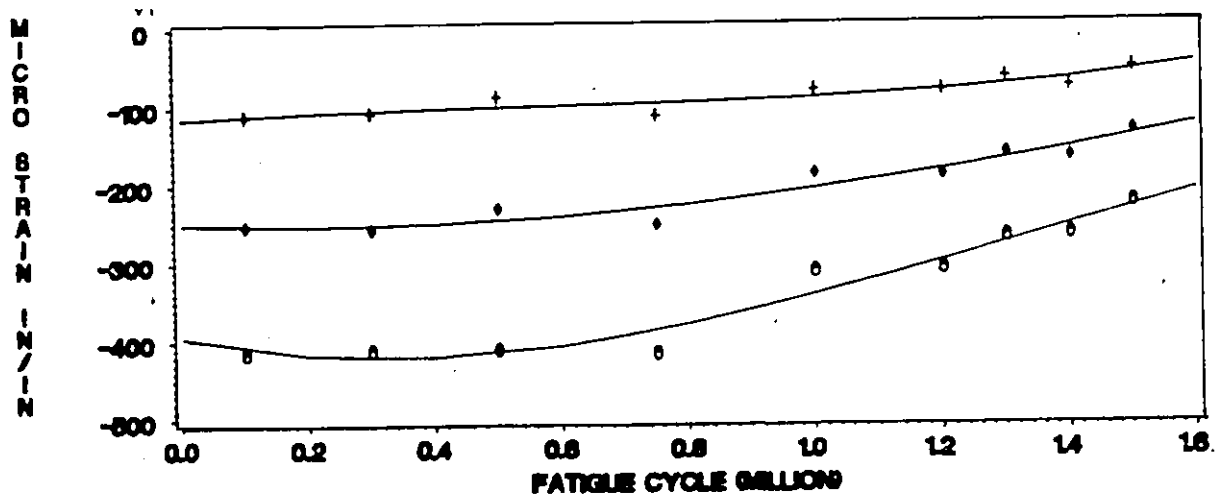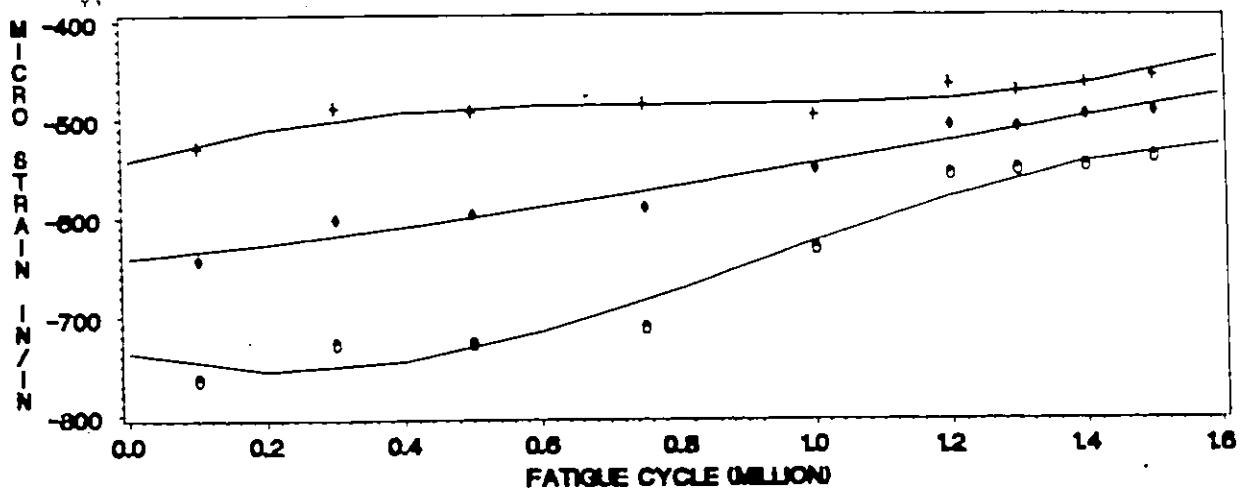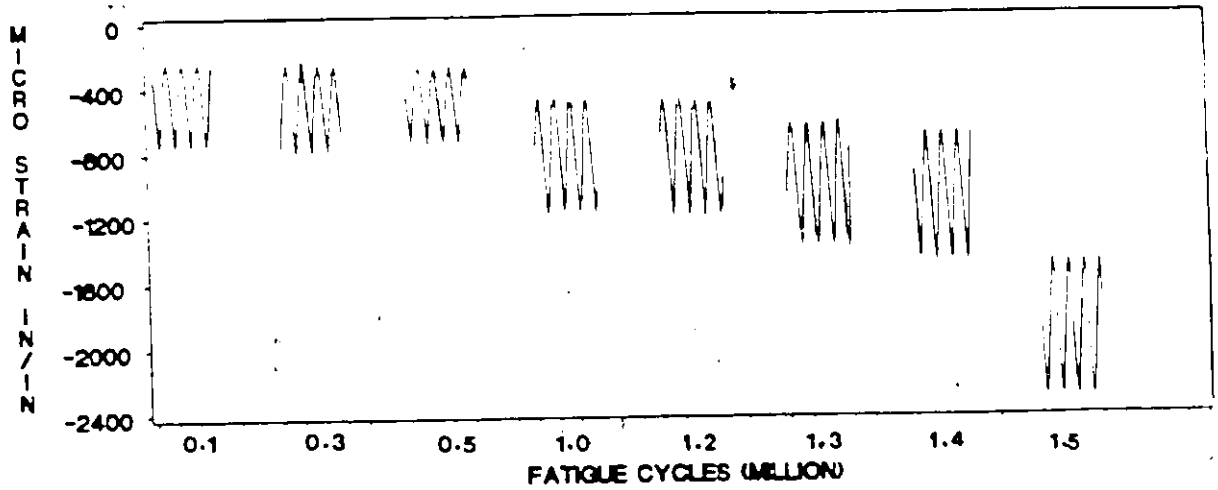FATIGUE READINGS OF STRAINGAGE 25
BEAM 4
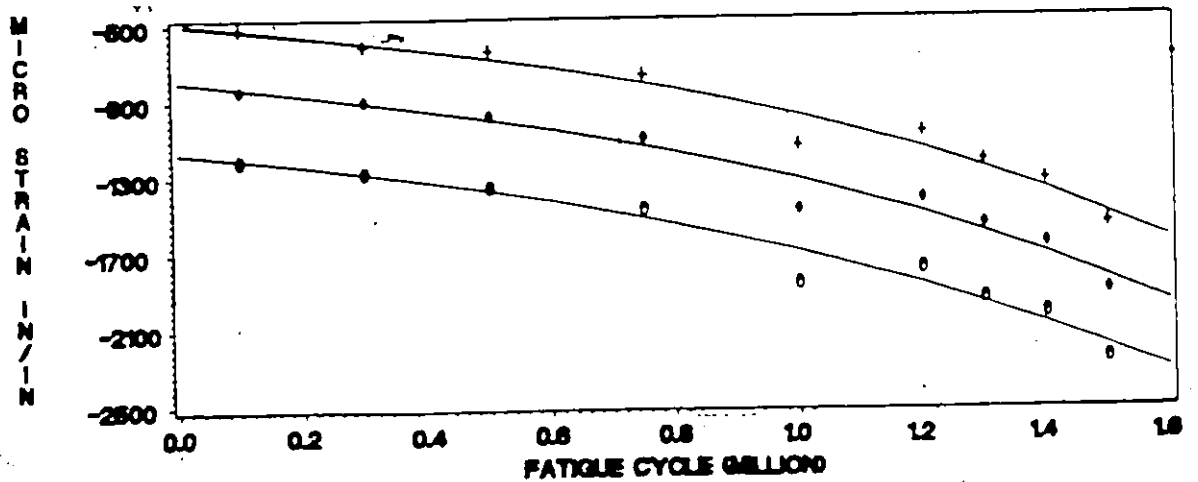
Figure 5.61: Strain Variation of gage #25 of Beams 3 and 4 With Increasing Fatigue Cycles

FATIGUE READINGS OF STRAINGAGE 26
BEAM 4
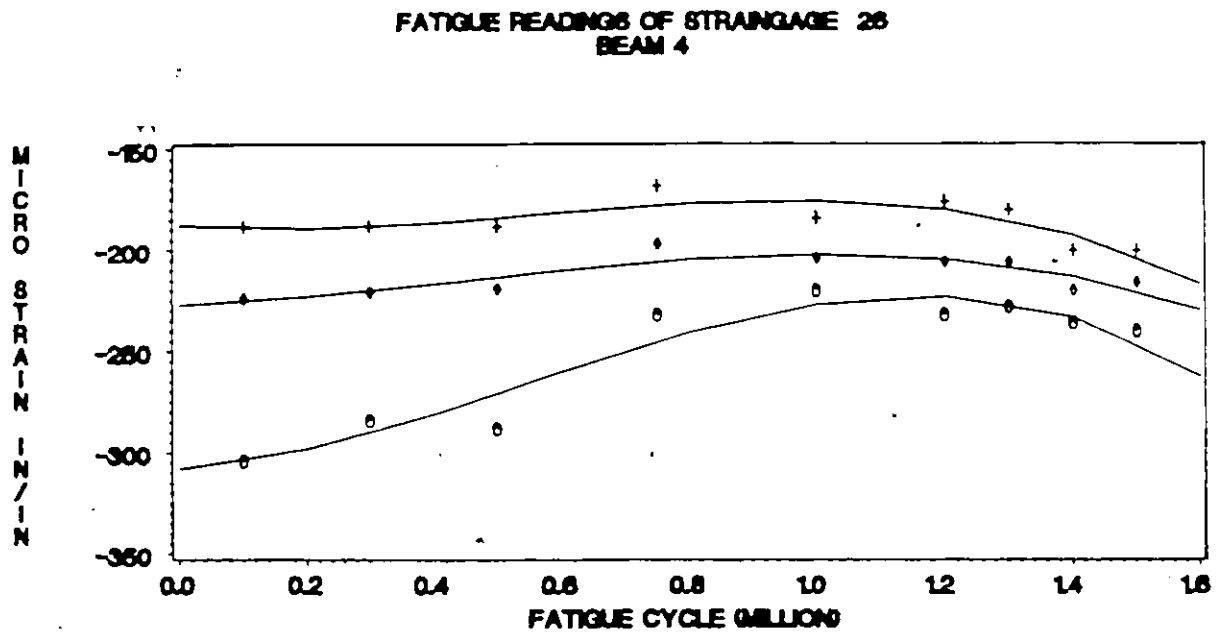
Figure 5.62: Strain Variation of gage #26 of Beam #4 With Increasing Fatigue Cycles
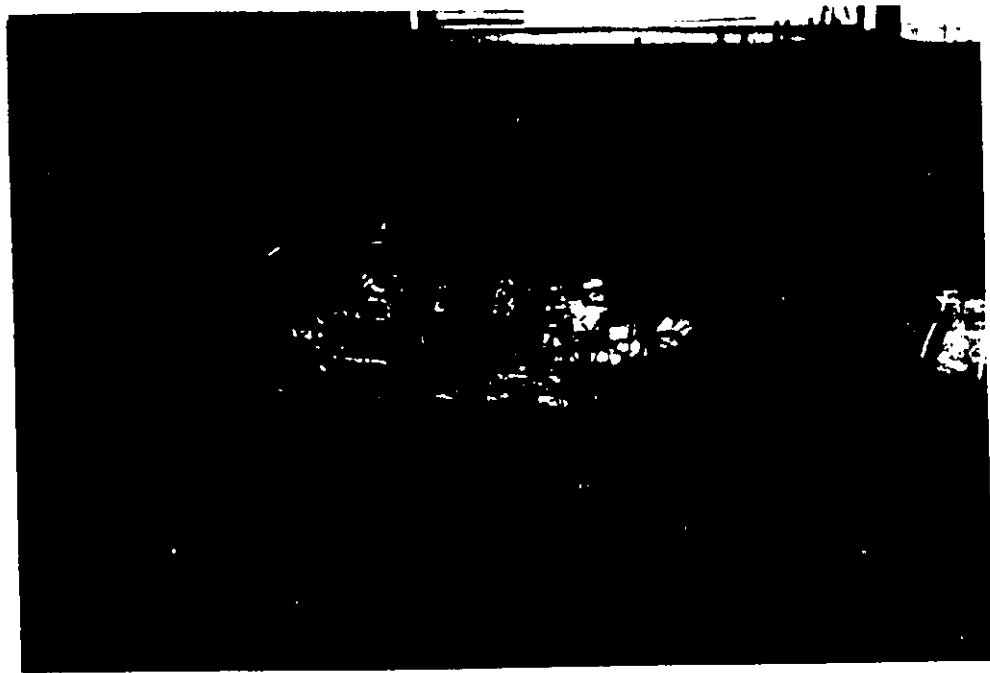
Figure 5.63:   Beam #1 Final Failure Mode and the Opening
                Region After Failure
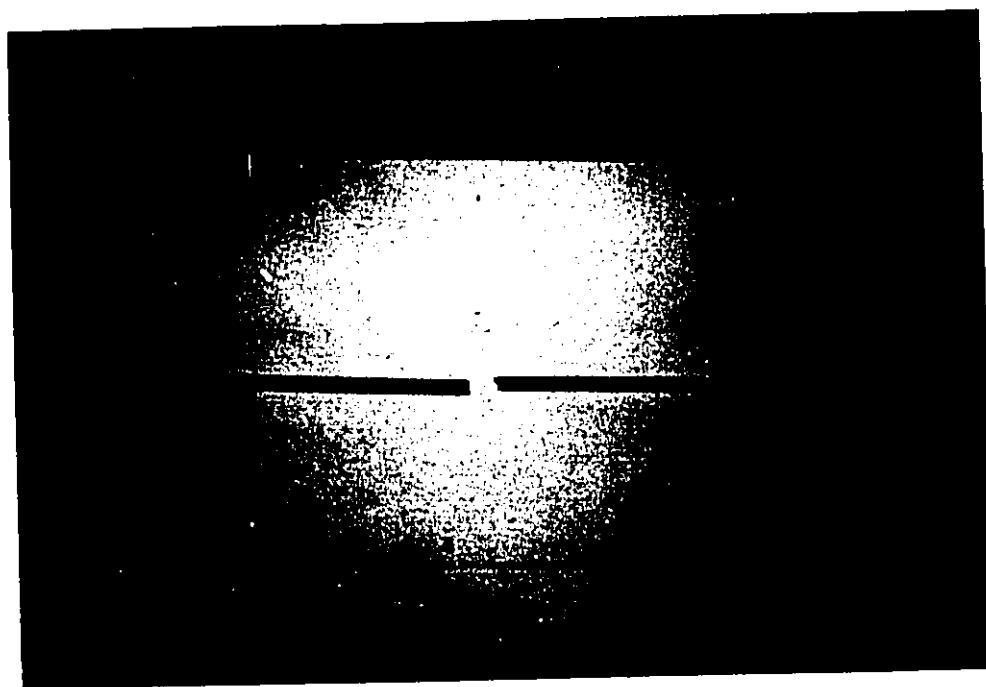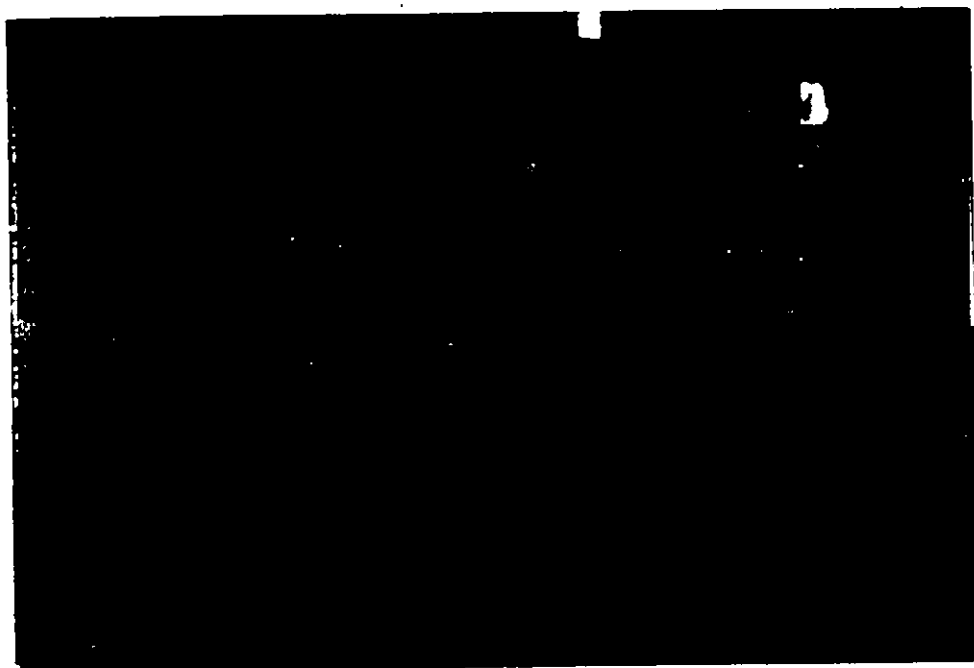
Figure 5.64: Beam #2 Cracking Patterns at Midspan and the Fatigued Prestressing Wire
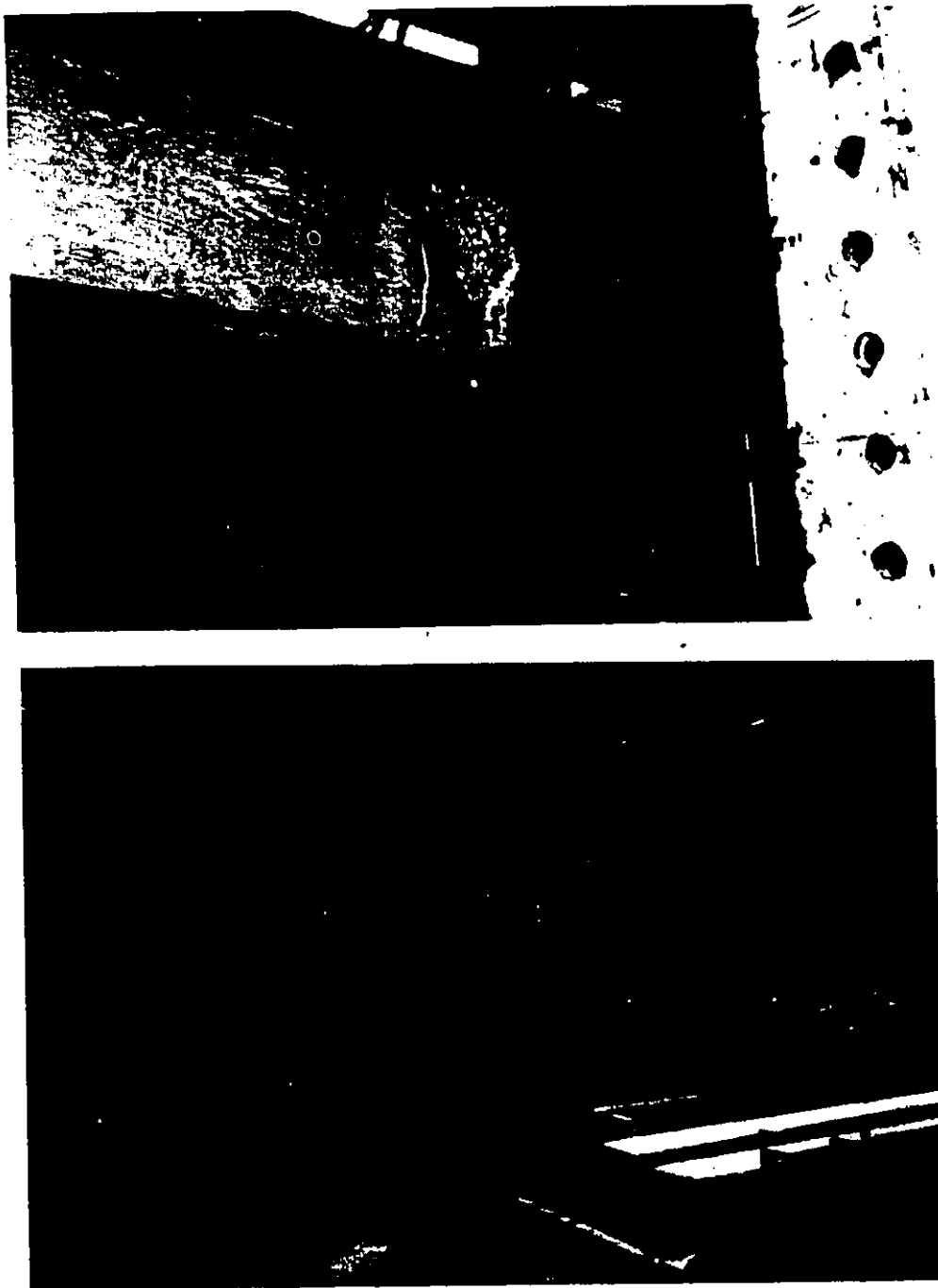
Figure 5.65:   Beam #3 Final Failure Mode
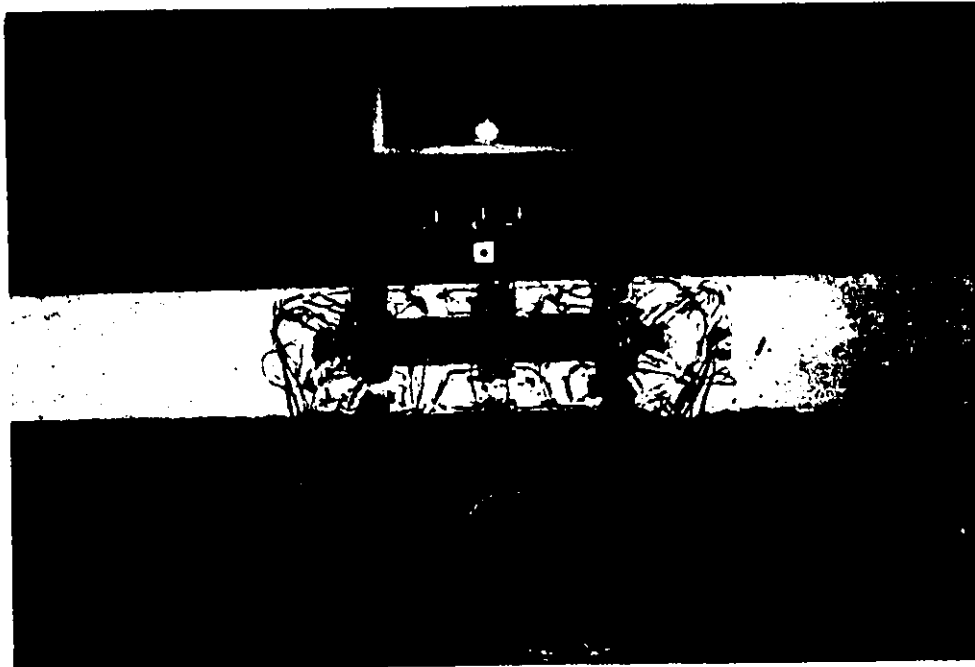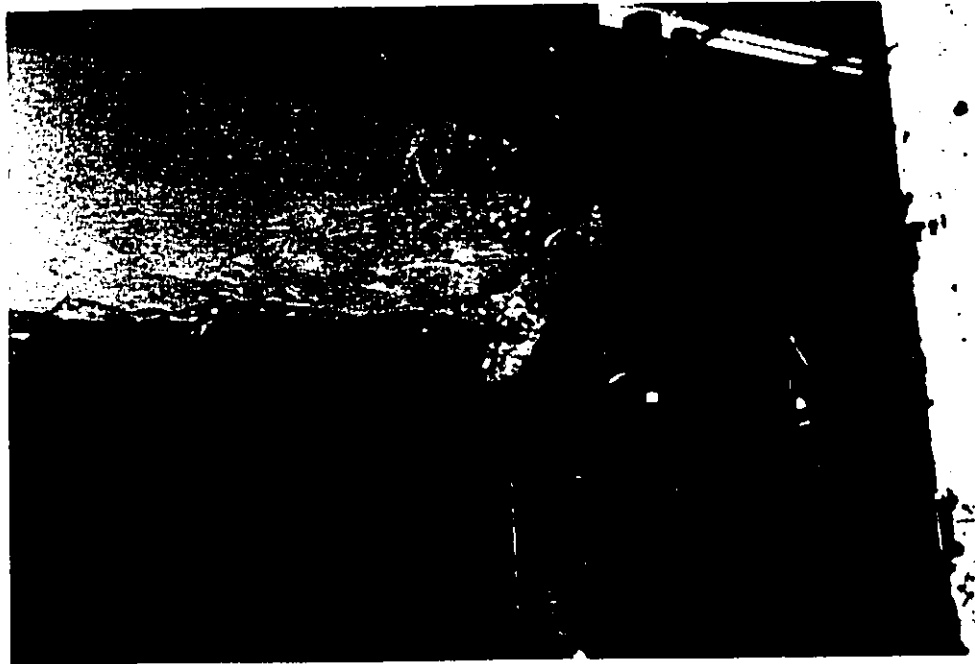
Figure 5.66: Beam #4 Final Failure Mode and the Opening Region After Failure
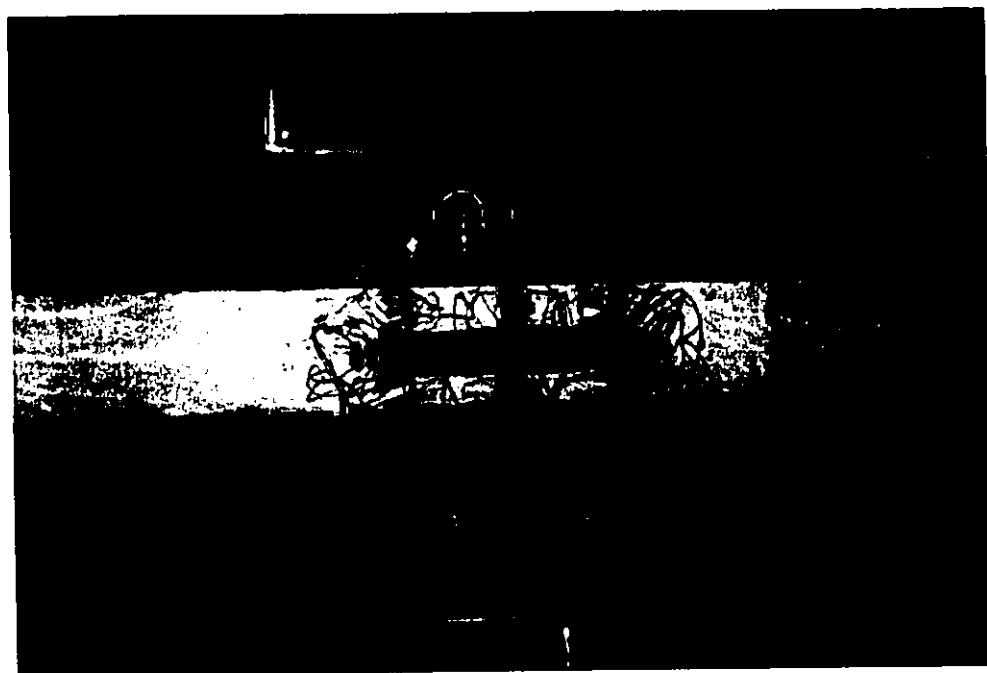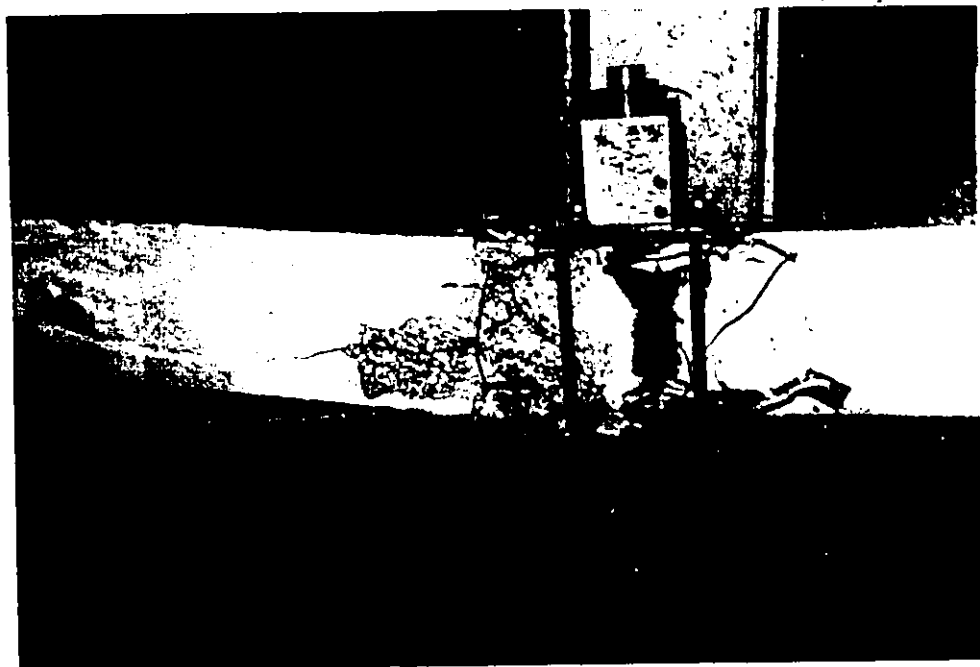
Figure 5.67: Beam #5 Final Failure Mode and the Opening Region After Failure

Figure 5.69:   Beam #6   Bottom Chord Mechanism and   the Final
                Static Failure Mode
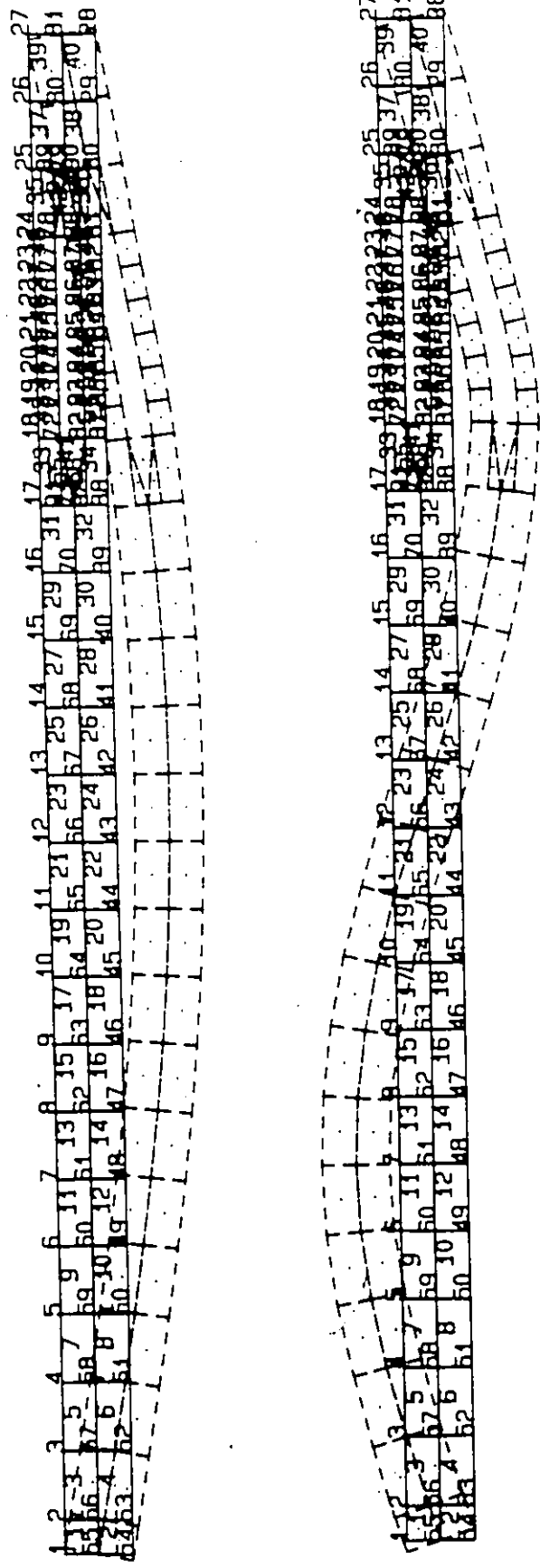
Figure 5.69: First and Second Mode Shapes for Rectangular Beam B8 (Side Opening)
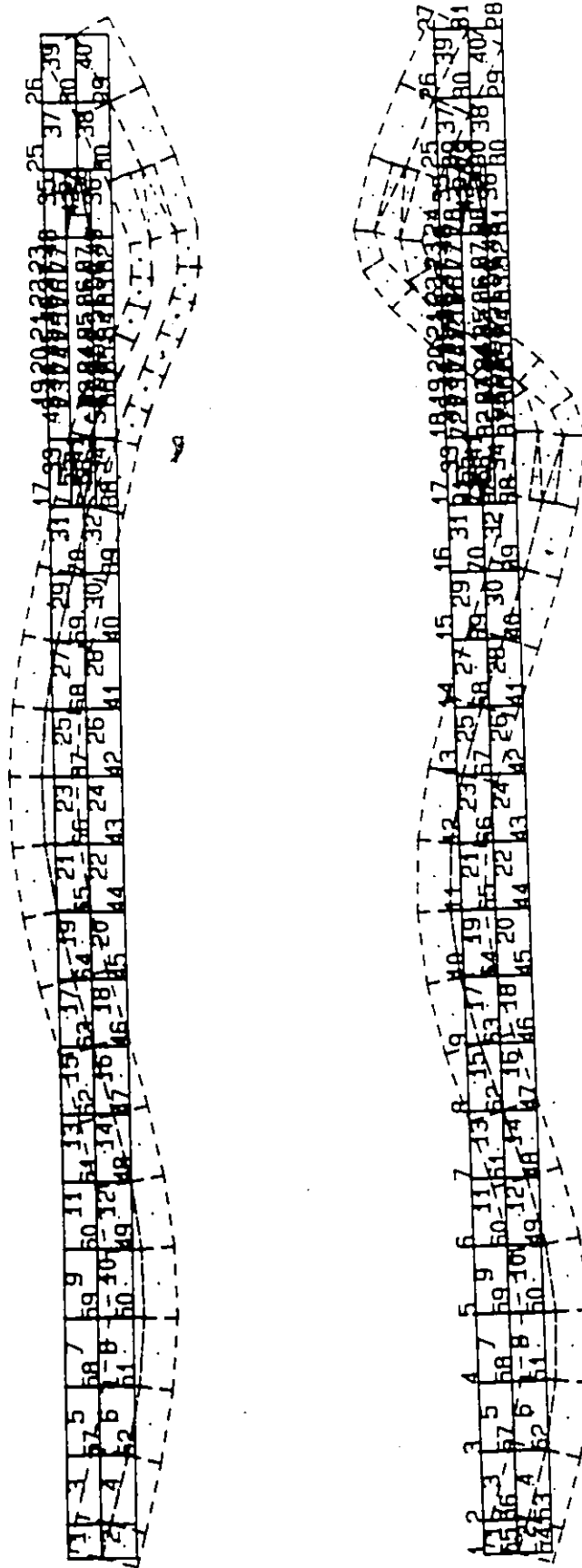
Figure 5.70: Third and Fourth Mode Shapes for Rectangular Beam #9 (Side Opening)

220
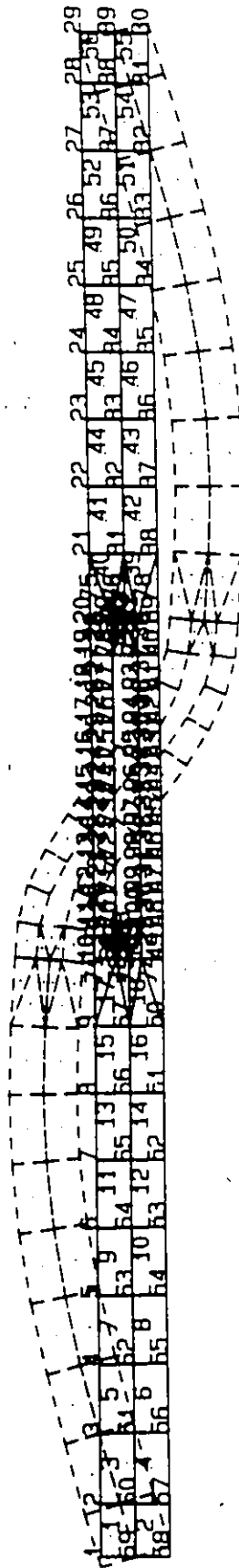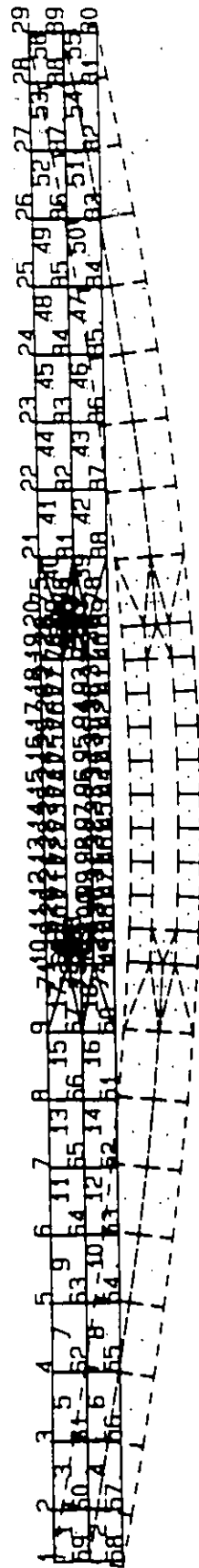
Figure 5.71: First and Second Mode Shapes for Rectangular
Beam #4 (Midspan Opening)
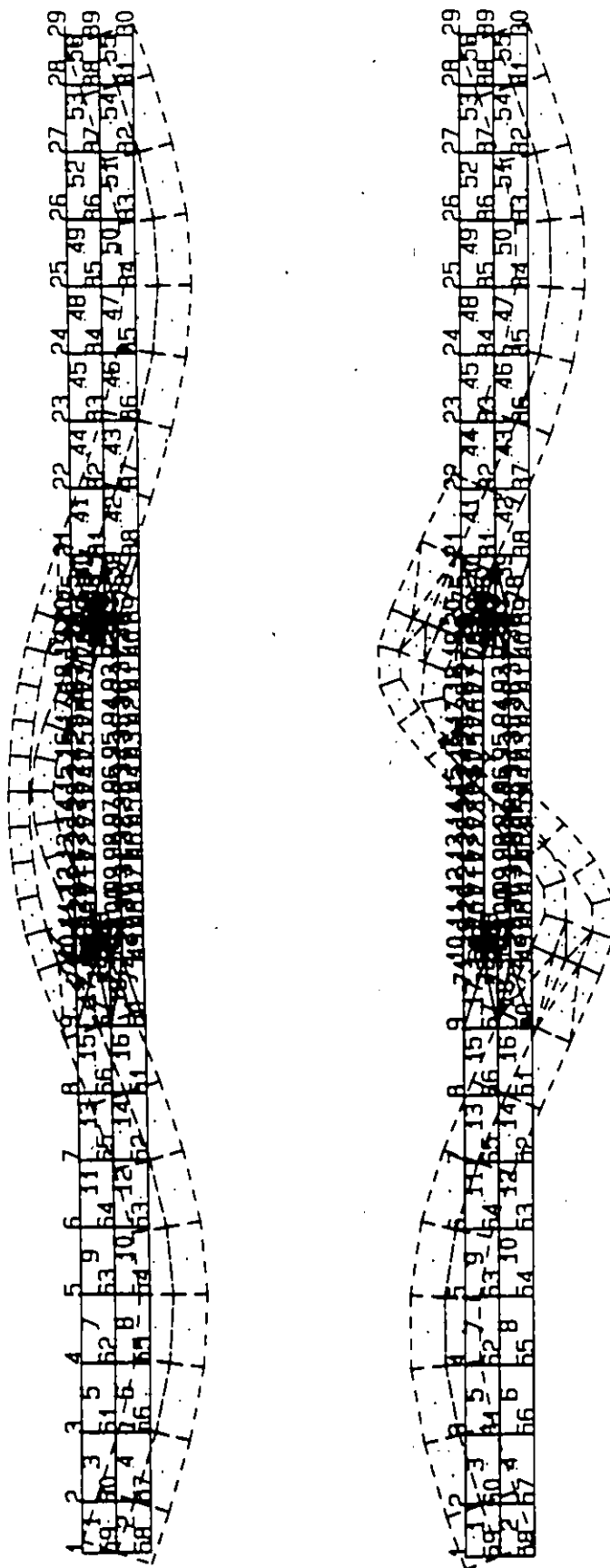
Figure 5.72: Third and Fourth Mode Shapes for Rectangular Beam #4 (Midspan Opening)
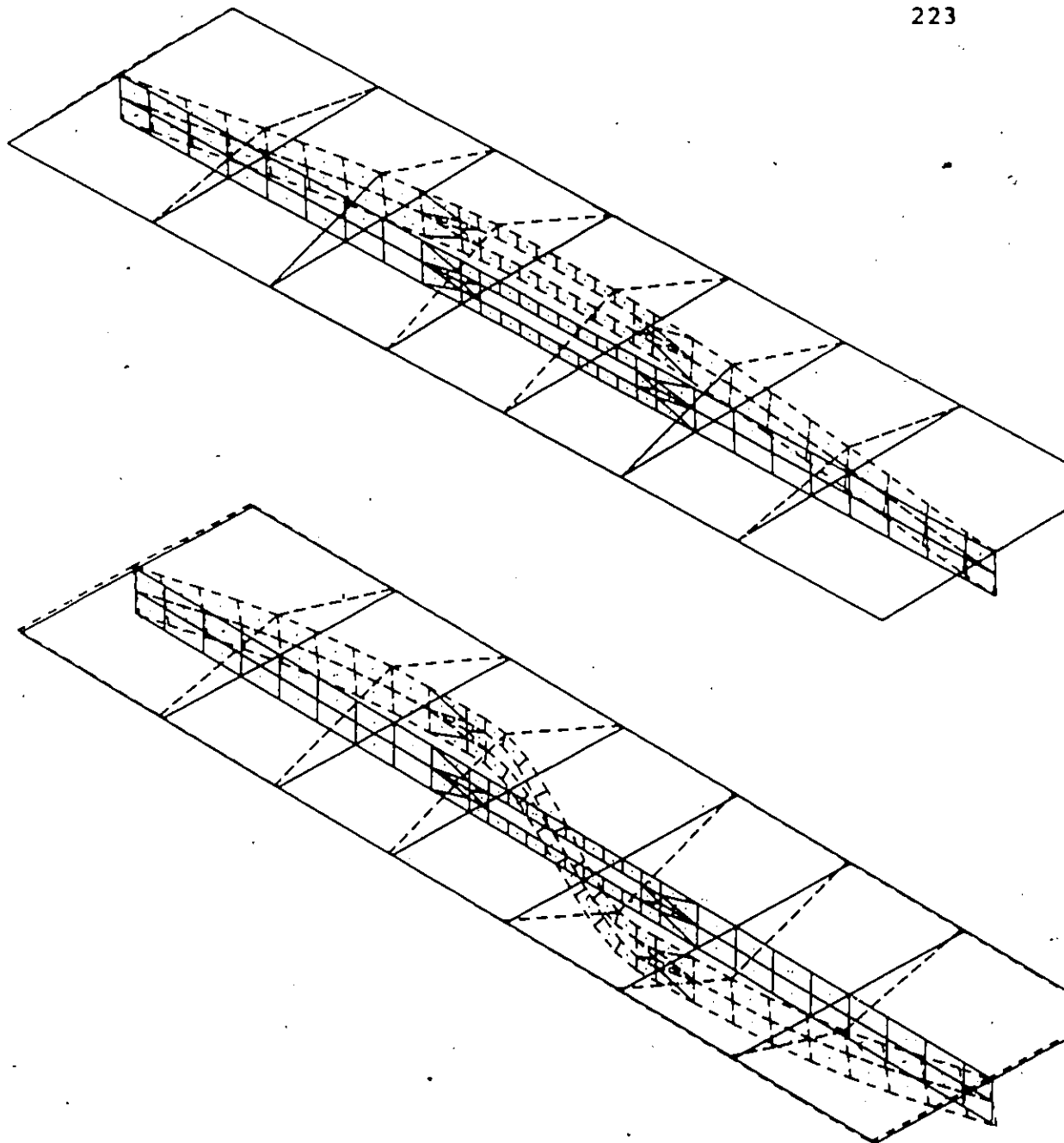
Figure 5.73: First and Second Mode Shapes for Tee Beam #4
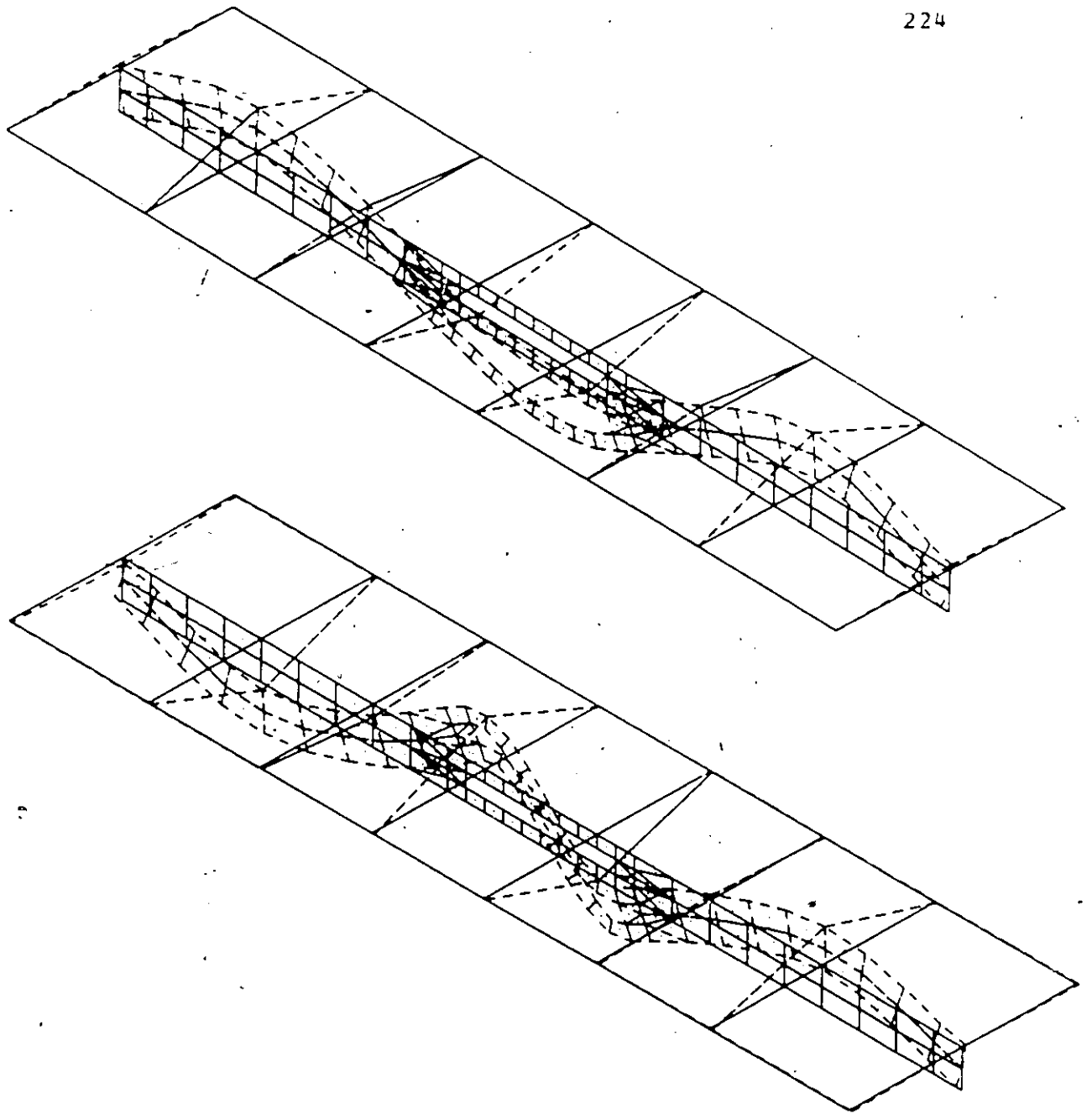
Figure 5.74: Third and Fourth Mode Shapes for Tee Beam #4
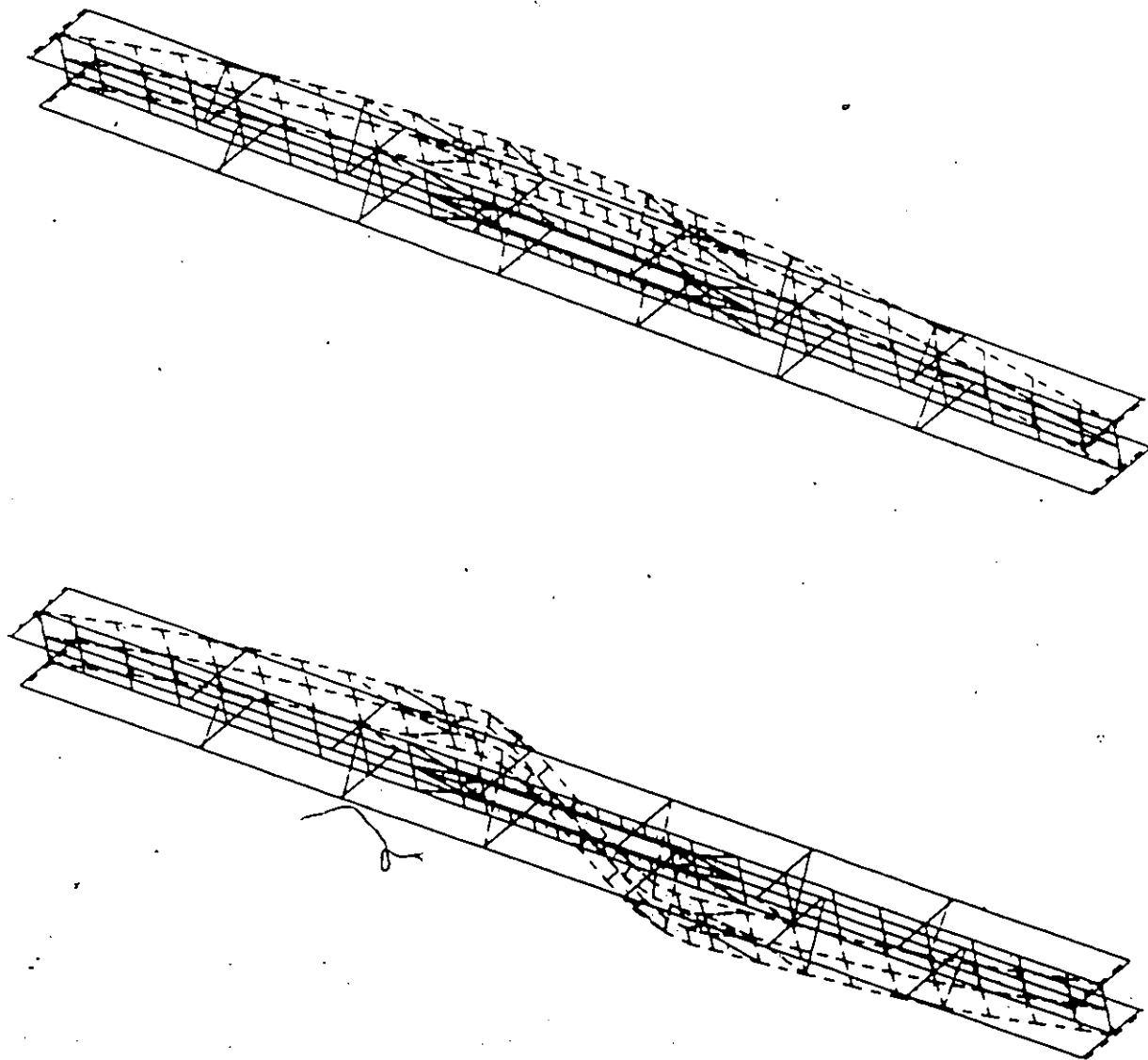
Figure 5.75:   First and Second Mode Shapes for I Beam #3

Appendix E

TABLES

Table 3.1: Rectangular Beams With Openings in the Shear Span

BEAM#	BEAM DIMENSIONS			OPENING SIZE		OPENING LOCATION	
	B (in)	H (in)	L (in)	h (in)	w (in)	ℓ (in)	c (in)
1	3	8	180	SOLID	SOLID	----	----
2	3	8	180	3	4	24	4
3	3	8	180	3	8	24	4
4	3	8	180	3	12	24	4
5	3	8	180	3	16	24	4
6	3	8	180	3.	20	24	4
7	3	8	180	3	24	24	4
8	3	8	180	3	32	24	4

Table 3.2: Rectangular Beams With Openings at midspan

BEAM#	BEAM DIMENSIONS			OPENING SIZE		OPENING LOCATION	
	B (in)	H (in)	L (in)	h (in)	w (in)	ℓ (in)	c (in)
1	3	8	180	3	8	86	4
2	3	8	180	3	16	82	4
3	3	8	180	3	24	78	4
4	3	8	180	3	32	74	4

Table 3.3:   Rectangular Beams With Two Openings in the Shear Span

BEAM#	BEAM DIMENSIONS			OPENING #1 SIZE		OPENING #2 SIZE		OPENING #1 LOCATION		CHORD LENGTH
	B (in)	H (in)	L (in)	h (in)	w (in)	h_2 (in)	w_2 (in)	ℓ (in)	c (in)	(in)
1	3	8	180	3	4	3	4	24	4	16
2	3	8	180	3	8	3	8	24	4	8
3	3	8	180	3	8	3	12	24	4	4

Table 3.4:   T-Beams With Openings at Midspan

BEAM#	TEE BEAM DIMENSIONS					OPENING SIZE		OPENING LOCATION	
	WEB		FLANGE						
	B (in)	H (in)	B_1 (in)	H_1 (in)	L (in)	h (in)	w (in)	ℓ (in)	c (in)
1	3	8	48	7	180	SOLID	SOLID	--	--
2	3	8	48	7	180	3	16	82	4
3	3	8	48	7	180	3	24	78	4
4	3	8	48	7	180	3	32	74	4
5	3	8	16	3	180	SOLID	SOLID	--	--
6	3	8	16	3	180	3	32	74	4

Table 3.5:   I-Beams With Openings at midspan

	WEB		TOP FLANGE			BOTTOM FLANGE		OPENING SIZE		OPENING LOCATION	
BEAM#	B (in)	H (in)	B_1 (in)	H_1 (in)	L (in)	B_2 (in)	H_2 (in)	h (in)	w (in)	ℓ (in)	c (in)
1	3	8	12	3	180	12	3	SOLID	SOLID	--	--
2	3	8	12	3	180	12	3	3	16	82	4
3	3	8	12	3	180	12	3	3	32	74	4

Table 4.1:   Characteristics of the Tested Rectangular Beams

	BEAM DIMENSIONS			OPENING SIZE		OPENING LOCATION		ECC. AND PREST. FORCE P		CONCRETE COMPRESSIVE STRENGTH
BEAM#	B (in)	H (in)	L (in)	h (in)	w (in)	ℓ (in)	c (in)	e (in)	P (kips)	f'_c (psi)
1	3	8	180	3	8	24	4.0	1.17	23.1	6925
2	3	8	180	3	12	24	4.0	1.17	23.4	7153
3	3	8	180	3	16	24	4.0	1.17	24.1	6885
4	3	8	180	3	16	24	4.5	1.17	24.4	7043
5	3	8	180	3	16	24	3.5	1.17	24.2	6808
6	3	8	180	3	16	82	4.0	1.17	23.2	6350

Table 5.1:   Experimental Free Vibration Natural Frequencies
             by the Hammer Test

FREQUENCY

BEAM #	f_1 (Hz)	f_2 (Hz)	f_3 (Hz)
1	16.5 ** 18.0	69.5 ** 70.5	148.0 ** 149.0
2	16.5 ** 18.5	69.5 ** 72.5	148.5 ** 150.0
3	16.5 ** 18.0	69.5 ** 71.0	150.5 ** 149.5
4	17.0 ** 18.0	70.5 ** 71.5	149.5 ** 154.5
5	17.0 ** 18.0	71.5 ** 71.5	144.0 ** 144.0
6	19.0	68.0	151.5

Note:

** Frequency Values With the Beam Tied and

the Loading Jack Resting at Midspan

Table 5.2:   Loading Amplitudes for Dynamic and fatigue tests

MAXIMUM LOADING AMPLITUDE

BEAM#	STATIC PRECOMPRESSION (kips)	SINE WAVE SWEEP TEST (kips)	FATIGUE TEST (kips)
1	0.15	0.83	1.28
2	0.08	0.45	0.83
3	0.08	0.45	1.28
4	0.08	0.45	1.28
5	0.08	0.45	1.28
6	0.08	0.45	1.28

Note:

Cracking Load = 1.6 kips

80% of the Cracking Load = 1.28 kips

50% of the Cracking Load = 0.83 kips

30% of the Cracking Load = 0.45 kips

Table 5.3: Experimental Sine Wave Sweep Test Results Before
and After Fatigue Loading

FUNDAMENTAL FREQUENCY

BEAM #	BEFORE FATIGUE (Hz)	AFTER FATIGUE (Hz)	CYCLE NUMBER (million)	FAILURE CYCLE (million)
1	20.0	18.9	1.20	1.27
2	18.9	17.9	1.80	2.15
3	17.8	16.9	1.48	1.67
4	18.0	16.9	1.60	1.69
5	17.8	16.9	1.50	1.57
6	19.4	18.0	0.35	0.40

Table 5.4:   Solid Beam   Natural Frequencies   by Beam   Theory
(SAP-IV)

BEAM#	B (in)	H (in)	L (in)	f_1 (Hz)	f_2 (Hz)	f_3 (Hz)	f_4 (Hz)
		BEAM DIMENSIONS			FREQUENCY		
1	3	8	180	16.5	65.9	146.8	263.5

Table 5.5:   Rectangular Beam Natural Frequencies for Varying
Opening Length in the Shear Span

FREQUENCY

BEAM#	f_1 (Hz)	f_2 (Hz)	f_3 (Hz)	f_4 (Hz)
1	17.2	67.9	150.1	263.1
2	17.2	68.1	150.7	263.4
3	17.2	68.4	151.8	263.8
4	17.2	68.6	153.0	260.0
5	17.2	68.9	153.9	245.2
6	17.1	69.2	153.7	220.1
7	17.0	69.2	150.5	198.5
8	16.9	70.5	109.5 **	187.2

Note:
**   Local Mode

Table 5.6:   Rectangular Beam Natural Frequencies for Varying
             Opening Length at Midspan

FREQUENCY

BEAM #	f_1 (Hz)	f_2 (Hz)	f_3 (Hz)	f_4 (Hz)
1	17.7	69.0	152.0	267.5
2	18.0	66.6	154.4	235.7
3	18.3	61.7	156.5	200.8
4	18.5	54.8	157.8	181.8

Table 5.7:   Rectangular Beam Natural Frequencies for Varying
             Opening Length and Number in the Shear Span

FREQUENCY

BEAM #	f_1 (Hz)	f_2 (Hz)	f_3 (Hz)	f_4 (Hz)
1	17.2	68.3	151.0	262.0
2	17.2	69.1	152.5	257.6
3	17.2	69.5	152.7	247.6

Table 5.8: T-Beam Natural Frequencies for Varying Opening Length and Cross Section at Midspan

FREQUENCY

BEAM#	f_1 (Hz)	f_2 (Hz)	f_3 (Hz)	f_4 (Hz)
1	22.6	51.4	107.2	-169.3
2	22.4	45.8	105.8	124.53
3	22.4	37.8	102.1	105.9
4	22.4	33.0	99.0	108.6
5	29.0	84.2	175.4	288.3
6	30.0	57.8	176.0	179.8

Table 5.9: I-Beam Natural Frequencies for Varying Opening Length at Midspan

FREQUENCY

BEAM#	f_1 (Hz)	f_2 (Hz)	f_3 (Hz)	f_4 (Hz)
1	35.8	114.5	212.1	319.8
2	36.4	93.8	215.6	229.9
3	37.1	64.8	198.7	221.6

BIBLIOGRAPHY

Abdus Salam, S., Harrop, J., (1979). "Prestressed Concrete
    Beams with Transverse-Circular Holes", Journal of
    Structural Division, ASCE, Vol. 105, No. ST3, pp.
    635-652.

Abeles, P.W., (1965). "Studies on Crack Widths and
    Deformation Under Sustained and Fatigue Loading", PCI
    Journal, Vol. 10, pp. 43-52.

Balaguru, P.N., (1981). "Analysis of Prestressed Concrete
    Beams for Fatigue Loading", PCI Journal, Vol. 26, pp.
    70-94.

Barney, G.B., Hanson, M.H., Corley, W.G and Parmelee, R.A.,
    (1977). "Behaviour and Design of Prestressed Concrete
    Beams with Large Web Openings", PCI Journal, Vol. 22,
    pp. 33-61.

Bathe, K.J., Wilson, F.L. and Paterson, P.E., (1974). "A
    Structural Analysis Program for Static and Dynamic
    Response of Linear Systems", (SAP-IV), Report #EERC
    72-11.

Coles, B.C., Hamilton, W.A., (1969). "Repetitive Dynamic
    Loading on Pretensioned Prestressed Beams", ACI Journal,
    Vol. 66, pp. 745-747.

"Design and Control of Concrete Mixes", (1981). Canadian
    Portland Cement Association, Third Edition, 131pp.

Dinakaran, V., Sastry, M.K.L.N., (1984). "Behaviour of
    Post-tensioned Prestressed Concrete T-Beams with Large
    Web Openings", Indian Concrete Journal, Vol. 58, No. 2,
    pp. 34-38,55.

El-laithy, A.M., (1978). "Influence of Openings on the
    Behaviour of Rectangular Post-tensioned Prestressed
    Concrete Beams", M.A.Sc. thesis, University of Windsor,
    Windsor, Ontario, 193pp.

Grace, N.F.F., (1986). "Free Vibration of Prestressed
    Continuous Composite Bridges and Skew Orthotropic

Plates", Ph.D. thesis, University of Windsor, Windsor, Ontario, 345pp.

Grace, N.F.P., Kennedy, J.B., (1985). "Dynamic Analysis of Orthotropic Plate Structures", Journal of Engineering Mechanics, Vol. 111, No. 8, pp. 1027-1037.

Grace, N.F.P, Kennedy, J.B., (1984). "Dynamic-Fatigue Response of Continuous Composite Bridges", Proceedings of Japan-U.S. Seminar on Composite Construction, Seattle, Washington, July 18-21.

Hanson, J.M., Hulsbos, C.L. and VanHorn, D.A., (1970). "Fatigue Tests of Prestressed Concrete I-Beams", Journal of Structural Division, ASCE, Vol. 96, No. ST11, pp. 2443-2464.

Inomata, P.S., (1971). "Comparative Study on Behaviour of Prestressed and Reinforced Concrete Beams Subject to Loading Reversals", PCI Journal, Vol. 16, pp.21-37.

Jacobs, M., Rankin and Hill, (1968). "The Behaviour of Prestressed Concrete Beams Under Reversed Cyclic Loading", The second Annual Australasian Conference on the Mechanics of Structures and Materials, Sydney, pp. 25.1-25.15 .

Johns, K.C., Belanger, M.D., (1981). "Dynamic Stiffness of Concrete Beams", ACI Journal, Vol. 78, pp. 210-205.

Kennedy, J.B., El-laithy, A.M., (1982). "Cracking at Openings in Prestressed Beams at Transfer", Journal of Structural Division, ASCE, Vol. 108, No. ST6, pp. 1250-1265.

Kulkarni, G.G., Ng, S.F., (1979). "Behaviour of Limited Prestressed Beams Under Repeated Loads", Can. J. Civil Eng., Vol. 6, pp. 544-556.

Mansur, M.A., Ong, K.C.G., (1985). "Epoxy Repaired Beams", Concrete International, ACI Institute, Vol. 7, pp.46-50.

Mansur, M.A., Tan, K.H. and Lee, S.L., (1985). "Design Method for Reinforced Concrete Beams With Large Openings", ACI Journal, Vol. 82, pp. 517-524.

Marshall, P.W., Ozell, A.M., (1960). "Behaviour of Prestressed Concrete Under Dynamic Loading", PCI Journal, Vol. 5, No. 2, pp. 74-84.

Paz, M., (1985). "Structural Dynamics", Second Edition, Van Nostrand Reinhold, New York, 561pp.

Price, K.M., Edwards, A.D., (1971). "Fatigue Strength of Prestressed and Reinforced Concrete Beams Subject to Loading Reversals", PCI Journal, Vol. 16, pp. 21-37.

Regan, H.S., Warwaruk, J., (1967). "Tee Members with Large Web Openings", PCI Journal, Vol. 12, pp. 52-65.

Rockey, K.C., Evans H.R., Griffiths D.W and Nethercot, D.A., (1983). "The Finite Element Method", Second Edition, Granada Publishing Limited, London, 239pp.

Sargious, M., Dilger, W., (1977). "Prestressed Concrete Deep Beams with Openings", PCI Journal, Vol. 22, pp. 64-79.

Sokolovsky, A.M., Livolant, M., Gauvain, J. and Hoffmann, A., (1980). "Study of Progressive Damage to Reinforced Concrete Structures Submitted to Dynamic Reversed Load", Nuclear Technology, Vol. 49, pp. 19-26.

Stanton, J.F., Mcniven, H.D., (1983). "Towards an Optimum Model For the Response of Reinforced Concrete Beams to Cyclic Loads", Earthquake Engineering and Structural Dynamics, Vol. 11, pp. 299-312.

"STRUDL-DYNAL, PLOTS and DANGS", (1985). The Structural Design Language Engineering User's Manual, Release 6.7, McDonnell Douglas Automation Company.

Thomson, W.T., (1981). "Theory of Vibration with Applications", Second Edition, Prentice-Hall, New Jersey, 493pp.

Timoshenko, S., (1955). "Vibration Problems in Engineering", Third Edition, D. Van Nostrand, New York, 468pp.

"Vibration Testing Instrumentation and Data Analysis", (1975). Proceedings of ASME/DED Vibrations Conference, Washington D.C., 141pp.

Warner, R.F., Hulsbos, C.L., (1962). "Probable Fatigue Life of Prestressed Concrete Flexural Members", Report to Pennsylvania Dept. of Highways, Fritz Eng. Lab No. 223.24A, 212pp.

Warner, R.F., (1960). "Research on fatigue and Shear in Prestressed Concrete", PCI Journal, Vol. 5, pp. 73-77.

Zivriev, K.S., (1964). "Research on Response of Prestressed
    Structures to Dynamic Loading", PCI Journal, Vol. 9, pp.
    27-32.

VITA AUCTORIS

SAADALLAH CHAMI

The author was born on July 15, 1963 in Beirut, Lebanon. In June of 1980, he completed his secondary school education at Jarvis Collegiate in Toronto, Ontario. In September of 1980, he joined the faculty of Engineering at the University of Windsor, Windsor, Ontario. In May of 1984, he completed the requirements for a Bachelor of Applied Science degree in Civil Engineering from the University of Windsor.

In September of 1984, he joined the department of Civil Engineering at the University of Windsor as a teaching and research assistant. In August of 1987, he completed the requirements for a Master of Applied Science degree in Civil Engineering.